U.S.NRC
United States Nuclear Regulatory Commission
*Protecting People and the Environment*

**RIL 2023-07**
**NIST TN 2263**

# REPORT ON HIGH ENERGY ARCING FAULT EXPERIMENTS

## Experimental Results from Medium-Voltage Bus Duct and Switchgear Enclosures

Date Published: September 2023

Prepared by:
G. Taylor
Office of Nuclear Regulatory Research

A.D. Putorti Jr.
National Institute of Standards and Technology

Mark Henry Salley, NRC Project Manager

This report was published as National Institute of Standards and Technology (NIST) Technical Note 2263 as part of a series of experiments funded by the U.S. Nuclear Regulatory Commission's Office of Research. The report has been re-published as an NRC Research Information Letter (RIL).

# Disclaimer

Legally binding regulatory requirements are stated only in laws, NRC regulations, licenses, including technical specifications, or orders; not in Research Information Letters (RILs). A RIL is not regulatory guidance, although NRC's regulatory offices may consider the information in a RIL to determine whether any regulatory actions are warranted.

Certain commercial equipment, instruments, or materials are identified in this paper to specify the experimental procedure adequately. Such identification is not intended to imply recommendation or endorsement by the U.S. Nuclear Regulatory Commission or the National Institute of Standards and Technology, nor is it intended to imply that the materials or equipment identified are necessarily the best available for any application.

NIST Technical Note
NIST TN 2263

# Report on High Energy Arcing Fault Experiments

*Experimental Results from Medium-Voltage Bus Duct and Switchgear Enclosures*

Final Report

G. Taylor
A. Putorti Jr.
S. Bareham
C. Brown
W.C. Tam
R. Falkenstein-Smith
S. Fink
M. Heck
E. Hnetkovsky
N. Melly
K. Hamburger
K. Miller

This publication is available free of charge from:
https://doi.org/10.6028/NIST.TN.2263

NIST NATIONAL INSTITUTE OF STANDARDS AND TECHNOLOGY
U.S. DEPARTMENT OF COMMERCE

**NIST Technical Note**
**NIST TN 2263**

# Report on High Energy Arcing Fault Experiments

## *Experimental Results from Medium-Voltage Bus Duct and Switchgear Enclosures*

Final Report

A. Putorti Jr., S. Bareham, C. Brown,
W.C. Tam, R. Falkenstein-Smith,
S. Fink, M. Heck, E. Hnetkovsky
*Fire Research Division*
*Engineering Laboratory*

G. Taylor, N. Melly, K. Hamburger,
K. Miller
*Office of Nuclear Regulatory Research*
*U.S. Nuclear Regulatory Commission*

This publication is available free of charge from:
https://doi.org/10.6028/NIST.TN.2263

September 2023


U.S. Department of Commerce
*Gina M. Raimondo, Secretary*

National Institute of Standards and Technology
*Laurie E. Locascio, NIST Director and Under Secretary of Commerce for Standards and Technology*

NIST TN 2263
September 2023





**Publication History**
Approved by the NIST Editorial Review Board on 2023-09-06

**How to Cite this NIST Technical Series Publication**
Taylor, G., Putorti Jr., A., Bareham, S., Brown, C.U., Tam, W.C., Falkenstein-Smith, R., Fink, S., Heck, M., Hnetkovsky, E., Melly, N., Hamburger, K., and Miller, K. (2023) Report on High Energy Arcing Fault Experiments: Experimental Results from Medium-Voltage Bus Duct and Switchgear Enclosures. (National Institute of Standards and Technology, Gaithersburg, MD), NIST Technical Note (TN) NIST TN 2263.
https://doi.org/10.6028/NIST.TN.2263

**NIST Author ORCID iDs**
G. Taylor: 0009-0001-0098-0075
A. Putorti Jr.: 0000-0001-9015-4959
S. Bareham: 0000-0001-6667-7055
C. Brown: 0000-0002-0426-2249
W.C. Tam: 0000-0003-3913-0243
R. Falkenstein-Smith: 0000-0001-7039-5835
S. Fink: 0009-0005-1698-1696
M. Heck: 0000-0002-6279-5908
E. Hnetkovsky: 0009-0001-0360-311X
N. Melly: 0009-0001-9645-284X
K. Hamburger: 0009-0008-6042-4063

**Contact Information**
gabriel.taylor@nrc.gov
anthony.putorti@nist.gov

## Abstract

This report documents an experimental program designed to investigate high energy arcing fault (HEAF) phenomena for medium-voltage, metal-enclosed bus ducts and switchgear. This report covers full-scale laboratory experiments using representative nuclear power plant (NPP) three-phase electrical equipment. Electrical, thermal, and pressure data were recorded for each experiment and documented in this report. This report covers experiments performed on two medium-voltage switchgear units and eight non-segregated phase bus ducts. The data collected supports characterization of the medium-voltage HEAF hazard, and these results will be used to complement the data used for HEAF hazard modeling tools and support potential improvements in fire probabilistic risk assessment (PRA) methods.

The experiments were performed at KEMA Labs in Chalfont, Pennsylvania. The experimental design, setup, and execution were performed by staff from the NRC, the National Institute of Standards and Technology (NIST), Sandia National Laboratories (SNL) and KEMA Labs. These experiments were sponsored by member countries of the HEAF 2 international agreement under the auspices of the Organisation for Economic Co-operation and Development (OECD).

The HEAF experiments were performed between August 22 and September 2, 2022. The HEAF experiments were performed on two near-identical units of General Electric metal-clad medium-voltage switchgear and eight units of non-segregated phase bus duct. A three-phase arcing fault was initiated on the equipment's bus bars. These experiments used nominal system voltages of either 4.16 kV (AC) or 6.9 kV (AC). Arc durations in the experiments ranged from approximately 2 s to 4 s with fault currents ranging from approximately 28 kA to 32 kA. Real-time electrical operating conditions, including voltage, current, and frequency, were measured during the experiments. Heat fluxes and incident energies were measured with plate thermometers and slug calorimeters at various locations around the electrical enclosures. Particulate samples were taken for subsequent analysis. The experiments were documented with normal and high-speed videography, infrared imaging, and photography.

Insights from the experimental series include timing information related to enclosure breach, event progression, mass loss measurements for electrodes and enclosures, peak pressure rise, along with visual and thermal imaging data to better understand and characterize the hazard. These results will be used to evaluate the adequacy of existing HEAF hazard modeling tools and for potential improvements to fire probabilistic risk assessment methods related to HEAF.

## Keywords

High Energy Arcing Fault, Arc Flash, Electrical Enclosure, Switchgear, Bus Duct, Electric Arc, Fire Probabilistic Risk Analysis, Fire Probabilistic Safety Analysis

## Table of Contents

## List of Tables

## List of Figures

## Executive Summary

**PRIMARY AUDIENCE:** Fire protection, electrical, and probabilistic risk assessment engineers conducting or reviewing fire risk assessments related to high energy arcing faults (HEAFs).

**SECONDARY AUDIENCE:** Engineers, reviewers, utility managers, and other stakeholders who conduct, review, or manage fire protection programs and need to understand the underlying technical basis for the hazards associated with high energy arcing faults.

**KEY RESEARCH QUESTION:** How does conductor and/or enclosure material influence the HEAF hazard for medium-voltage equipment?

### RESEARCH OVERVIEW

Operating experience has shown that high energy arcing faults pose a hazard to the safe operation of nuclear facilities. Current regulations and probabilistic risk assessment methods were developed using limited information, and the inherent uncertainties required the use of safety margins to bound the hazard. The NRC and its collaborative research partners have significantly advanced the understanding of HEAF phenomena, such as an improved understanding of plant configurations, operational history, target fragility, source characterization, hazard modeling and associated improvements to fire PRA. The experiments documented in this report aim to provide additional data to improve realism and complement previous experimental results. This report documents a set of experiments performed in 2022.

A series of medium-voltage, metal-enclosed indoor switchgear and medium-voltage, non-segregated bus duct arcing experiments were performed. Each experiment consisted of an arcing fault initiated within the unit on either aluminum or copper bus bars. Nominal system voltages of either 4.16 kV (AC) or 6.9 kV (AC) were used, depending on equipment ratings. Fault durations of 2 s to 4 s and current levels between 30 kA and 32 kA (AC rms) were used. Numerous measurements were taken to characterize the environment within and surrounding the enclosure, including pressure, external heat flux, and external incident energy. Time-resolved electrical measurements of the fault conditions were also recorded.

This report documents the experiments performed, including the experimental methods, experimental facility, experimental devices, instrumentation, observations, and results. Videos and photometric data files are provided by laboratories contracted to the NRC, and information on accessing that information is identified. This report does not provide detailed evaluation of the results or comparisons of the results to other methods or data. Those efforts will be documented in subsequent report(s).

### KEY FINDINGS

This research yields data that characterizes the effects of electrical arcing faults. The results from this research include:

- Switchgear experiments 2-10 and 2-12 using copper bus bars did not experience a breach, while previous experiments using identical switchgear using aluminum bus bars did under similar fault conditions.
- Bus duct experiments demonstrated thermal exposures that were similar to those predicted by numerical simulations performed prior to the experiments. The arc migration

and duct enclosure failures were not well predicted based on past testing and impacted the ability of the measurement devices to record the most severe exposures.

## WHY THIS MATTERS

This report provides empirical evidence to assist U.S. NRC staff, OECD HEAF 2 member countries, and stakeholders who are evaluating the adequacy of current methods. The information provided will support advances in state-of-the-art methods and tools to assess the high energy arcing fault hazard in nuclear facilities. This information may also be applicable to fossil fuel and alternative energy facilities and other buildings with low- and medium-voltage electrical distribution equipment such as switchgear and bus ducts.

## HOW TO APPLY RESULTS

Engineers and scientist advancing hazard and fire probabilistic risk assessment methods should focus on Section 3 of this report.

## LEARNING AND ENGAGEMENT OPPORTUNITIES

Users of this report may be interested in the following opportunities:

Nuclear Energy Agency (NEA) HEAF Project to conduct experiments to explore the basic configurations, failure modes and effects of HEAF events. Primary objectives include (1) development of a peer-reviewed guidance document that could be readily used to assist regulators and (2) joint nuclear safety project report covering all experimentation and data captured. More information on the project and opportunities to participate in the program can be found online at https://www.oecd-nea.org/.

## Citations

This report was prepared by the following:

National Institute of Standards and Technology (NIST)
Engineering Laboratory; Fire Research Division
Gaithersburg, Maryland 20899
Anthony D. Putorti Jr.
Scott Bareham
Christopher Brown
Wai Cheong Tam
Ryan Falkenstein-Smith
Stephen Fink
Michael Heck
Edward Hnetkovsky

U.S. Nuclear Regulatory Commission
Washington, DC 20555-0001
Kenneth Hamburger
Nicholas Melly
Kenneth Miller
Gabriel Taylor

## ABBREVIATIONS AND ACRONYMS

| | |
|---|---|
| AC | alternating current |
| ASTM | ASTM International |
| AWG | American Wire Gauge |
| CT | current transformer |
| DC | direct current |
| EDT | eastern daylight time |
| EMI | electro-magnetic interference |
| EPRI | Electric Power Research Institute |
| GE | General Electric |
| GI | generic issue |
| GIRP | Generic Issue Review Panel |
| HEAF | high energy arcing fault |
| IEEE | Institute of Electrical and Electronic Engineers |
| IN | information notice |
| IR | infra-red |
| KEMA | Keuring van Elektrotechnische Materialen te Arnhem |
| MD | management directive |
| NEA | Nuclear Energy Agency |
| NEC | National Electric Code |
| NIST | National Institute of Standards and Technology |
| NRC | Nuclear Regulatory Commission |
| NRR | Office of Nuclear Reactor Regulation |
| NSBD | non-segregated bus duct |
| OECD | Organisation for Economic Co-operation and Development |
| PIRT | Phenomena Identification and Ranking Table |
| PRA | probabilistic risk assessment |
| PT | plate thermometer |
| RES | Office of Nuclear Regulatory Research |
| RIL | research information letter |
| SNL | Sandia National Laboratories |
| $T_{cap}$ | tungsten thermal capacitance |
| U.S. | United States of America |

# 1. Introduction

Infrequent events such as fires at a nuclear power plant can pose a significant risk to safe plant operations. Licensees combat this risk by having robust fire protection programs designed to minimize the likelihood and consequences of fire. These programs provide reasonable assurance of adequate protection from known fire hazards. However, several hazards remain subject to a large degree of uncertainty, requiring significant safety margins in plant analyses.

One such hazard comprises an electrical arcing fault involving electrical distribution equipment and components. While the electrical faults and subsequent fires are considered in existing fire protection programs, recent research [1] has indicated that elements of the electrical fault can exacerbate the damage potential of the event. The increased damage potential could exceed the protection provided by existing fire protection features for specific fire scenarios and increase plant risk estimated in fire probabilistic risk assessments (PRAs).

The U.S. Nuclear Regulatory Commission (NRC) Office of Nuclear Regulatory Research (RES) studies fire and explosion hazards to ensure the safe operation of nuclear facilities. This includes developing data, tools, and methodologies to support risk and safety assessments. Through recent research efforts and collaboration with international partners, a non-negligible number of reportable high energy arcing fault (HEAF) events have been identified as occurring in nuclear facilities [2]. HEAF events pose a unique hazard in nuclear facilities and additional research in this area is needed to ensure that the hazard is accurately characterized and assessed for its impact on nuclear safety.

## 1.1. Background

In June 2013, an Organisation for Economic Co-operation and Development (OECD) / Nuclear Energy Agency (NEA) report [2] on international operating experience documented 48 HEAF events, accounting for approximately 10 percent of the total fire events reported. These HEAF events are often accompanied by loss of essential power and complicated shutdowns. Existing PRA methodology for HEAF analysis is prescribed in NUREG/CR-6850 "EPRI/NRC-RES Fire PRA Methodology for Nuclear Power Facilities Vol. 2 [3]," and its Supplement 1 [4]. To confirm these methods, the NRC led an international experimental campaign from 2014 to 2016. This experimental campaign is referred to as "Phase 1 Experimenting." The results of these experiments [5] uncovered a potential increase in the hazard severity.

In response to this new information, the NRC issued Information Notice 2017-004, "High Energy Arcing Faults in Electrical Equipment Containing Aluminum Components (IN 2017-04)," detailing the relevant aspects of the licensee event reports and Phase 1 experimental results in August of 2017 [1]. Additionally, RES staff proposed a potential safety concern as a generic issue (GI) in a letter dated May 6, 2016 [6]. The Generic Issue Review Panel (GIRP) completed its screening evaluation [7] for the proposed Generic Issue (GI) PRE-GI-018, "High-Energy Arc Faults (HEAFs) Involving Aluminum," and concluded that the proposed issue met all seven screening criteria outlined in Management Directive (MD) 6.4, "Generic Issues Program." Therefore, the GIRP recommended that this issue continue into the Assessment Stage of the GI program. The GIRP has completed an assessment plan, issued August 23, 2018 [8]. In September

of 2021, the NRC determined that the pre-GI-018 no longer met the Criterion 5 of the NRC MD 6.4, concluding that the risk and safety significance of HEAFs involving aluminum cannot be adequately determined in a timely manner without performing additional, long-term research to develop the methodology for such a determination [9].

In a revised approach to resolving the knowledge gap, the NRC staff applied the BeRiskSMART framework. This approach consists of two coordinated tracks for (1) research activity in coordination with the Electric Power Research Institute (EPRI) and (2) use of the NRC process LIC-504, "Integrated Risk-Informed Decisionmaking Process for Emergent Issues [10]," to apply best available information and NRC risk assessment tools to determine whether any regulatory action was needed. The NRC LIC-504 process was completed in July 2022, finding both increase and decreases in plant risk with a determination of no significant risk increase in total HEAF risk for the two plants evaluated.

Under the research approach with EPRI, the NRC developed tools to estimate the HEAF hazard [11, 12], a hazard-specific target fragility characterization [13] and an updated HEAF fire PRA method [14] to provide guidance for evaluating the risk from a HEAF. As part of the modeling effort, the team identified several scenarios where experimental data was either not available to validate the model's predictive capabilities or lacking for comparison purposes. These scenarios included medium-voltage non-segregated bus ducts and medium-voltage switchgear.

Due to the lack of data, possible modeling uncertainty, and potential risk significance of these configurations, the NRC Office of Nuclear Reactor Regulation issued a Research Assistance Request (NRR-2022-014-RAR) to NRC/RES to perform high energy arcing fault experimenting in cooperation with the OECD. This report documents this effort to perform a limited series of experiments to acquire the needed data. The NRC developed an experimental plan in collaboration with its international collaborative partners under the OECD/NEA program, NRC/NRR RAR request, and based on information from a Phenomena Identification and Ranking Table (PIRT) exercise performed in 2017 [15].

## 1.2. Objectives

The research objectives for this experimental series include: quantitatively characterize the thermal and pressure conditions created by HEAFs occurring in electrical enclosures (switchgear and bus ducts) and document the experiments and results.

## 1.3. Scope

The scope of this research includes evaluating the HEAF hazard on medium-voltage electrical switchgear containing copper bus and medium-voltage non-segregated bus ducts with specific combinations of enclosure material (steel or aluminum) and bus bar material (copper or aluminum). This characterization involves measurement and documentation of electrical and thermal parameters, along with physical evidence. The results from this effort will be used to provide empirical evidence for use by the OECD HEAF 2 member countries and by NRC staff to evaluate the prediction capabilities of the recently developed hazard models. Detailed data analysis for specific applications is beyond the scope of this report.

## 1.4. Approach

The approach taken for this work follows practices from past efforts [5, 16-18]. Specifically, the experimental device (medium-voltage switchgear and bus ducts) is faulted between the three phases. The laboratory provided electrical energy to the experimental device at specified parameters (system voltage, current, duration). Measurements internal and external to the gear were made using robust measurement devices fielded by the National Institute of Standards and Technology (NIST). Sandia National Laboratories (SNL) provided high-speed visual and thermal imaging and those results are presented in a separate report. Measurements were recorded, scaled, and reported. Feedback received during the developmental stage of this project was incorporated into the experimental approach. This included the arc locations, fault current magnitudes, and the durations of the experiments.

## 2. Experimental Method

This section provides information on methods used to perform the experiments[1], including experimental planning, overview of the experimental facility, the tested devices, and the various instruments that were used.

### 2.1. Experiment Planning

The experimental plan was developed and shared with the OECD member countries and NRC/NRR. Lessons learned from the Phase 1 and generic issue experiments, results from the Phenomena Identification and Ranking Table (PIRT) exercise, and existing literature were used to develop the initial experimental plan. The experimental plan is a living document and has undergone several revisions over time as new information emerges. Review and feedback by the OECD/NEA and other stakeholders were incorporated into the experimental plan. The central component of the experimental plan is the experimental matrix which specifies the key parameters for each experiment. A graphical matrix for electrical enclosures is presented in Fig. 1 and Fig. 2. The experiments shown in red were completed in 2018 [16], green experiments are the subject of the experimental series documented in this report, and white experiments have not been completed. This report covers Experiment 2-10, Experiment 2-12 and Experiments 2-25 through 2-32. The key parameters that are evaluated in this experimental campaign are arc duration and arcing current.

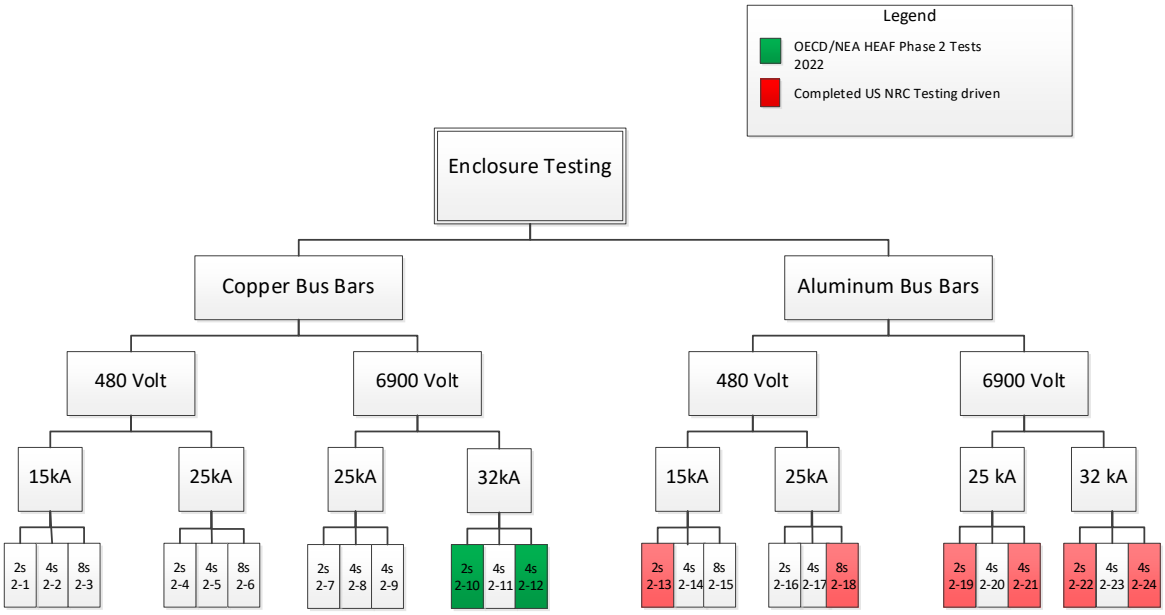


[1] The term 'test' implies the use of a standardized test method promulgated by a standards development organization such as the International Organization for Standardization (ISO), ASTM International, Institute of Electrical and Electronics Engineers (IEEE), etc. The experiments described in this report are not standard tests and were specifically developed to examine HEAF phenomena. The term 'test' is used in some contexts to preserve continuity with previous programs or to describe facilities where standard tests are frequently performed. Standard test methods, where they exist, are used for some measurements.

Fig. 1. Graphical Phase 2 Experimental Matrix for Electrical Enclosure

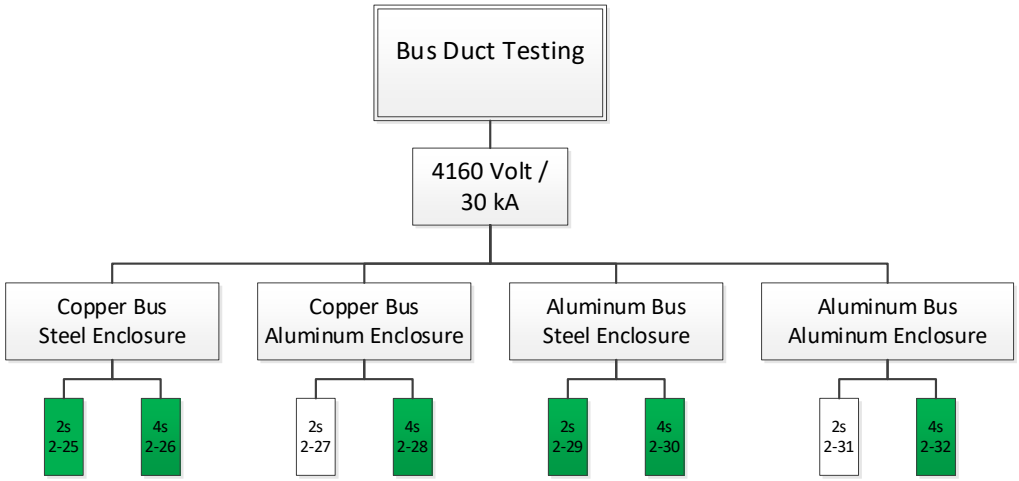


Fig. 2. Graphical Phase 2 Experimental Matrix for Non-segregated Bus Duct

One change that deviated from the plan was that experiment 2-29 was not performed. During the testing of experiment 2-30, a laboratory equipment failure occurred and resulted in the experiment 2-30 parameters not being met. The importance of the results from experiment 2-30 and the lack of spare equipment resulted in the team making the decision to not perform experiment 2-29. The equipment planned to be tested for experiment 2-29 was used to re-run an experiment. The re-run experiment is identified in this report as experiment 2-30B. Details on the failure are described in Section 3.7.

## 2.2. Experimental Facility

The full-scale experiments were performed at KEMA Labs (referred to in the remainder of this report as "KEMA"), located in Chalfont, Pennsylvania, in August and September 2022. The experimental facility was chosen for its ability to meet the requirements of the program; specifically, the electrical voltages, currents, and energies needed for sustained arcing within the test enclosures and to permit fire conditions for a period after termination of the arc. KEMA provided the electrical measurements required to characterize the power supplied to the enclosures during the arcing experiments. KEMA also provided incident energy measurements using ASTM F1959 calorimeters.

The test cell is a cubical space with one open side. The open side was equipped with a roll-up door for security and weather protection when not in use. The open side of the cell faces the operator control room, with a courtyard area in between. The control room is equipped with impact-resistant glazing so that the operators, clients, and guests can observe the experiments. A door in the rear of the cell leads to the exterior and a climate-controlled van where NIST data acquisition equipment was located and operated.

Test cell #9 was used during this experiment series to perform the medium-voltage experiments. The cell is shown in Fig. 3. Detailed drawings of the facility are provided in Appendix A.1. Drawings of the cell are courtesy of KEMA.

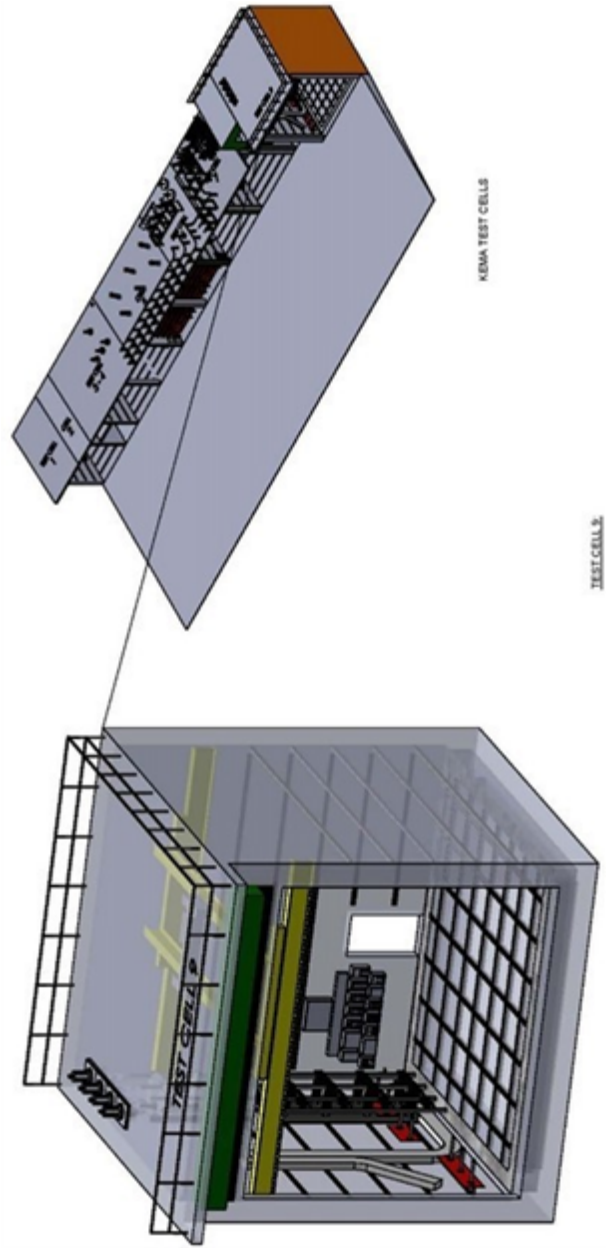


Fig. 3 Isometric drawing of test cell # 9 (left) and location of test cell #9 (right with respect to KEMA facility).

## 2.3. Experimental Devices

Two types of equipment were used during this experimental series. One type was a medium-voltage switchgear similar to the devices tested in 2018 [16]. The other type of equipment was medium-voltage non-segregated bus duct. Descriptions of both follow.

### 2.3.1. Medium-Voltage Switchgear

The two metal-clad switchgear units were General Electric[2] Type M-36, used and refurbished from an ISO 9001-certified medium-voltage circuit breaker and electrical power distribution supplier. The units were approximately 92 cm (36 in) wide by 202 cm (79.5 in) long and 229 cm (90 in) high. Main buses were extended outside of the enclosure approximately 46 cm (18 in) to allow for connection to the laboratory's power supply. A shorter grounding stab also extended outside the enclosure. Fig. 4 presents photographs of one of the units without the metal cladding. The photo on the left is taken from the rear of the enclosure closest to the "primary cable compartment." Note that the bus bars have been removed in this photo to be weighed and measured. The photo on the right is a side view with the breaker compartment on the left. The only differences between the two enclosures were the protective relaying and internal control wiring configuration located on the front door and secondary enclosure. Fig. 5 provides a drawing and isometric view of the enclosure used in experiments 2-10 and 2-12.

Fig. 4. Type M-36 Metal Clad Enclosure (note: bus bar and breaker not shown)

[2] Certain commercial equipment, instruments, or materials are identified in this paper to specify the experimental procedure adequately. Such identification is not intended to imply recommendation or endorsement by the U.S. Nuclear Regulatory Commission or the National Institute of Standards and Technology, nor is it intended to imply that the materials or equipment identified are necessarily the best available for any application.

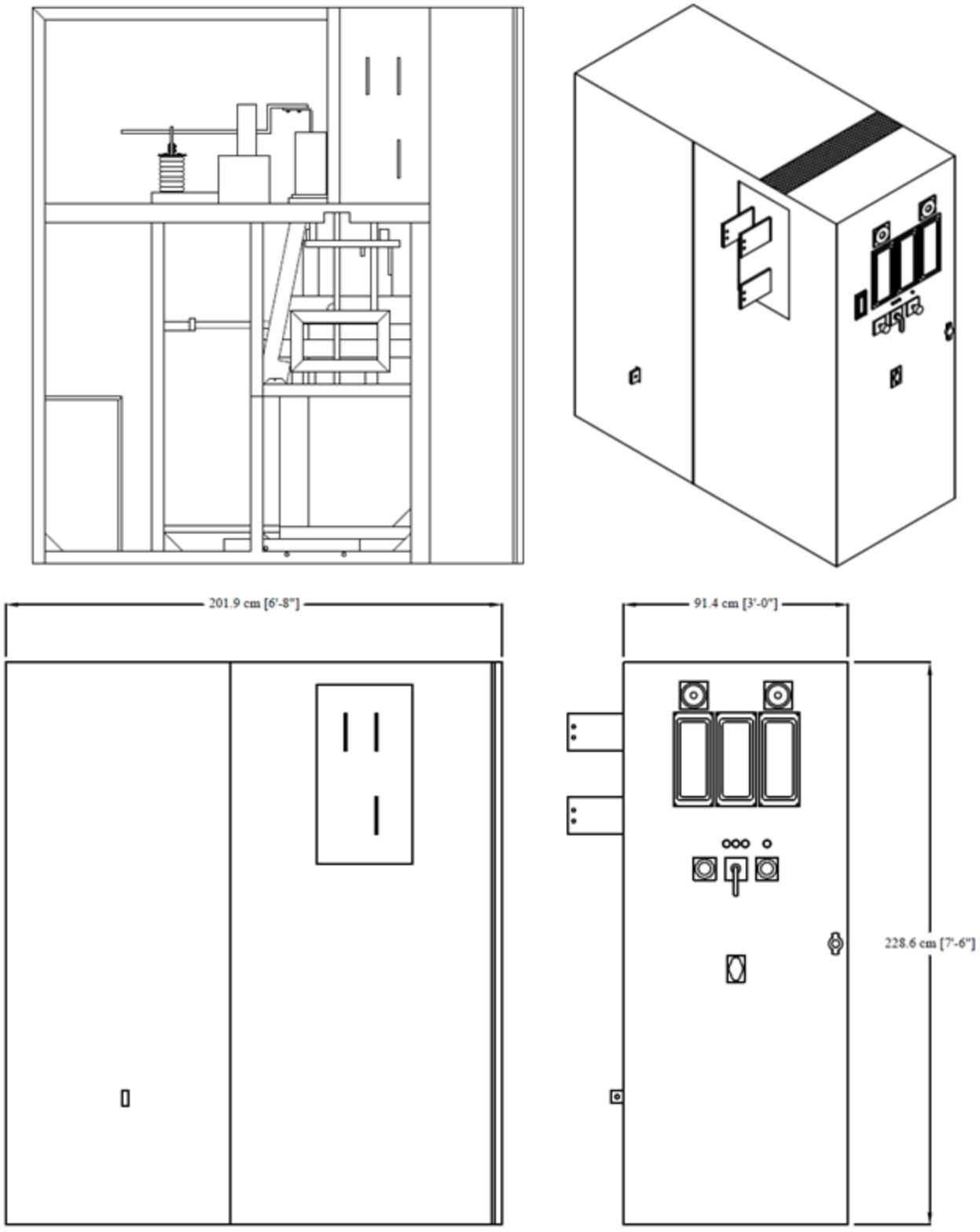


Fig. 5. Drawing of Medium-Voltage Electrical Enclosure - Experimental Device (all measurements are approximate)

Copper bus bars were used for the main bus conductors and primary cable compartment buses. The breaker socket/tube conductors were copper. The original equipment contained insulation on the primary cable compartment buses, but the insulation was removed to be consistent with the 2018 experimental series for comparative purposes [16]. In the U.S., equipment can be found with and without insulation on the bus bars. Unlike the 2018 experimental series, the current transformers (CTs) were included in the experiments. This inclusion added realism in the experimental configuration as switchgear found in the field typically have CTs as part of the protection circuit. The CT's secondary sides were shorted to minimize the concern of high voltage conditions due to open circuit CTs. Field-installed cable potheads or cable clamp terminations were not included. The absence of bus cabling reduced the amount of combustible load but is consistent with previous experiments.

Each unit contained one medium-voltage circuit breaker. All breakers were GE Magne-blast Type AM-7.2-500 circuit breakers. The breaker ratings are shown in Table 1 and a photo of a breaker removed from the enclosure is shown in Fig. 6. After receipt of the equipment, the breakers were tested by the electrical contractor to ensure functionality. The breaker in the experiment enclosure was closed prior to, and remained closed during, the arc experiment. Prior to the experiments, Megger testing was performed with and without the breaker closed.

A Megger test consists of applying a DC voltage across an insulator and measuring the resulting current. Ohms law allows for the measurement of the insulation resistance, typically in the megaohm range for a good insulator. This ensured the equipment and breaker were functional prior to each experiment.

Table 1. GE AM-7.2 Breaker Nominal Rating and Characteristics

| Parameter | Value | Parameter | Value |
|---|---|---|---|
| Rated Max Voltage | 8.25 kV | Breaker Type | AM-7.2-500 |
| Rated Amps | 1.2 kA | Rated voltage range factor | 1.25 |
| Frequency | 60 Hz | Impulse Withstand | 95 kV |
| Rated Short Circuit Amps | 33 kA | Close / Latch Capability | 66 kA |
| Weight | 680 kg (1 500 lb) | Date Manufactured | February 1976 |

Fig. 6. Photo of AM-7.2-500 GE Magne-blast breaker

Initiation of the arc followed the process outlined in Annex E.4 of IEEE C.37.20.7, “IEEE Guide for Experimenting Switchgear Rated Up to 52kV for Internal Arcing Faults” [19]. A nominally 0.511 mm diameter (24 American Wire Gauge [AWG]) tinned copper wire was placed at the cable termination points on the primary cable compartment copper bus bars at the ends of the horizontal bar. This configuration is shown in Fig. 7. The shorting wire was placed on the bus conductors prior to securing the back panel of the electrical enclosure. The air gap spacing between each phase bus bar in the primary cable compartment was approximately 17.4 cm [6.88 in] and the bus bar centerline spacing was approximately 25.1 cm [9.88 in]. These copper bus bars were approximately 0.96 cm [0.38 in] thick and 7.6 cm [3.0 in] wide. This configuration resulted in the switchgear configured in a bus-tie or load circuit breaker configuration.

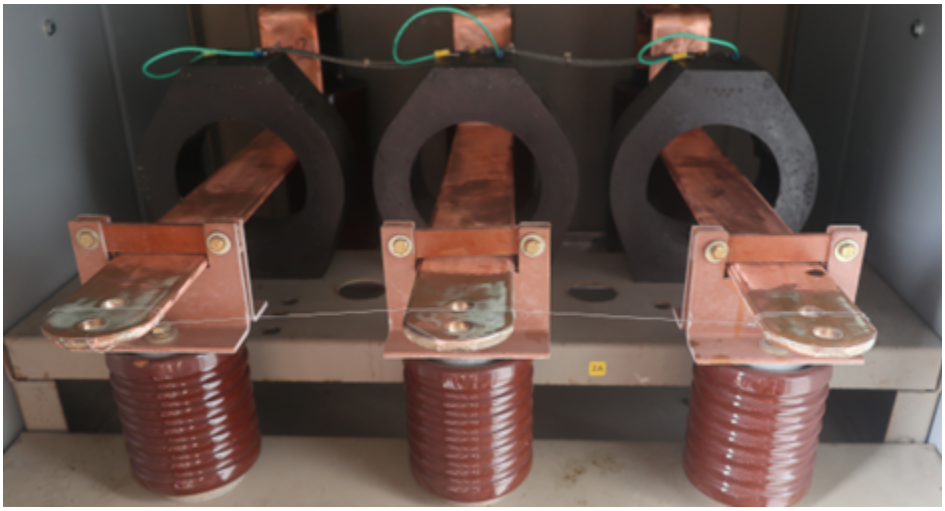

Fig. 7.Photograph of tinned copper wire used to create the short

The combustible loading within the enclosure was minimal. The primary enclosure contained polyolefin heat shrink tubing on the bus bars; however, the location where this material was located was separated from the primary cable compartment buses by metal cladding. The

material was not on the primary cable compartment buses as discussed previously. The secondary enclosure contained protective relays, fuse holders, control switches, meters, resistors, and associated insulated conductors. The insulation on the SIS-insulated conductors represented most of the combustible loading in the secondary enclosure. Some of the wiring had been cut and removed prior to receipt of the equipment. It was unclear if the equipment supplier removed it, or if it was removed by the previous owner. The amount of combustible material varied between enclosures, but was minimal and separated from the arc location by metal cladding. Fig. 8 shows this loading.

Fig. 8. Photo of combustible component loading in the secondary enclosure

### 2.3.2. Medium-Voltage Bus Duct

Eight medium-voltage non-segregated bus ducts (NSBD) were acquired. Six of the NSBD were procured new from a domestic vendor. The two remaining bus ducts were harvested from a U.S. nuclear power plant undergoing decommissioning. The two harvested ducts provide representative samples to ensure realism in the experimental program. The configurations of the ducts differed to address the program objective of evaluating the influence of material on the HEAF evolution. Table 2 presents the configurations. Duplicate samples only differed by the duration of the arc.

Table 2. NSBD Configurations

| Experiment # | Bus Material | Duct Material | Nominal Arc Duration | Acquired |
|---|---|---|---|---|
| **2-25** | Copper | Steel | 2 s | New |
| **2-26** | Copper | Steel | 4 s | New |
| **2-27** | Copper | Aluminum | 2 s | New |
| **2-28** | Copper | Aluminum | 4 s | New |
| **2-30** | Aluminum | Steel | 4 s | New |
| **2-30B*** | Aluminum | Steel | 4 s | New |
| **2-31** | Aluminum | Aluminum | 2 s | Harvested |
| **2-32** | Aluminum | Aluminum | 4 s | Harvested |

* Experiment #2-29 was not performed as discussed above, Experiment #2-30B replaces Experiment #2-29

Table 3. NSBD nominal Ratings and characteristics of bus conductors

| RATING | COPPER | ALUMINIUM | ALUMINUM (Decom.) |
|---|---|---|---|
| **Nominal operating voltage** | 4 160 V | 4 160 V | 4 160 V |
| **Rated voltage** | 5 000 V | 5 000 V | 5 000 V |
| **Continuous rating** | 2 000 A | 2 000 A | 2 000 A |
| **Momentary** | 80 000 A (asym.) 51 613 (sym.) | 80 000 A (asym.) 51 613 (sym.) | No Documentation |
| **BIL rating** | 19 kV | 19 kV | No Documentation |
| **System Frequency** | 60 Hz | 60 Hz | No Documentation |
| **Enclosure Thickness** | 3.18 mm (0.125 in) | 3.18 mm (0.125 in) | Top and Bottom 2.54 mm (0.100 in)<br><br>Sides 3.56 mm (0.140 in) |
| **Insulation** | 3M Heat Shrinkable Tubing for Bus Bar | 3M Heat Shrinkable Tubing for Bus Bar | 3M Heat Shrink Tubing |
| **Supports** | Polyester | Polyester | Fiberglass |

## 2.4. Instrumentation

Thermal, pressure, and HEAF byproduct measurements were made using a variety of instruments and techniques, identified in Table 4. A full description of these instruments and their application is provided in RIL 2021-10 Experimental Results from Medium Voltage Electrical Enclosures [16], except for the sheathed thermocouples and the calculation of the total incident energy from the plate thermometers.

A sheathed thermocouple (Type-K, 3.2 mm (0.125 in) nominal diameter, sheathed, ungrounded) was installed in the switchgear used in the bus experiment. The uncertainty in the temperature of the sheathed thermocouple is given by the manufacturer as the greater of ± 2.2 °C (± 4.0 °F) or ± 0.75 percent with a 99 percent confidence interval.

The total incident energy measured by the plate thermometers is calculated in a similar way to the ASTM F1959 Slug Calorimeters described in [16, 20], but with an additional correction for the emissivity of heat-treated Inconel 600, which is approximately 0.85.

The total incident energy, $Q''_{PT}$ (kJ/m$^2$), from the PT is calculated by:

$$Q''_{PT} = \frac{\rho_{ST} \cdot \bar{C}_{ST} \cdot \delta \cdot \left(T_{PT,\,max} - T_{PT,\,initial}\right)}{\varepsilon_{PT}} \quad (1)$$

where $T_{PT,\,initial}$ is the temperature of the plate prior to the experiment (K), $T_{PT,\,max}$ is the maximum temperature of the plate during the experiment (K), $\varepsilon_{PT}$ is the plate emissivity, 0.85 at 480 °C as rolled and oxidized and specified by the alloy manufacturer, $\rho_{ST}$ is the alloy plate density, 8 470 kg/m$^3$ from the alloy manufacturer, $\bar{C}_{ST}$ is the average temperature dependent alloy plate heat capacity [21] over the initial to maximum plate temperatures, and δ is the alloy plate thickness, 0.79 mm ± 0.03 mm. The ASTM F1959 standard also refers to the incident energy as the total energy per unit area (cal/cm$^2$ or kJ/m$^2$). The total incident energy during the experiment is reported in the plate thermometer summary table for each sensor location in each experiment. The uncertainty in the reported values of the total incident energy is ± 15%, with a coverage factor of k=2, which corresponds to a confidence interval of approximately 95%, as determined using the NIST Uncertainty Machine [22].

Table 4. Experimental Measurement Instrumentation and Techniques

| Measurements | Instrument / Technique |
|---|---|
| Temperature | Infrared (IR) Imaging, Plate Thermometer (PT), sheathed thermocouple |
| Heat flux (time-varying) | Plate Thermometer (PT) |
| Heat flux (average) | Plate Thermometer (PT), Thermal Capacitance Slug ($T_{cap}$ slug) |
| Incident Energy | ASTM F1959 Slug calorimeter (ASTM slug), Thermal Capacitance Slug ($T_{cap}$ slug) |
| Pressure | Piezoelectric pressure transducer |
| Arc plasma / fire dimensions | Videography, IR Imaging |
| Surface deposit analysis | Sample collection (carbon tape / aerogels) |
| Qualitative damage | Cable samples (cable coupons) |

### 2.4.1. Instrument Placement – Switchgear Experiments

The majority of the thermal instrumentation devices were located on instrument racks with the face of the instrument located approximately 91 cm (36 in) from the exterior of the metal-clad enclosure. One additional instrument rack (Rack 3) was located approximately 183 cm (72 in) from the expected arc breach side of the electrical enclosure. Rack 3 had its sensors shifted up approximately 102 mm (4 in) to reduce shadowing effects from the Rack 2 located between Rack 3 and the enclosure. An instrumentation rack was also located above the enclosure. This instrumentation rack (Rack 5) was secured to the electrical enclosure with 90-degree angle red GPO-3 board (glass reinforced thermoset polyester) and nominal ¼ in-20 fasteners. The sensors on Rack 5 are located approximately 91 cm (36 in) from the top of the enclosure's metal cladding. This instrumentation rack configuration is shown in Fig. 9 and Fig. 10. Details of the instrument locations are presented in Appendix A, with a photograph showing the instrumentation racks around the experimental device during setup in Fig. 11. The expanded uncertainty in the measurement of the distances from the instrumentation racks to the electrical enclosure is ± 13 mm (0.5 in) with a coverage factor of 2 and an estimated confidence interval of 95 percent.

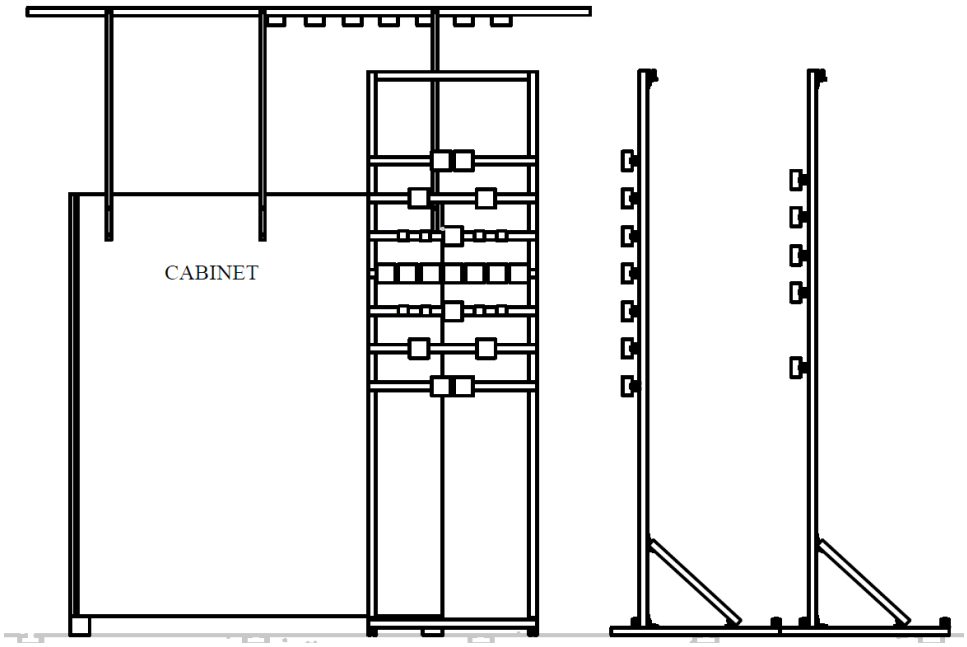


Fig. 9. Elevation view of instrument rack configuration around electrical enclosure

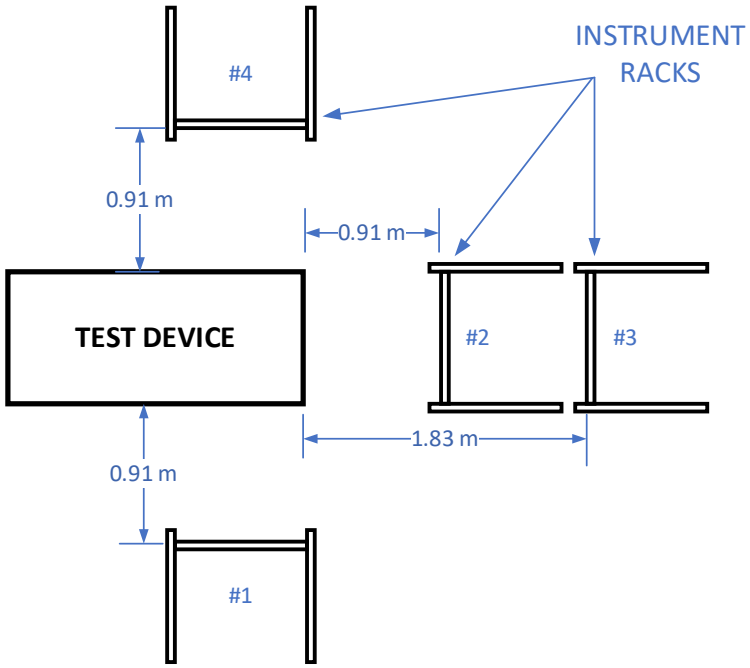


Fig. 10. Plan view of instrument rack configuration around electrical enclosure. The enclosure is approximately 0.927 m (36.5 in) wide, 2.019 m (79.5 in) deep, and 2.286 m (90.0 in) tall

Fig. 11. Photo of instrumentation racks during experimental setup

### 2.4.2. Instrument Placement - Bus Duct Experiments

Following the same scheme as the switchgear experiments, the majority of the thermal instrumentation devices were located on instrument racks with the face of the instrument located approximately 91 cm (36 in) from the exterior of the bus duct enclosure. One additional instrument rack (Rack 5) was located approximately 183 cm (72 in) from the expected arc breach side of the bus duct enclosure (below the duct). An instrumentation rack (Rack 3) was also located above the bus duct enclosure. The sensors on Rack 3 are located approximately 91 cm (36 in) from the top of the enclosure metal cladding. This instrumentation rack configuration is shown in Fig. 12 and Fig. 13. Fig. 14 is a photograph showing the instrumentation racks around the experiment device and the sheathed thermocouple in the side of the switchgear. The sheathed thermocouple penetrates the side panel of the switchgear 20 cm (8.0 in) form the top, and 46 cm (18.0 in) from the rear. The tip of the sheathed thermocouple is located 21.6 cm (8.5 in) inside the switchgear so that it intersects the centerline of the bus duct above. The expanded uncertainty in the measurement of the distances from the instrumentation racks to the bus duct enclosure is ± 13 mm (0.5 in) with a coverage factor of 2 and an estimated confidence interval of 95 percent. The expanded uncertainty in the measurement of the location of the sheathed thermocouples is ± 6 mm (0.25 in) with a coverage factor of 2 and an estimated confidence interval of 95 percent.

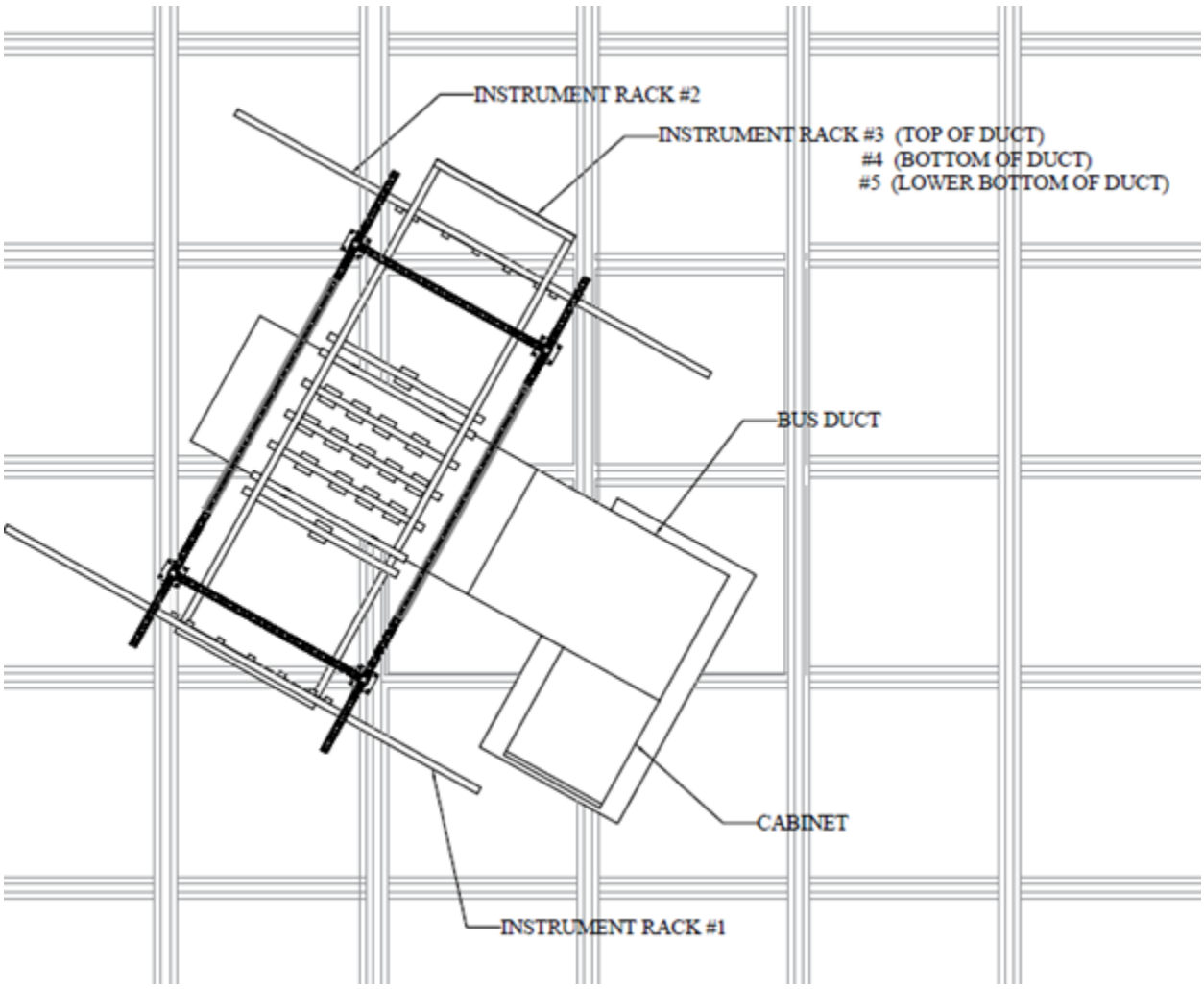


Fig. 12. Plan view of bus duct configuration in test cell #9

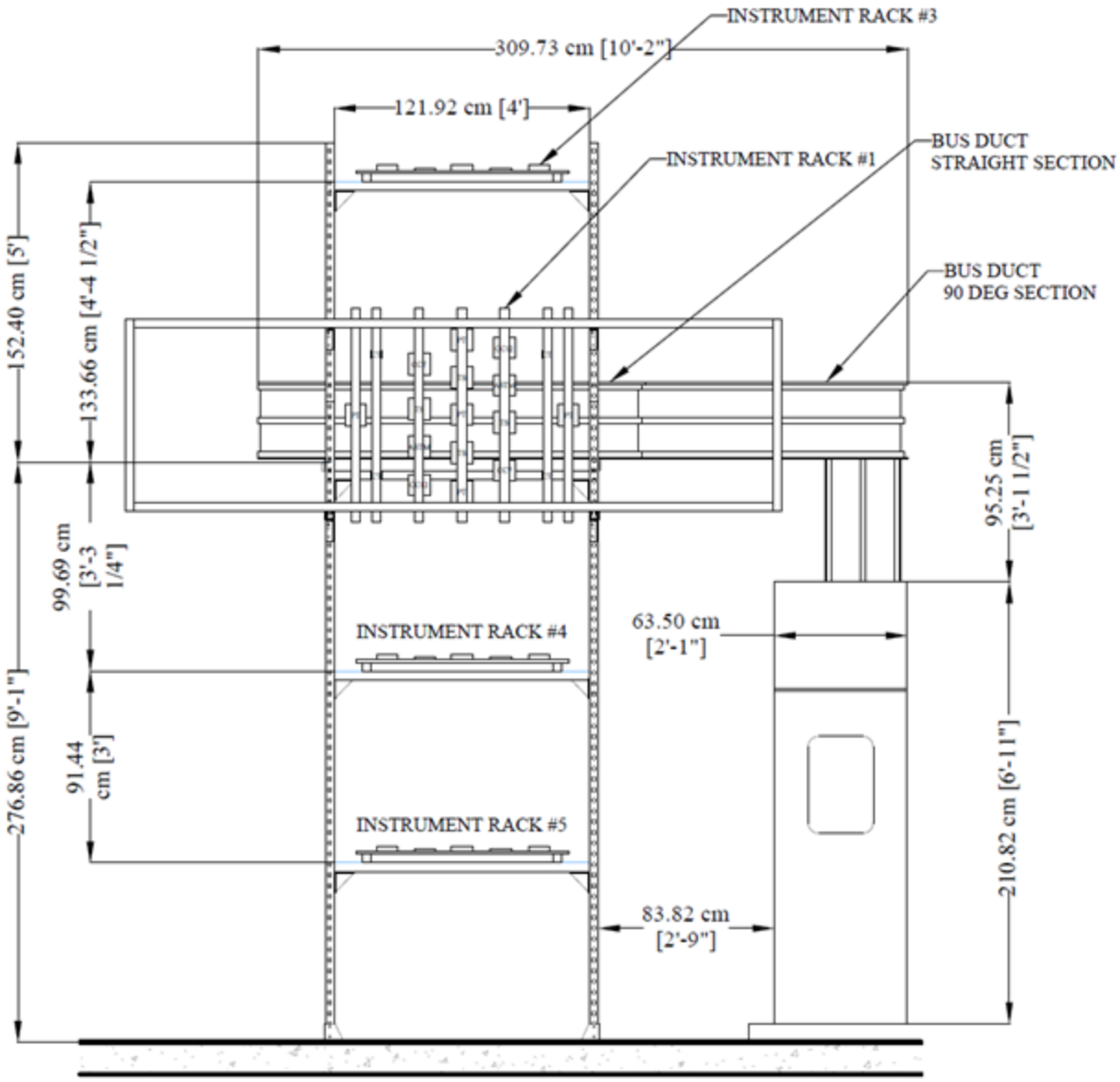


Fig. 13. Elevation view of instrument configuration

Fig. 14. Photo of bus duct instrumentation configuration prior to experiment

## 3. Experimental Results

The KEMA Labs performed calibration runs to ensure that the power circuits selected met the desired experimental parameters. The calibrations are measured at a shorting bus within the laboratory's facility, and the actual experimental conditions will be slightly different because of the additional circuit length of the experimental device and its connections. The calibration experiments are presented in Table 5 with detail provided in the KEMA report (Appendix E).

Table 5. Circuit calibration parameters (measurements are ± 3 percent)

| Voltage (kV) | Current Symmetrical (kA) | Current Peak (kA) | Circuit |
|---|---|---|---|
| **32.6** | 32.6 | 66.7 to 86.3 | S01 |
| **4.16** | 29.9 | 60.7 to 81.1 | S02 |

The calibration experiments were performed for about 10 cycles to ensure stabilization of the waveform. The duration of the arc during an actual experiment was controlled by the ability to maintain the arc within the enclosure and the breaking of the circuit by KEMA's protective device(s). Provided that the arc did not prematurely extinguish, KEMA ensured that the arc duration parameter was met by automatically triggering their protectives devices to open at the specified duration. Because of KEMA's desire to ensure the desired duration is met, there is a delay in the opening of the circuit (breaker opening time), and as such, the actual durations were longer than the desired durations. Table 6 presents the experimental parameter variations performed for these series of experiments.

Table 6. Summary of Experiments (measurements are ± 3 percent)

| Experiment No. # | Voltage (kV) | | | Current (kA) | | Duration (s) | | Material | | Notes |
|---|---|---|---|---|---|---|---|---|---|---|
| | System | Actual | Arc | Planned | Actual | Planned | Actual | Conductor | Enclosure | |
| **2-10** | 6.90 | 6.91 | 0.728 | 32 | 31.6 | 2 | 2.04 | Copper | Steel | Switchgear |
| **2-12** | 6.90 | 6.90 | 1.109 | 32 | 31.2 | 4 | 2.87 | Copper | Steel | Switchgear |
| **2-25** | 4.16 | 4.17 | 0.654 | 30 | 29.1 | 2 | 2.02 | Copper | Steel | Bus duct |
| **2-26** | 4.16 | 4.17 | 0.620 | 30 | 28.7 | 4 | 4.02 | Copper | Steel | Bus duct |
| **2-27** | 4.16 | 4.17 | 0.794 | 30 | 29.1 | 2 | 2.04 | Copper | Aluminum | Bus duct |
| **2-28** | 4.16 | 4.17 | 0.839 | 30 | 28.4 | 4 | 4.03 | Copper | Aluminum | Bus duct |
| **2-30** | 4.16 | 4.17 | 0.942 | 30 | 28.4 | 4 | 4.05 | Aluminum | Steel | Bus duct, laboratory power supply failure resulted in arcing outside and away from experiment device. |
| **2-30B** | 4.16 | 4.17 | 0.711 | 30 | 28.8 | 4 | 4.03 | Aluminum | Steel | Bus duct, re-run of Experiment 2-30. Replaces Experiment 2-29. |
| **2-31** | 4.16 | 4.17 | 0.684 | 30 | 29.7 | 2 | 2.03 | Aluminum | Aluminum | Bus duct |
| **2-32** | 4.16 | 4.17 | 0.794 | 30 | 28.7 | 4 | 4.04 | Aluminum | Aluminum | Bus duct |

## 3.1. Experiment 2-10 – 6.9kV, 32kA, 2 s Duration, Load Configuration

Experiment 2-10 was performed on August 22, 2022, at 2:52 PM eastern daylight time (EDT). The temperature was approximately 27 °C (81 °F), approximately 91 percent relative humidity and approximately 101.1 kPa of pressure. The weather was mostly cloudy with a wind of approximately 4.8 km/h (3 mi/h) out of the southeast.

The arc was located near the ends of bus bar in the cable connection compartment of the switchgear. Power flow resulted in a load experiment configuration. The arcing wire installed on the bus and marked up illustrations of the arc wire location is presented in Fig. 15.

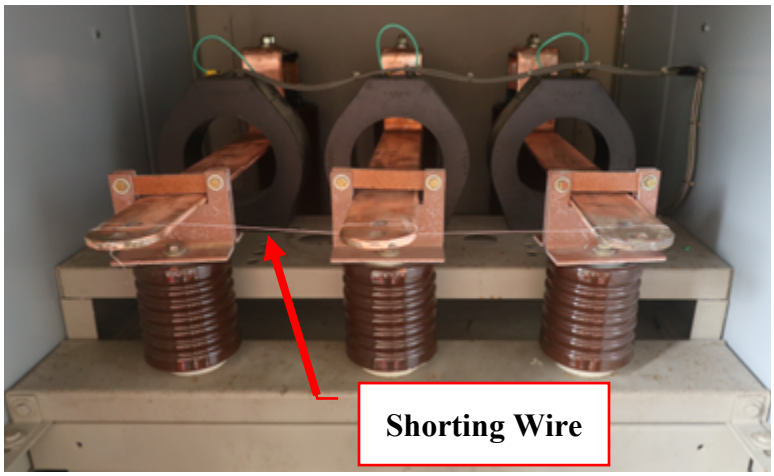


Fig. 15. Shorting wire location Experiment 2-10.

### 3.1.1. Observations

Observations documented below are based on review of video and thermal imaging that was taken during the experiment. The observations are provided in Table 7 and include an approximate time reference. Corresponding images are provided in Fig. 16, with thermography images presented in Fig. 17.

The arc lasted for the expected duration of 2.05 s. Pressure was higher than observed in aluminum experiments (Experiment 2-21 [16]). Excessive panel buckling was observed on the rear panel. No enclosure breach was observed on any sides. No cable damage was observed. The switchgear door was opened due HEAF generated pressure. Lack of physical protection on KEMA's incoming power supply, combined with the switchgear door swinging open past 90-degrees due to arc-induced overpressure, resulted in the door contacting the Phase A connection for approximately 143 ms, resulting in a shorting path outside of the intended locations. Arc energy was 75.0 MJ.

Table 7. Observations from Experiment 2-10

| Time (ms) | Observation |
|---|---|
| **0** | Initial light observed in bottom rear louver |
| **83** | Door opens |
| **445** | Door hits Phase A power supply and arcs for 143 ms |
| **600** | End of door arcing |
| **2 017** | End of arc |
| **4 504** | First visual of cabinet after smoke rises above cabinet |
| **20 000** | Image at 20 s following arc initiation |


Fig. 16. Sequence of Images from Experiment 2-10 (image time stamps are in seconds).

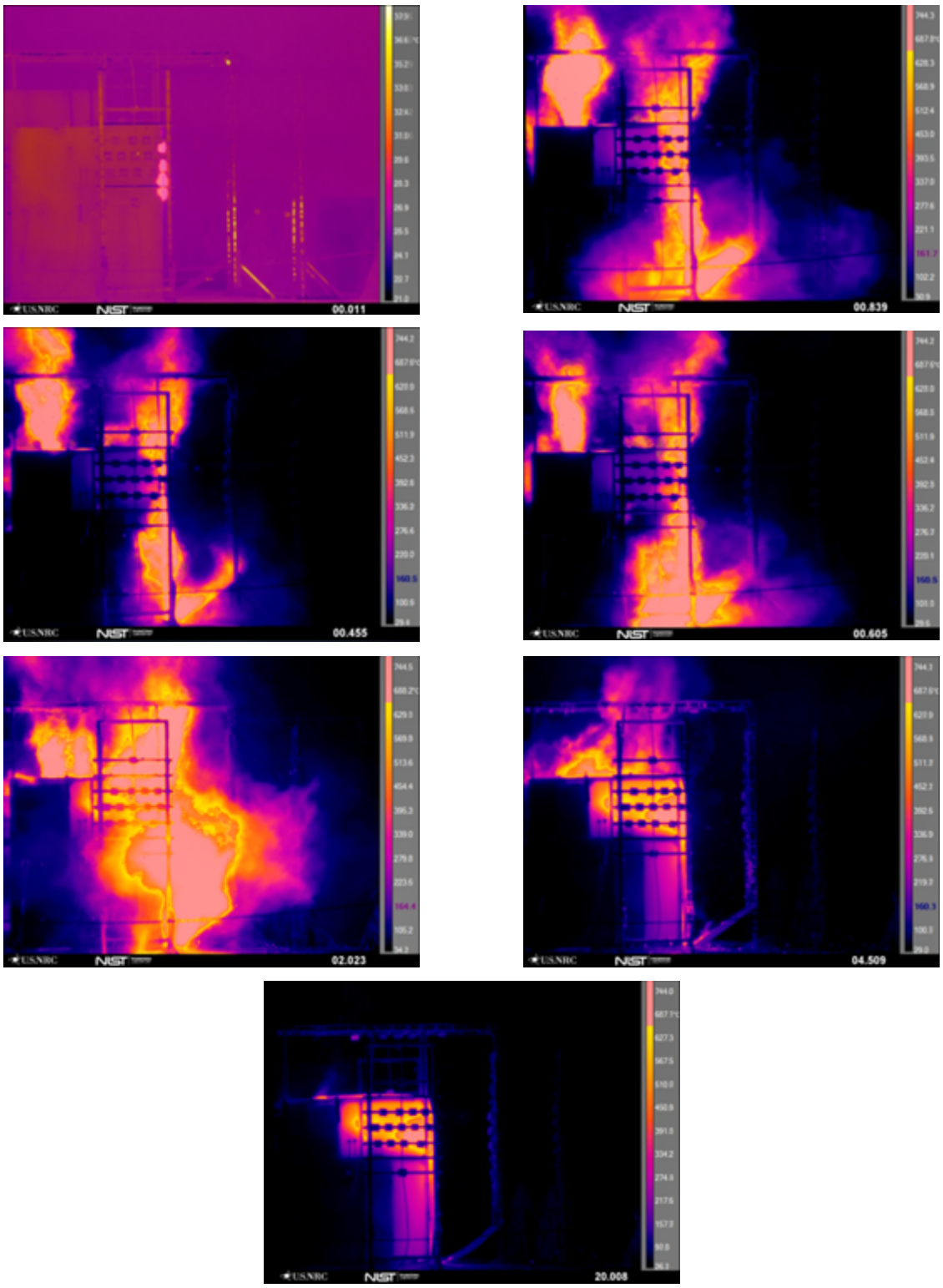


Fig. 17. Sequence of Thermal Images from Experiment 2-10 (image time stamp in seconds)

Photographs of the enclosure following the experiment are presented in Fig. 18. The enclosure did not experience a breach due to thermal burn through.


Fig. 18. Enclosure Post-Experiment 2-10.

An image of the bus bars removed from the enclosure after the experiment are shown in Fig. 19. The total mass loss of the bus bars was 2 035g ± 1g. Additional details are presented in Appendix C.

Fig. 19. Photo of Experiment 2-10 bus bars post-experiment (arc location shown right).

### 3.1.2. Measurements

Measurements made during Experiment 2-10 are presented below. These measurements include:

- Thermal
  - Heat flux – Plate Thermometers, Tcap Slug Calorimeters
  - Incident Energy – ASTM Slug Calorimeters, Tcap Slug Calorimeters, Plate Thermometers
- Pressure
  - Internal pressure
- Mass Loss
  - Pre- / Post-experimental measurements
- Electrical
  - Voltage profiles
  - Current profiles
  - Power and energy profiles

#### 3.1.2.1. Thermal Measurements

Thermal measurements from the active instruments are reported below for Experiment 2-10. These include PT measurements in Table 8, ASTM Slug Calorimeter measurements in Table 9, and $T_{cap}$ slug measurements in Table 10. The maximum reading is identified with bold text. Some of the instruments were inoperable prior to the experiment as noted. This is likely due to the failure of the thermocouple junction that occurred during transportation. These sensors were initially installed for a series of HEAF experiments in 2019, but a change in project direction resulted in the sensors not being used. This resulted in the sensors being un-installed, transported for storage, then transported back to KEMA in 2022 and re-installed. The extra handling and transportation likely caused the failure of some instruments.

Table 8. Summary of plate thermometer measurements Experiment 2-10

| Rack No. | Plate No. | Location | Max Heat Flux ($kW/m^2$) Greater of ± 1 $kW/m^2$ or ± 5 % | Average Heat Flux During Arc ($kW/m^2$) Greater of ±1 $kW/m^2$ or ± 5 % | Total Incident Energy ($kJ/m^2$) ± 15 % | Notes |
|---|---|---|---|---|---|---|
| **1** | 1 | Top | 270 | 162 | 360 | |
| **1** | 3 | Mid-Right | **499** | **173** | 400 | |
| **1** | 5 | Mid-Center | - - - | - - - | - - - | Inoperable prior to experiment (IPE) |
| **1** | 7 | Mid-Left | 77 | 63 | 270 | |
| **1** | 9 | Bottom | 307 | 161 | 330 | |
| **2** | 10 | Top | 109 | 92 | 350 | |
| **2** | 12 | Mid-Right | - - - | - - - | - - - | IPE |
| **2** | 14 | Mid-Center | 93 | 77 | **540** | |
| **2** | 16 | Mid-Left | 97 | 84 | 490 | |
| **2** | 18 | Bottom | 139 | 108 | 440 | |
| **3** | 19 | Top | 45 | 37 | 120 | |
| **3** | 21 | Mid-Right | - - - | - - - | - - - | IPE |
| **3** | 23 | Mid-Center | 52 | 37 | 130 | |
| **3** | 25 | Mid-Left | 48 | 39 | 130 | |
| **3** | 27 | Bottom | 53 | 40 | 140 | |
| **4** | 28 | Top | - - - | - - - | - - - | IPE |
| **4** | 30 | Mid-Right | 84 | 51 | 250 | |
| **4** | 32 | Mid-Center | 118 | 75 | 300 | |
| **4** | 34 | Mid-Left | - - - | - - - | - - - | IPE |
| **4** | 36 | Bottom | 221 | 111 | 270 | |
| **5** | 37 | Front | 230. | 164 | 390 | |
| **5** | 39 | Center-Right | 154 | 125 | 370 | |
| **5** | 41 | Center-Mid | 179 | 123 | 410 | |
| **5** | 43 | Center-Left | 258 | 99 | 340 | |
| **5** | 45 | Back | - - - | - - - | - - - | IPE |

Table 9. Summary of ASTM slug calorimeter measurements, Experiment 2-10

| Rack No. | ASTM No. | Location | Incident Energy ($kJ/m^2$) Greater of ± 18 $kJ/m^2$ or ± 4 % | Time to Max Temperature (s) ± 3 % | Comment |
|---|---|---|---|---|---|
| **1** | A | Top | 374 | 61.3 | |
| **1** | B | Bottom | 339 | 91.7 | |
| **2** | C | Top | 553 | 65.0 | |
| **2** | D | Bottom | **610** | 66.9 | |
| **3** | E | Top | - - - | - - - | IPE |
| **3** | F | Bottom | 166 | 61.7 | |
| **4** | G | Top | 306 | 93.5 | |
| **4** | H | Bottom | 350 | 78.8 | |
| **5** | I | Front | 435 | 4.9 | |
| **5** | J | Back | 360 | 94.4 | |

Table 10. Summary of $T_{cap}$ slug measurements, Experiment 2-10

| Rack No. | $T_{cap}$ No. | Location | Heat Flux During Arc (kW/m$^2$) Greater of ± 1.5 kW/m$^2$ or ± 2.9 % | Incident Energy During Arc Phase (kJ/m$^2$) Greater of ± 2.4 kJ/m$^2$ or ± 5 % | Total Incident Energy (kJ/m$^2$) Greater of ± 2.4 kJ/m$^2$ or ± 5 % |
|---|---|---|---|---|---|
| **1** | 2 | Top | 114.0 | 189.7 | 929.7 |
| **1** | 4 | Mid-Right | **121.9** | **208.0** | 926.6 |
| **1** | 6 | Mid-Left | 71.5 | 112.0 | 883.1 |
| **1** | 8 | Bottom | 97.0 | 152.2 | 927.2 |
| **2** | 11 | Top | 71.3 | 123.0 | 1 285.7 |
| **2** | 13 | Mid-Right | 68.9 | 111.5 | 1 355.9 |
| **2** | 15 | Mid-Left | - - - | - - - | - - - |
| **2** | 17 | Bottom | 83.6 | 142.4 | **1 429.6** |
| **3** | 20 | Top | - - - | - - - | - - - |
| **3** | 22 | Mid-Right | 32.5 | 55.5 | 329.5 |
| **3** | 24 | Mid-Left | 33.1 | 59.6 | 342.1 |
| **3** | 26 | Bottom | 28.8 | 45.6 | 367.6 |
| **4** | 29 | Front | 62.2 | 103.2 | 822.5 |
| **4** | 31 | Center-Right | 59.2 | 100.2 | 836.3 |
| **4** | 33 | Center-Left | 90.4 | 144.4 | 870.3 |
| **4** | 35 | Back | - - - | - - - | - - - |
| **5** | 38 | Front | 108.0 | 185.6 | 1 071.1 |
| **5** | 40 | Center-Right | 116.3 | 191.6 | 1 088.6 |
| **5** | 42 | Center-Left | 99.6 | 152.4 | 1 017.3 |
| **5** | 44 | Back | 102.4 | 161.9 | 1 202.4 |

### 3.1.2.2. Pressure Measurements

The pressure profiles for the first two tenths of a second are shown in Fig. 20. P Pressure is measured at two locations (primary cable connection compartment and the breaker compartment). At each measurement location there are two pressure transducers. The 0 kPa to 207 kPa (0 psia to 30 psia) and 0 kPa to 345 kPa (0 psia to 50 psia) transducer recordings at a specific location were consistent. After the initial pressure spike, the pressure rapidly decays to a relative steady state. The peak pressure is higher in the primary cable connection compartment as would be expected since this is the compartment where the arc is initiated. The maximum change in pressure in the primary cable connection compartment is approximately 49.1 kPa (7.1 psi)

above ambient at its peak. The maximum change in pressure in the breaker compartment is approximately 17.0 kPa (2.5 psi) above ambient.

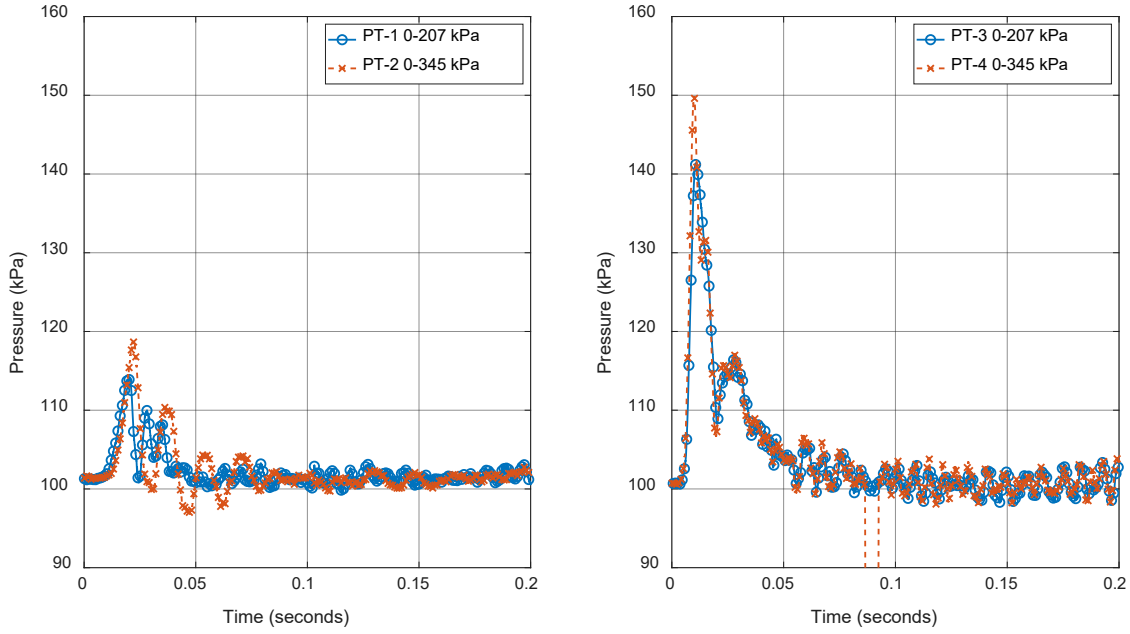


Fig. 20. Pressure measurements from Experiment 2-10 (breaker compartment (left); Main bus [arcing compartment] – (right)). Measurement uncertainty ± 3 percent.

### 3.1.2.3. Electrical Measurements

Experiment 2-10 used KEMA circuit S01 and is reported in Appendix E. Full-level circuit checks (calibration experiments) were performed prior to the experiment to verify the experimental parameters were acceptable. For this experiment the calibration experiments configured the power system to 6.88 kV, 32.58 kA symmetrical, and 86.3 kA peak. The KEMA report (Appendix E) identifies this experiment as 220822-9003. Key experimental measurements are presented in Table 11. Plots of the electrical measurements are presented in Appendix B.

Table 11. Key measurement from Experiment 2-10. Measurement uncertainty ± 3 percent.

| Phase | Units | A | B | C |
|---|---|---|---|---|
| **Applied voltage, phase-to-ground** | $kV_{RMS}$ | 3.99 | 3.99 | 3.99 |
| **Applied voltage, phase-to-phase** | $kV_{RMS}$ | 6.91 | | |
| **Making current** | $kA_{peak}$ | 55.1 | 62.2 | -70.6 |
| **Current, AC component, beginning** | $kA_{RMS}$ | 33.1 | 33.9 | 33.9 |
| **Current, AC component, middle** | $kA_{RMS}$ | 31.4 | 32.1 | 30.5 |
| **Current, AC component, end** | $kA_{RMS}$ | 29.7 | 31.0 | 30.4 |
| **Current, AC component, average** | $kA_{RMS}$ | 31.6 | 32.1 | 31.1 |
| **Current, AC component, three-phase average** | $kA_{RMS}$ | 31.6 | | |
| **Duration** | s | 2.05 | 2.05 | 2.04 |
| **Arc Energy** | MJ | 75.01 | | |

## 3.2. Experiment 2-12 – 6.9kV, 32kA, 4 s Duration, Load Configuration

Experiment 2-12 was performed on August 23, 2022, at 10:32 AM eastern daylight time (EDT). The temperature was approximately 25 °C (71 °F), approximately 82 percent relative humidity and approximately 100.3 kPa of pressure. The weather was partly cloudy with a wind of approximately 11.3 km/h (7 mi/h) out of the west northwest.

The arc was located near the top of the main bus bar in the load section of the switchgear. The arcing wire installed on the bus and marked up illustrations of the arc wire location is presented in Fig. 21.

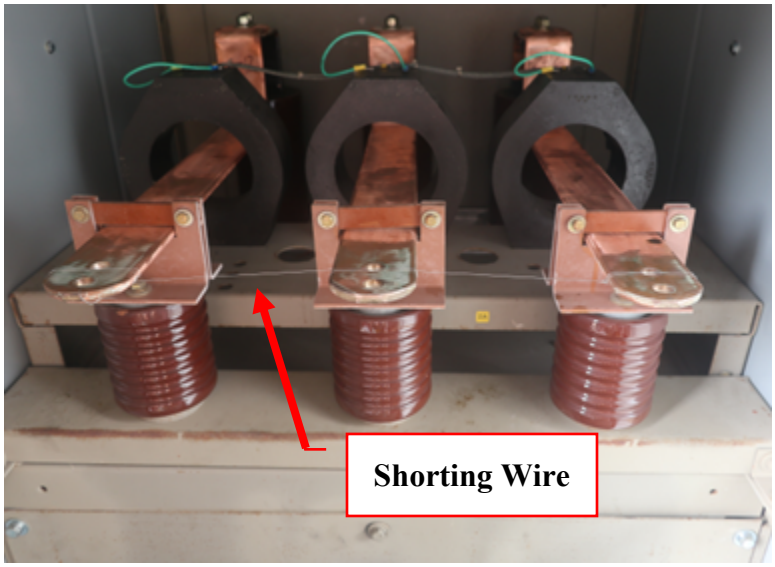


Fig. 21. Shorting wire location Experiment 2-12

### 3.2.1. Observations

Observations documented below are based on review of video and thermal imaging that was taken during the experiment. The observations are provided in Table 12, and include an approximate time reference. Corresponding images are provided in Fig. 23, with thermography images presented in Fig. 24.

The arc did not last for expected duration and self-extinguished at 2.88 s. It appeared that the arc migrated towards the front of the cabinet and severed the bus bar at the connections to the breaker bottles as shown in Fig. 22. Excessive panel buckling was observed on the rear panel. The enclosure breached on the top near the vent above the main bus. No enclosure breach was observed on any sides or the back panel. No visible cable damage was observed. The switchgear door was opened due to HEAF generated enclosure pressure. The arc energy was 129 MJ.

Fig. 22. Photo of severed bus bars at insulating bushing (breaker stab bottles).

Table 12. Observations from Experiment 2-12

| Time (ms) | Observation |
|---|---|
| **0** | Initial light observed in top rear louver |
| **66** | Door opens |
| **250** | Luminescent flash zone reaches top rack 5 and half-way between rack 2 and 3 |
| **433** | Particle ejecta observed near rack 1 and 5 |
| **1 267** | Smoke beginning to obscure visual |
| **2 886** | End of arc |
| **4 003** | Smoke begins to clear |
| **5 005** | Flames emit from vent on top of enclosure |


Fig. 23. Sequence of Images from Experiment 2-12 (image time stamps are in seconds).

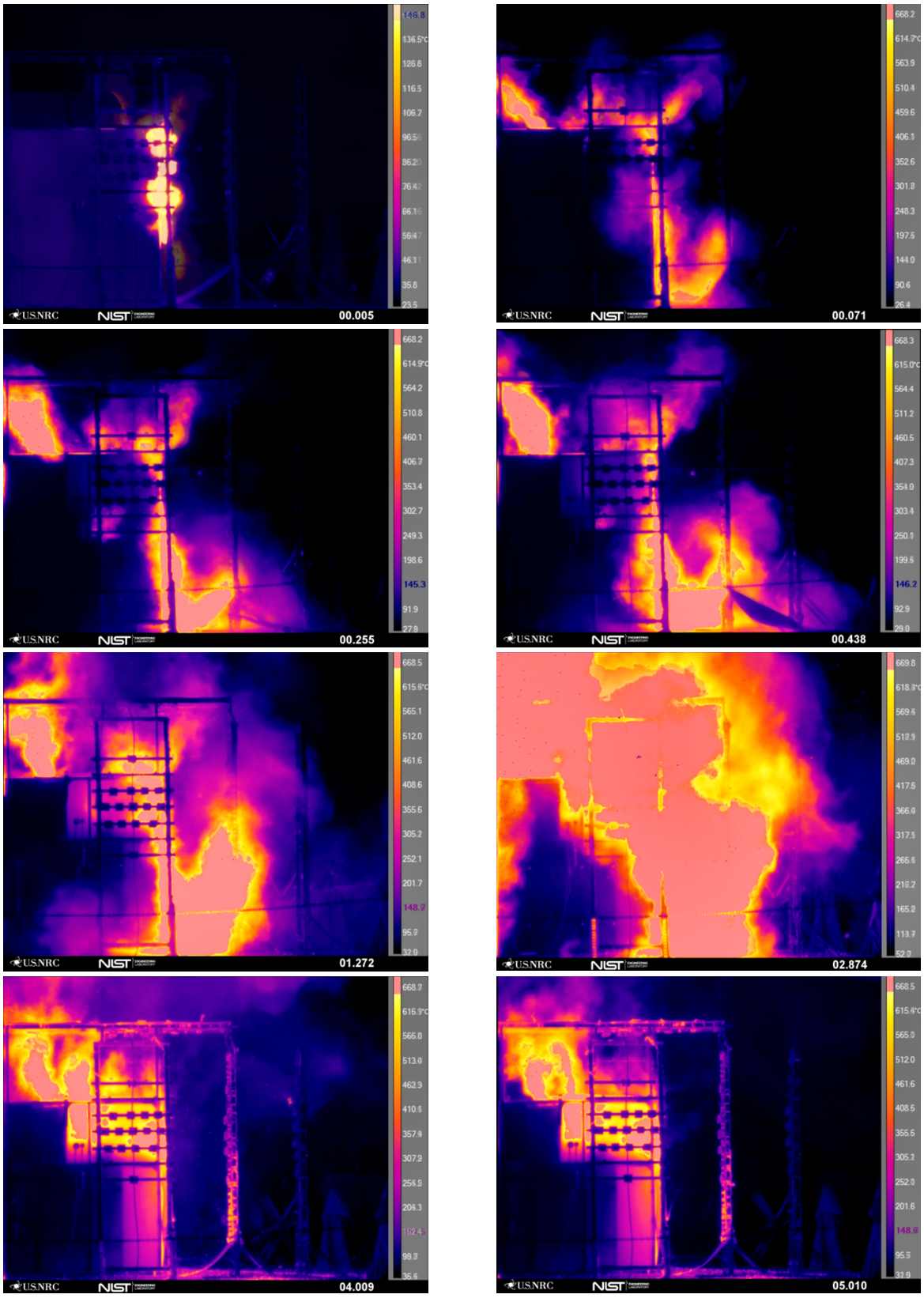


Fig. 24. Sequence of Thermal Images from Experiment 2-12 (image time stamp in seconds)

A photograph of the enclosure following the experiment is presented in Fig. 25. The enclosure experienced a breach on the top panel with two openings near the vent. A majority of the vent grating area was missing from the exposure as shown in Fig. 26.

Fig. 25. Enclosure Post-Experiment 2-12.

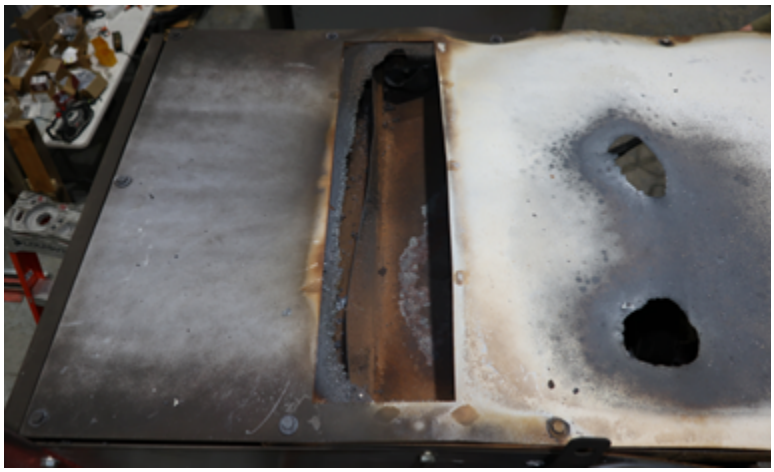

Fig. 26. Enclosure Breach (top panel)

An image of the bus bars removed from the enclosure after the experiment are shown in Fig. 27. The total mass loss of the bus bars was 3 349 g ± 1g. Additional details are presented in Appendix C.

Fig. 27. Photo of Experiment 2-12 bus bars post-experiment (arc location shown right).

### 3.2.2. Measurements

Measurements made during Experiment 2-12 are presented below. These measurements include:

- Thermal
  - Heat flux – Plate Thermometers, Tcap Slug Calorimeters
  - Incident Energy –ASTM Slug Calorimeters, Tcap Slug Calorimeters, Plate Thermometers
- Pressure
  - Internal pressure
- Mass Loss
  - Pre- / Post-experimental measurements
- Electrical
  - Voltage profiles
  - Current profiles
  - Power and energy profiles

### 3.2.2.1. Thermal Measurements

Thermal measurements from the active instruments are reported below for Experiment 2-12. These include PT measurements in Table 13, ASTM Slug Calorimeter measurements in Table 14, and $T_{cap}$ slug measurements in Table 15. The maximum reading is identified with bold text.

Table 13. Summary of plate thermometer measurements Experiment 2-12

| Rack No. | Plate No. | Location | Max Heat Flux (kW/m$^2$) Greater of ± 1 kW/m$^2$ or ± 5 % | Average Heat Flux During Arc (kW/m$^2$) Greater of ±1 kW/m$^2$ or ± 5 % | Total Incident Energy (kJ/m$^2$) ± 15 % | Notes |
|---|---|---|---|---|---|---|
| **1** | 1 | Top | 843 | 229 | 670 | |
| **1** | 3 | Mid-Right | 395 | 147 | 510 | |
| **1** | 5 | Mid-Center | 453 | 133 | 520 | |
| **1** | 7 | Mid-Left | 295 | 98 | 490 | |
| **1** | 9 | Bottom | 173 | 102 | 350 | |
| **2** | 10 | Top | 234 | 133 | 550 | |
| **2** | 12 | Mid-Right | - - - | - - - | - - - | Inoperable prior to experiment (IPE) |
| **2** | 14 | Mid-Center | 222 | 129 | 790 | |
| **2** | 16 | Mid-Left | 214 | 142 | 720 | |
| **2** | 18 | Bottom | 372 | 223 | 820 | |
| **3** | 19 | Top | 100 | 51 | 200 | |
| **3** | 21 | Mid-Right | - - - | - - - | - - - | IPE |
| **3** | 23 | Mid-Center | 121 | 64 | 230 | |
| **3** | 25 | Mid-Left | 122 | 59 | 220 | |
| **3** | 27 | Bottom | 144 | 80 | 270 | |
| **4** | 28 | Top | 270. | 129 | 450 | |
| **4** | 30 | Mid-Right | 149 | 77 | 460 | |
| **4** | 32 | Mid-Center | 274 | 110 | 510 | |
| **4** | 34 | Mid-Left | 221 | 132 | 500 | |
| **4** | 36 | Bottom | 197 | 98 | 350 | |
| **5** | 37 | Front | 491 | 232 | 680 | |
| **5** | 39 | Center-Right | **1 481** | **234** | 800 | |

| Rack No. | Plate No. | Location | Max Heat Flux (kW/m$^2$) Greater of ± 1 kW/m$^2$ or ± 5 % | Average Heat Flux During Arc (kW/m$^2$) Greater of ±1 kW/m$^2$ or ± 5 % | Total Incident Energy (kJ/m$^2$) ± 15 % | Notes |
|---|---|---|---|---|---|---|
| **5** | 41 | Center-Mid | 1 100 | 206 | 850 | |
| **5** | 43 | Center-Left | 565 | 156 | 640 | |
| **5** | 45 | Back | 1 137 | 226 | **960** | |

Table 14. Summary of ASTM slug calorimeter measurements, Experiment 2-12

| Rack No. | ASTM No. | Location | Incident Energy (kJ/m$^2$) Greater of ± 18 kJ/m$^2$ or ± 4 % | Time to Max Temperature (s) ± 3 % | Comment |
|---|---|---|---|---|---|
| **1** | A | Top | 603 | 45.70 | |
| **1** | B | Bottom | 500 | 75.91 | |
| **2** | C | Top | 824 | 54.18 | |
| **2** | D | Bottom | **930** | 52.32 | |
| **3** | E | Top | 294 | 42.79 | |
| **3** | F | Bottom | 234 | 39.35 | |
| **4** | G | Top | 568 | 81.86 | |
| **4** | H | Bottom | 564 | 57.87 | |
| **5** | I | Front | 699 | 53.38 | |
| **5** | J | Back | 811 | 62.08 | |

Table 15. Summary of $T_{cap}$ slug measurements, Experiment 2-12

| Rack No. | Tcap No. | Location | Heat Flux During Arc (kW/m²) Greater of ± 1.5 kW/m² or ± 2.9 % | Incident Energy During Arc Phase (kJ/m²) Greater of ± 2.4 kJ/m² or ± 5 % | Total Incident Energy (kJ/m²) Greater of ± 2.4 kJ/m² or ± 5 % |
|---|---|---|---|---|---|
| **1** | 2 | Top | 199.2 | 357.4 | 1 472.9 |
| **1** | 4 | Mid-Right | 202.8 | 386.9 | 1 380.7 |
| **1** | 6 | Mid-Left | 157.7 | 294.4 | 1 429.0 |
| **1** | 8 | Bottom | 141.7 | 259.2 | 1 317.1 |
| **2** | 11 | Top | 146.2 | 310.4 | 1 825.2 |
| **2** | 13 | Mid-Right | 146.5 | 291.2 | 1 921.3 |
| **2** | 15 | Mid-Left | 150.0 | 354.5 | 1 978.6 |
| **2** | 17 | Bottom | 190.2 | 423.3 | 2 057.5 |
| **3** | 20 | Top | 53.0 | 104.7 | 489.8 |
| **3** | 22 | Mid-Right | 67.7 | 141.8 | 513.0 |
| **3** | 24 | Mid-Left | 67.3 | 140.4 | 520.9 |
| **3** | 26 | Bottom | 63.5 | 132.7 | 580.7 |
| **4** | 29 | Front | 98.5 | 163.9 | 1 405.2 |
| **4** | 31 | Center-Right | 88.8 | 168.8 | 1 457.9 |
| **4** | 33 | Center-Left | 138.1 | 303.8 | 1 424.6 |
| **4** | 35 | Back | 135.8 | 339.2 | 1 473.5 |
| **5** | 38 | Front | 240.8 | 391.6 | 1 722.4 |
| **5** | 40 | Center-Right | 255.8 | 403.0 | 1 989.1 |
| **5** | 42 | Center-Left | 259.4 | 458.6 | 1 883.9 |
| **5** | 44 | Back | **333.1** | **498.2** | **2 256.7** |

### 3.2.2.2. Pressure Measurements

The pressure profiles for the first two tenths of a second are shown in Fig. 28. Pressure is measured at two locations (primary cable connection compartment and the breaker compartment). At each measurement location there are two pressure transducers. The 0 kPa to 207 kPa (0 psia to 30 psia) and 0 kPa to 345 kPa (0 psia to 50 psia) transducer recordings at a specific location were consistent. After the initial pressure spike, the pressure rapidly decays to a relative steady state. The peak pressure is higher in the primary cable connection compartment as would be expected since this is the compartment where the arc is initiated. The maximum change in pressure in the primary cable connection compartment is approximately 51.9 kPa (7.5 psi) above ambient at its peak. The maximum change in pressure in the breaker compartment is approximately 18.5 kPa (2.7 psi) above ambient.

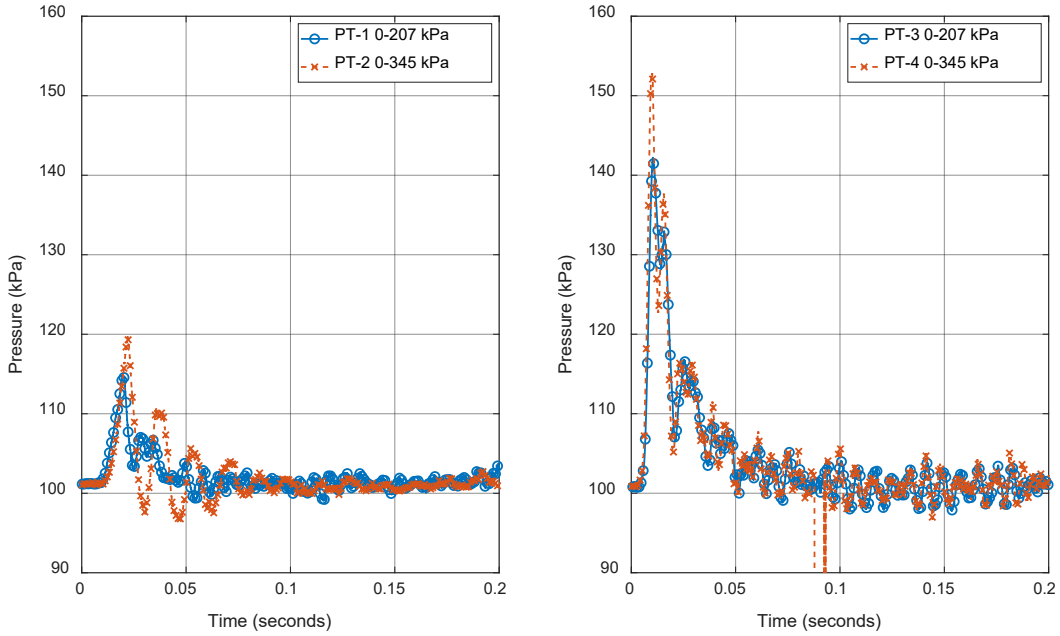


Fig. 28. Pressure measurements from Experiment 2-12 (breaker compartment (left); Main bus [arcing compartment] – (right)). Measurement uncertainty ± 3 percent.

### 3.2.2.3. Electrical Measurements

Experiment 2-12 used KEMA circuit S01 and is reported in Appendix E. Full-level circuit checks (calibration experiments) were performed prior to the experiment to verify the experimental parameters were acceptable. For this experiment the calibration experiments configured the power system to 6.900 kV and 32.6 kA symmetrical. The KEMA report (Appendix E) identifies this experiment as 220823-9001. Key experimental measurements are presented in Table 16. Plots of the electrical measurements are presented in Appendix B.

Table 16. Key measurement from Experiment 2-12. Measurement uncertainty ± 3 percent.

| Phase | Units | A | B | C |
|---|---|---|---|---|
| **Applied voltage, phase-to-ground** | $kV_{RMS}$ | 3.98 | 3.99 | 3.98 |
| **Applied voltage, phase-to-phase** | $kV_{RMS}$ | | 6.90 | |
| **Making current** | $kA_{peak}$ | 55.2 | 65.0 | -71.2 |
| **Current, AC component, beginning** | $kA_{RMS}$ | 33.1 | 34.6 | 33.7 |
| **Current, AC component, middle** | $kA_{RMS}$ | 29.4 | 31.4 | 29.8 |
| **Current, AC component, end** | $kA_{RMS}$ | 0 | 0 | 0 |
| **Current, AC component, average** | $kA_{RMS}$ | 30.8 | 32.2 | 30.7 |
| **Current, AC component, three-phase average** | $kA_{RMS}$ | | 31.23 | |
| **Duration** | s | 2.87 | 2.87 | 2.87 |
| **Arc Energy** | MJ | | 129.1 | |

## 3.3. Experiment 2-25 – 4.16 kV, 30 kA, 2 s Duration, Copper Bus, Steel Enclosure

Experiment 2-25 was performed on August 24, 2022, at 11:50 AM eastern daylight time (EDT). The temperature was approximately 28 °C (83 °F), approximately 61 percent relative humidity and approximately 100.8 kPa of pressure. The weather was fair with a wind of approximately 3.2 km/h (2 mi/h) out of the west-northwest.

The arc wire was located at center of the duct section. A strip of insulation, approximately 2.5cm (1 in) long, was removed from each of the three bus conductors, and the arcing wire was wrapped around each conductor. The arcing wire installed on the bus is presented in Fig. 29.

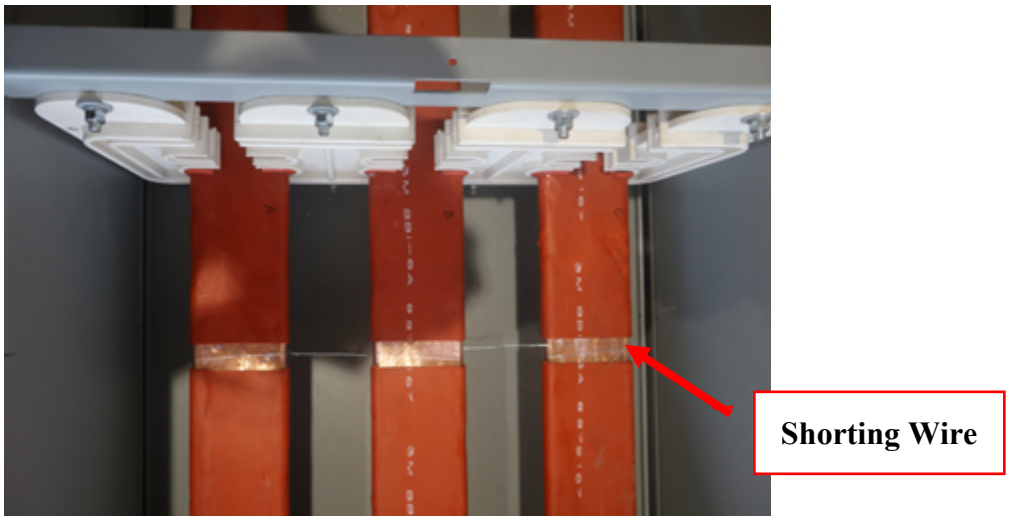


Fig. 29. Shorting wire location Experiment 2-25

### 3.3.1. Observations

Observations documented below are based on review of video and thermal imaging that was taken during the experiment. The observations are provided in Table 17 and include an approximate time reference. Corresponding images are provided in Fig. 30, with thermography images presented in Fig. 31.

The bus duct enclosure experienced failure of the fasteners holding the bus duct top and bottom covers resulting in an open configuration within 0.07s from the initiation of the arc. The manner in which these covers deflected resulted in directing much of the thermal exposure away from the instrumentation and back towards the laboratory's power supply. During the experiment there were two arc induced breaches of the lower cover while the cover was still attached to the duct structure. One of the breaches occurred where the lower cover was restrained by a steel beam of the bus duct support structure. No visible damage to the cable samples on the instrument rack was observed, however, the insulation material on the bus bars separated from conductors melted and ignited, causing a dripping liquid fire. Post-experiment inspection identified that the arc migrated to the end of the bus bars and sustained the majority of the arc time near the ends of the bus bar. It appears that the arc migrated away from the arc initiation location and stabilized near the internal bus bar support (away from power supply). Minor degradation of the bus bar was observed at arc initiation point, with more extensive damage observed near the far internal

bus bar supports. No phases were completely severed. It appears that the bus orientation may have influenced the manner and speed in which the bus insulation was removed from the arc exposure during the experiment.

Table 17. Observations from Experiment 2-25

| Time (ms) | Observation |
|---|---|
| **0** | Initial light observed |
| **216** | Luminescent flash zone beyond first instrument rack immediately above bus duct |
| **517** | Particle ejecta reaches first instrument rack immediately above enclosure |
| **950** | Particle ejecta near power supply end of duct |
| **1 184** | Flame exiting switchgear |
| **1 484** | Particle ejecta impacts cell wall (right) |
| **2 001** | End of arc |
| **3 003** | One second after end of arc with smoke clearing |

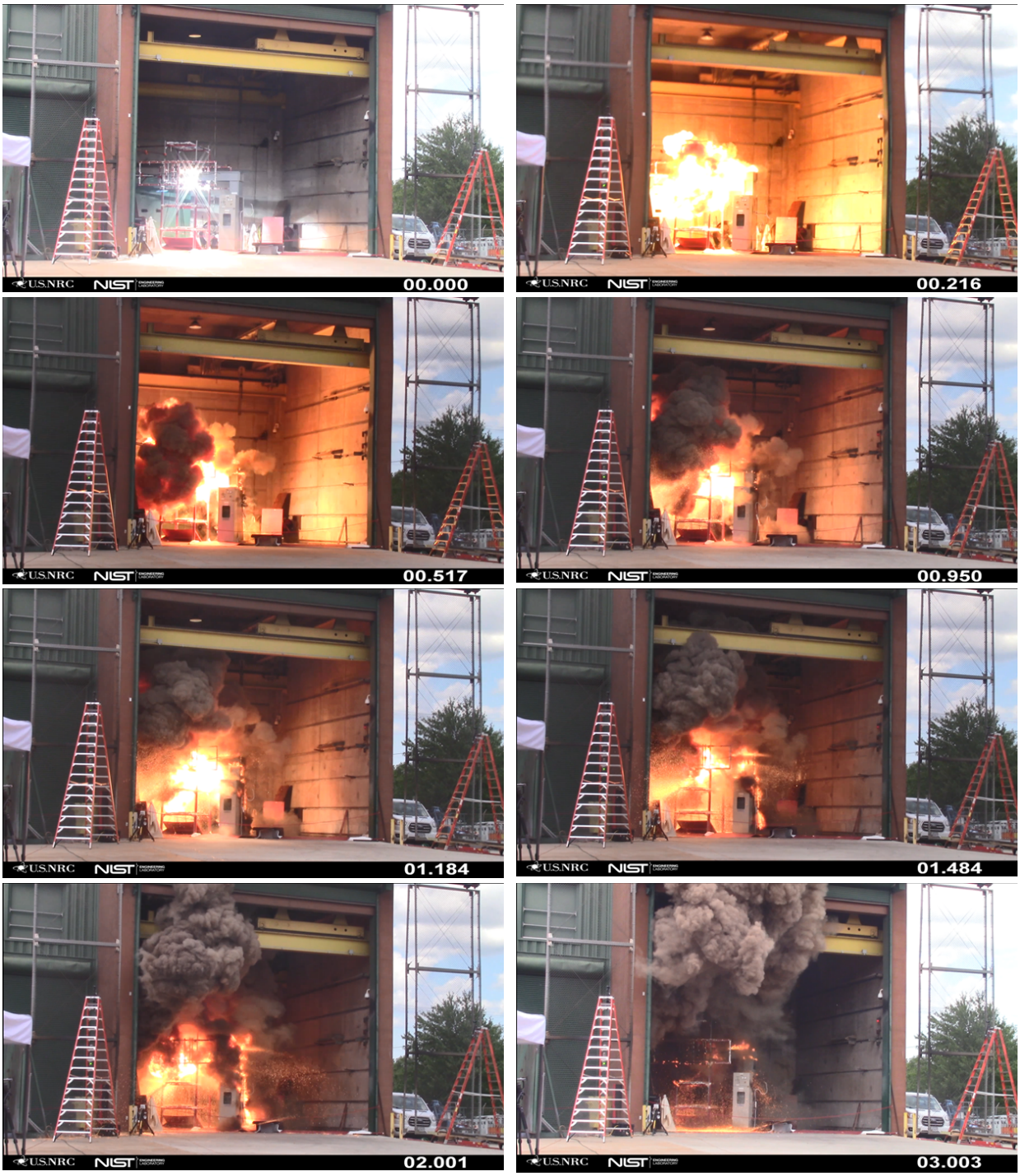


Fig. 30. Sequence of Images from Experiment 2-25 (image time stamps are in seconds).

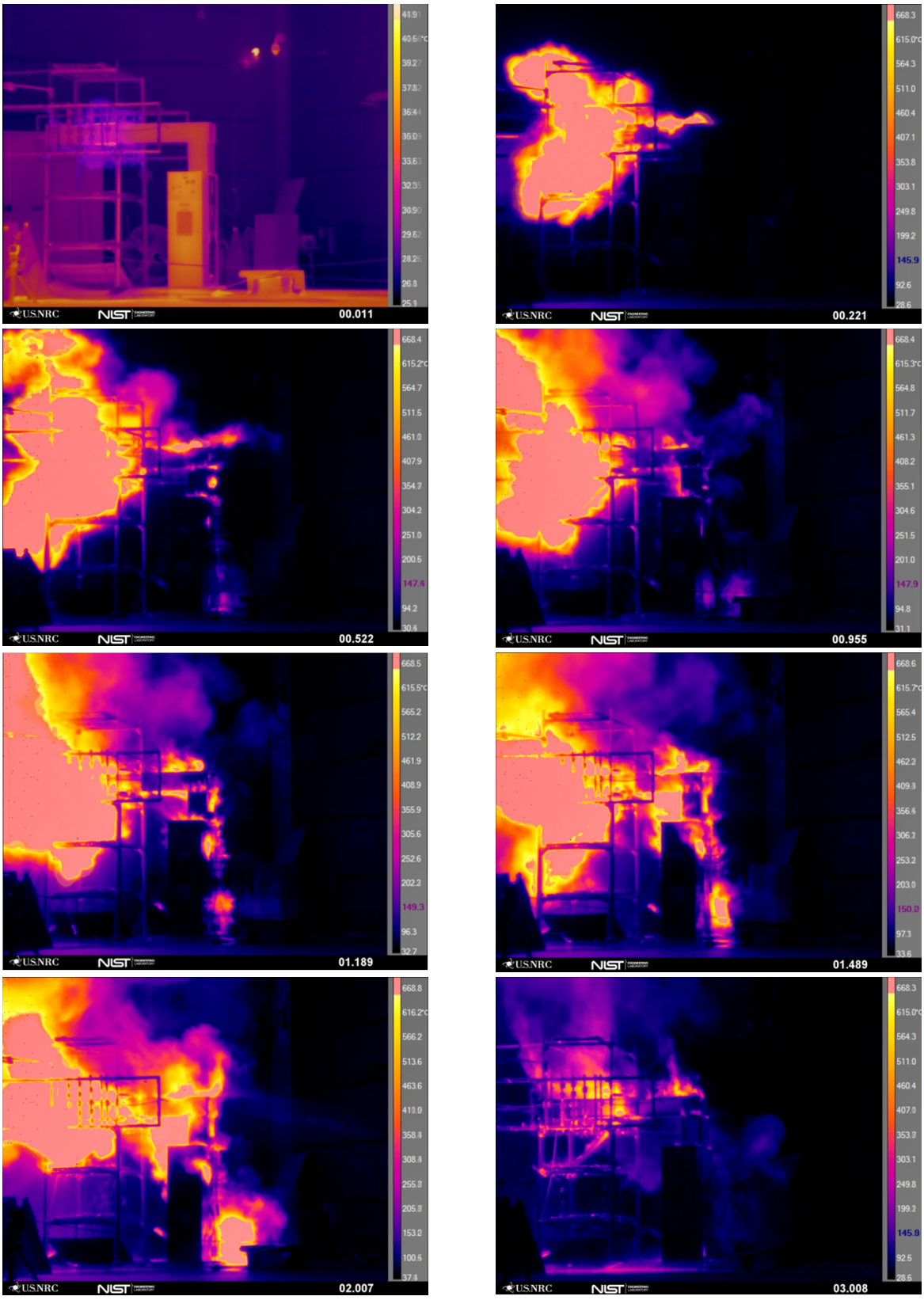


Fig. 31. Sequence of Thermal Images from Experiment 2-25 (image time stamp in seconds)

Photograph of the enclosure following the experiment is presented in Fig. 32. The enclosure did breach from both fastener failure and thermal effects.

Fig. 32. Enclosure Post-Experiment 2-25.

An image of the bus bars in the enclosure after the experiment are shown in Fig. 33. The total mass loss of the bus bars was 3 848.5 g ± 1 g. Additional details are presented in Appendix C.

Fig. 33. Photo of Experiment 2-25 bus bars post-experiment (arc location shown center).

### 3.3.2. Measurements

Measurements made during Experiment 2-25 are presented below. These measurements include:

- Thermal
  - Heat flux – Plate Thermometers, Tcap Slug Calorimeter
  - Incident Energy – ASTM Slug Calorimeters, Tcap Slug Calorimeters, Plate Thermometers
  - Temperature – Thermocouple inside of switchgear
- Pressure
  - Internal pressure
- Mass Loss
  - Pre- / Post-experimental measurements
- Electrical
  - Voltage profiles
  - Current profiles
  - Power and energy profiles

#### 3.3.2.1. Thermal Measurements

Thermal measurements from the active instruments are reported below for Experiment 2-25. These include PT measurements in Table 18, ASTM Slug Calorimeter measurements in Table 19 and $T_{cap}$ slug measurements in Table 20. The maximum reading is identified with bold text. The maximum temperature of the sheathed thermocouple located in the switchgear was 387 °C ± 3 °C.

Table 18. Summary of plate thermometer measurements Experiment 2-25

| Rack No. | Plate No. | Location | Max Heat Flux ($kW/m^2$) Greater of ± 1 $kW/m^2$ or ± 5 % | Average Heat Flux During Arc ($kW/m^2$) Greater of ±1 $kW/m^2$ or ± 5 % | Total Incident Energy ($kJ/m^2$) ± 15 % | Notes |
|---|---|---|---|---|---|---|
| **1** | 1 | Top | 466 | 311 | 600 | |
| **1** | 3 | Mid-Right | **2 102** | **994** | **1920** | |
| **1** | 5 | Mid-Center | 704 | 447 | 850 | |
| **1** | 7 | Mid-Left | 349 | 277 | 527 | |
| **1** | 9 | Bottom | - - - | - - - | - - - | Inoperable prior to experiment (IPE) |
| **2** | 10 | Top | - - - | - - - | - - - | IPE |
| **2** | 12 | Mid-Right | 378 | 247 | 480 | |

| Rack No. | Plate No. | Location | Max Heat Flux (kW/m$^2$) Greater of ± 1 kW/m$^2$ or ± 5 % | Average Heat Flux During Arc (kW/m$^2$) Greater of ±1 kW/m$^2$ or ± 5 % | Total Incident Energy (kJ/m$^2$) ± 15 % | Notes |
|---|---|---|---|---|---|---|
| **2** | 14 | Mid-Center | 630 | 362 | 700 | |
| **2** | 16 | Mid-Left | 693 | 424 | 800 | |
| **2** | 18 | Bottom | 461 | 314 | 600 | |
| **3** | 19 | Top | 333 | 195 | 390 | |
| **3** | 21 | Mid-Right | 241 | 150 | 310 | |
| **3** | 23 | Mid-Center | 148 | 129 | 290 | |
| **3** | 25 | Mid-Left | 139 | 99 | 240 | |
| **3** | 27 | Bottom | 266 | 170 | 340 | |
| **4** | 28 | Top | 530 | 351 | 680 | |
| **4** | 30 | Mid-Right | 1 119 | 303 | 710 | |
| **4** | 32 | Mid-Center | 1 570 | 496 | 990 | |
| **4** | 34 | Mid-Left | - - - | - - - | - - - | IPE |
| **4** | 36 | Bottom | 711 | 308 | 570 | |
| **5** | 37 | Front | - - - | - - - | - - - | IPE |
| **5** | 39 | Center-Right | 282 | 121 | 300 | |
| **5** | 41 | Center-Mid | 1 060 | 281 | 830 | |
| **5** | 43 | Center-Left | 384 | 176 | 390 | |
| **5** | 45 | Back | 150 | 112 | 250 | |

Table 19. Summary of ASTM slug calorimeter measurements, Experiment 2-25

| Rack No. | ASTM No. | Location | Incident Energy (kJ/m$^2$) Greater of ± 18 kJ/m$^2$ or ± 4 % | Time to Max Temperature (s) ± 3 % | Comment |
|---|---|---|---|---|---|
| **1** | A | Top | **1 195** | 2.43 | |
| **1** | B | Bottom | 717 | 2.68 | |
| **2** | C | Top | 620 | 2.38 | |
| **2** | D | Bottom | 785 | 3.30 | |
| **3** | E | Top | 348 | 6.47 | |
| **3** | F | Bottom | 324 | 8.40 | |

| Rack No. | ASTM No. | Location | Incident Energy (kJ/m$^2$) Greater of ± 18 kJ/m$^2$ or ± 4 % | Time to Max Temperature (s) ± 3 % | Comment |
|---|---|---|---|---|---|
| **4** | G | Top | 457 | 20.25 | |
| **4** | H | Bottom | 478 | 3.71 | |
| **5** | I | Top | 246 | 6.37 | |
| **5** | J | Bottom | 252 | 4.3 | |

Table 20. Summary of $T_{cap}$ slug measurements, Experiment 2-25

| Rack No. | $T_{cap}$ No. | Location | Heat Flux During Arc (kW/m$^2$) Greater of ± 1.5 kW/m$^2$ or ± 2.9 % | Incident Energy During Arc Phase (kJ/m$^2$) Greater of ± 2.4 kJ/m$^2$ or ± 5 % | Total Incident Energy (kJ/m$^2$) Greater of ± 2.4 kJ/m$^2$ or ± 5 % |
|---|---|---|---|---|---|
| **1** | 2 | Top | 271.8 | 560.2 | 1043.3 |
| **1** | 4 | Mid-Right | **560.0** | **1 070.7** | 1 479.8 |
| **1** | 6 | Mid-Left | 294.3 | 639.8 | 885.1 |
| **1** | 8 | Bottom | 276.2 | 566.2 | 1060.3 |
| **2** | 11 | Top | 276.6 | 532.0 | 851.1 |
| **2** | 13 | Mid-Right | 291.0 | 572.3 | 813.1 |
| **2** | 15 | Mid-Left | 296.6 | 594.1 | 922.6 |
| **2** | 17 | Bottom | 173.4 | 310.4 | 922.5 |
| **3** | 20 | Top | 108.0 | 220.2 | 692.0 |
| **3** | 22 | Mid-Right | 85.0 | 180.9 | 684.5 |
| **3** | 24 | Mid-Left | 78.7 | 154.9 | 707.7 |
| **3** | 26 | Bottom | 106.8 | 185.7 | 716.2 |
| **4** | 29 | Front | 150.8 | 268.9 | 813.1 |
| **4** | 31 | Center-Right | 313.6 | 539.9 | **1 591.0** |
| **4** | 33 | Center-Left | 224.8 | 370.2 | 863.9 |
| **4** | 35 | Back | 223.2 | 373.2 | 1 173.7 |
| **5** | 38 | Front | 70.4 | 127.7 | 374.8 |
| **5** | 40 | Center-Right | 110.0 | 212.5 | 452.2 |
| **5** | 42 | Center-Left | 119.2 | 217.7 | 414.5 |
| **5** | 44 | Back | 75.6 | 142.4 | 389.9 |

### 3.3.2.2. Pressure Measurements

The pressure profiles for the first two tenths of a second are shown in Fig. 34. Only one pressure probe, 0 kPa to 207 kPa (0 psia to 30 psia), was used due to a problem installing the second probe. After the initial pressure spike, the pressure rapidly decays to a relative steady state. The maximum change in pressure is approximately 33.7 kPa (4.9 psi) above ambient at its peak.

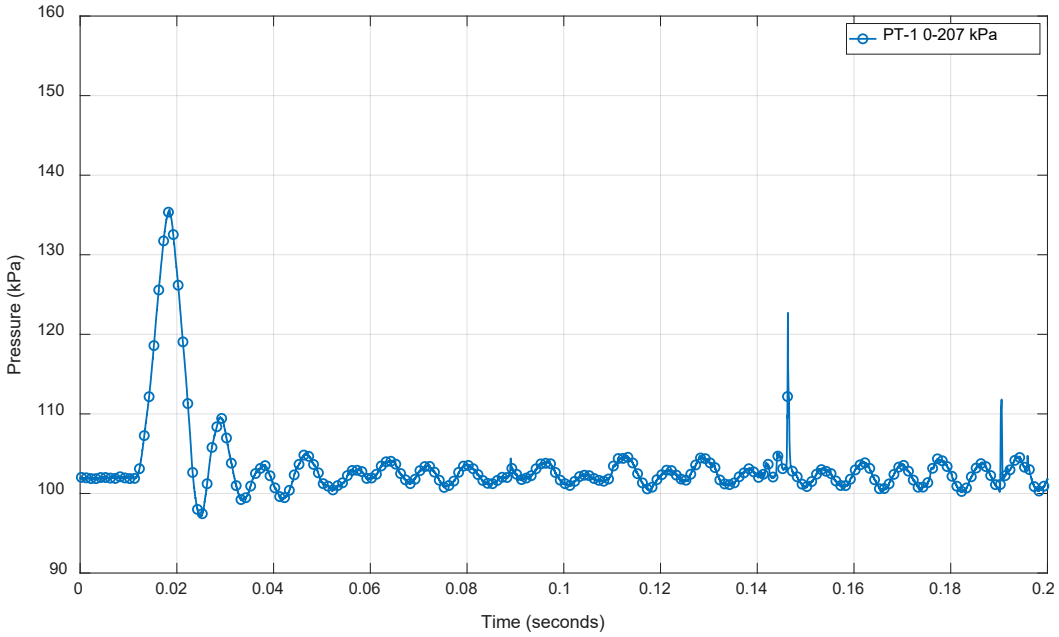


Fig. 34. Pressure measurements from Experiment 2-25 located in connected switchgear. Measurement uncertainty ± 3 percent.

#### 3.3.2.3. Electrical Measurements

Experiment 2-25 used KEMA circuit S02 and is reported in Appendix E. Full-level circuit checks (calibration experiments) were performed prior to the experiment to verify the experimental parameters were acceptable. For this experiment the calibration experiments configured the power system to 4.157 kV, 29.941 kA symmetrical, and 81.0 kA peak. The KEMA report (Appendix E) identifies this experiment as 220824-9003. Key experimental measurements are presented in Table 21. Plots of the electrical measurements are presented in Appendix B.

Table 21. Key measurement from Experiment 2-25. Measurement uncertainty ± 3 percent.

| Phase | Units | A | B | C |
|---|---|---|---|---|
| **Applied voltage, phase-to-ground** | $kV_{RMS}$ | 2.41 | 2.41 | 2.41 |
| **Applied voltage, phase-to-phase** | $kV_{RMS}$ | | 4.17 | |
| **Making current** | $kA_{peak}$ | 50.3 | 62.8 | -63.7 |
| **Current, AC component, beginning** | $kA_{RMS}$ | 32.5 | 32.5 | 29.9 |
| **Current, AC component, middle** | $kA_{RMS}$ | 30.2 | 29.3 | 27.2 |
| **Current, AC component, end** | $kA_{RMS}$ | 28.1 | 29.7 | 26.4 |
| **Current, AC component, average** | $kA_{RMS}$ | 30.2 | 29.7 | 27.3 |
| **Current, AC component, three-phase average** | $kA_{RMS}$ | | 29.1 | |
| **Duration** | s | 2.02 | 2.02 | 2.02 |
| **Arc Energy** | MJ | | 54.0 | |

## 3.4. Experiment 2-26 – 4.16 kV, 30 kA, 4 s Duration, Copper Bus, Steel Enclosure

Experiment 2-26 was performed on August 25, 2022, at 9:12 AM eastern daylight time (EDT). The temperature was approximately 22 °C (72 °F), approximately 78 percent relative humidity and approximately 101.9 kPa of pressure. The weather was mostly sunny with a wind of approximately 1.6 km/h (1 mi/h) out of the northwest.

The arc wire was located at center of the started duct section. A strip of insulation, approximately 2.5cm (1 in) long, was removed from each of the three bus conductors and the arcing wire was wrapped around each conductor. The arcing wire installed on the bus is presented in Fig. 35.

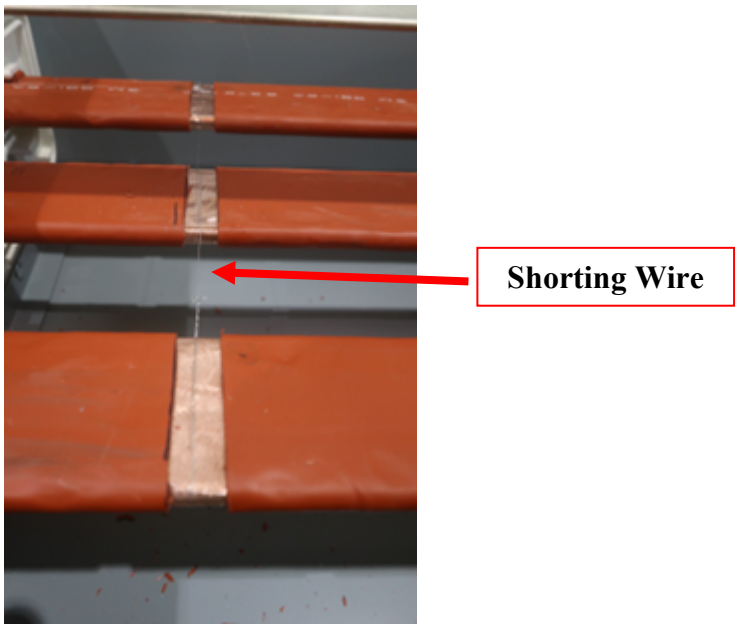


Fig. 35. Shorting wire location Experiment 2-26

### 3.4.1. Observations

Observations documented below are based on review of video and thermal imaging that was taken during the experiment. The observations are provided in Table 22 and include an approximate time reference. Corresponding images are provided in Fig. 36, with thermography images presented in Fig. 37.

Similar to experiment 2-25, the bus duct enclosure experienced failure of the fasteners holding the duct top and bottom covers resulting in an open configuration within 0.04s from the initiation of the arc. The manner in which these covers deflected resulted in directing much of the thermal exposure away from the instrumentation and back towards the laboratory's power supply. None of the panels experienced breach due to thermal exposure. The lower splice plate cover was dislocated from the duct and found on the ground after the experiment. The breather screen was missing. It is unknown if thermal or pressure effects caused the loss of the breather screen. Post-experiment inspection identified that the arc migrated to the end of the bus bars and sustained the majority of the arc time near the ends of the bus bar. No cable damage was observed.

Table 22. Observations from Experiment 2-26

| Time (ms) | Observation |
|---|---|
| **0** | Initial light observed |
| **116** | Luminescent flash zone reaches first instrument rack immediately above and below duct enclosure |
| **433** | Flames emerge from switchgear right |
| **1 768** | Lower panel dislodged from structure and resting on support structure |
| **2 218** | Particle ejecta observable below duct on power supply side |
| **2 585** | Particle ejecta observed and 90-degree duct bend |
| **4 003** | End of arc |
| **15 015** | Post-experiment after smoke has cleared to observe visual of duct |


Fig. 36. Sequence of Images from Experiment 2-26 (image time stamps are in seconds).

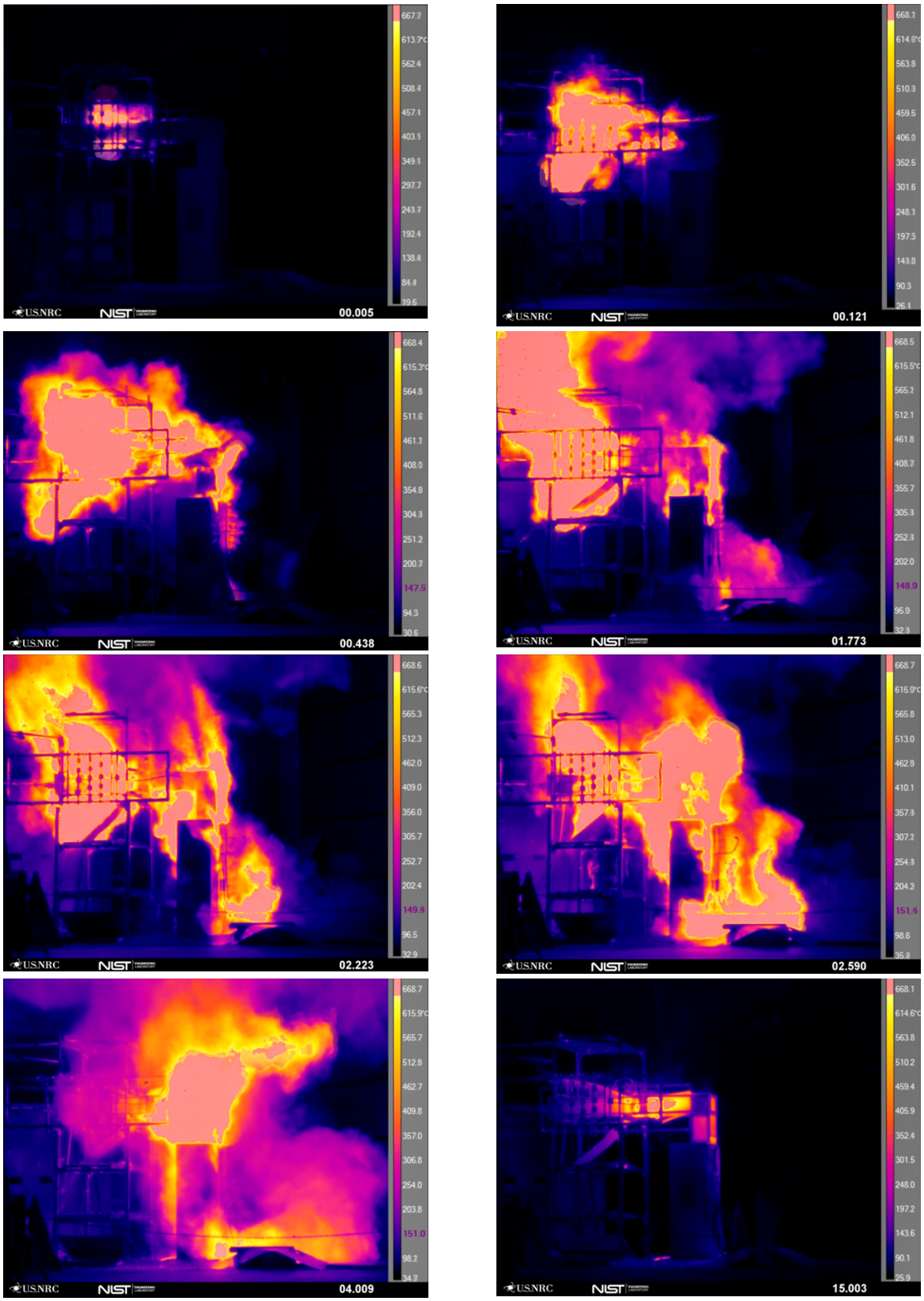


Fig. 37. Sequence of Thermal Images from Experiment 2-26 (image time stamp in seconds)

Photograph of the enclosure following the experiment is presented in Fig. 38. The enclosure did not experience a breach due to thermal effects.


Fig. 38. Enclosure Post-Experiment 2-26.

The bus bars in the duct enclosure after the experiment are shown in Fig. 39. The total mass lost from the bus bars was 5 991.0 g ± 1 g. Additional details are presented in Appendix C.

Fig. 39. Photo of Experiment 2-26 bus bars post-experiment (arc location shown center).

### 3.4.2. Measurements

Measurements made during Experiment 2-26 are presented below. These measurements include:

- Thermal
  - Heat flux – Plate Thermometers, Tcap Slug Calorimeters
  - Incident Energy – ASTM Slug Calorimeters, Tcap Slug Calorimeters, Plate Thermometers
  - Temperature – Thermocouple inside of switchgear
- Pressure
  - Internal pressure
- Mass Loss
  - Pre- / Post-experimental measurements
- Electrical
  - Voltage profiles
  - Current profiles
  - Power and energy profiles

#### 3.4.2.1. Thermal Measurements

Thermal measurements from the active instruments are reported below for Experiment 2-26. These include PT measurements in Table 23, ASTM Slug Calorimeter measurements in Table 24, and $T_{cap}$ slug measurements in Table 25. The maximum value is identified with bold text. The maximum temperature of the sheathed thermocouple located in the switchgear was approximately 1 413 °C, which exceeds the maximum manufacture calibrated Type K thermocouple temperature of 1 372 °C ± 10 °C.

Table 23. Summary of plate thermometer measurements Experiment 2-26

| Rack No. | Plate No. | Location | Max Heat Flux (kW/m²) Greater of ± 1 kW/m² or ± 5 % | Average Heat Flux During Arc (kW/m²) Greater of ±1 kW/m² or ± 5 % | Total Incident Energy (kJ/m²) ± 15 % | Notes |
|---|---|---|---|---|---|---|
| **1** | 1 | Top | 474 | 187 | 680 | |
| **1** | 3 | Mid-Right | 388 | 177 | 710 | |
| **1** | 5 | Mid-Center | 511 | 224 | 830 | |
| **1** | 7 | Mid-Left | 615 | **260** | **960** | |
| **1** | 9 | Bottom | 507 | 182 | 660 | |
| **2** | 10 | Top | - - - | - - - | - - - | Inoperable prior to |

| Rack No. | Plate No. | Location | Max Heat Flux ($kW/m^2$) Greater of ± 1 $kW/m^2$ or ± 5 % | Average Heat Flux During Arc ($kW/m^2$) Greater of ±1 $kW/m^2$ or ± 5 % | Total Incident Energy ($kJ/m^2$) ± 15 % | Notes |
|---|---|---|---|---|---|---|
| | | | | | | experiment (IPE) |
| **2** | 12 | Mid-Right | **641** | 232 | 860 | |
| **2** | 14 | Mid-Center | 599 | 235 | 870 | |
| **2** | 16 | Mid-Left | 443 | 186 | 680 | |
| **2** | 18 | Bottom | 338 | 166 | 600 | |
| **3** | 19 | Top | 290 | 134 | 500 | |
| **3** | 21 | Mid-Right | - - - | - - - | - - - | IPE |
| **3** | 23 | Mid-Center | 185 | 103 | 420 | |
| **3** | 25 | Mid-Left | 161 | 85 | 490 | |
| **3** | 27 | Bottom | 219 | 122 | 450 | |
| **4** | 28 | Top | 342 | 142 | 520 | |
| **4** | 30 | Mid-Right | 186 | 106 | 420 | |
| **4** | 32 | Mid-Center | 147 | 66 | 260 | |
| **4** | 34 | Mid-Left | 91 | 38 | 150 | |
| **4** | 36 | Bottom | 222 | 128 | 530 | |
| **5** | 37 | Front | 104 | 41 | 160 | |
| **5** | 39 | Center-Right | 601 | 115 | 420 | |
| **5** | 41 | Center-Mid | 62 | 49 | 180 | |
| **5** | 43 | Center-Left | 187 | 61 | 220 | |
| **5** | 45 | Back | 73 | 56 | 230 | |

Table 24. Summary of ASTM slug calorimeter measurements, Experiment 2-26

| Rack No. | ASTM No. | Location | Incident Energy ($kJ/m^2$) Greater of ± 18 $kJ/m^2$ or ± 4 % | Time to Max Temperature (s) ± 3 % | Comment |
|---|---|---|---|---|---|
| **1** | A | Top | **1 007** | 4.04 | |
| **1** | B | Bottom | 860 | 4.13 | |
| **2** | C | Top | 975 | 4.43 | |
| **2** | D | Bottom | 866 | 4.48 | |
| **3** | E | Top | 449 | 7.10 | |
| **3** | F | Bottom | 491 | 50.43 | |
| **4** | G | Top | 409 | 9.64 | |
| **4** | H | Bottom | 241 | 9.49 | |
| **5** | I | Top | 220 | 5.61 | |
| **5** | J | Bottom | 204 | 5.66 | |

Table 25. Summary of $T_{cap}$ slug measurements, Experiment 2-26

| Rack No. | $T_{cap}$ No. | Location | Heat Flux During Arc (kW/m$^2$) Greater of ± 1.5 kW/m$^2$ or ± 2.9 % | Incident Energy During Arc Phase (kJ/m$^2$) Greater of ± 2.4 kJ/m$^2$ or ± 5 % | Total Incident Energy (kJ/m$^2$) Greater of ± 2.4 kJ/m$^2$ or ± 5 % |
|---|---|---|---|---|---|
| **1** | 2 | Top | 184.4 | 625.8 | 1 142.3 |
| **1** | 4 | Mid-Right | 298.2 | 832.5 | 1 069.0 |
| **1** | 6 | Mid-Left | **376.6** | **1 046.0** | 1 255.6 |
| **1** | 8 | Bottom | 277.6 | 776.6 | 969.4 |
| **2** | 11 | Top | 268.0 | 794.0 | 1 167.8 |
| **2** | 13 | Mid-Right | 329.3 | 930.4 | 1 121.3 |
| **2** | 15 | Mid-Left | 242.5 | 778.8 | 1 101.5 |
| **2** | 17 | Bottom | 175.9 | 562.3 | 1 085.0 |
| **3** | 20 | Top | 129.5 | 411.0 | 1 113.2 |
| **3** | 22 | Mid-Right | 112.4 | 348.2 | 983.4 |
| **3** | 24 | Mid-Left | 94.1 | 321.1 | **1 262.3** |
| **3** | 26 | Bottom | 117.1 | 372.0 | 1 125.0 |
| **4** | 29 | Front | 73.8 | 295.1 | 702.3 |
| **4** | 31 | Center-Right | 86.2 | 288.8 | 1 066.7 |
| **4** | 33 | Center-Left | 46.9 | 185.0 | 621.0 |
| **4** | 35 | Back | 70.5 | 227.3 | 851.7 |
| **5** | 38 | Front | 46.4 | 180.4 | 345.9 |
| **5** | 40 | Center-Right | 58.1 | 223.6 | 537.3 |
| **5** | 42 | Center-Left | 45.3 | 176.0 | 349.8 |
| **5** | 44 | Back | 48.4 | 192.6 | 505.3 |

### 3.4.2.2. Pressure Measurements

The pressure profiles for the first two tenths of a second are shown in Fig. 40. After the initial pressure spike, the pressure rapidly decays to a relative steady state. Only one pressure probe, 0 kPa to 207 kPa (0 psia to 30 psia) was used due to a problem installing the second probe. The maximum change in pressure in the connected switchgear unit is approximately 37.8 kPa (5.5 psi) above ambient at its peak.

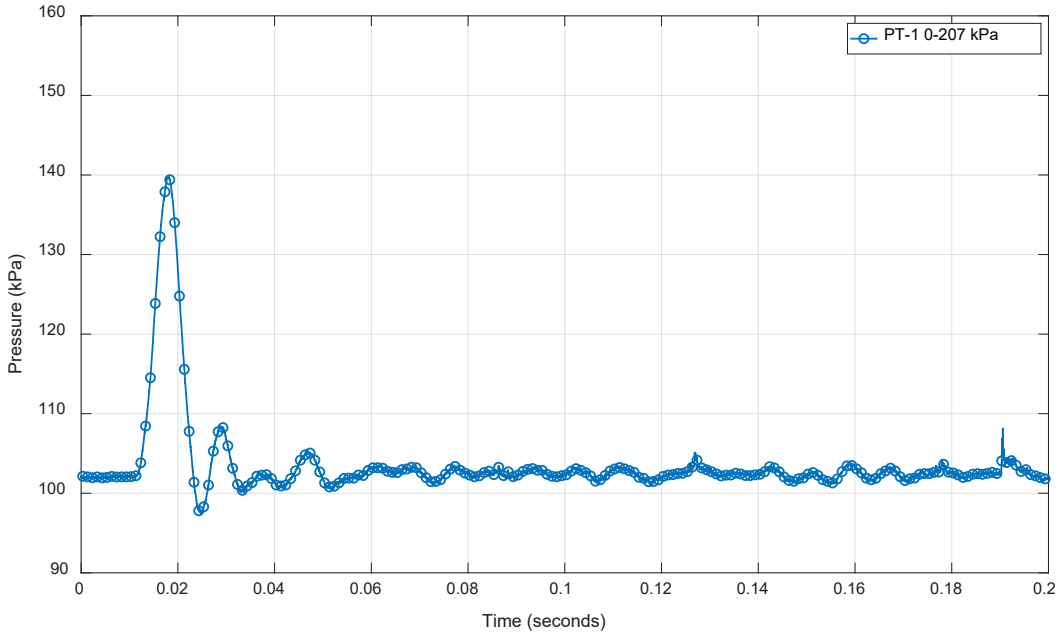


Fig. 40. Pressure measurements from Experiment 2-26 (breaker compartment (left); Main bus [arcing compartment] – (right)). Measurement uncertainty ± 3 percent.

### 3.4.2.3. Electrical Measurements

Experiment 2-26 used KEMA circuit S02 and is reported in Appendix E. Full-level circuit checks (calibration experiments) were performed prior to the experiment to verify the experimental parameters were acceptable. The KEMA report (Appendix E) identifies this experiment as 220825-9001. Key experimental measurements are presented in Table 26. Plots of the electrical measurements are presented in Appendix B.

Table 26. Key measurement from Experiment 2-26. Measurement uncertainty ± 3 percent.

| Phase | Units | A | B | C |
|---|---|---|---|---|
| **Applied voltage, phase-to-ground** | $kV_{RMS}$ | 2.41 | 2.41 | 2.41 |
| **Applied voltage, phase-to-phase** | $kV_{RMS}$ | | 4.17 | |
| **Making current** | $kA_{peak}$ | 49.8 | 63.9 | -64.2 |
| **Current, AC component, beginning** | $kA_{RMS}$ | 31.5 | 33.3 | 29.5 |
| **Current, AC component, middle** | $kA_{RMS}$ | 28.6 | 29.7 | 26.6 |
| **Current, AC component, end** | $kA_{RMS}$ | 26.1 | 27.7 | 25.3 |
| **Current, AC component, average** | $kA_{RMS}$ | 28.8 | 30.1 | 27.1 |
| **Current, AC component, three-phase average** | $kA_{RMS}$ | | 28.7 | |
| **Duration** | s | 4.02 | 4.02 | 4.02 |
| **Arc Energy** | MJ | | 101 | |

## 3.5. Experiment 2-27 – 4.16 kV, 30 kA, 2 s Duration, Copper Bus, Aluminum Enclosure

Experiment 2-27 was performed on August 29, 2022, at 11:02 AM eastern daylight time (EDT). The temperature was approximately 27 °C (81 °F), approximately 69 percent relative humidity and approximately 101.3 kPa of pressure. The weather was partly cloudy with a wind of approximately 15 km/h (9 mi/h) out of the southwest.

The arc wire was located at center of the straight duct section. A strip of insulation, approximately 2.5cm (1 in) long, was removed from each of the three bus conductors and the arcing wire was wrapped around each conductor. The arcing wire installed on the bus and marked up illustrations of the arc wire location is presented in Fig. 41.

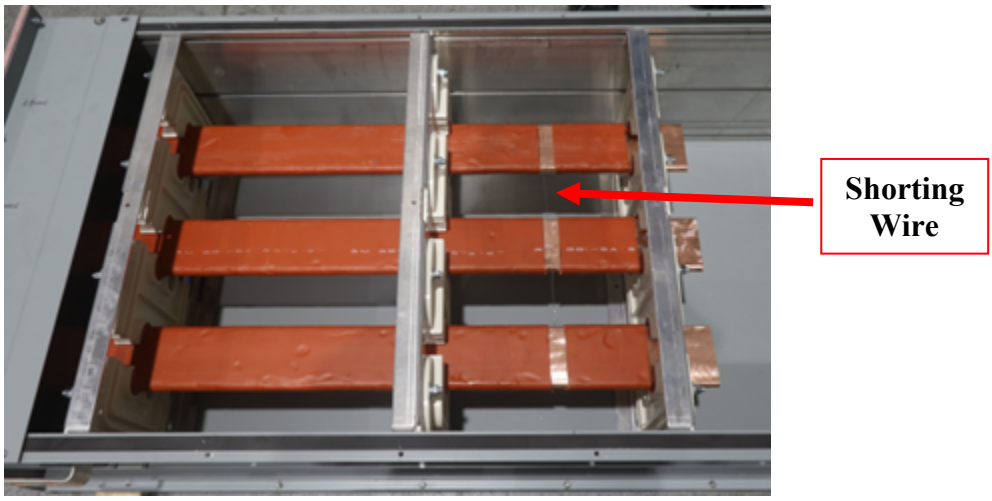


Fig. 41. Shorting wire location Experiment 2-27

### 3.5.1. Observations

The observations documented below are based on review of the video and thermal imaging that was recorded during the experiment. The observations are provided in Table 27 and include an approximate time reference. Corresponding images are provided in Fig. 42, with thermography images presented in Fig. 43.

This was the first aluminum bus duct enclosure experiment of the series and was also the first experiment with the bus bars shortened to prevent arc migration beyond sensor locations. The arc successfully stabilized above the instrumentation rack and lasted for the expected duration (2.04 s). After the HEAF event $CO_2$ fire suppression agent was applied to the duct and local hot spots on the racks and floor.

A large portion of the bus duct enclosure was destroyed during experiment. Aluminum slag was found throughout the test cell with the majority of slag deposited below the duct. No identifiable enclosure pieces or parts were located in the debris. The walls and ceiling of the test cell were coated with white powder (assumed to be aluminum and aluminum oxide). Slag was found in the courtyard up to approximately 20 m (65 ft) from the enclosure. No visible damage to the cable

samples was observed. Approximately 51 mm (2 in) of copper material was consumed in the experiment.

Table 27. Observations from Experiment 2-27

| Time (ms) | Observation |
|---|---|
| **0** | Initial light observed |
| **250** | Particle ejecta observed at 90 degree elbow |
| **633** | Particle ejecta observed outside test cell |
| **1 000** | Smoke reaches overhead crane and expansive particulate ejecta |
| **2 001** | End of arc |
| **12 012** | Smoke clearing cell 10 s after arc termination |


Fig. 42. Sequence of Images from Experiment 2-27 (image time stamps are in seconds).

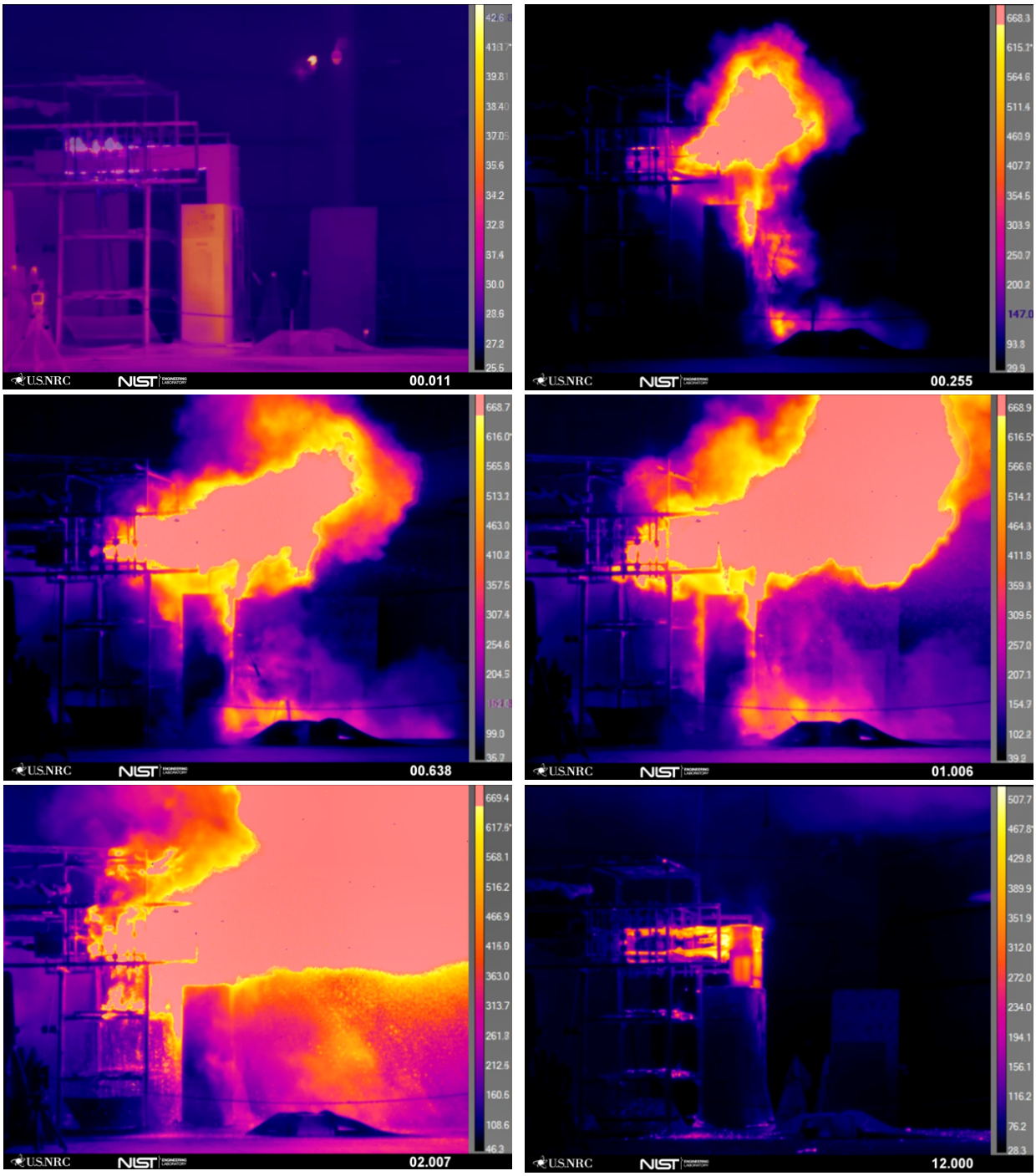


Fig. 43. Sequence of Thermal Images from Experiment 2-27 (image time stamp in seconds)

A photograph of the enclosure following the experiment is presented in Fig. 44. The enclosure did experience a breach. Most of the bus duct beyond the end of the bus bars was missing on the horizontal straight section. In addition, the end of the 90-degree duct elbow experienced a breach with most of the material missing post-experiment.

Fig. 44. Enclosure Post-Experiment 2-27.

An image of the bus bars and enclosure after the experiment is shown in Fig. 45. The total mass loss of the bus bars was 2 459.0 g ±1 g. Additional details are presented in Appendix E.

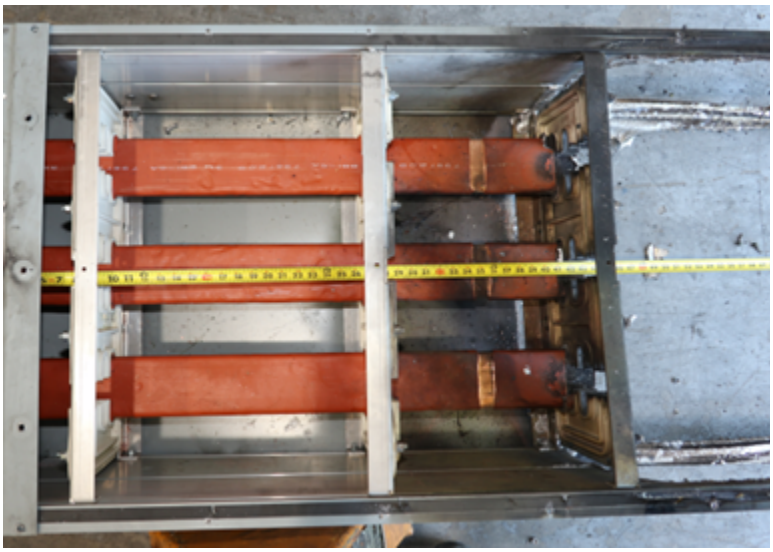

Fig. 45. Photo of Experiment 2-27 bus bars post-experiment (arc location shown center).

### 3.5.2. Measurements

Measurements made during Experiment 2-27 are presented below. These measurements include:

- Thermal
  - Heat flux – Plate Thermometers, Tcap Slug Calorimeters
  - Incident Energy – ASTM Slug Calorimeters, Tcap Slug Calorimeters, Plate Thermometers
  - Temperature – Thermocouple inside of switchgear

- Pressure
  - Internal pressure
- Mass Loss
  - Pre- / Post-experimental measurements
- Electrical
  - Voltage profiles
  - Current profiles
  - Power and energy profiles

#### 3.5.2.1. Thermal Measurements

Thermal measurements from the active instruments are reported below for Experiment 2-27. These include PT measurements in Table 28, ASTM Slug Calorimeter measurements in Table 29, and $T_{cap}$ slug measurements in Table 30. The maximum value is identified with bold text. The maximum temperature of the sheathed thermocouple located in the switchgear exceeded the maximum manufacture calibrated Type K thermocouple temperature of 1 372 °C ± 10 °C and failed shortly thereafter.

Table 28. Summary of plate thermometer measurements Experiment 2-27

| Rack No. | Plate No. | Location | Max Heat Flux (kW/m²) Greater of ± 1 kW/m² or ± 5 % | Average Heat Flux During Arc (kW/m²) Greater of ±1 kW/m² or ± 5 % | Total Incident Energy (kJ/m²) ± 15 % | Notes |
|---|---|---|---|---|---|---|
| **1** | 1 | Top | - - - | - - - | - - - | Inoperable prior to experiment (IPE) |
| **1** | 3 | Mid-Right | 381 | 186 | 370 | |
| **1** | 5 | Mid-Center | 805 | 418 | 800 | |
| **1** | 7 | Mid-Left | 562 | 352 | 680 | |
| **1** | 9 | Bottom | 327 | 167 | 330 | |
| **2** | 10 | Top | 554 | 411 | 810 | |
| **2** | 12 | Mid-Right | 341 | 201 | 400 | |
| **2** | 14 | Mid-Center | 424 | 256 | 510 | |
| **2** | 16 | Mid-Left | 366 | 190 | 360 | |
| **2** | 18 | Bottom | 397 | 202 | 380 | |
| **3** | 19 | Top | 469 | 269 | 510 | |
| **3** | 21 | Mid-Right | 364 | 172 | 350 | |
| **3** | 23 | Mid-Center | 520 | 237 | 450 | |

| Rack No. | Plate No. | Location | Max Heat Flux ($kW/m^2$) Greater of ± 1 $kW/m^2$ or ± 5 % | Average Heat Flux During Arc ($kW/m^2$) Greater of ±1 $kW/m^2$ or ± 5 % | Total Incident Energy ($kJ/m^2$) ± 15 % | Notes |
|---|---|---|---|---|---|---|
| **3** | 25 | Mid-Left | 526 | 312 | 600 | |
| **3** | 27 | Bottom | 481 | 207 | 400 | |
| **4** | 28 | Top | 500 | 247 | 510 | |
| **4** | 30 | Mid-Right | 1 333 | **628** | 1460 | |
| **4** | 32 | Mid-Center | 1 576 | 606 | **1910** | |
| **4** | 34 | Mid-Left | 313 | 169 | 1520 | |
| **4** | 36 | Bottom | 564 | 260 | 520 | |
| **5** | 37 | Front | 610 | 114 | 240 | |
| **5** | 39 | Center-Right | 1 612 | 489 | 1360 | |
| **5** | 41 | Center-Mid | 1 009 | 238 | 1310 | |
| **5** | 43 | Center-Left | - - - | - - - | - - - | IPE |
| **5** | 45 | Back | **2 293** | 420 | 1500 | |

Table 29. Summary of ASTM slug calorimeter measurements, Experiment 2-27

| Rack No. | ASTM No. | Location | Incident Energy ($kJ/m^2$) Greater of ± 18 $kJ/m^2$ or ± 4 % | Time to Max Temperature (s) ± 3 % | Comment |
|---|---|---|---|---|---|
| **1** | A | Top | 65 | 300 | |
| **1** | B | Bottom | 651 | 3.17 | |
| **2** | C | Top | 627 | 3.45 | |
| **2** | D | Bottom | 534 | 3.75 | |
| **3** | E | Top | 537 | 3.50 | |
| **3** | F | Bottom | 424 | 7.05 | |
| **4** | G | Top | 961 | 8.72 | |
| **4** | H | Bottom | **1673** | 20.42 | |
| **5** | I | Top | 588 | 24.25 | |
| **5** | J | Bottom | | | No data |

Table 30. Summary of $T_{cap}$ slug measurements, Experiment 2-27

| Rack No. | $T_{cap}$ No. | Location | Heat Flux During Arc (kW/m$^2$) Greater of ± 1.5 kW/m$^2$ or ± 2.9 % | Incident Energy During Arc Phase (kJ/m$^2$) Greater of ± 2.4 kJ/m$^2$ or ± 5 % | Total Incident Energy (kJ/m$^2$) Greater of ± 2.4 kJ/m$^2$ or ± 5 % |
|---|---|---|---|---|---|
| **1** | 2 | Top | 323.7 | 503.4 | 1 060.0 |
| **1** | 4 | Mid-Right | 298.3 | 445.8 | 865.0 |
| **1** | 6 | Mid-Left | **427.8** | **710.9** | 954.1 |
| **1** | 8 | Bottom | 276.8 | 423.6 | 784.7 |
| **2** | 11 | Top | 209.2 | 358.2 | 774.5 |
| **2** | 13 | Mid-Right | 280.9 | 469.6 | 621.6 |
| **2** | 15 | Mid-Left | 294.6 | 499.6 | 697.0 |
| **2** | 17 | Bottom | 207.3 | 317.4 | 572.1 |
| **3** | 20 | Top | 190.7 | 275.5 | 628.5 |
| **3** | 22 | Mid-Right | 217.7 | 330.8 | 599.8 |
| **3** | 24 | Mid-Left | 238.0 | 338.8 | 711.5 |
| **3** | 26 | Bottom | 182.0 | 265.3 | 618.4 |
| **4** | 29 | Front | 337.1 | 477.3 | 957.8 |
| **4** | 31 | Center-Right | 271.7 | 356.3 | 1 750.3 |
| **4** | 33 | Center-Left | 209.4 | 302.2 | 1 853.2 |
| **4** | 35 | Back | 342.4 | 383.6 | 2 422.0 |
| **5** | 38 | Front | 335.0 | 317.0 | 4 275.9 |
| **5** | 40 | Center-Right | 169.1 | 186.7 | **2 670.0** |
| **5** | 42 | Center-Left | 86.3 | 136.4 | 394.8 |
| **5** | 44 | Back | 118.8 | 171.4 | 1 251.6 |

### 3.5.2.2. Pressure Measurements

The pressure profiles for the first two tenths of a second are shown in Fig. 46. After the initial pressure spike, the pressure rapidly decays to a relative steady state. The maximum change in pressure in the switchgear enclosure is approximately 24 kPa (3.5 psi) above ambient at its peak.

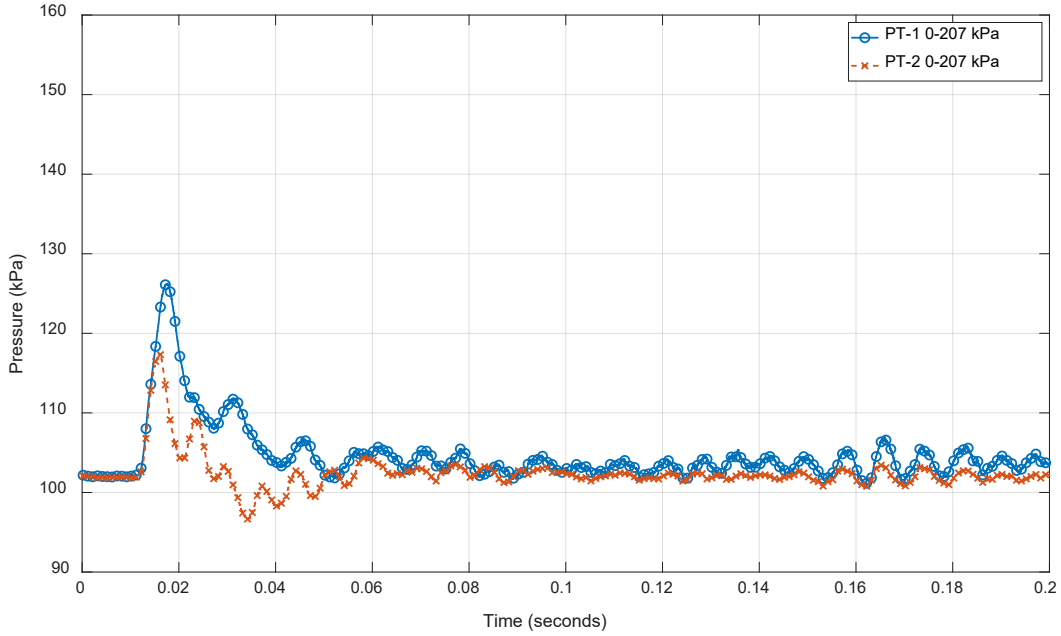


Fig. 46. Pressure measurements from Experiment 2-27. Measurement uncertainty ± 3 percent.

### 3.5.2.3. Electrical Measurements

Experiment 2-27 used KEMA circuit S02 and is reported in Appendix E. Full-level circuit checks (calibration experiments) were performed prior to the experiment to verify the experimental parameters were acceptable. The KEMA report (Appendix E) identifies this experiment as 220829-9001. Key experimental measurements are presented in Table 31. Plots of the electrical measurements are presented in Appendix B.

Table 31. Key measurement from Experiment 2-27. Measurement uncertainty ± 3 percent.

| Phase | Units | A | B | C |
|---|---|---|---|---|
| **Applied voltage, phase-to-ground** | $kV_{RMS}$ | 2.41 | 2.41 | 2.41 |
| **Applied voltage, phase-to-phase** | $kV_{RMS}$ | | 4.17 | |
| **Making current** | $kA_{peak}$ | 50.7 | 63.3 | -65.0 |
| **Current, AC component, beginning** | $kA_{RMS}$ | 31.4 | 32.8 | 30.0 |
| **Current, AC component, middle** | $kA_{RMS}$ | 28.9 | 29.9 | 28.1 |
| **Current, AC component, end** | $kA_{RMS}$ | 27.6 | 29.1 | 27.0 |
| **Current, AC component, average** | $kA_{RMS}$ | 29.0 | 30.4 | 28.1 |
| **Current, AC component, three-phase average** | $kA_{RMS}$ | | 29.1 | |
| **Duration** | s | 2.04 | 2.04 | 2.03 |
| **Arc Energy** | MJ | | 76.75 | |

## 3.6. Experiment 2-28 – 4.16 kV, 30 kA, 4 s Duration, Copper Bus, Aluminum Enclosure

Experiment 2-28 was performed on August 30, 2022, at 9:19 AM eastern daylight time (EDT). The temperature was approximately 26 °C (78 °F), approximately 84 percent relative humidity and approximately 100.6 kPa of pressure. The weather was mostly cloudy with a wind of approximately 11 km/h (7 mi/h) out of the south.

The arc wire was located at center of the duct section. A strip of insulation, approximately 2.5cm (1 in) long, was removed from each of the three bus conductors and the arcing wire was wrapped around each conductor. The arcing wire installed on the bus and marked up illustrations of the arc wire location is presented in Fig. 47.

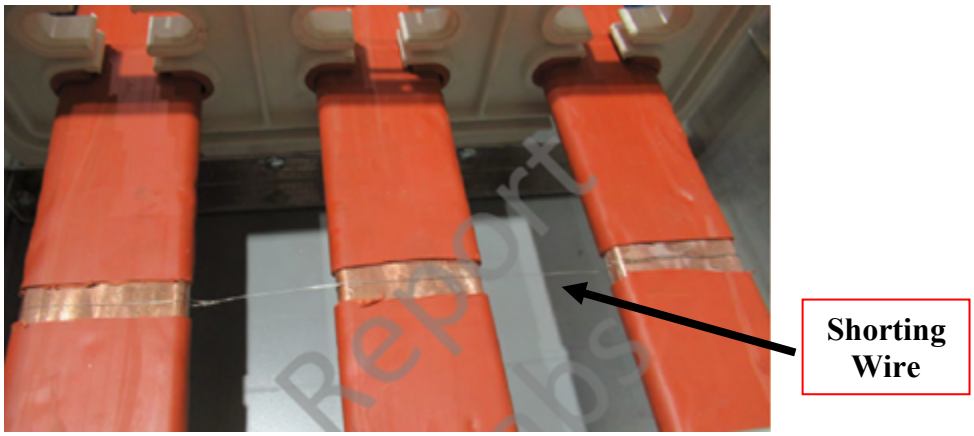


Fig. 47. Shorting wire location Experiment 2-28 [photo from KEMA report]

### 3.6.1. Observations

Observations documented below are based on review of video and thermal imaging that was taken during the experiment. The observations are provided in Table 32 and include an approximate time reference. Corresponding images are provided in Fig. 50, with thermography images presented in Fig. 51.

The arc successfully stabilized at the end of the bus bars and lasted for the expected duration (4.03 s). After the HEAF event, $CO_2$ fire suppression agent was applied to the duct and local hot spots on the racks and floor.

More of the duct enclosure was consumed during this experiment than the previous Cu/Al experiment with a 2 s arc duration (Experiment 2-27). Aluminum slag was found throughout the test cell and courtyard with the majority of the slag found below the duct. Some enclosure parts such as fasteners and metal straps were located outside the test cell. Aluminum yielding was evident on the far side of the 90 degree duct. The test cell wall was coated with white powder (assumed to be aluminum and aluminum oxide), but it was difficult to determine the extent due to residual deposits from the previous experiment.

Exposed cable insulation was observed along a long run of cable placed down the central axis of the instrumentation rack. Cable jacket was missing, with a portion hanging from the cable. After

the racks were removed, no cable damage was observed that would be expected to affect functionality. However, these cables were made from a thermoplastic material and may have undergone a rehealing process that has been observed in other fire experiments. The state of functionality during the experiment could not be confirmed by observation. No visible cable damage was observed an any cable coupon sample on the instrument racks. While the arc stabilized at the end of the bus bars, observations of the cable jacket damage and thermal imaging appear to indicate that most of the energy was released beyond the instrumentation rack locations. Fig. 48 and Fig. 49 show the locations on the cable where jacket material was removed during the HEAF experiment.

Fig. 48. Location of cable jacket damage relative to equipment. (Red arrows identify locations missing cable jacket and in some cases conductor jacket)

Fig. 49. Close-up of cable on Rack 2 from Experiment 2-28.

Table 32. Observations from Experiment 2-28

| Time (ms) | Observation |
|---|---|
| **0** | Initial light observed |
| **250** | Particle ejecta observed |
| **684** | Particle ejecta reaches right cell wall |
| **1 501** | Particle ejecta observed outside of cell |
| **2 285** | Extensive particle ejecta outside of cell |
| **2 485** | Shrapnel observed in air above small yard camera tripod and between tripod and ladder. |
| **4 003** | End of arc |
| **14 014** | Smoke clearing cell 10 s after arc termination |


Fig. 50. Sequence of Images from Experiment 2-28 (image time stamps are in seconds).

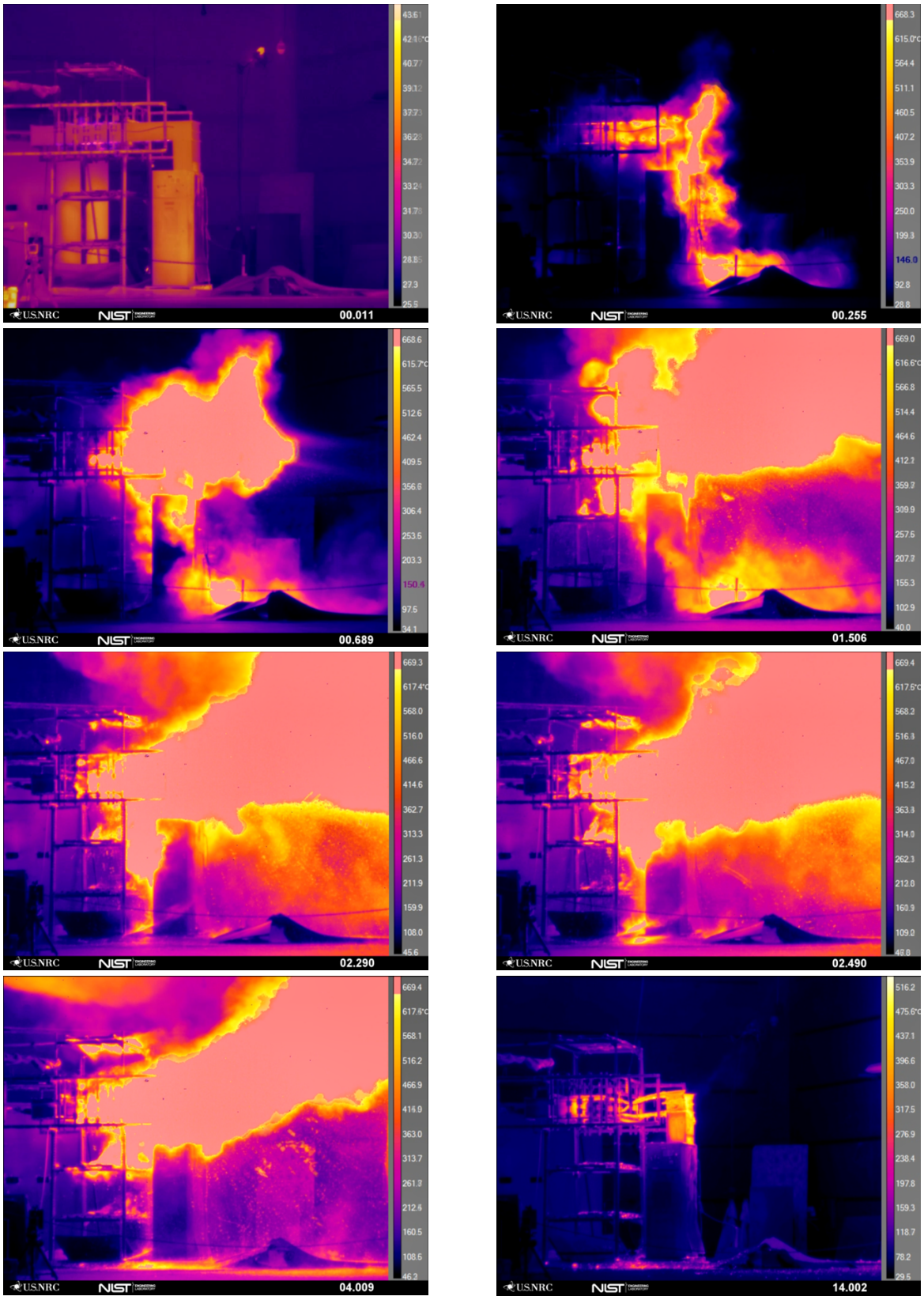


Fig. 51. Sequence of Thermal Images from Experiment 2-28 (image time stamp in seconds)

The enclosure following the experiment is presented in Fig. 52. The enclosure did experience a breach. Most of the bus duct beyond the end of the bus bars is missing on the horizontal straight section. In addition, the end of the 90-degree duct elbow experienced a breach with most of the material missing post-experiment.

Fig. 52. Enclosure Post-Experiment 2-28.

An image of the bus bars removed from the enclosure after the experiment is shown in Fig. 53. The total mass loss of the bus bars was 5 096.5 g ±1 g. Additional details are presented in Appendix C.

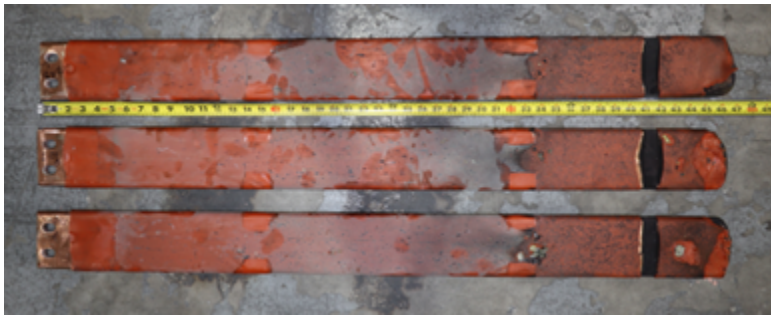

Fig. 53. Photo of Experiment 2-28 bus bars post-experiment (arc location shown right).

### 3.6.2. Measurements

Measurements made during Experiment 2-28 are presented below. These measurements include:

- Thermal
  - Heat flux – Plate Thermometers, Tcap Slug Calorimeters
  - Incident Energy – ASTM Slug Calorimeters, Tcap Slug Calorimeters, Plate Thermometers
  - Temperature – Thermocouple inside of switchgear

- Pressure
  - Internal pressure
- Mass Loss
  - Pre- / Post-experimental measurements
- Electrical
  - Voltage profiles
  - Current profiles
  - Power and energy profiles

#### 3.6.2.1. Thermal Measurements

Thermal measurements from the active instruments are reported below for Experiment 2-28. These include PT measurements in Table 33, ASTM Slug Calorimeter measurements in Table 34, and $T_{cap}$ slug measurements in Table 35. The maximum reading is identified with bold text. The maximum temperature of the sheathed thermocouple located in the switchgear was 1 367 °C ± 10 °C.

Table 33. Summary of plate thermometer measurements Experiment 2-28

| Rack No. | Plate No. | Location | Max Heat Flux (kW/m²) Greater of ± 1 kW/m² or ± 5 % | Average Heat Flux During Arc (kW/m²) Greater of ±1 kW/m² or ± 5 % | Total Incident Energy (kJ/m²) ± 15 % | Notes |
|---|---|---|---|---|---|---|
| **1** | 1 | Top | 856 | 551 | 2 090 | |
| **1** | 3 | Mid-Right | 408 | 286 | 1 070 | |
| **1** | 5 | Mid-Center | 702 | 520 | 1 940 | |
| **1** | 7 | Mid-Left | 605 | 422 | 1 570 | |
| **1** | 9 | Bottom | 370 | 273 | 1 030 | |
| **2** | 10 | Top | 1 056 | 628 | 2 440 | |
| **2** | 12 | Mid-Right | 366 | 269 | 1 010 | |
| **2** | 14 | Mid-Center | 500 | 356 | 1 340 | |
| **2** | 16 | Mid-Left | 1 480 | 268 | 1 000 | |
| **2** | 18 | Bottom | 338 | 238 | 880 | |
| **3** | 19 | Top | 566 | 380 | 1 420 | |
| **3** | 21 | Mid-Right | 542 | 283 | 1 090 | |
| **3** | 23 | Mid-Center | 732 | 437 | 1 630 | |
| **3** | 25 | Mid-Left | 909 | 563 | 2 130 | |
| **3** | 27 | Bottom | - - - | - - - | - - - | EMI |
| **4** | 28 | Top | 1 277 | 426 | 1 620 | |
| **4** | 30 | Mid-Right | 1 310 | **640** | **2 520** | |
| **4** | 32 | Mid-Center | 1 540 | 507 | 2 390 | |

| Rack No. | Plate No. | Location | Max Heat Flux ($kW/m^2$) Greater of ± 1 $kW/m^2$ or ± 5 % | Average Heat Flux During Arc ($kW/m^2$) Greater of ±1 $kW/m^2$ or ± 5 % | Total Incident Energy ($kJ/m^2$) ± 15 % | Notes |
|---|---|---|---|---|---|---|
| **4** | 34 | Mid-Left | 827 | 509 | 2 300 | |
| **4** | 36 | Bottom | 1 433 | 531 | 1 980 | |
| **5** | 37 | Front | 507 | 148 | 560 | |
| **5** | 39 | Center-Right | 2 121 | 307 | 1 230 | |
| **5** | 41 | Center-Mid | 1 832 | 382 | 1 670 | |
| **5** | 43 | Center-Left | **3 358** | 125 | 2 350 | |
| **5** | 45 | Back | 563 | 158 | 600 | |

Table 34. Summary of ASTM slug calorimeter measurements, Experiment 2-28

| Rack No. | ASTM No. | Location | Incident Energy ($kJ/m^2$) Greater of ± 18 $kJ/m^2$ or ± 4 % | Time to Max Temperature (s) ± 3 % | Comment |
|---|---|---|---|---|---|
| **1** | A | Top | 1 869 | 4.74 | |
| **1** | B | Bottom | 1 912 | 4.79 | |
| **2** | C | Top | 1 332 | 4.84 | |
| **2** | D | Bottom | 1 518 | 5.81 | |
| **3** | E | Top | 1 387 | 5.90 | |
| **3** | F | Bottom | 1 610 | 6.14 | |
| **4** | G | Top | - - - | - - - | No Signal |
| **4** | H | Bottom | **1 915** | 5.38 | |
| **5** | I | Top | 656 | 8.82 | |
| **5** | J | Bottom | 934 | 14.77 | |

Table 35. Summary of $T_{cap}$ slug measurements, Experiment 2-28

| Rack No. | $T_{cap}$ No. | Location | Heat Flux During Arc (kW/m$^2$) Greater of ± 1.5 kW/m$^2$ or ± 2.9 % | Incident Energy During Arc Phase (kJ/m$^2$) Greater of ± 2.4 kJ/m$^2$ or ± 5 % | Total Incident Energy (kJ/m$^2$) Greater of ± 2.4 kJ/m$^2$ or ± 5 % |
|---|---|---|---|---|---|
| **1** | 2 | Top | 555.1 | 1 729.5 | 2 754.2 |
| **1** | 4 | Mid-Right | 513.4 | 1 638.3 | 2 383.6 |
| **1** | 6 | Mid-Left | 641.3 | 2 062.2 | 2 458.0 |
| **1** | 8 | Bottom | 494.7 | 1 557.8 | 2 242.8 |
| **2** | 11 | Top | 509.2 | 1 421.8 | 2 319.1 |
| **2** | 13 | Mid-Right | 471.4 | 1 476.7 | 1 745.9 |
| **2** | 15 | Mid-Left | 523.8 | 1 629.4 | 2 016.5 |
| **2** | 17 | Bottom | 361.8 | 1 051.8 | 1 507.0 |
| **3** | 20 | Top | 483.2 | 1 246.0 | 1 951.1 |
| **3** | 22 | Mid-Right | 511.1 | 1 340.0 | 1 799.2 |
| **3** | 24 | Mid-Left | 605.2 | 1 592.6 | 2 289.4 |
| **3** | 26 | Bottom | 534.5 | 1 286.2 | 2 088.2 |
| **4** | 29 | Front | 279.0 | 685.4 | 2 484.9 |
| **4** | 31 | Center-Right | 757.3 | **2 033.1** | 3 430.6 |
| **4** | 33 | Center-Left | 581.9 | 1 636.5 | **3 729.5** |
| **4** | 35 | Back | 565.0 | 1 408.8 | 2 686.1 |
| **5** | 38 | Front | 191.9 | 531.5 | 2 785.6 |
| **5** | 40 | Center-Right | 317.0 | 825.3 | 2 064.3 |
| **5** | 42 | Center-Left | 173.7 | 534.6 | 704.9 |
| **5** | 44 | Back | 177.3 | 505.8 | 807.8 |

### 3.6.2.2. Pressure Measurements

The pressure profiles for the first two tenths of a second are shown in Fig. 54. After the initial pressure spike, the pressure rapidly decays to a relative steady state. The maximum change in pressure in the switchgear is approximately 20 kPa (2.9 psi) above ambient at its peak.

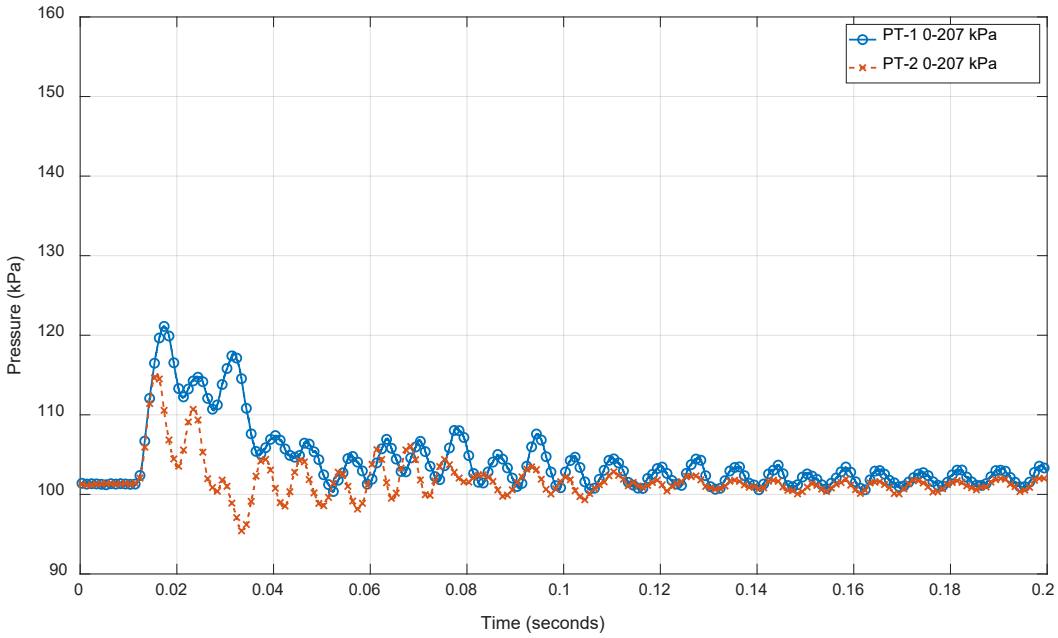


Fig. 54. Pressure measurements from Experiment 2-28. Measurement uncertainty ± 3 percent.

### 3.6.2.3. Electrical Measurements

Experiment 2-28 used KEMA circuit S02 and is reported in Appendix E. Full-level circuit checks (calibration experiments) were performed prior to the experiment to verify the experimental parameters were acceptable. The KEMA report (Appendix E) identifies this experiment as 220830-9001. Key experimental measurements are presented in Table 36. Plots of the electrical measurements are presented in Appendix B.

Table 36. Key measurement from Experiment 2-28. Measurement uncertainty ± 3 percent.

| Phase | Units | A | B | C |
|---|---|---|---|---|
| **Applied voltage, phase-to-ground** | $kV_{RMS}$ | 2.41 | 2.41 | 2.41 |
| **Applied voltage, phase-to-phase** | $kV_{RMS}$ | | 4.17 | |
| **Making current** | $kA_{peak}$ | 51.7 | 65.2 | -66.8 |
| **Current, AC component, beginning** | $kA_{RMS}$ | 31.9 | 33.3 | 29.8 |
| **Current, AC component, middle** | $kA_{RMS}$ | 27.6 | 29.3 | 27.4 |
| **Current, AC component, end** | $kA_{RMS}$ | 26.0 | 27.9 | 25.4 |
| **Current, AC component, average** | $kA_{RMS}$ | 28.1 | 29.7 | 27.5 |
| **Current, AC component, three-phase average** | $kA_{RMS}$ | | 28.4 | |
| **Duration** | s | 4.03 | 4.03 | 4.03 |
| **Arc Energy** | MJ | | 152.6 | |

## 3.7. Experiment 2-30 – 4.16 kV, 30 kA, 4 s Duration, Aluminum Bus, Steel Enclosure

Experiment 2-30 was performed on August 26, 2022, at 8:49 AM eastern daylight time (EDT). The temperature was approximately 24 °C (76 °F), approximately 85 percent relative humidity and approximately 100.7 kPa of pressure. The weather was partly cloudy with a wind of approximately 8 km/h (5 mi/h) out of the southwest.

The arc wire was located at the center of the duct section. A strip of insulation, approximately 2.5 cm (1 in) long, was removed from each of the three bus conductors and the arcing wire was wrapped around each conductor. The arcing wire and installation location are presented in Fig. 55.

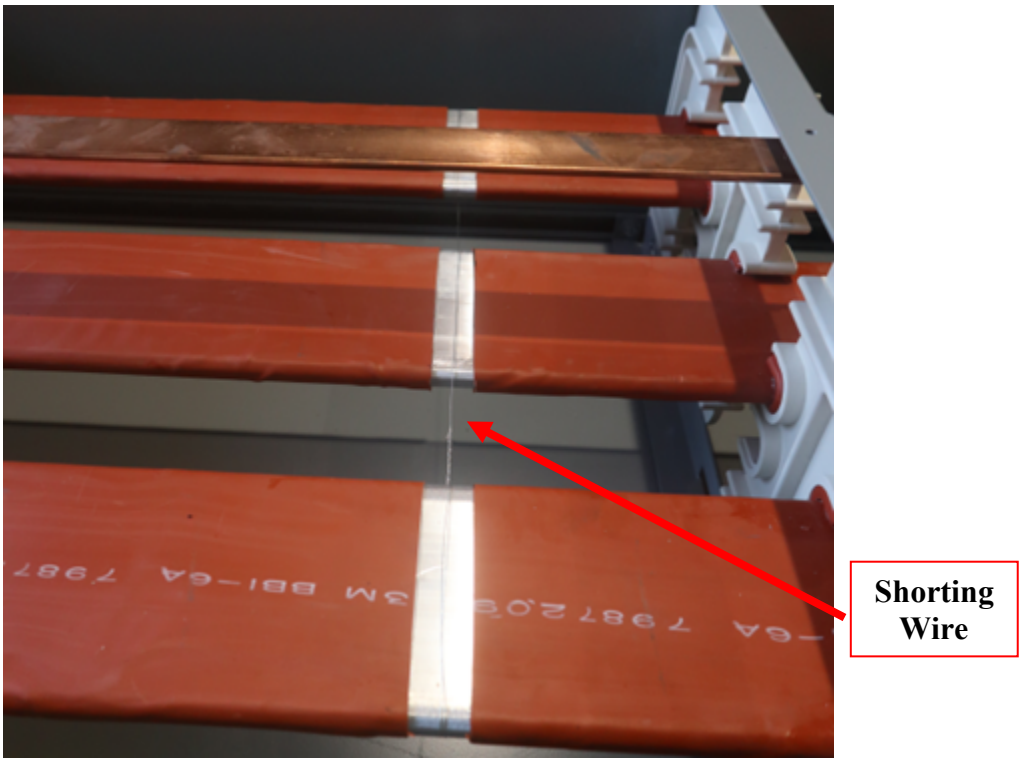


Fig. 55. Shorting wire location Experiment 2-30. Note that the bus duct is inverted in this photo. Unsheathed ground bar is located on the bottom of the enclosure.

### 3.7.1. Observations

The observations documented below are based on review of video and thermal imaging that was taken during the experiment. The observations are provided in Table 37 and include an approximate time reference. Corresponding images are provided in Fig. 57, with thermography images presented in Fig. 58.

Fig. 56 shows changes made to reinforce the panel bolting and provide additional pressure relief. These changes were discussed with the NRC/EPRI working group members, who agreed that the changes would help make the experiments consistent with operating experience.

During the HEAF experiment, the arc migrated away from the arc initiation location and stabilized near the end of the bus bars (away from power supply). Arc migration toward the switchgear resulted in arc ejecta and energy release being directed away from the center of the instrumentation racks which limited the thermal energy reaching the instruments. The arc lasted the expected 4.05 s.

Minor degradation of the bus bars was observed at the arc initiation point, while more extensive damage occurred near the ends of the bus bars. Enclosure breaching from arc damage was observed on all four sides of the bus duct. No visible cable damage was observed, however, the red insulation material on the bus bars separated from the conductors and ignited causing a dripping liquid fire. After the HEAF event, $CO_2$ fire suppression agent was applied to the duct and local hot spots on the racks and floor.

This experiment caused damage to the KEMA power supply bus. The A phase incoming power supply was severely damaged and impacted the resulting A phase arc voltage measurements. The cause of the incident was most likely a loose bolted connection on the A phase connection between the A phase incoming power supply and the A phase bus duct conductor. The loose connection caused a high resistance connection which began arcing at the start of power flow. After the KEMA supply buses in the test cell were cleaned and hi-pot tested, the system was found to be acceptable and the experimental series continued.


Fig. 56. Photo showing changes to duct enclosure to increase ability of panel to remain intact. Approximately, (13 mm (0.5 in) air gap offset from bus duct flange and end panel – far left; Extra bolts to secure panel – left; Panel bolts added to splice plate end of straight bus duct section - right)

Table 37. Observations from Experiment 2-30

| Time (ms) | Observation |
|---|---|
| **0** | Initial light observed |
| **100** | Luminescent flash zone reaches rack 3 and 4 |
| **266** | Particle ejecta observed |
| **1 000** | Particle ejecta observed outside of cell |
| **2 886** | Cell fully engulfed with smoke |
| **4 003** | End of arc |
| **7 007** | Smoke clear near hot duct section |


Fig. 57. Sequence of Images from Experiment 2-30 (image time stamps are in seconds).

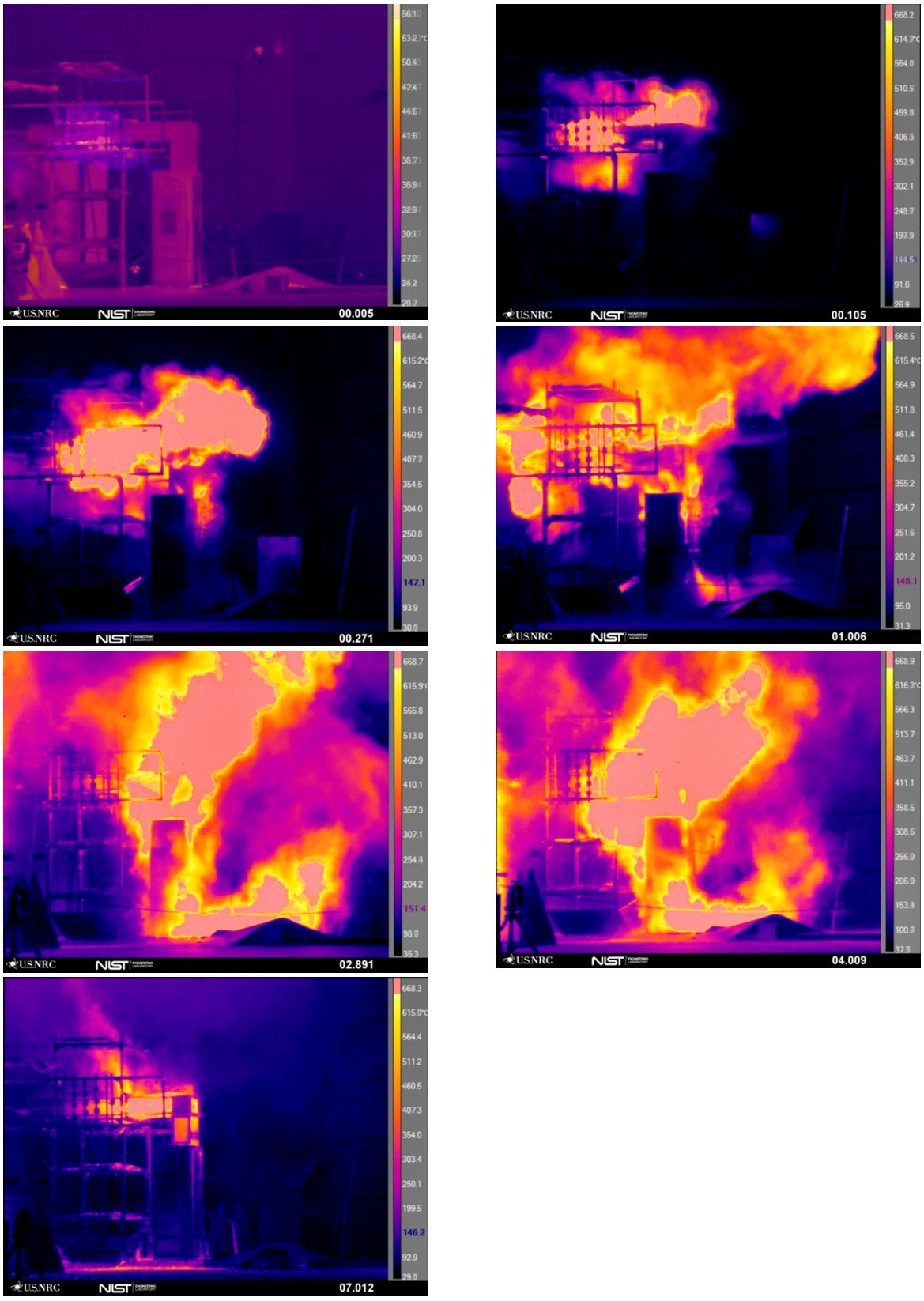


Fig. 58. Sequence of Thermal Images from Experiment 2-30 (image time stamp in seconds)

A photograph of the enclosure following the experiment is presented in Fig. 59. The enclosure did experience a breach. Openings were observed on all sides of the bus duct near the ends of the bus bar.

Fig. 59. Enclosure Post-Experiment 2-30.

An image of the bus bars in the enclosure after the experiment are shown in Fig. 60. The total mass loss of the bus bars was 4 445.5 g ±1 g. Additional details are presented in Appendix C.

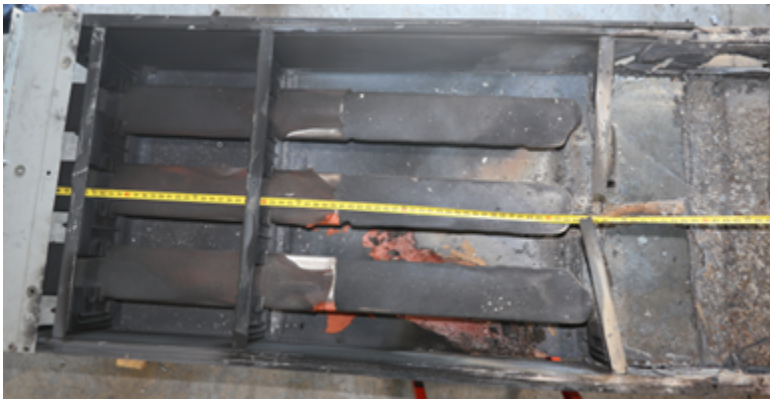

Fig. 60. Photo of Experiment 2-30 bus bars post-experiment (arc location shown right).

### 3.7.2. Measurements

Measurements made during Experiment 2-30 are presented below. These measurements include:

- Thermal
  - Heat flux – Plate Thermometers, Tcap Slug Calorimeters
  - Incident Energy – ASTM Slug Calorimeters, Tcap Slug Calorimeters, Plate Thermometers
  - Temperature – Thermocouple inside of switchgear
- Pressure
  - Internal pressure
- Mass Loss
  - Pre- / Post-experimental measurements
- Electrical
  - Voltage profiles
  - Current profiles
  - Power and energy profiles

#### 3.7.2.1. Thermal Measurements

Thermal measurements from the active instruments are reported below for Experiment 2-30. These include PT measurements in Table 38, ASTM Slug Calorimeter measurements in Table 39, and $T_{cap}$ slug measurements in Table 40. The maximum reading is identified with bold text. The maximum temperature of the sheathed thermocouple located in the switchgear was approximately 1 402 °C, which exceeds the maximum manufacturer calibrated Type K thermocouple temperature of 1 372 °C ± 10 °C. The thermocouple failed shortly after reporting this temperature.

Table 38. Summary of plate thermometer measurements Experiment 2-30

| Rack No. | Plate No. | Location | Max Heat Flux (kW/m$^2$) Greater of ± 1 kW/m$^2$ or ± 5 % | Average Heat Flux During Arc (kW/m$^2$) Greater of ±1 kW/m$^2$ or ± 5 % | Total Incident Energy (kJ/m$^2$) ± 15 % | Notes |
|---|---|---|---|---|---|---|
| **1** | 1 | Top | 453 | 166 | 690 | |
| **1** | 3 | Mid-Right | 396 | 101 | 410 | |
| **1** | 5 | Mid-Center | 516 | 128 | 530 | |
| **1** | 7 | Mid-Left | 370 | 104 | 470 | |
| **1** | 9 | Bottom | 194 | 79 | 320 | |
| **2** | 10 | Top | 463 | 218 | 870 | |
| **2** | 12 | Mid-Right | 602 | 196 | 750 | |
| **2** | 14 | Mid-Center | 955 | 277 | 1 040 | |

| Rack No. | Plate No. | Location | Max Heat Flux (kW/m$^2$) Greater of ± 1 kW/m$^2$ or ± 5 % | Average Heat Flux During Arc (kW/m$^2$) Greater of ±1 kW/m$^2$ or ± 5 % | Total Incident Energy (kJ/m$^2$) ± 15 % | Notes |
|---|---|---|---|---|---|---|
| **2** | 16 | Mid-Left | - - - | - - - | - - - | Inoperable prior to experiment (IPE) |
| **2** | 18 | Bottom | 503 | 156 | 580 | |
| **3** | 19 | Top | 211 | 94 | 480 | |
| **3** | 21 | Mid-Right | - - - | - - - | - - - | IPE |
| **3** | 23 | Mid-Center | 211 | 102 | 650 | |
| **3** | 25 | Mid-Left | 272 | 127 | 760 | |
| **3** | 27 | Bottom | 219 | 114 | 500 | |
| **4** | 28 | Top | 507 | 143 | 630 | |
| **4** | 30 | Mid-Right | **4 094** | **433** | **1 950** | |
| **4** | 32 | Mid-Center | 1 248 | 235 | 900 | |
| **4** | 34 | Mid-Left | 225 | 109 | 550 | |
| **4** | 36 | Bottom | 554 | 172 | 680 | |
| **5** | 37 | Front | 116 | 55 | 330 | |
| **5** | 39 | Center-Right | 250 | 102 | 840 | |
| **5** | 41 | Center-Mid | 599 | 110 | 570 | |
| **5** | 43 | Center-Left | 542 | 109 | 400 | |
| **5** | 45 | Back | 151 | 76 | 400 | |

Table 39. Summary of ASTM slug calorimeter measurements, Experiment 2-30.

| Rack No. | ASTM No. | Location | Incident Energy (kJ/m$^2$) Greater of ± 18 kJ/m$^2$ or ± 4 % | Time to Max Temperature (s) ± 3 % | Comment |
|---|---|---|---|---|---|
| **1** | A | Top | 619 | 24.85 | |
| **1** | B | Bottom | 273 | 15.23 | |
| **2** | C | Top | 893 | 6.46 | |
| **2** | D | Bottom | 922 | 5.00 | |
| **3** | E | Top | 604 | 46.39 | |
| **3** | F | Bottom | 664 | 53.84 | |
| **4** | G | Top | **1 000** | 48.98 | |
| **4** | H | Bottom | 730 | 61.57 | |
| **5** | I | Top | 419 | 9.50 | |
| **5** | J | Bottom | 351 | 13.5 | |

Table 40. Summary of $T_{cap}$ slug measurements, Experiment 2-30.

| Rack No. | $T_{cap}$ No. | Location | Heat Flux During Arc (kW/m$^2$) Greater of ± 1.5 kW/m$^2$ or ± 2.9 % | Incident Energy During Arc Phase (kJ/m$^2$) Greater of ± 2.4 kJ/m$^2$ or ± 5 % | Total Incident Energy (kJ/m$^2$) Greater of ± 2.4 kJ/m$^2$ or ± 5 % |
|---|---|---|---|---|---|
| **1** | 2 | Top | 83.2 | 305.4 | 1 444.9 |
| **1** | 4 | Mid-Right | 78.7 | 308.2 | 1 352.3 |
| **1** | 6 | Mid-Left | 91.2 | 376.1 | 1 229.3 |
| **1** | 8 | Bottom | 69.9 | 259.2 | 1 058.3 |
| **2** | 11 | Top | 454.9 | **1 092.3** | 1 654.6 |
| **2** | 13 | Mid-Right | 305.7 | 807.3 | 1 471.3 |
| **2** | 15 | Mid-Left | **466.9** | 1 086.0 | 1 585.9 |
| **2** | 17 | Bottom | 393.7 | 885.5 | 1 205.7 |
| **3** | 20 | Top | 102.5 | 351.8 | 1 803.9 |
| **3** | 22 | Mid-Right | 77.1 | 263.2 | 1 531.0 |
| **3** | 24 | Mid-Left | 96.8 | 347.5 | 2 097.4 |
| **3** | 26 | Bottom | 79.1 | 311.4 | 1 751.2 |
| **4** | 29 | Front | 258.4 | 643.1 | 2 127.5 |
| **4** | 31 | Center-Right | 259.3 | 646.3 | **2 464.7** |
| **4** | 33 | Center-Left | 160.1 | 552.1 | 1 826.9 |
| **4** | 35 | Back | 100.1 | 184.1 | 294.1 |
| **5** | 38 | Front | 83.0 | 245.1 | 779.0 |
| **5** | 40 | Center-Right | 108.0 | 328.6 | 903.8 |
| **5** | 42 | Center-Left | 71.6 | 240.0 | 696.4 |
| **5** | 44 | Back | 86.5 | 281.7 | 778.2 |

### 3.7.2.2. Pressure Measurements

The pressure profiles for the first two tenths of a second are shown in Fig. 61. After the initial pressure spike, the pressure rapidly decays to a relative steady state. The maximum change in pressure in the primary cable connection compartment is approximately 28.3 kPa (4.1 psi) above ambient at its peak.

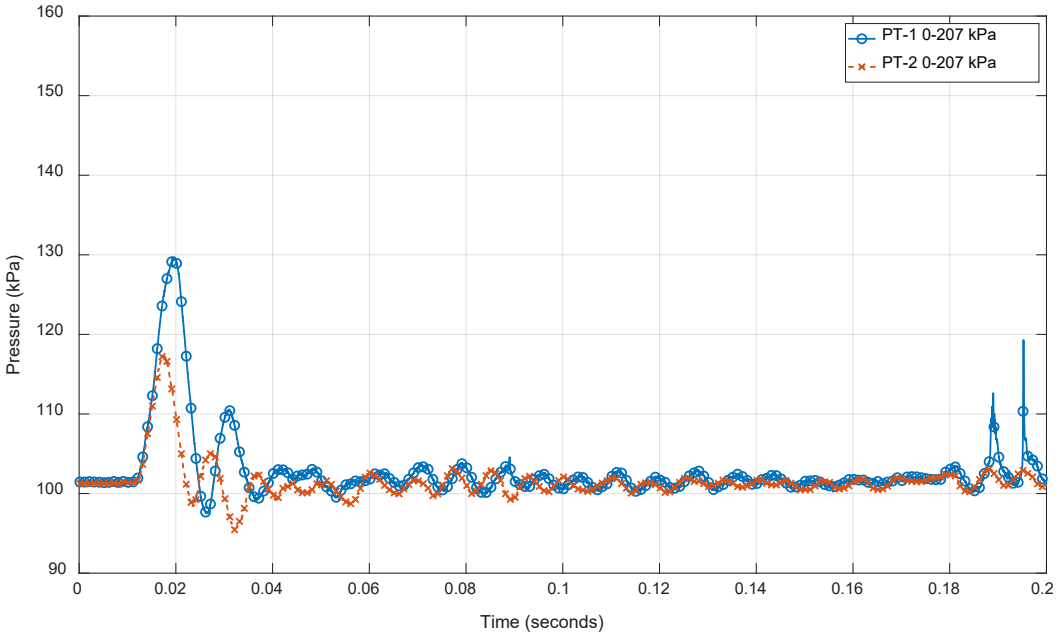


Fig. 61. Pressure measurements from Experiment 2-30 (breaker compartment (red dashes with “x” markers); Main bus [arcing compartment] – (blue line with “o” markers)).
Measurement uncertainty ± 3 percent.

### 3.7.2.3. Electrical Measurements

Experiment 2-30 used KEMA circuit S02 and is reported in Appendix E. Full-level circuit checks (calibration experiments) were performed prior to the experiment to verify the experimental parameters were acceptable. The KEMA report (Appendix E) identifies this experiment as 220826-9001. Key experimental measurements are presented in Table 41. Plots of the electrical measurements are presented in Appendix B.

Table 41. Key measurements from Experiment 2-30. Measurement uncertainty ± 3 percent.

| Phase | Units | A | B | C |
|---|---|---|---|---|
| **Applied voltage, phase-to-ground** | $kV_{RMS}$ | 2.41 | 2.41 | 2.41 |
| **Applied voltage, phase-to-phase** | $kV_{RMS}$ | | 4.17 | |
| **Making current** | $kA_{peak}$ | 48.7 | 64.2 | -63.9 |
| **Current, AC component, beginning** | $kA_{RMS}$ | 30.4 | 33.3 | 27.7 |
| **Current, AC component, middle** | $kA_{RMS}$ | 27.6 | 33.2 | 25.7 |
| **Current, AC component, end** | $kA_{RMS}$ | 24.2 | 31.6 | 25.2 |
| **Current, AC component, average** | $kA_{RMS}$ | 28.0 | 31.0 | 26.4 |
| **Current, AC component, three-phase average** | $kA_{RMS}$ | | 28.4 | |
| **Duration** | s | 4.05 | 4.05 | 4.04 |
| **Arc Energy** | MJ | | 170.8 | |

## 3.8. Experiment 2-30B – 4.16 kV, 30 kA, 4 s Duration, Aluminum Bus, Steel Enclosure

Experiment 2-30B was performed on August 31, 2022, at 10:13 AM eastern daylight time (EDT). The temperature was approximately 27.2 °C (75 °F), approximately 71 percent relative humidity and approximately 100.3 kPa of pressure. The weather was fair with wind of approximately 13 km/h (8 mi/h) out of the west.

The arc wire was located at center of the duct section. A strip of insulation, approximately 2.5cm (1 in) long, was removed from each of the three bus conductors and the arcing wire was wrapped around each conductor. The arc wire installed on the bus is shown in Fig. 62.

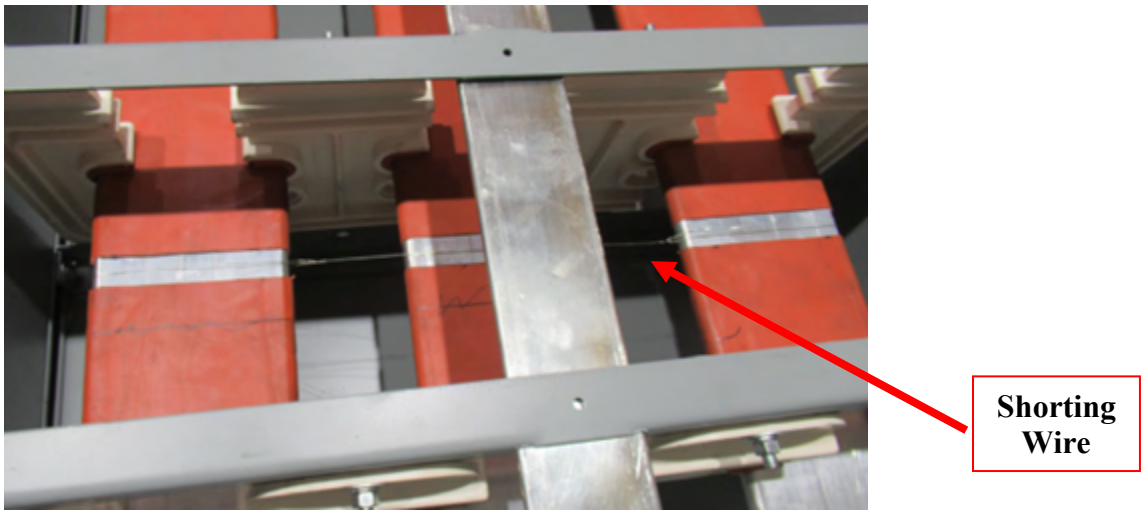


Fig. 62. Shorting wire location Experiment 2-30B. Note, image is from bottom of bus duct with uninsulated ground bus showing in center of image.

### 3.8.1. Observations

Observations documented below are based on a review of the video and thermal imaging that was recorded during the experiment. The observations are provided in Table 42 and include an approximate time reference. Corresponding images are provided in Fig. 63, with thermography images presented in Fig. 64.

This experiment was a repeat of Experiment 2-30, due to the laboratory power supply issue affecting that experiment. During the HEAF, the duct enclosure remained intact without mechanical fastener failure and panel blow off. The arc stabilized at the end of the bus bars, and the enclosure breached on all sides near and slightly beyond the arc location. The enclosure breach was localized to the sensor location. No visible cable damage was observed on any cable coupon sample on the instrument racks. The arc lasted for the expected duration (4.03 s). After the HEAF experiment, $CO_2$ fire suppression agent was applied to the duct and local hot spots on the racks and floor.

Table 42. Observations from Experiment 2-30B

| Time (ms) | Observation |
|---|---|
| **0** | Initial light observed |
| **83** | Luminescent flash zone reaches rack 3 and 4 directly above and below duct |
| **300** | Particle ejecta observed |
| **1 401** | Particle ejecta impinges on right cell wall and smoke reaches overhead crane |
| **3 470** | Particle ejecta observed outside cell and smoke fills most of cell |
| **4 003** | End of arc |
| **5 005** | Hot liquid material falling from duct 1 s after end of arc |
| **8 007** | Smoke clears from view of duct |

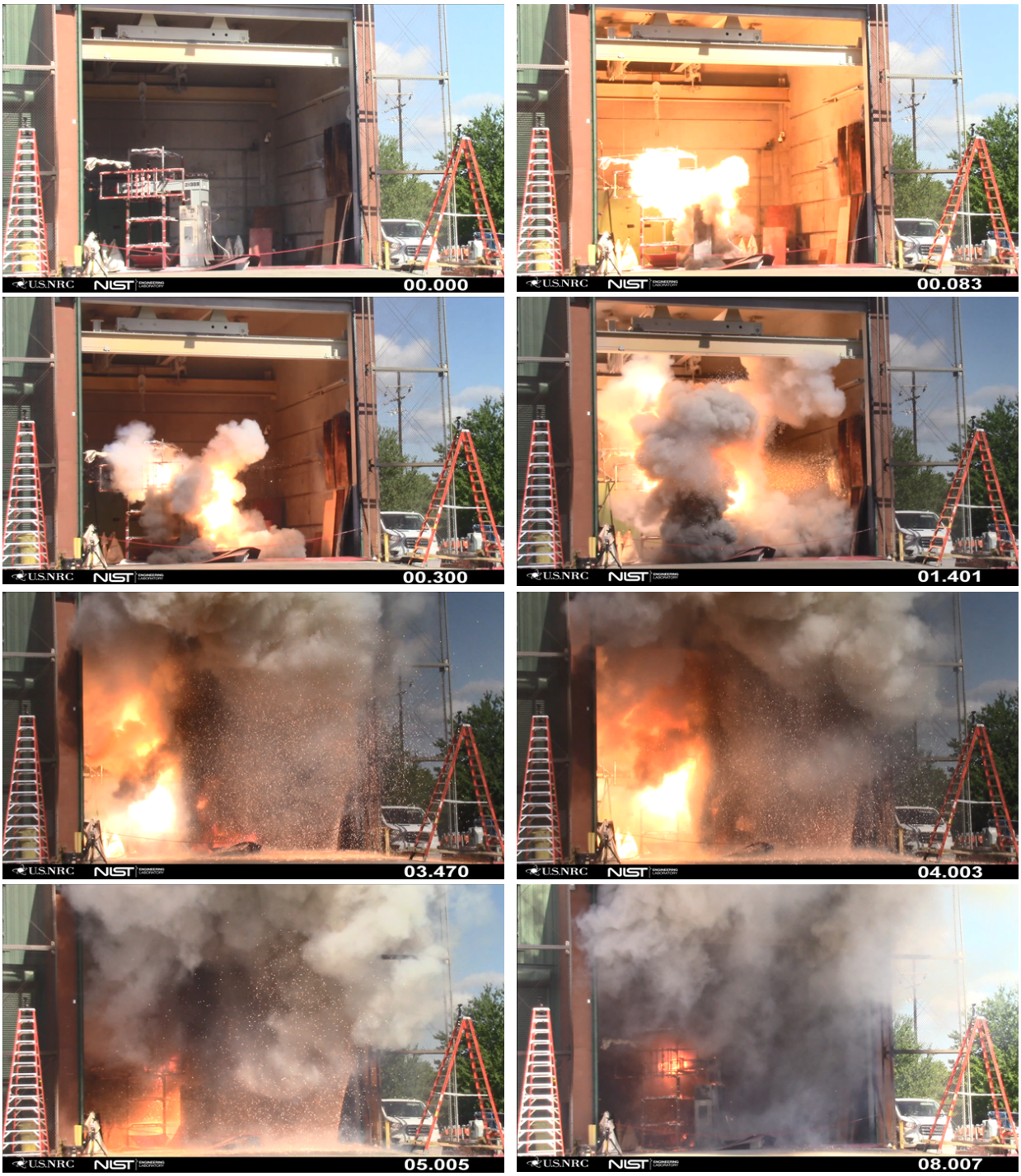


Fig. 63. Sequence of Images from Experiment 2-30B (image time stamps are in seconds).

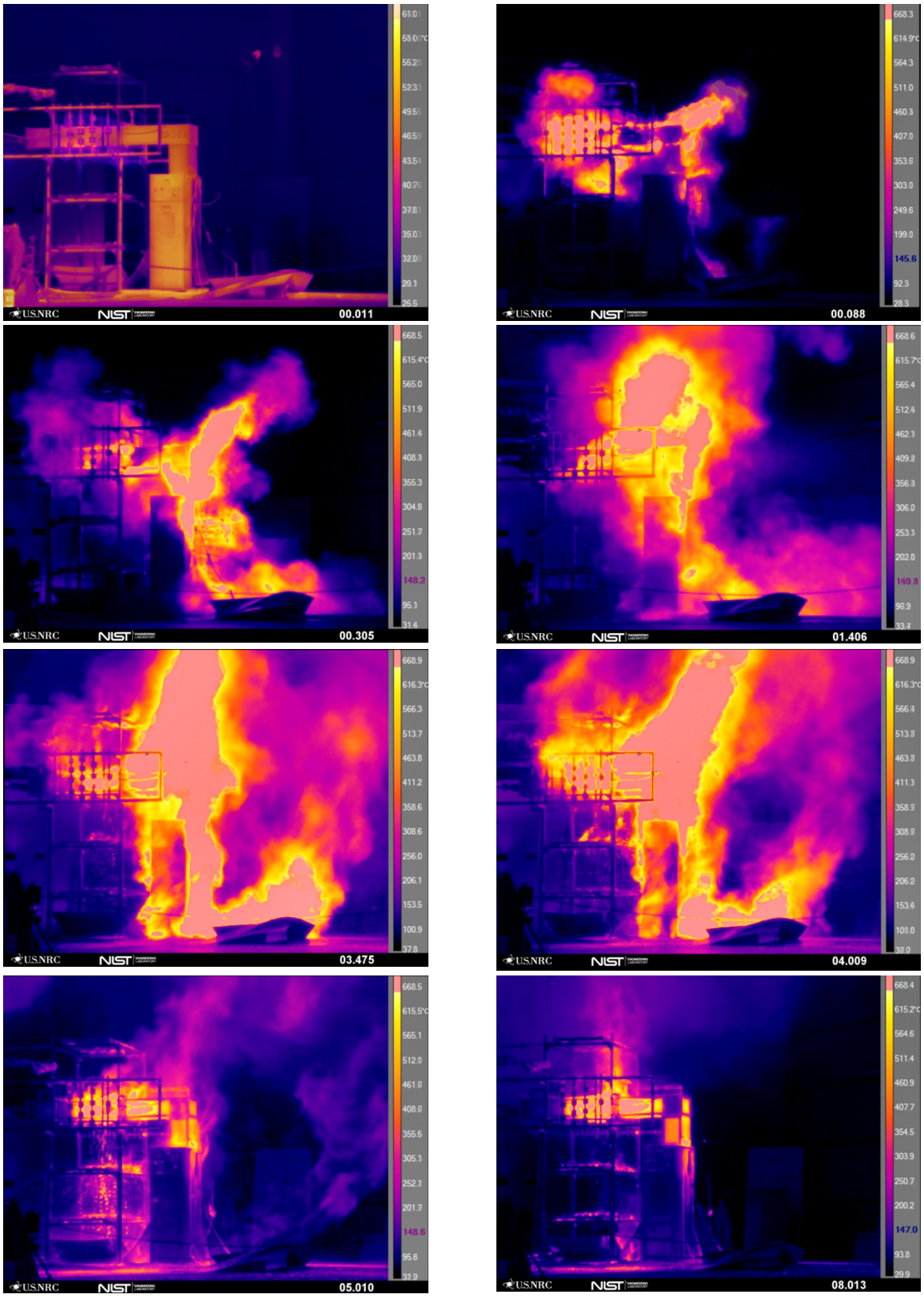


Fig. 64. Sequence of Thermal Images from Experiment 2-30B (image time stamp in seconds)

Photograph of the enclosure following the experiment is presented in Fig. 65. The enclosure did experience a breach. Openings were observed on all sides of the bus duct near the ends of the bus bar.


Fig. 65. Enclosure Post-Experiment 2-30B.

An image of the bus bars removed from the enclosure after the experiment is shown in Fig. 66. The total mass loss of the bus bars was 3 605.0 g ±1 g. Additional details are presented in Appendix C.

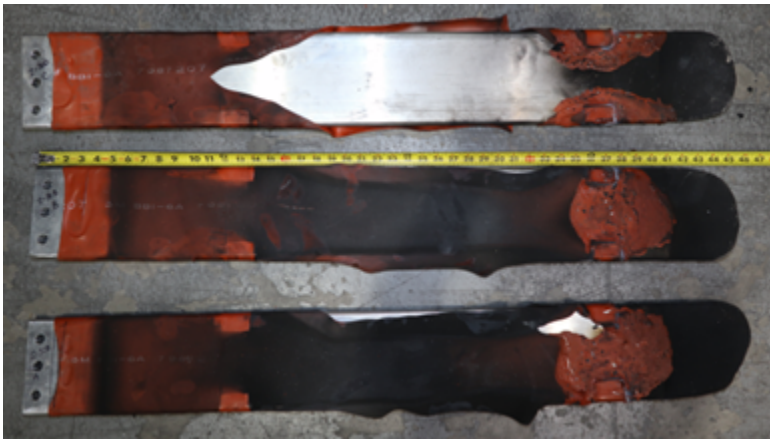

Fig. 66. Photo of Experiment 2-30B bus bars post-experiment (arc location shown center).

### 3.8.2. Measurements

Measurements made during Experiment 2-30B are presented below. These measurements include:

- Thermal
  - Heat flux – Plate Thermometers, Tcap Slug Calorimeters
  - Incident Energy – ASTM Slug Calorimeters, Tcap Slug Calorimeters, Plate Thermometers
  - Temperature – Thermocouple inside of switchgear
- Pressure
  - Internal pressure
- Mass Loss
  - Pre- / Post-experimental measurements
- Electrical
  - Voltage profiles
  - Current profiles
  - Power and energy profiles

#### 3.8.2.1. Thermal Measurements

Thermal measurements from the active instruments are reported below for Experiment 2-30B. These include PT measurements in Table 43, ASTM Slug Calorimeter measurements in Table 44, and $T_{cap}$ slug measurements in Table 45. The maximum reading is identified with bold text. The maximum temperature of the sheathed thermocouple located in the switchgear was approximately 1 576 °C, which exceeds the maximum manufacturer calibrated Type K thermocouple temperature of 1 372 °C ± 10 °C. The thermocouple failed shortly thereafter.

Table 43. Summary of plate thermometer measurements Experiment 2-30B

| Rack No. | Plate No. | Location | Max Heat Flux (kW/m$^2$) Greater of ± 1 kW/m$^2$ or ± 5 % | Average Heat Flux During Arc (kW/m$^2$) Greater of ±1 kW/m$^2$ or ± 5 % | Total Incident Energy (kJ/m$^2$) ± 15 % | Notes |
|---|---|---|---|---|---|---|
| **1** | 1 | Top | 344 | 229 | 920 | |
| **1** | 3 | Mid-Right | 243 | 132 | 630 | |
| **1** | 5 | Mid-Center | 459 | 177 | 890 | |
| **1** | 7 | Mid-Left | 804 | 255 | 1 040 | |
| **1** | 9 | Bottom | 335 | 151 | 620 | |
| **2** | 10 | Top | 465 | 245 | 960 | |
| **2** | 12 | Mid-Right | 470 | 198 | 820 | |
| **2** | 14 | Mid-Center | 1 085 | 298 | 1 170 | |
| **2** | 16 | Mid-Left | 313 | 131 | 570 | |

| Rack No. | Plate No. | Location | Max Heat Flux (kW/m$^2$) Greater of ± 1 kW/m$^2$ or ± 5 % | Average Heat Flux During Arc (kW/m$^2$) Greater of ±1 kW/m$^2$ or ± 5 % | Total Incident Energy (kJ/m$^2$) ± 15 % | Notes |
|---|---|---|---|---|---|---|
| **2** | 18 | Bottom | 267 | 116 | 510 | |
| **3** | 19 | Top | 455 | 208 | 980 | |
| **3** | 21 | Mid-Right | 342 | 156 | 920 | |
| **3** | 23 | Mid-Center | 422 | 236 | 1 270 | |
| **3** | 25 | Mid-Left | 692 | 371 | 1 510 | |
| **3** | 27 | Bottom | 358 | 206 | 980 | |
| **4** | 28 | Top | 338 | 142 | 980 | |
| **4** | 30 | Mid-Right | 390 | 173 | 1 300 | |
| **4** | 32 | Mid-Center | 5 161 | **610** | **4 800** | |
| **4** | 34 | Mid-Left | 289 | 104 | 920 | |
| **4** | 36 | Bottom | 1 673 | 269 | 1 720 | |
| **5** | 37 | Front | 1 246 | 103 | 1 410 | |
| **5** | 39 | Center-Right | - - - | - - - | - - - | Inoperable prior to experiment (IPE) |
| **5** | 41 | Center-Mid | **5 809** | 167 | 3 830 | |
| **5** | 43 | Center-Left | 1 558 | 56 | 1 680 | |
| **5** | 45 | Back | 589 | 53 | 630 | |

Table 44. Summary of ASTM slug calorimeter measurements, Experiment 2-30B

| Rack No. | ASTM No. | Location | Incident Energy (kJ/m$^2$) Greater of ± 18 kJ/m$^2$ or ± 4 % | Time to Max Temperature (s) ± 3 % | Comment |
|---|---|---|---|---|---|
| **1** | A | Top | 1 132 | 18.74 | |
| **1** | B | Bottom | 1 088 | 13.49 | |
| **2** | C | Top | 1 068 | 14.66 | |
| **2** | D | Bottom | 824 | 15.09 | |
| **3** | E | Top | 1 413 | 38.74 | |
| **3** | F | Bottom | 1 439 | 31.74 | |
| **4** | G | Top | **2 572** | 20.86 | |
| **4** | H | Bottom | 1 532 | 41.19 | |
| **5** | I | Top | 624 | 21.84 | |
| **5** | J | Bottom | 500 | 22.99 | |

Table 45. Summary of $T_{cap}$ slug measurements, Experiment 2-30B

| Rack No. | $T_{cap}$ No. | Location | Heat Flux During Arc (kW/m$^2$) Greater of ± 1.5 kW/m$^2$ or ± 2.9 % | Incident Energy During Arc Phase (kJ/m$^2$) Greater of ± 2.4 kJ/m$^2$ or ± 5 % | Total Incident Energy (kJ/m$^2$) Greater of ± 2.4 kJ/m$^2$ or ± 5 % |
|---|---|---|---|---|---|
| **1** | 2 | Top | 337.7 | **988.8** | 2 238.2 |
| **1** | 4 | Mid-Right | 255.1 | 718.6 | 1 898.8 |
| **1** | 6 | Mid-Left | 321.7 | 672.2 | 1 654.8 |
| **1** | 8 | Bottom | 223.3 | 554.6 | 1 688.2 |
| **2** | 11 | Top | 362.0 | 913.2 | 2 190.5 |
| **2** | 13 | Mid-Right | 332.1 | 780.2 | 2 081.5 |
| **2** | 15 | Mid-Left | 345.3 | 812.3 | 2 111.8 |
| **2** | 17 | Bottom | 388.1 | 827.0 | 1 881.4 |
| **3** | 20 | Top | 335.4 | 962.3 | 3 114.5 |
| **3** | 22 | Mid-Right | 260.8 | 692.9 | 2 793.7 |
| **3** | 24 | Mid-Left | 298.3 | 692.2 | 3 567.0 |
| **3** | 26 | Bottom | 288.6 | 755.4 | 2 967.2 |
| **4** | 29 | Front | 231.3 | 511.8 | 3 117.6 |
| **4** | 31 | Center-Right | **461.7** | 688.4 | **10 266.2** |
| **4** | 33 | Center-Left | 181.1 | 333.8 | 2 857.6 |
| **4** | 35 | Back | 226.1 | 358.7 | 3 484.0 |
| **5** | 38 | Front | 59.5 | 142.3 | 1 088.7 |
| **5** | 40 | Center-Right | 160.8 | 308.9 | 1 492.1 |
| **5** | 42 | Center-Left | 76.9 | 175.9 | 1 064.1 |
| **5** | 44 | Back | 85.9 | 165.5 | 1 047.1 |

### 3.8.2.2. Pressure Measurements

The pressure profiles for the first two tenths of a second are shown in Fig. 67. After the initial pressure spike, the pressure rapidly decays to a relative steady state. The maximum change in pressure in the switchgear enclosure is approximately 24.0 kPa (3.5 psi) above ambient at its peak.

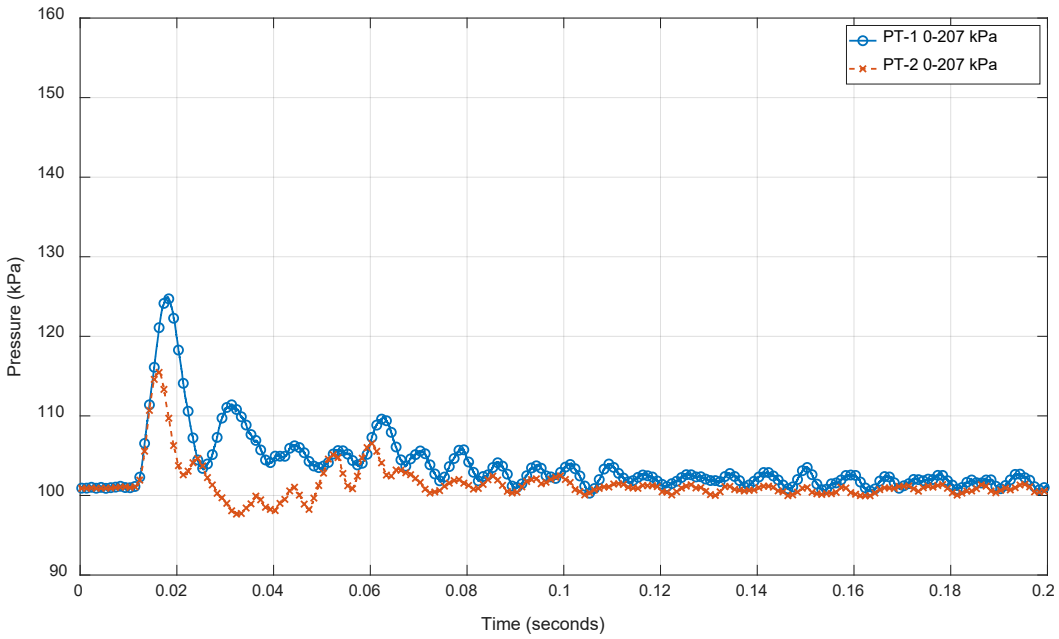


Fig. 67. Pressure measurements from Experiment 2-30B (breaker compartment (red dashed line with "x" marker); Main bus [arcing compartment] – (Blue solid line with "o" marker)). Measurement uncertainty ± 3 percent.

### 3.8.2.3. Electrical Measurements

Experiment 2-30B used KEMA circuit S02 and is reported in Appendix E. Full-level circuit checks (calibration experiments) were performed prior to the experiment to verify the experimental parameters were acceptable. The KEMA report (Appendix E) identifies this experiment as 220831-9001. Key experimental measurements are presented in Table 46. Plots of the electrical measurements are presented in Appendix B.

Table 46. Key measurement from Experiment 2-30B. Measurement uncertainty ± 3 percent.

| Phase | Units | A | B | C |
|---|---|---|---|---|
| **Applied voltage, phase-to-ground** | $kV_{RMS}$ | 2.41 | 2.41 | 2.41 |
| **Applied voltage, phase-to-phase** | $kV_{RMS}$ | | 4.17 | |
| **Making current** | $kA_{peak}$ | 49.2 | 63.7 | -65.0 |
| **Current, AC component, beginning** | $kA_{RMS}$ | 30.3 | 32.4 | 28.9 |
| **Current, AC component, middle** | $kA_{RMS}$ | 27.3 | 30.9 | 27.6 |
| **Current, AC component, end** | $kA_{RMS}$ | 25.7 | 28.6 | 26.5 |
| **Current, AC component, average** | $kA_{RMS}$ | 28.4 | 30.0 | 27.9 |
| **Current, AC component, three-phase average** | $kA_{RMS}$ | | 28.8 | |
| **Duration** | s | 4.03 | 4.03 | 4.03 |
| **Arc Energy** | MJ | | 134.3 | |

## 3.9. Experiment 2-31 – 4.16 kV, 30 kA, 2 s Duration, Aluminum Bus, Aluminum Enclosure

Experiment 2-31 was performed on September 1, 2022, at 9:19 AM eastern daylight time (EDT). The temperature was approximately 22 °C (72 °F), approximately 61 percent relative humidity and approximately 100.7 kPa of pressure. The weather was fair with wind of approximately 11 km/h (7 mi/h) out of the west-southwest.

The arc wire was located at the center of the duct section. A strip of insulation, approximately 2.5cm (1 in) long, was removed from each of the bus conductors (nine in total) and the arcing wire was wrapped around all conductors. The arcing wire and installation location are shown in Fig. 68.

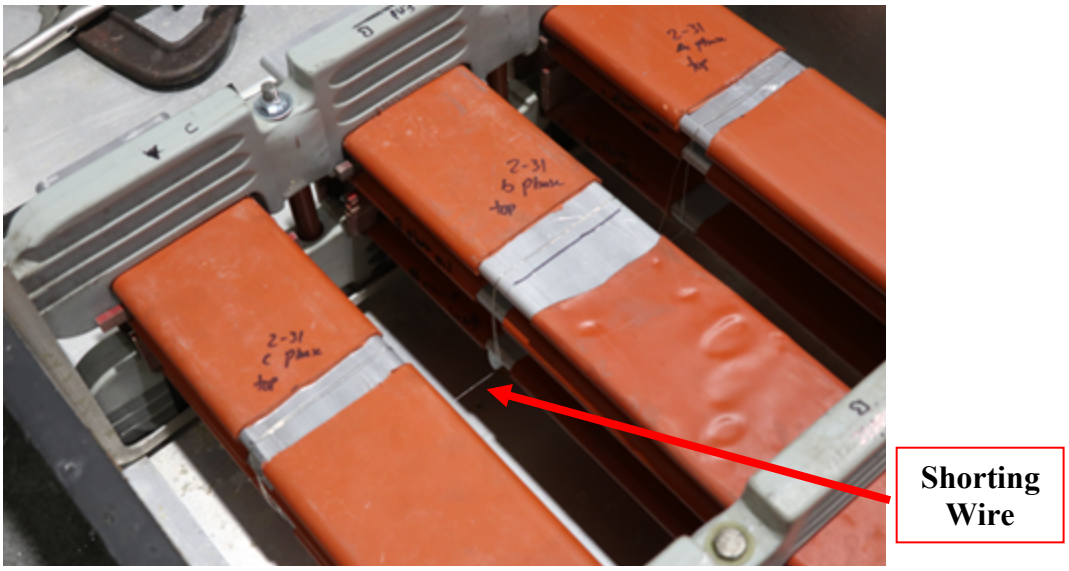


Fig. 68. Shorting wire location Experiment 2-31

### 3.9.1. Observations

Observations documented below are based on review of video and thermal imaging that was taken during the experiment. The observations are provided in Table 47 and include an approximate time reference. Corresponding images are provided in Fig. 69, with thermography images presented in Fig. 70.

This was the first aluminum enclosure with aluminum bus bars examined in the series of experiments. The bus duct assembly was acquired from a nuclear facility undergoing decommissioning and had the same voltage and continuous current carrying rating as other ducts examined in this series. The duct had three conductors per phase, with all conductors constructed of aluminum.

After the experiment, aluminum slag was found throughout the test cell and courtyard with the majority of slag found below the duct. No visible damage was observed an any of the cable coupon samples mounted on the instrument racks. Carbon dioxide ($CO_2$) fire suppression agent was applied to the duct and local hot spots on the racks and floor. The arc lasted for the expected duration of 2.02 s.

Table 47. Observations from Experiment 2-31

| Time (ms) | Observation |
|---|---|
| **0** | Initial light observed |
| **333** | Particle ejecta observed |
| **617** | Particle ejecta reaches right wall of test cell |
| **1 234** | Smoke reaches overhead crane |
| **2 035** | End of arc |
| **12 012** | Smoke beginning to clear test cell 10 s after end of arc |


Fig. 69. Sequence of Images from Experiment 2-31 (image time stamps are in seconds).

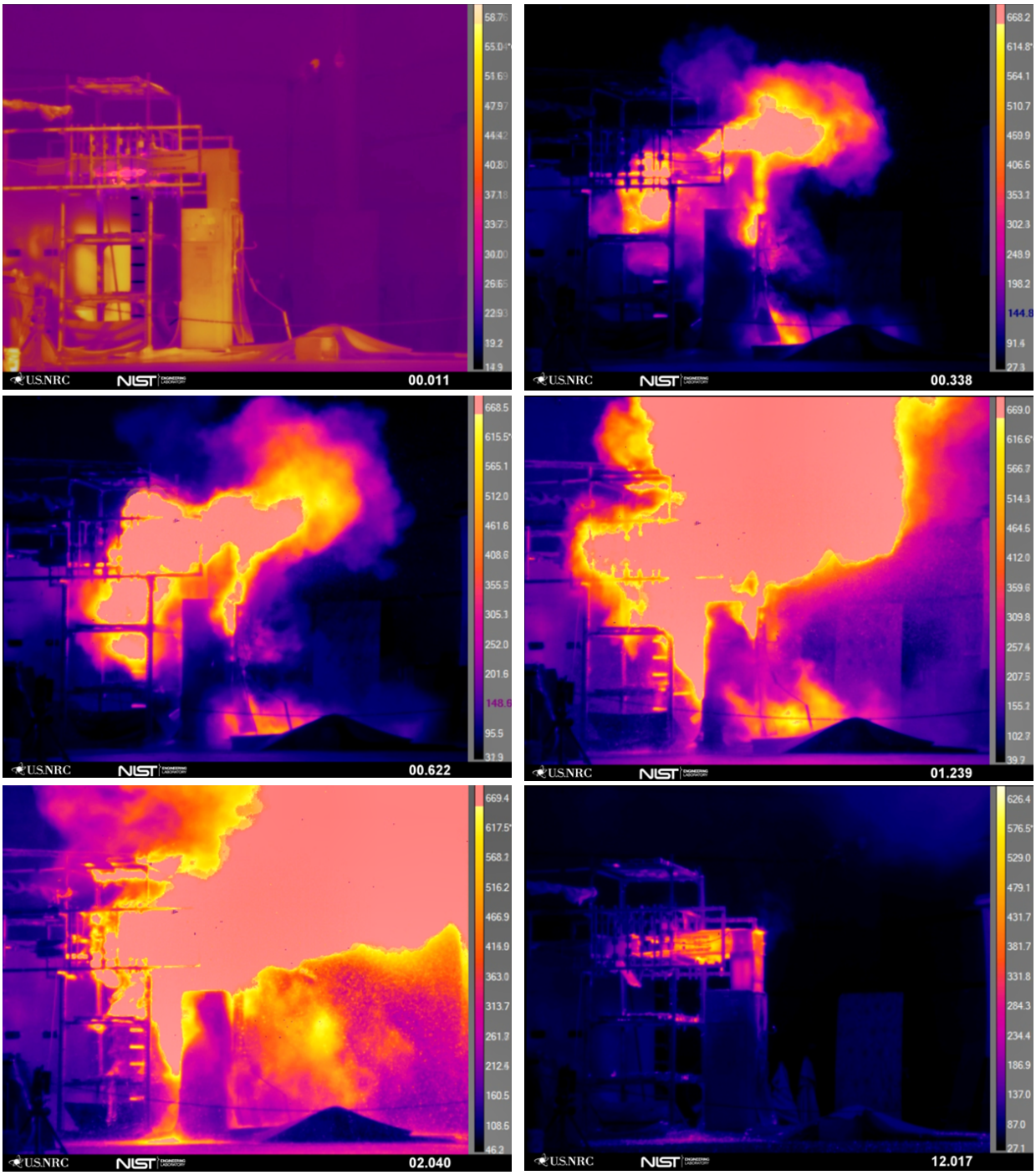


Fig. 70. Sequence of Thermal Images from Experiment 2-31 (image time stamp in seconds)

A photograph of the enclosure following the experiment is shown in Fig. 71. The enclosure did experience a breach, with most of the straight section duct beyond the bus bar ends missing post-experiment. In addition, there were openings in the aluminum 90-degree duct elbow.

Fig. 71. Enclosure Post-Experiment 2-31.

An image of the bus bars in the partially disassembled enclosure after the experiment is shown in Fig. 72. The total mass loss of the bus bars was 2 985.0 g ±1 g. Additional details are presented in Appendix C.

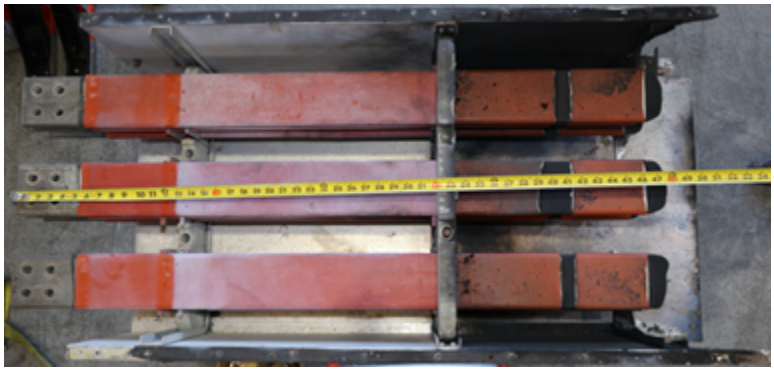

Fig. 72. Photo of Experiment 2-31 bus bars post-experiment (arc location shown right).

### 3.9.2. Measurements

Measurements made during Experiment 2-31 are presented below. These measurements include:

- Thermal
  - Heat flux – Plate Thermometers, Tcap Slug Calorimeter
  - Incident Energy – ASTM Slug Calorimeters. Tcap Slug Calorimeters, Plate Thermometers
  - Temperature – Thermocouple inside of switchgear
- Pressure
  - Internal pressure
- Mass Loss
  - Pre- / Post-experimental measurements
- Electrical
  - Voltage profiles
  - Current profiles
  - Power and energy profiles

#### 3.9.2.1. Thermal Measurements

Thermal measurements from the active instruments are reported below for Experiment 2-31. These include PT measurements in Table 48, ASTM Slug Calorimeter measurements in Table 49, and $T_{cap}$ slug measurements in Table 50. The maximum reading is identified with bold text. The maximum temperature of the sheathed thermocouple located in the switchgear was 960 °C ± 7 °C.

Table 48. Summary of plate thermometer measurements Experiment 2-31

| Rack No. | Plate No. | Location | Max Heat Flux (kW/m²) Greater of ± 1 kW/m² or ± 5 % | Average Heat Flux During Arc (kW/m²) Greater of ±1 kW/m² or ± 5 % | Total Incident Energy (kJ/m²) ± 15 % | Notes |
|---|---|---|---|---|---|---|
| **1** | 1 | Top | 1 210 | 770 | 1 490 | |
| **1** | 3 | Mid-Right | 485 | 384 | 770 | |
| **1** | 5 | Mid-Center | 535 | 384 | 880 | |
| **1** | 7 | Mid-Left | 836 | 540 | 1 050 | |
| **1** | 9 | Bottom | 546 | 356 | 670 | |
| **2** | 10 | Top | 1 506 | **875** | **1 690** | |
| **2** | 12 | Mid-Right | 751 | 501 | 970 | |
| **2** | 14 | Mid-Center | 752 | 529 | 1 070 | |

| Rack No. | Plate No. | Location | Max Heat Flux (kW/m$^2$) Greater of ± 1 kW/m$^2$ or ± 5 % | Average Heat Flux During Arc (kW/m$^2$) Greater of ±1 kW/m$^2$ or ± 5 % | Total Incident Energy (kJ/m$^2$) ± 15 % | Notes |
|---|---|---|---|---|---|---|
| **2** | 16 | Mid-Left | 632 | 436 | 830 | |
| **2** | 18 | Bottom | 446 | 329 | 630 | |
| **3** | 19 | Top | 870 | 533 | 1 030 | |
| **3** | 21 | Mid-Right | 860 | 530 | 1 030 | |
| **3** | 23 | Mid-Center | 1 098 | 659 | 1 330 | |
| **3** | 25 | Mid-Left | 1 198 | 736 | 1 430 | |
| **3** | 27 | Bottom | 846 | 528 | 1 020 | |
| **4** | 28 | Top | 698 | 527 | 1 030 | |
| **4** | 30 | Mid-Right | **1 551** | 841 | 1 650 | |
| **4** | 32 | Mid-Center | 1 278 | 693 | 1 470 | |
| **4** | 34 | Mid-Left | 492 | 453 | 870 | |
| **4** | 36 | Bottom | 829 | 550 | 1 050 | |
| **5** | 37 | Front | 237 | 175 | 400 | |
| **5** | 39 | Center-Right | 198 | 142 | 270 | |
| **5** | 41 | Center-Mid | 212 | 165 | 320 | |
| **5** | 43 | Center-Left | 827 | 194 | 430 | |
| **5** | 45 | Back | 207 | 143 | 310 | |

Table 49. Summary of ASTM slug calorimeter measurements, Experiment 2-31

| Rack No. | ASTM No. | Location | Incident Energy (kJ/m$^2$) Greater of ± 18 kJ/m$^2$ or ± 4 % | Time to Max Temperature (s) ± 3 % | Comment |
|---|---|---|---|---|---|
| **1** | A | Top | **1 574** | 3.38 | |
| **1** | B | Bottom | 1 244 | 3.00 | |
| **2** | C | Top | 1 107 | 3.30 | |
| **2** | D | Bottom | 901 | 2.93 | |
| **3** | E | Top | 1 550 | 2.89 | |
| **3** | F | Bottom | - - - | - - - | No Data |
| **4** | G | Top | 1 404 | 4.07 | |
| **4** | H | Bottom | 1 239 | 3.13 | |
| **5** | I | Top | 342 | 4.23 | |
| **5** | J | Bottom | 963 | 17.91 | |

Table 50. Summary of $T_{cap}$ slug measurements, Experiment 2-31

| Rack No. | $T_{cap}$ No. | Location | Heat Flux During Arc (kW/m$^2$) Greater of ± 1.5 kW/m$^2$ or ± 2.9 % | Incident Energy During Arc Phase (kJ/m$^2$) Greater of ± 2.4 kJ/m$^2$ or ± 5 % | Total Incident Energy (kJ/m$^2$) Greater of ± 2.4 kJ/m$^2$ or ± 5 % |
|---|---|---|---|---|---|
| **1** | 2 | Top | 757.9 | 1 290.8 | 1 864.0 |
| **1** | 4 | Mid-Right | 519.9 | 852.0 | 1 450.8 |
| **1** | 6 | Mid-Left | 285.5 | 483.1 | 1 127.2 |
| **1** | 8 | Bottom | 402.4 | 619.6 | 1 281.4 |
| **2** | 11 | Top | 574.1 | 1 017.4 | 1 458.4 |
| **2** | 13 | Mid-Right | 450.0 | 749.2 | 1 350.1 |
| **2** | 15 | Mid-Left | 465.4 | 787.3 | 1 380.3 |
| **2** | 17 | Bottom | 410.5 | 718.5 | 1 130.3 |
| **3** | 20 | Top | 754.7 | 1 224.8 | 1 701.7 |
| **3** | 22 | Mid-Right | 663.3 | 997.6 | 1 649.2 |
| **3** | 24 | Mid-Left | 460.3 | 550.6 | 1 895.3 |
| **3** | 26 | Bottom | 621.8 | 949.8 | 1 674.9 |
| **4** | 29 | Front | 656.4 | 1 311.0 | 2 038.2 |
| **4** | 31 | Center-Right | 761.2 | 1 461.2 | **2 229.3** |
| **4** | 33 | Center-Left | 637.4 | 1 249.2 | 1 799.0 |
| **4** | 35 | Back | 765.8 | **1 482.8** | 2 178.1 |
| **5** | 38 | Front | 151.9 | 274.9 | 477.3 |
| **5** | 40 | Center-Right | 134.8 | 234.6 | 469.5 |
| **5** | 42 | Center-Left | 168.3 | 300.3 | 535.7 |
| **5** | 44 | Back | 155.9 | 278.3 | 511.8 |

### 3.9.2.2. Pressure Measurements

The pressure profiles for the first two tenths of a second are shown in Fig. 73. After the initial pressure spike, the pressure rapidly decays to a relatively steady state. The maximum change in pressure in the switchgear enclosure is approximately 23.4 kPa (3.4 psi) above ambient at its peak.

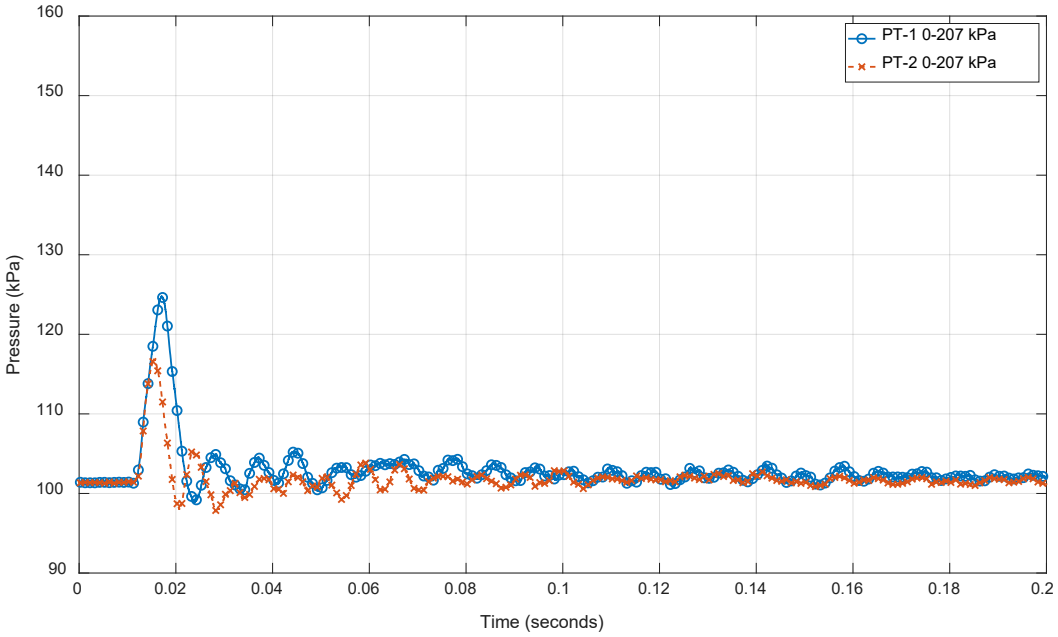


Fig. 73. Pressure measurements from Experiment 2-31. Measurement uncertainty ± 3 percent.

### 3.9.2.3. Electrical Measurements

Experiment 2-31 used KEMA circuit S02 and is reported in Appendix E. Full-level circuit checks (calibration experiments) were performed prior to the experiment to verify the experimental parameters were acceptable. The KEMA report (Appendix E) identifies this experiment as 220901-9001. Key experimental measurements are presented in Table 51. Plots of the electrical measurements are presented in Appendix B.

Table 51. Key measurement from Experiment 2-31. Measurement uncertainty ± 3 percent.

| Phase | Units | A | B | C |
|---|---|---|---|---|
| **Applied voltage, phase-to-ground** | $kV_{RMS}$ | 2.41 | 2.41 | 2.41 |
| **Applied voltage, phase-to-phase** | $kV_{RMS}$ | | 4.17 | |
| **Making current** | $kA_{peak}$ | 52.6 | 64.1 | -68.9 |
| **Current, AC component, beginning** | $kA_{RMS}$ | 31.7 | 33.5 | 31.1 |
| **Current, AC component, middle** | $kA_{RMS}$ | 28.8 | 31.2 | 28.8 |
| **Current, AC component, end** | $kA_{RMS}$ | 28.0 | 30.0 | 27.8 |
| **Current, AC component, average** | $kA_{RMS}$ | 29.2 | 31.1 | 29.0 |
| **Current, AC component, three-phase average** | $kA_{RMS}$ | | 29.7 | |
| **Duration** | s | 2.03 | 2.03 | 2.02 |
| **Arc Energy** | MJ | | 65.5 | |

## 3.10. Experiment 2-32 – 4.16 kV, 30 kA, 4 s Duration, Aluminum Bus, Aluminum Enclosure

Experiment 2-32 was performed on September 1, 2022, at 2:59 PM eastern daylight time (EDT). The temperature was approximately 29 °C (84 °F), approximately 34 percent relative humidity and approximately 100.6 kPa of pressure. The weather was fair with a wind of approximately 13 km/h (8 mi/h) out of the west.

The arc wire was located at the center of the duct section. A strip of insulation, approximately 2.5cm (1 in) long, was removed from each of the bus conductors (nine in total) and the arcing wire was wrapped around all conductors. The arcing wire and installation location are shown in Fig. 74.


Fig. 74. Shorting wire location Experiment 2-32.

### 3.10.1. Observations

Observations documented below are based on the review of video and thermal imaging that were recorded during the experiment. The observations are provided in Table 52 and include an approximate time reference. Corresponding images are provided in Fig. 75, with thermography images presented in Fig. 76.

This was the second aluminum enclosure with aluminum bus bars examined in the series of experiments. The bus duct assembly was acquired from a nuclear facility undergoing decommissioning, and had the same voltage and continuous current carrying rating as the other ducts tested in this series. This duct had three conductors per phase with all aluminum conductors. Due to the damage of all three aluminum 90 degree duct elbows on hand during the previous experiments, this experiment used a steel 90 degree duct elbow.

During the experiment, the arc stabilized at the end of the bus bars. After the HEAF experiment, $CO^2$ fire suppression agent was applied to the duct and local hot spots on the racks and floor. The arc lasted for the expected duration (4.04 s).

Post-test viewing of the cable samples running the length of the instrument racks indicated that they were likely functional, and that the highest thermal exposure was located outside the area covered by the instrument rack sensor matrix. These cables were made from a thermoplastic

material, however, and may have undergone a rehealing process that has been observed in other fire experiments.

Table 52. Observations from Experiment 2-32.

| Time (ms) | Observation |
|---|---|
| **0** | Initial light observed |
| **300** | Particle ejecta observed |
| **784** | Particle ejecta reaches right cell wall |
| **1 301** | Smoke reaches overhead crane and particle ejecta observed outside of the cell |
| **2 068** | Particle ejecta observed impinging on concrete pad outside of test cell, test cell mostly engulfed in smoke |
| **4 037** | End of arc |
| **6 740** | Smoke clearing cell with visual of duct |


Fig. 75. Sequence of Images from Experiment 2-32 (image time stamps are in seconds).

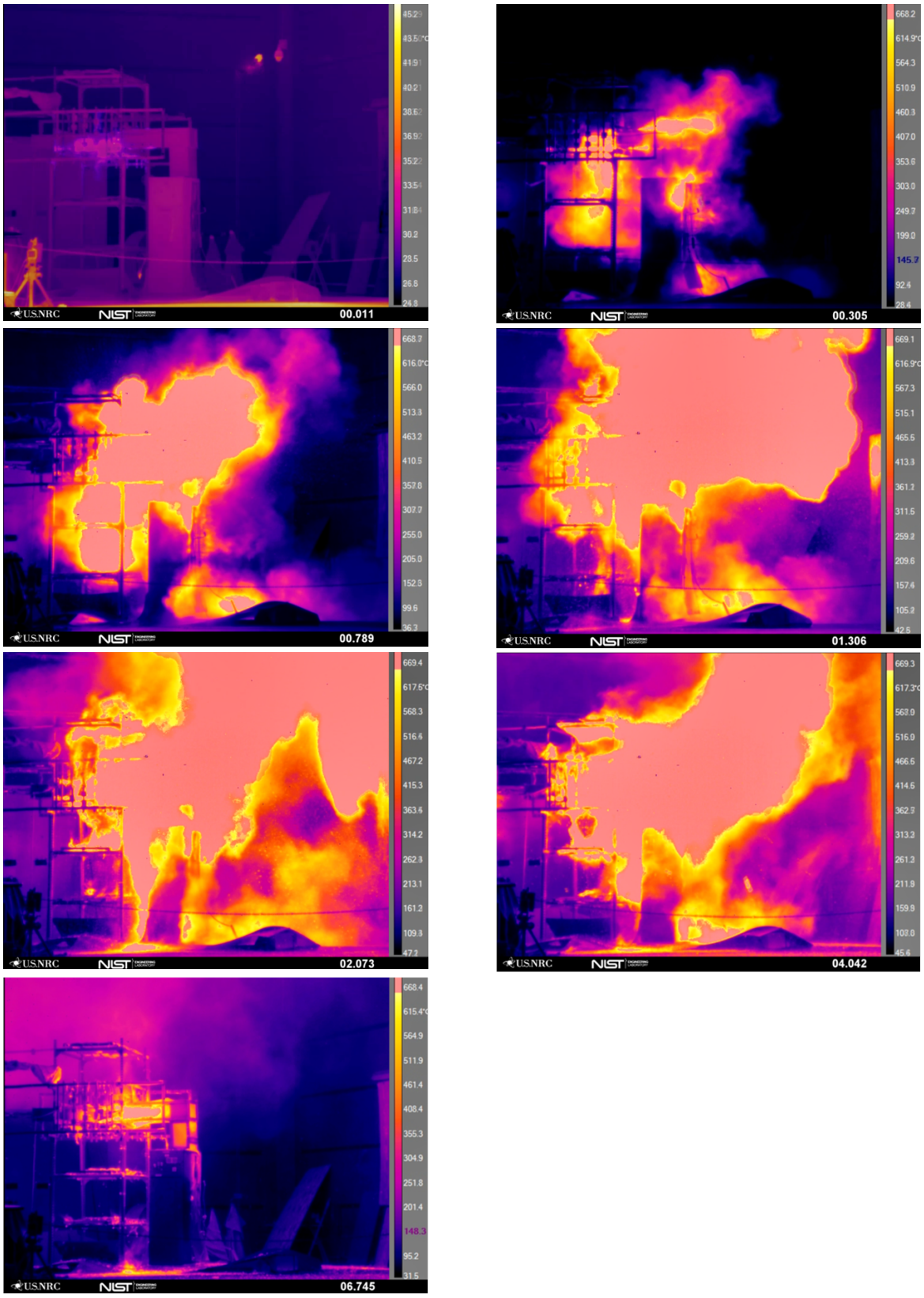


Fig. 76. Sequence of Thermal Images from Experiment 2-32 (image time stamp in seconds)

A photograph of the enclosure following the experiment is shown in Fig. 77. The enclosure did experience a breach. The aluminum bus duct straight section beyond the bus bars was destroyed. The 90-degree elbow was made of steel and remained intact. The Unistrut supports used to connect the 90-degree elbow to the straight section were deformed with some material loss.

Fig. 77. Enclosure Post-Experiment 2-32.

An image of the bus bars removed from the enclosure after the experiment are shown in Fig. 79. The total mass loss of the bus bars was 4 793 g ±1 g. Additional details are presented in Appendix E.

Fig. 78. Photo of Experiment 2-32 bus bars post-experiment

Fig. 79. Photo of Experiment 2-32 bus bars post experiment (arc location shown right)

### 3.10.2. Measurements

Measurements made during Experiment 2-32 are presented below. These measurements include:

- Thermal
  - Heat flux – Plate Thermometers, Tcap Slug Calorimeters
  - Incident Energy – ASTM Slug Calorimeters, Tcap Slug Calorimeters, Plate Thermometers
  - Temperature – Thermocouple inside of switchgear
- Pressure
  - Internal pressure
- Mass Loss
  - Pre- / Post-experimental measurements
- Electrical
  - Voltage profiles
  - Current profiles
  - Power and energy profiles

#### 3.10.2.1. Thermal Measurements

Thermal measurements from the active instruments are reported below for Experiment 2-32. These include PT measurements in Table 53, ASTM Slug Calorimeter measurements in Table 54, and $T_{cap}$ slug measurements in Table 55. The maximum reading is identified with bold text. The maximum temperature of the thermocouple located in the switchgear was

approximately 1 421 °C, which exceeds the maximum manufacturer calibrated Type K thermocouple temperature of 1 372 °C ± 10 °C.

Table 53. Summary of plate thermometer measurements Experiment 2-32

| Rack No. | Plate No. | Location | Max Heat Flux (kW/m²) Greater of ± 1 kW/m² or ± 5 % | Average Heat Flux During Arc (kW/m²) Greater of ±1 kW/m² or ± 5 % | Total Incident Energy (kJ/m²) ± 15 % | Notes |
|---|---|---|---|---|---|---|
| **1** | 1 | Top | **4 031** | **1 635** | **5 370** | |
| **1** | 3 | Mid-Right | 674 | 526 | 1 970 | |
| **1** | 5 | Mid-Center | 1 034 | 825 | 3 140 | |
| **1** | 7 | Mid-Left | - - - | - - - | - - - | EMI |
| **1** | 9 | Bottom | 1 199 | 512 | 1 910 | |
| **2** | 10 | Top | 2 699 | 1 228 | 4 380 | |
| **2** | 12 | Mid-Right | 782 | 596 | 2 320 | |
| **2** | 14 | Mid-Center | 1 312 | 732 | 2 820 | |
| **2** | 16 | Mid-Left | - - - | - - - | - - - | Inoperable prior to experiment (IPE) |
| **2** | 18 | Bottom | 587 | 434 | 1 640 | |
| **3** | 19 | Top | 952 | 736 | 2 830 | |
| **3** | 21 | Mid-Right | 980 | 615 | 2 390 | |
| **3** | 23 | Mid-Center | 1 308 | 984 | 3 670 | |
| **3** | 25 | Mid-Left | 1 259 | 970 | 3 630 | |
| **3** | 27 | Bottom | 968 | 695 | 2 680 | |
| **4** | 28 | Top | 1 036 | 788 | 3 100 | |
| **4** | 30 | Mid-Right | 2 965 | 1 490 | 5 030 | |
| **4** | 32 | Mid-Center | 1 161 | 910 | 3 430 | |
| **4** | 34 | Mid-Left | 915 | 672 | 2 600 | |
| **4** | 36 | Bottom | 1 421 | 859 | 3 250 | |
| **5** | 37 | Front | 960 | 260 | 970 | |
| **5** | 39 | Center-Right | 509 | 292 | 1 220 | |
| **5** | 41 | Center-Mid | 569 | 174 | 830 | |
| **5** | 43 | Center-Left | 1 725 | 291 | 1 840 | |
| **5** | 45 | Back | 402 | 260 | 1 440 | |

Table 54. Summary of ASTM slug calorimeter measurements, Experiment 2-32

| Rack No. | ASTM No. | Location | Incident Energy ($kJ/m^2$) Greater of ± 18 $kJ/m^2$ or ± 4 % | Time to Max Temperature (s) ± 3 % | Comment |
|---|---|---|---|---|---|
| **1** | A | Top | 3 599 | 5.52 | |
| **1** | B | Bottom | 2 532 | 4.28 | |
| **2** | C | Top | 2 747 | 5.33 | |
| **2** | D | Bottom | 1 624 | 5.93 | |
| **3** | E | Top | 2 739 | 5.29 | |
| **3** | F | Bottom | 2 769 | 5.34 | |
| **4** | G | Top | **3 610.** | 5.50 | |
| **4** | H | Bottom | 3 500. | 7.39 | |
| **5** | I | Top | 1 049 | 6.47 | |
| **5** | J | Bottom | 985 | 7.85 | |

Table 55. Summary of $T_{cap}$ slug measurements, Experiment 2-32

| Rack No. | $T_{cap}$ No. | Location | Heat Flux During Arc (kW/m$^2$) Greater of ± 1.5 kW/m$^2$ or ± 2.9 % | Incident Energy During Arc Phase (kJ/m$^2$) Greater of ± 2.4 kJ/m$^2$ or ± 5 % | Total Incident Energy (kJ/m$^2$) Greater of ± 2.4 kJ/m$^2$ or ± 5 % |
|---|---|---|---|---|---|
| **1** | 2 | Top | 1 221.1 | 3 900.9 | 4 933.9 |
| **1** | 4 | Mid-Right | 1 016.8 | 3 400.6 | 3 940.8 |
| **1** | 6 | Mid-Left | 869.3 | 2 836.0 | 3 773.9 |
| **1** | 8 | Bottom | 649.3 | 1 986.4 | 3 197.2 |
| **2** | 11 | Top | 1 018.7 | 2 992.9 | 4 303.3 |
| **2** | 13 | Mid-Right | 798.8 | 2 510.5 | 3 389.1 |
| **2** | 15 | Mid-Left | 798.8 | 2 414.2 | 3 515.3 |
| **2** | 17 | Bottom | 550.4 | 1 596.8 | 2 623.5 |
| **3** | 20 | Top | 1 145.8 | 3 532.4 | 4 601.5 |
| **3** | 22 | Mid-Right | 1 030.6 | 3 220.7 | 3 918.7 |
| **3** | 24 | Mid-Left | **1 155.4** | 3 602.3 | 4 554.3 |
| **3** | 26 | Bottom | 1 052.5 | 3 054.8 | 4 194.4 |
| **4** | 29 | Front | 927.9 | 3 034.9 | 4 799.1 |
| **4** | 31 | Center-Right | 1 135.2 | **4 058.0** | **5 994.6** |
| **4** | 33 | Center-Left | 1 147.6 | 3 902.6 | 4 660.1 |
| **4** | 35 | Back | 955.1 | 3302.1 | 4 720.8 |
| **5** | 38 | Front | 275.6 | 986.8 | 1 497.7 |
| **5** | 40 | Center-Right | 267.4 | 1 032.2 | 1 541.4 |
| **5** | 42 | Center-Left | 233.6 | 795.1 | 1 114.8 |
| **5** | 44 | Back | 263.6 | 918.2 | 1 503.0 |

### 3.10.2.2. Pressure Measurements

The pressure profiles for the first two tenths of a second are shown in Fig. 80. After the initial pressure spike, the pressure rapidly decays to a relative steady state. The maximum change in pressure in the switchgear enclosure is approximately 25.9 kPa (3.8 psi) above ambient at its peak.

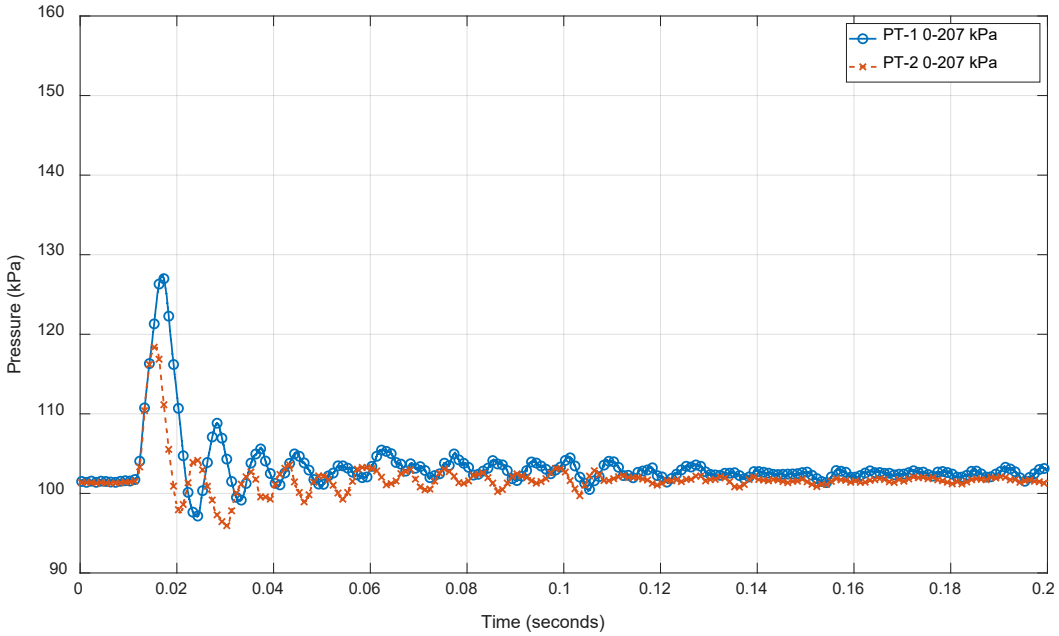


Fig. 80. Pressure measurements from Experiment 2-32. Measurement uncertainty ± 3 percent.

### 3.10.2.3. Electrical Measurements

Experiment 2-32 used KEMA circuit S02 and is reported in Appendix E. Full-level circuit checks (calibration experiments) were performed prior to the experiment to verify the experimental parameters were acceptable. The KEMA report (Appendix E) identifies this experiment as 220901-9002. Key experimental measurements are presented in Table 56. Plots of the electrical measurements are presented in Appendix B.

Table 56. Key measurement from Experiment 2-32. Measurement uncertainty ± 3 percent.

| Phase | Units | A | B | C |
|---|---|---|---|---|
| **Applied voltage, phase-to-ground** | $kV_{RMS}$ | 2.41 | 2.41 | 2.41 |
| **Applied voltage, phase-to-phase** | $kV_{RMS}$ | | 4.17 | |
| **Making current** | $kA_{peak}$ | 52.0 | 64.9 | -68.5 |
| **Current, AC component, beginning** | $kA_{RMS}$ | 31.2 | 33.4 | 30.9 |
| **Current, AC component, middle** | $kA_{RMS}$ | 27.4 | 30.1 | 27.2 |
| **Current, AC component, end** | $kA_{RMS}$ | 26.7 | 28.4 | 28.1 |
| **Current, AC component, average** | $kA_{RMS}$ | 28.1 | 30.0 | 28.1 |
| **Current, AC component, three-phase average** | $kA_{RMS}$ | | 28.7 | |
| **Duration** | s | 4.04 | 4.04 | 4.04 |
| **Arc Energy** | MJ | | 141.1 | |

## References

[1] NRC Information Notice 2017-04: High Energy Arcing Faults in Electrical Equipment Containing Aluminum Components, U.S. NRC, Washington, DC, August 2017.
[2] OECD Fire Project – Topical Report No. 1, Analysis of High Energy Arcing Faults (HEAF) Fire Events, Nuclear Energy Agency Committee on the Safety of Nuclear Installations, Organization for Economic Cooperation and Development, June 2013. http://www.oecd-nea.org/nsd/docs/2013/csni-r2013-6.pdf
[3] EPRI/NRC-RES Fire PRA Methodology for Nuclear Power Facilities, Volume 2: Detailed Methodology. Electric Power Research Institute (EPRI), Palo Alto, CA, and U.S. Nuclear Regulatory Commission, Office of Nuclear Regulatory Research (RES), Rockville, MD: 2005, EPRI TR-1011989 and NUREG/CR-6850.
[4] Fire Probabilistic Risk Assessment Methods Enhancements: Supplement 1 to NUREG/CR-6850 and EPRI 1011989, EPRI, Palo Alto, CA, and NRC, Washington, DC.: December 2009.
[5] NEA HEAF Project – TOPICAL REPORT No. 1, Experimental Results from the International High Energy Arcing Fault (HEAF) Research Program – Phase 1 Experimenting 2014 to 2016, Nuclear Energy Agency Committee on The Safety of Nuclear Installations, 2017
[6] Memorandum from Mark Henry Salley, to Thomas H. Boyce, Regarding submittal of possible generic issue concerning the damage caused by high energy arc faults in electrical equipment containing aluminum components, ADAMS Accession No. ML16126A096, May 2016.
[7] Memorandum from Joseph Giitter to Michael F. Weber, regarding Results of Generic Issue Review Panel Screening Evaluation for Proposed Generic Issue PRE-GI-018, 'High Energy Arcing Faults involving Aluminum,' ADAMS Accession No. ML16349A027, July 15, 2017.
[8] Memorandum from Michael Franovich and Michael Cheok to Raymond V. Furstenau, regarding Assessment Plan for Pre-GI-018, Proposed Generic Issue on High Energy Arc Faults Involving Aluminum, ADAMS Accession No. ML18172A189, August 22, 2018.
[9] Management Directive 6.4, Generic Issue Program, ADAMS Accession No. ML16349A027, January 2, 2015.
[10] LIC-504, Integrated Risk-Informed Decisionmaking Process for Emergent Issues, ADAMS Accession No. ML19253D401, March 4, 2020.
[11] Determining the Zone of Influence for High Energy Arcing Faults Using Fire Dynamics Simulator, RIL2022-09, EPRI 3002025123, Electric Power Research Institute (EPRI), Palo Alto, CA, and U.S. Nuclear Regulatory Commission, Office of Nuclear Regulatory Research (RES), Washington, DC, November 2022.
[12] Predicting High Energy Arcing Fault Zones of Influence for Aluminum Using a Modified Arc Flash Model, Evaluation of a modified model bias, uncertainty, parameter sensitivity and zone of influence estimation, Draft for public comment, ADAMS Accession No. ML22095A236.
[13] Target Fragilities for Equipment Vulnerable to High Energy Arcing Faults, RIL 2022-01, EPRI 3002023400, Electric Power Research Institute (EPRI), Palo Alto, CA, and U.S. Nuclear Regulatory Commission, Office of Nuclear Regulatory Research (RES), Washington, DC, May 2022.

[14] High Energy Arcing Fault Frequency and Consequence Modeling, Draft Report for Comment, NUREG-2262, EPRI 30020XXXX, Electric Power Research Institute (EPRI), Palo Alto, CA, and U.S. Nuclear Regulatory Commission, Office of Nuclear Regulatory Research (RES), Washington, DC, July 2022.
[15] An International Phenomena Identification and Ranking Table (PIRT) Expert Elicitation Exercise for High Energy Arcing Faults (HEAFs), U.S. NRC, Washington, DC, NUREG-2218, January 2018.
[16] Report on High Energy Arcing Fault Experiments, Experimental Results from Medium Voltage Electrical Enclosures, RIL 2021-10, NIST TN 2188, SAND2021-12049 R, U.S. Nuclear Regulatory Commission, Washington, DC, National Institute of Standards and Technology, Gaithersburg, MD, Sandia National Laboratories, Albuquerque, NM, November 2021. https://doi.org/10.6028/NIST.TN.2188
[17] Report on High Energy Arcing Fault Experiments, Experimental Results from Open Box Enclosures, RIL 2021-18, NIST TN 2198, SAND2021-16075 R, U.S. Nuclear Regulatory Commission, Washington, DC, National Institute of Standards and Technology, Gaithersburg, MD, Sandia National Laboratories, Albuquerque, NM, December 2021. https://doi.org/10.6028/NIST.TN.2198
[18] Report on High Energy Arcing Fault Experiments, Experimental Results from Low Voltage Switchgear Enclosures, RIL 2021-17, NIST TN 2197, U.S. Nuclear Regulatory Commission, Washington, DC, National Institute of Standards and Technology, Gaithersburg, MD, December 2021. https://doi.org/10.6028/NIST.TN.2197
[19] IEEE C37.010-1999, “IEEE Application Guide for AC High-Voltage Circuit Breakers Rated on a Symmetrical Current Basis,” The Institute of Electrical and Electronics Engineers, Inc., New York, NY, 2000.
[20] ASTM Standard F1959 / F1959M-14, 2014, “Standard Test Method for Determining the Arc Rating of Materials for Clothing,” ASTM International, West Conshohocken, PA, 2014.
[21] J. Clark and R. Tye (2003). Thermophysical Properties Reference Data for some Key Engineering Alloys. High Temperatures-High Pressures - HIGH TEMP-HIGH PRESS. 35-6. 1-14. 10.1068/htjr087.
[22] T. Lafarge and A. Possolo (2015) "The NIST Uncertainty Machine", NCSLI Measure Journal of Measurement Science, volume 10, number 3 (September), pages 20-27.

# Appendix A. Engineering Drawings

This appendix provides detailed drawings and information on the experiment facility, experiment objects, and instrumentation.

## A.1. Experimental Facility

Drawings of the experimental facility are presented in Fig. 81 through Fig. 83.

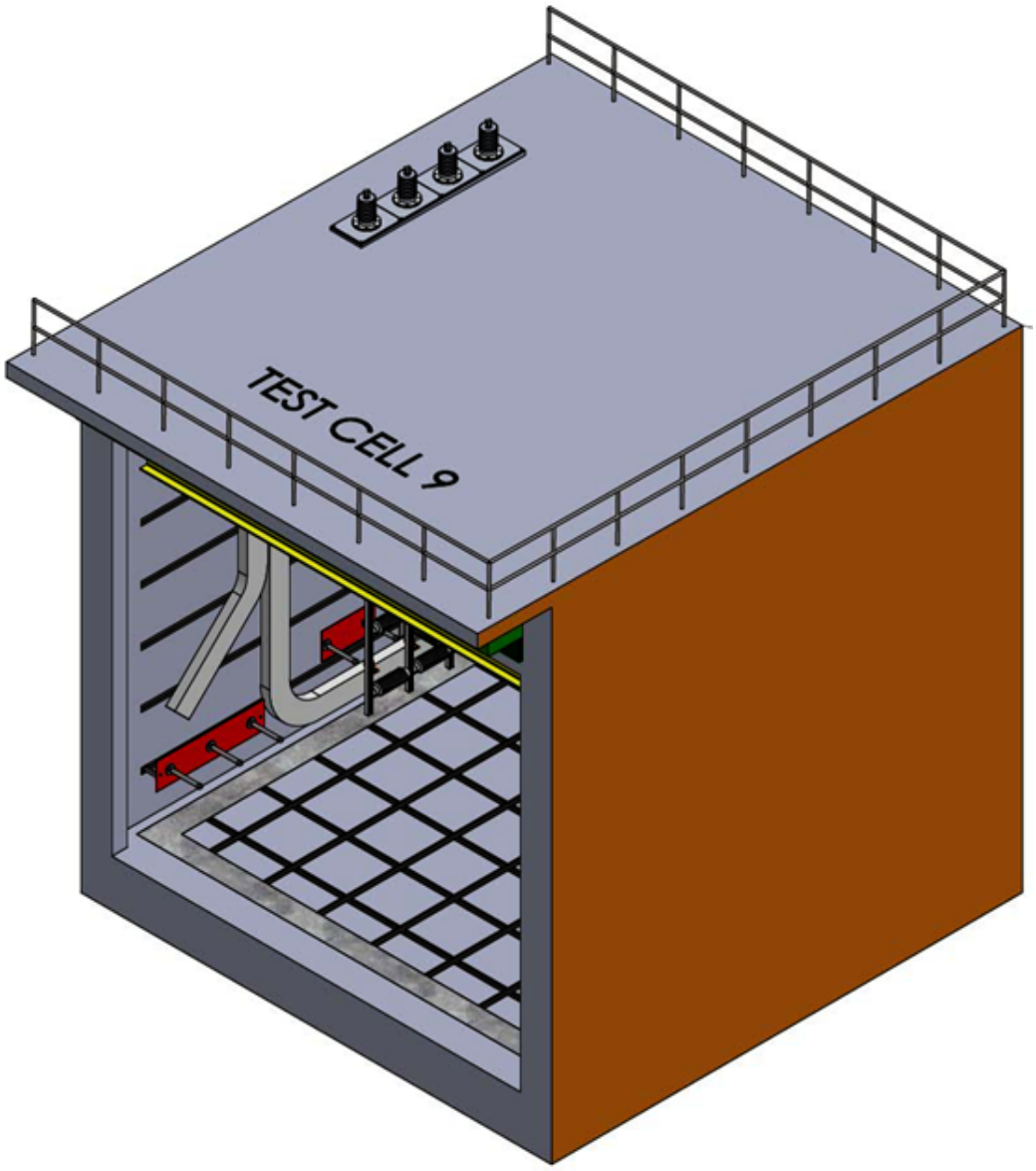


Fig. 81. Isometric drawing of test cell #9

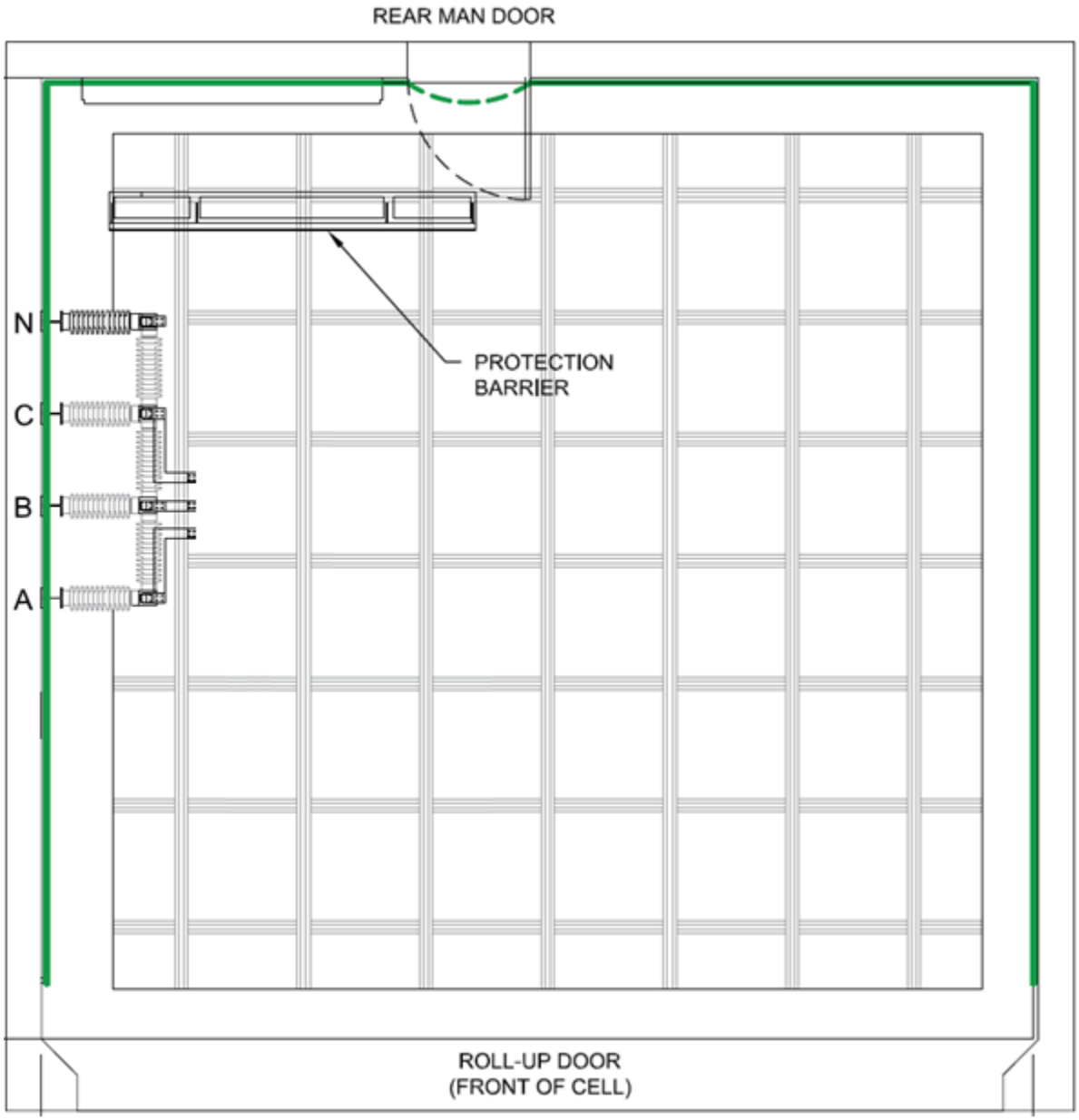


Fig. 82. Plan view of test cell #9.

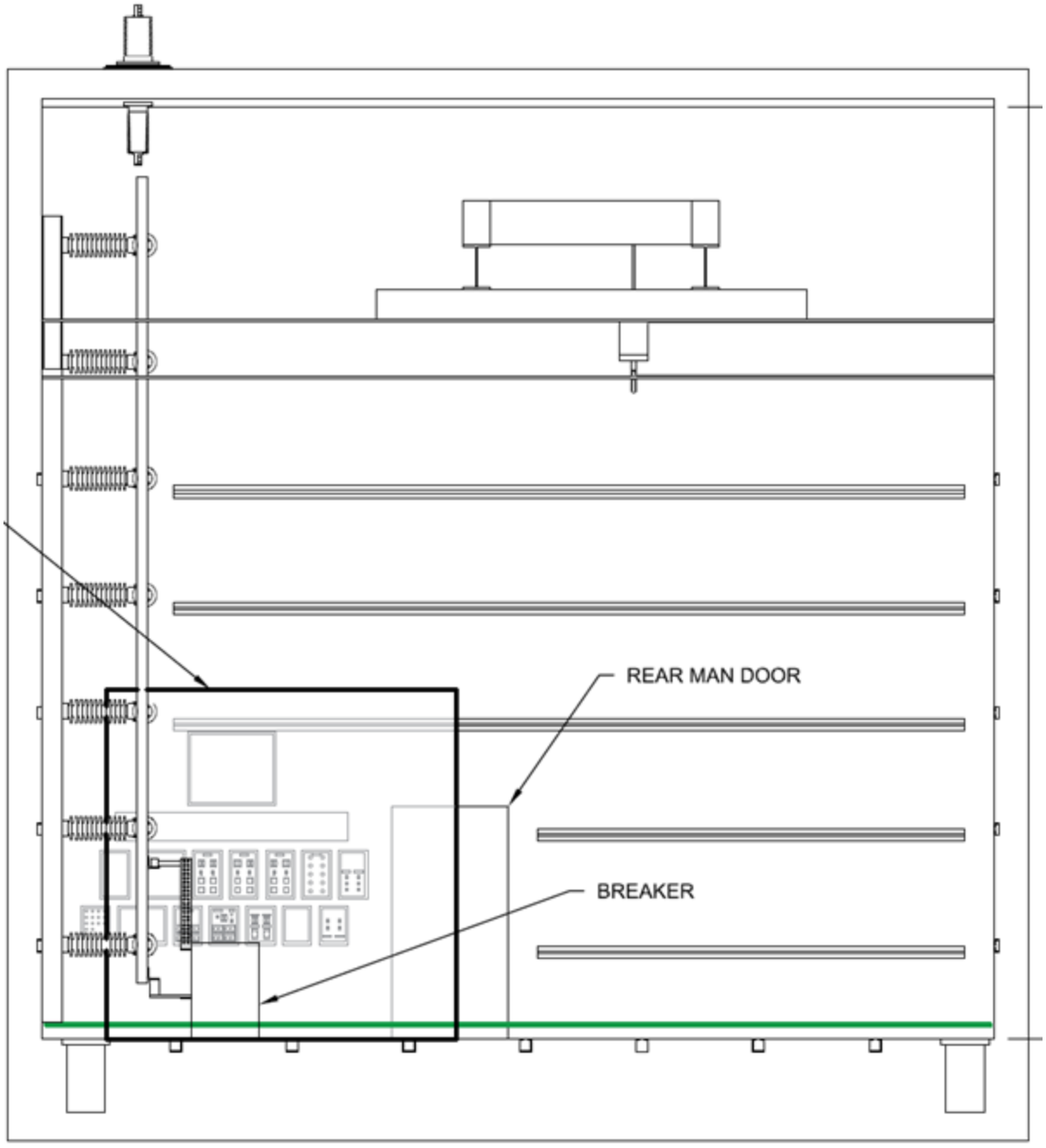


Fig. 83. Elevation view of test cell #9. Breaker shown in drawing is part of KEMA protection system and was not used during this experimental series. (unlabeled arrow indicates movable partition wall used to protect laboratory equipment within the cell)

## A.2. Support Drawings

### A.2.1. Medium-Voltage Switchgear Instrument Rack Drawings

Instrumentation rack drawings for switchgear experiments 2-10 and 2-12 are shown below in Fig. 84 to Fig. 90. As shown in Fig. 87 and Fig. 87, the instrumentation array for Rack 3 is shifted lower to reduce shielding from Rack 2 instruments.

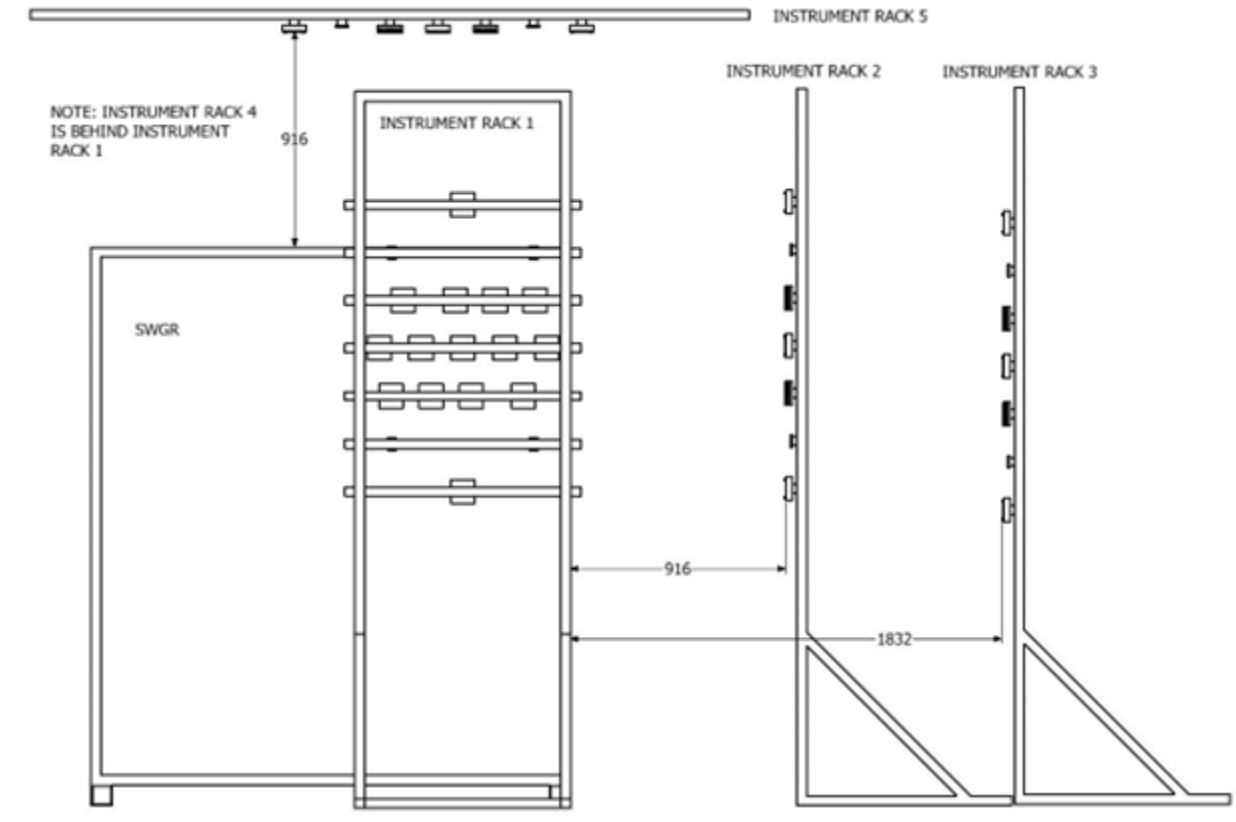


Fig. 84. Elevation view of instrument racks surrounding switchgear unit. (Note that Instrumentation Rack 4 is on the opposite side of the switchgear unit from Rack 1 and therefore not shown in this image. Dimensions in mm ± 5mm.)

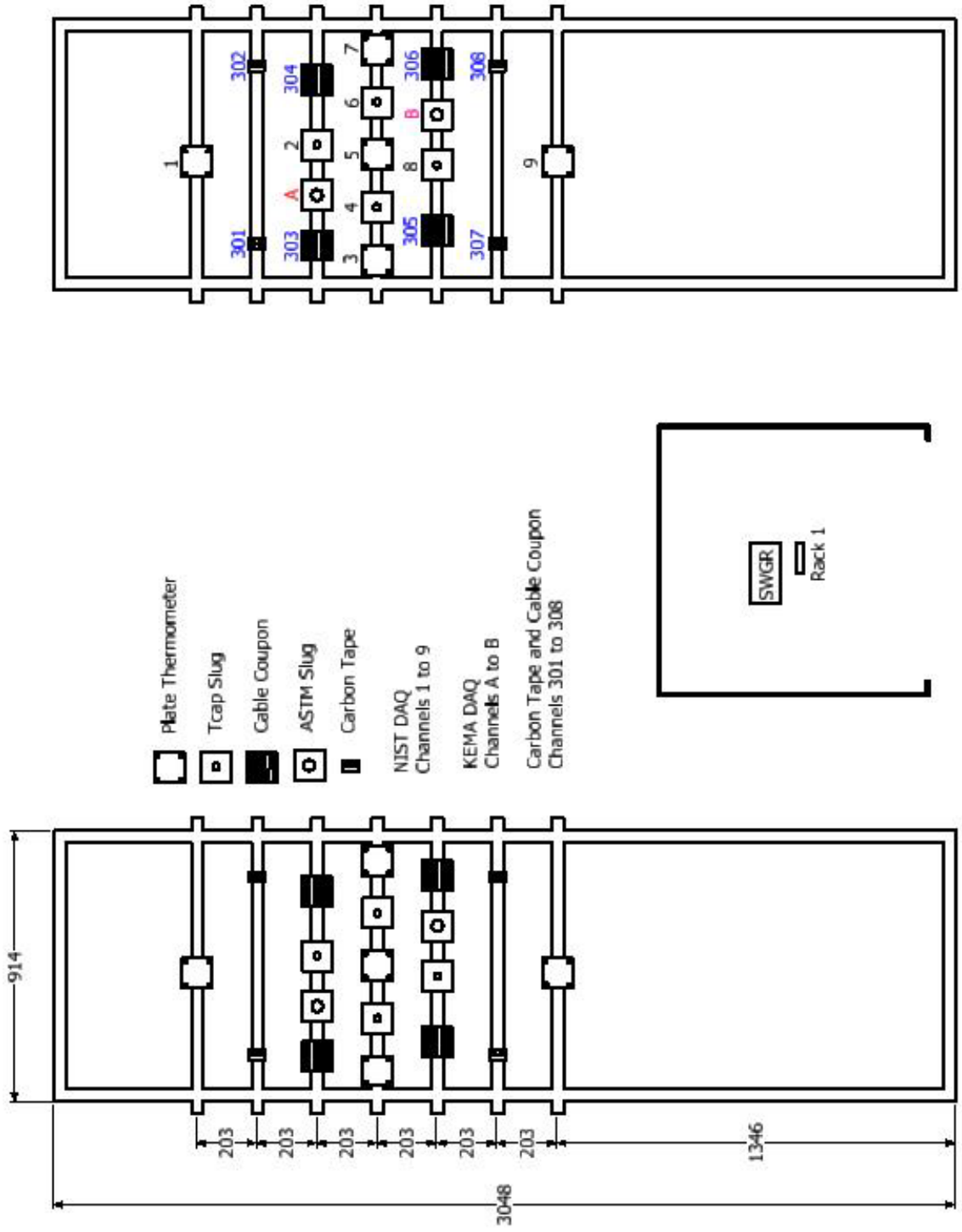


Fig. 85. Illustration of Vertical Instrumentation Rack 1 with data acquisition channels. Dimensions in mm ± 5 mm.

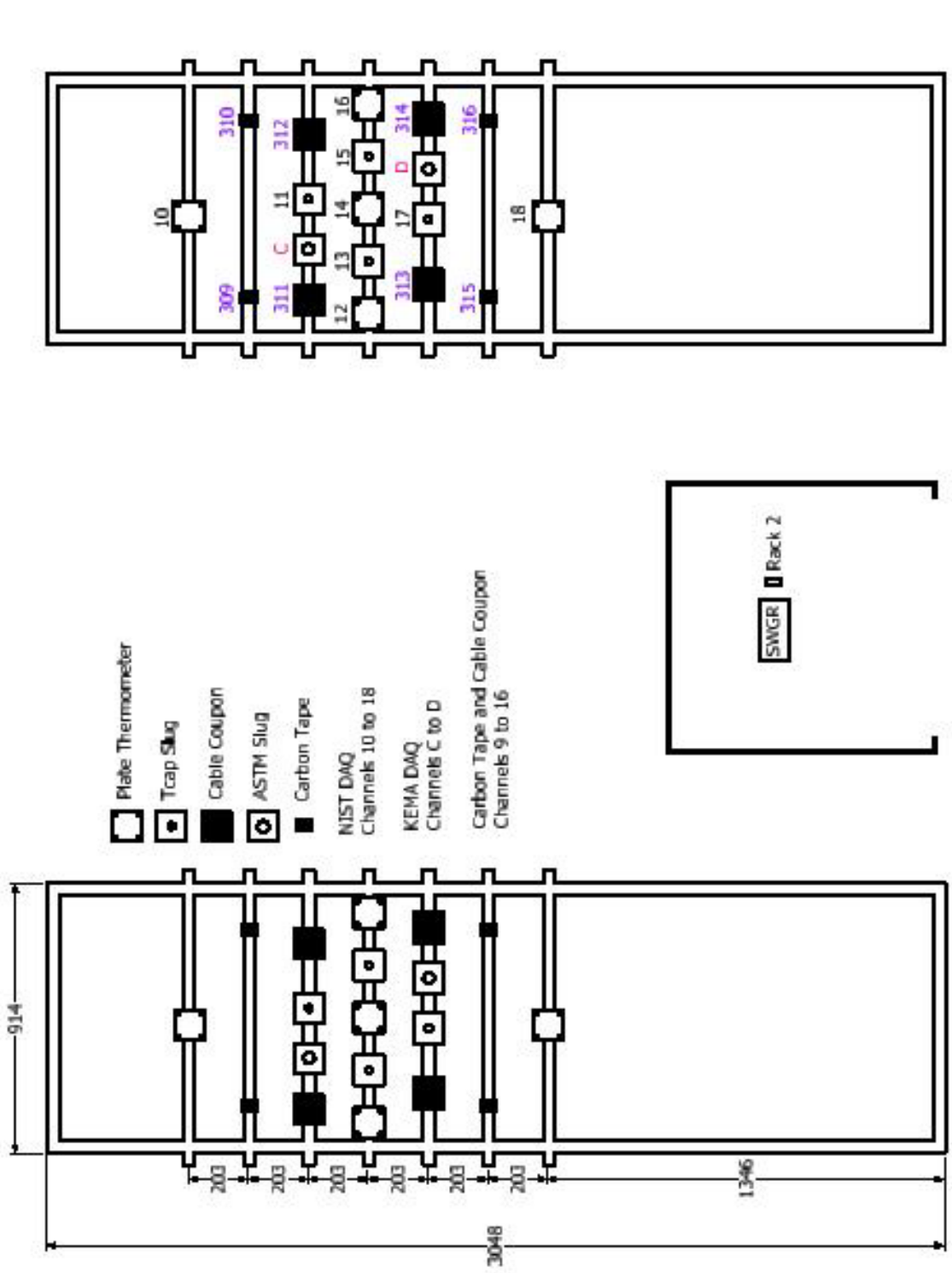


Fig. 86. Illustration of Vertical Instrumentation Rack 2 with data acquisition channels. Dimensions in mm ± 5 mm.

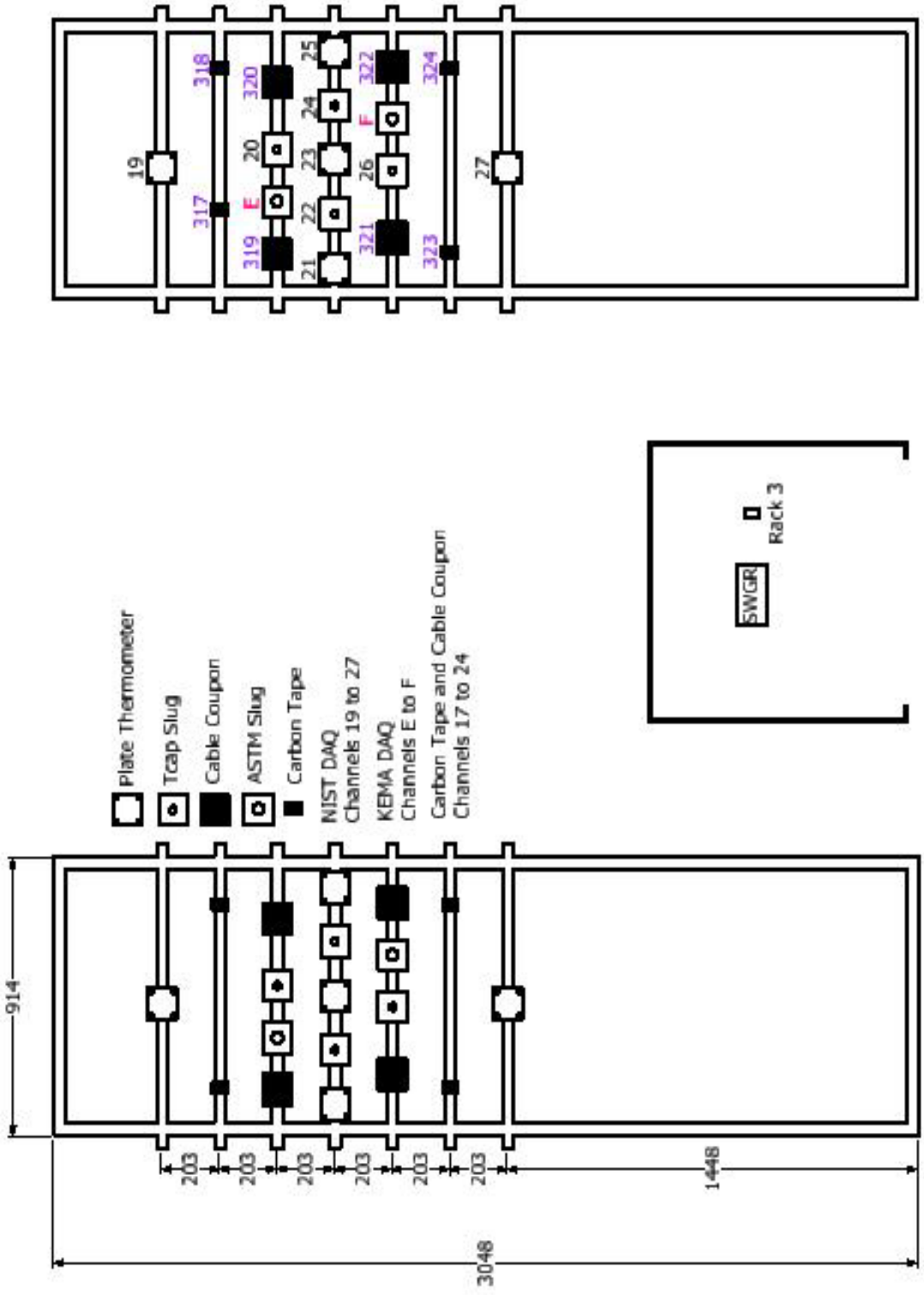


Fig. 87. Illustration of Vertical Instrumentation Rack 3 with data acquisition channels. Dimensions in mm ± 5mm.

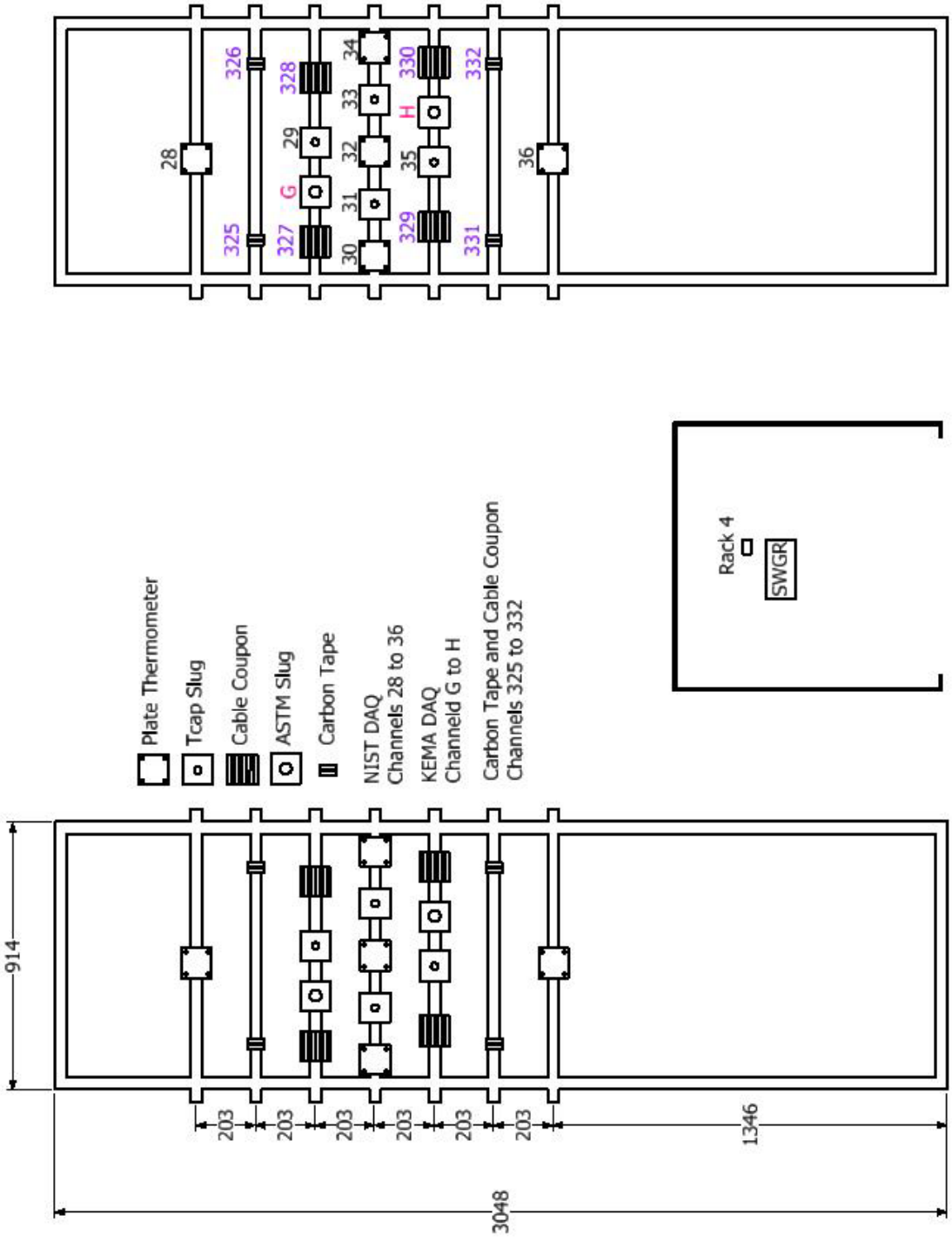


Fig. 88. Illustration of Vertical Instrumentation Rack 4 with data acquisition channels. Dimensions in mm ± 5 mm.

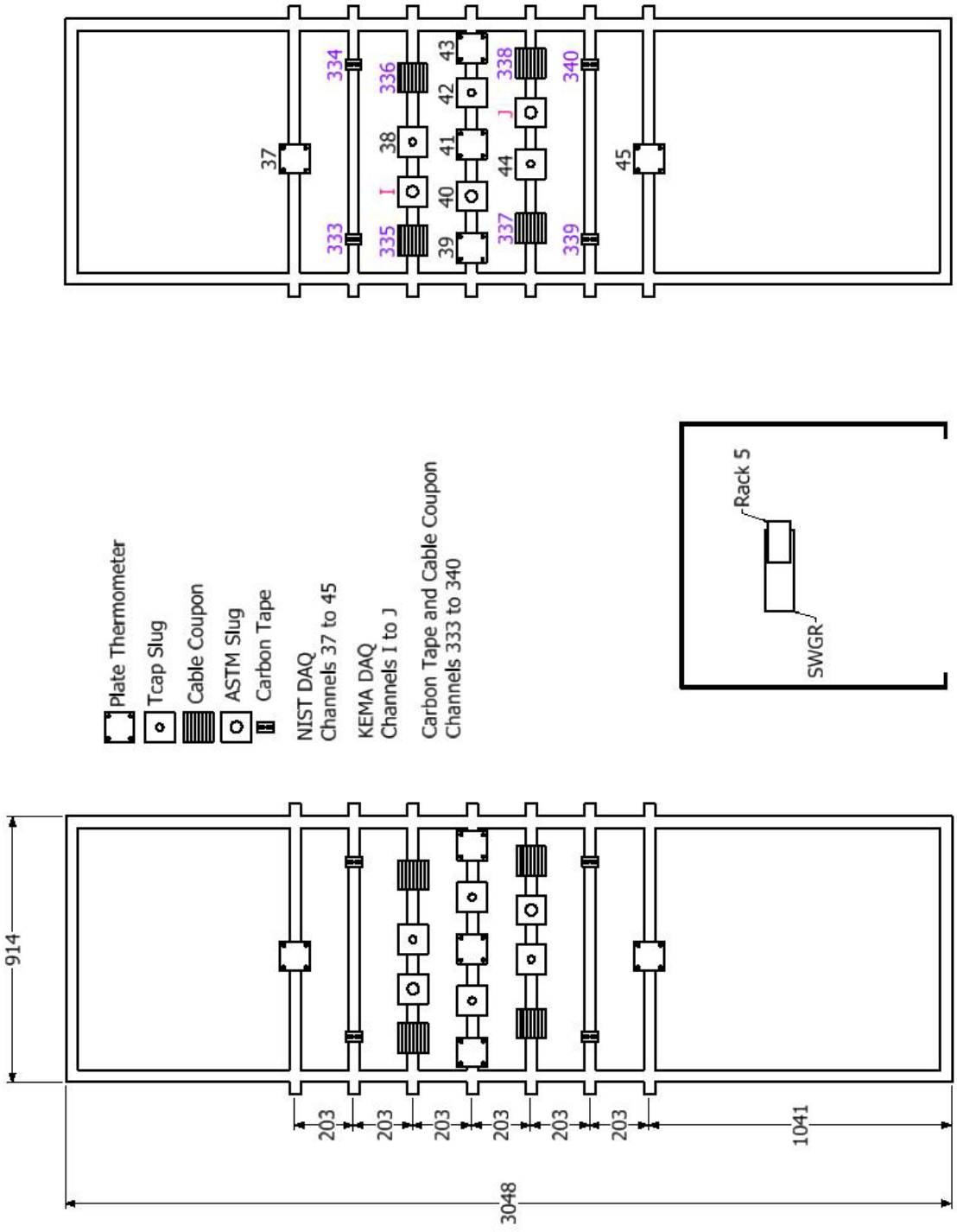


Fig. 89. Illustration of horizontal Instrumentation Rack 5 with data acquisition channels. Dimensions in mm ± 5mm.

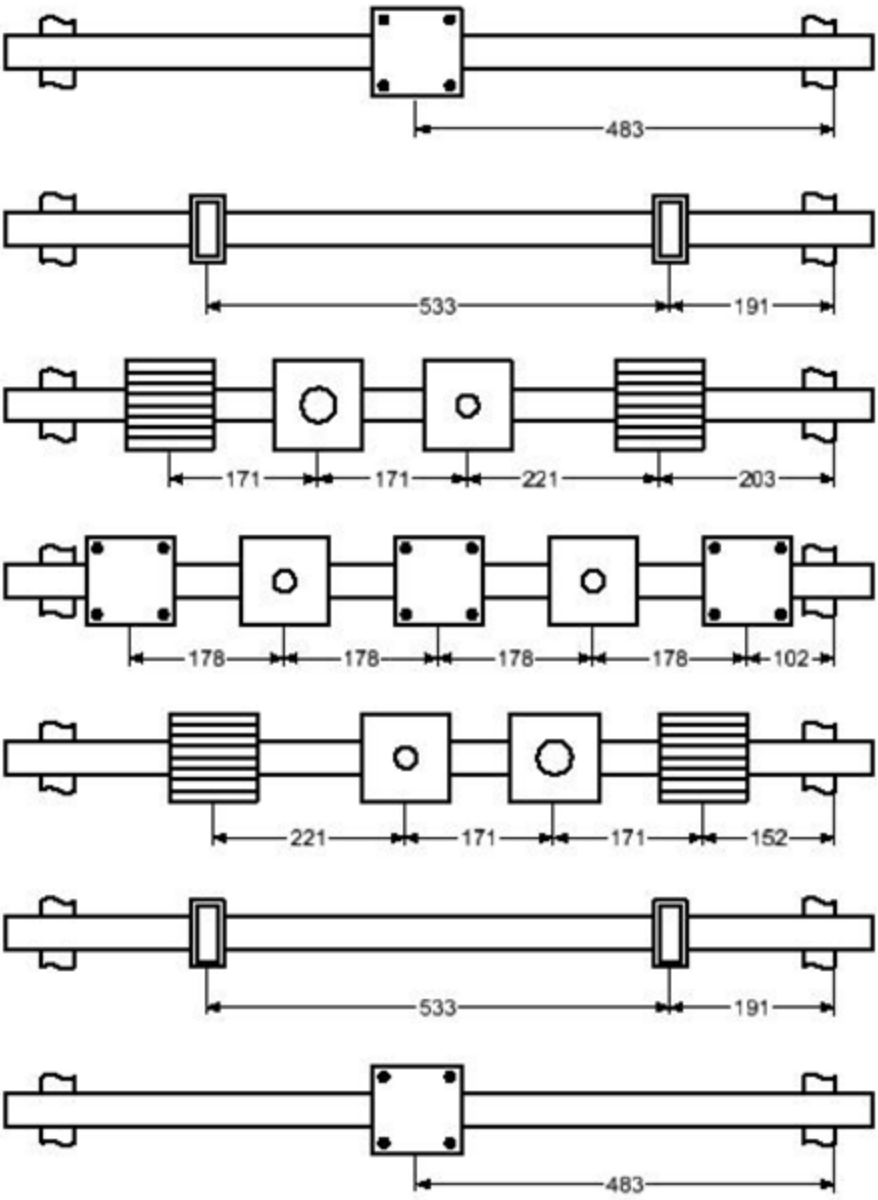


Fig. 90. Detailed Horizontal Locations of Instruments on Instrument Racks 1 - 5
Dimensions in mm ± 5 mm.

### A.2.2. Medium-voltage bus duct drawings

Instrumentation rack drawings for bus duct experiments are shown below in Fig. 91 to Fig. 102.

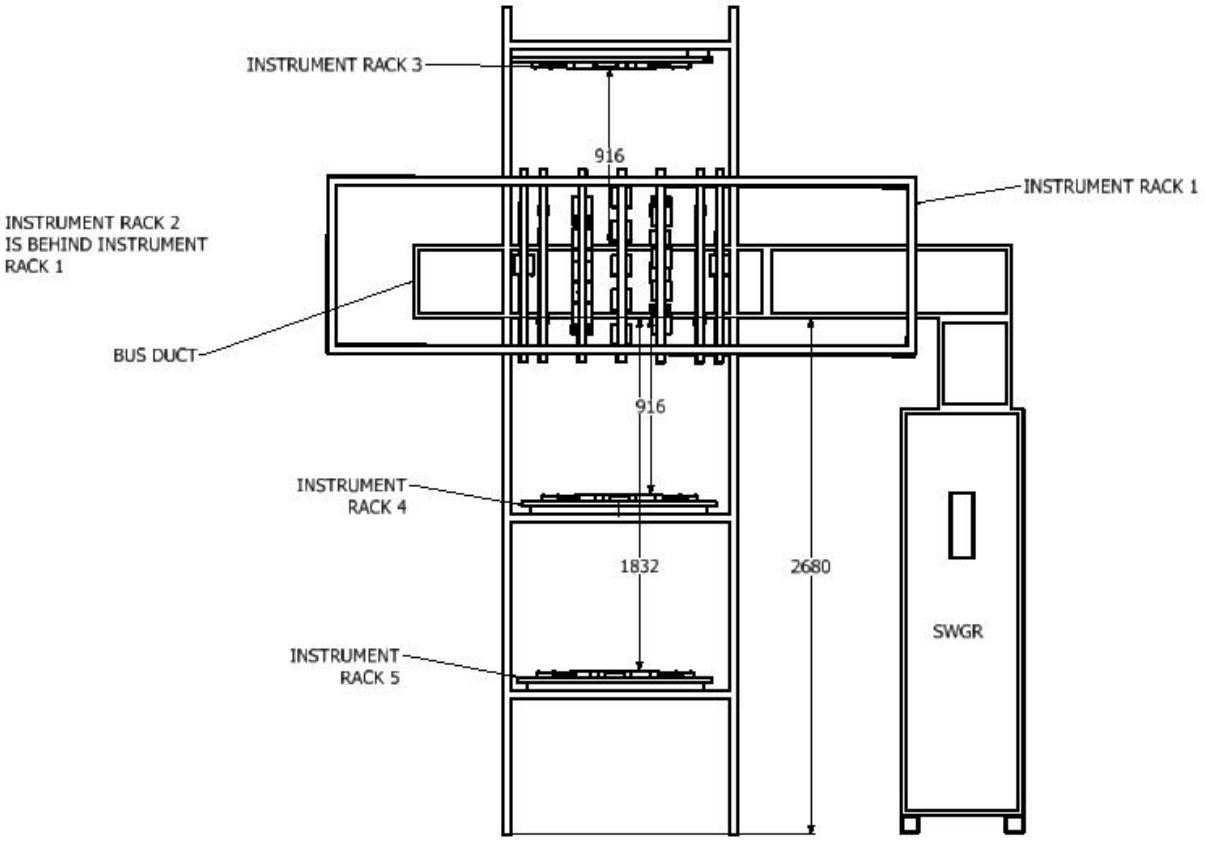


Fig. 91. Elevation view of instrument racks surrounding bus duct used in experiments 2-25 & 2-26. (Note that Instrumentation Rack 2 is on the opposite side of the bus duct from Rack 1 and therefore not shown in this image.) Dimensions in mm ± 5mm.

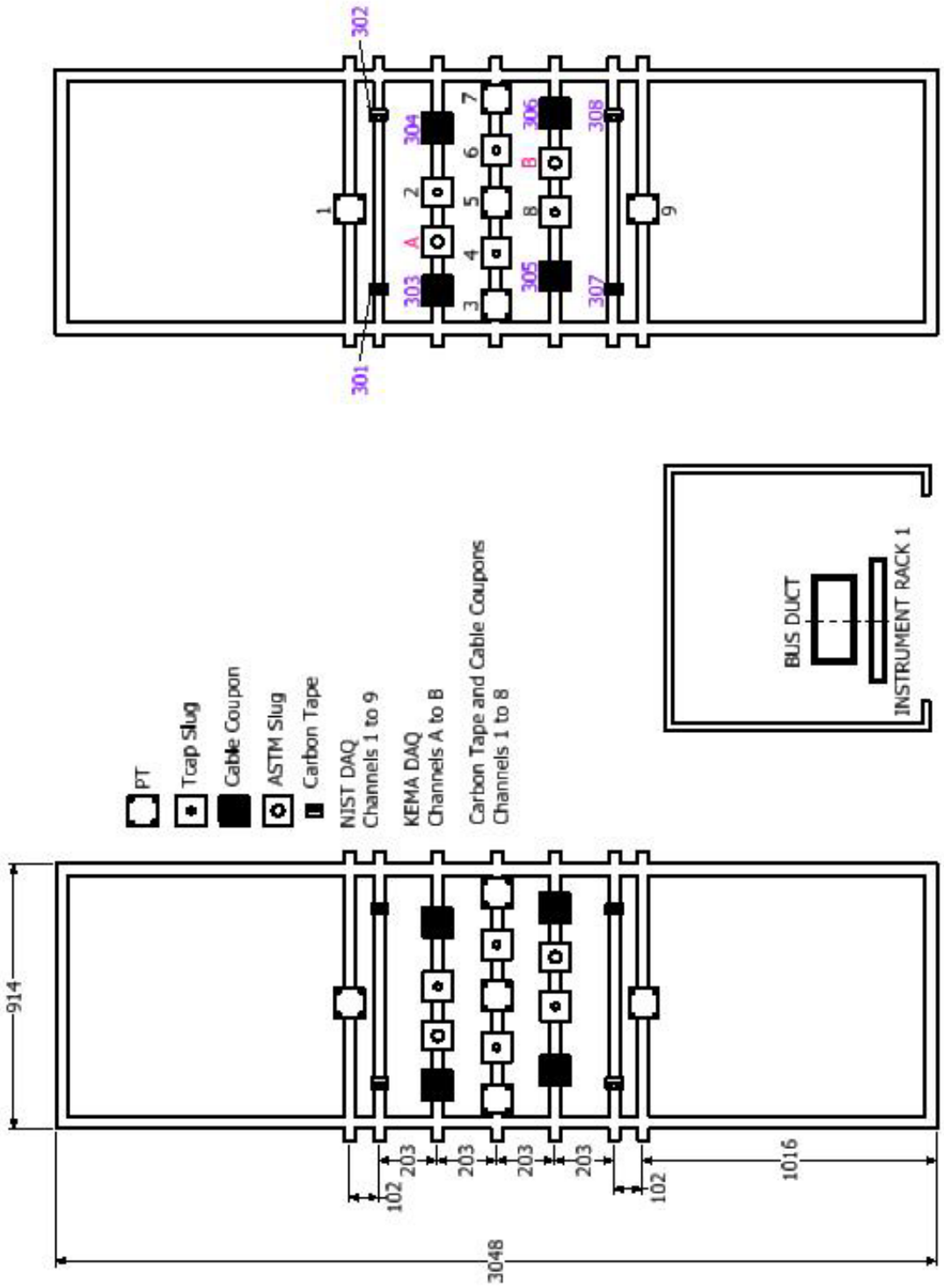


Fig. 92. Illustration of vertical Instrumentation Rack 1 used in experiments 2-25 & 2-26, with data acquisition channels. Dimensions in mm ± 5mm.

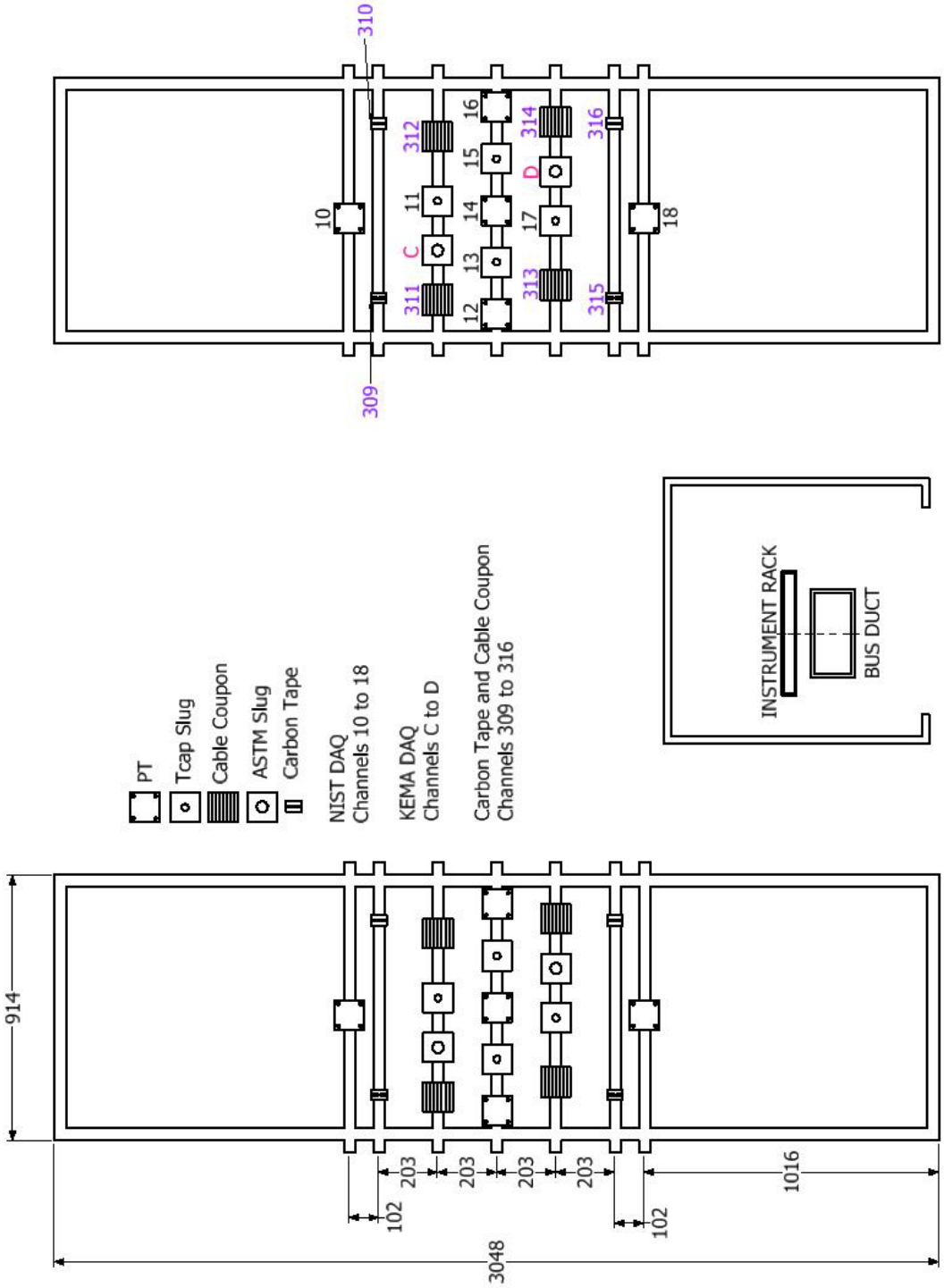


Fig. 93. Illustration of vertical Instrumentation Rack 2 used in experiments 2-25 & 2-26, with data acquisition channels. Dimensions in mm ± 5mm.

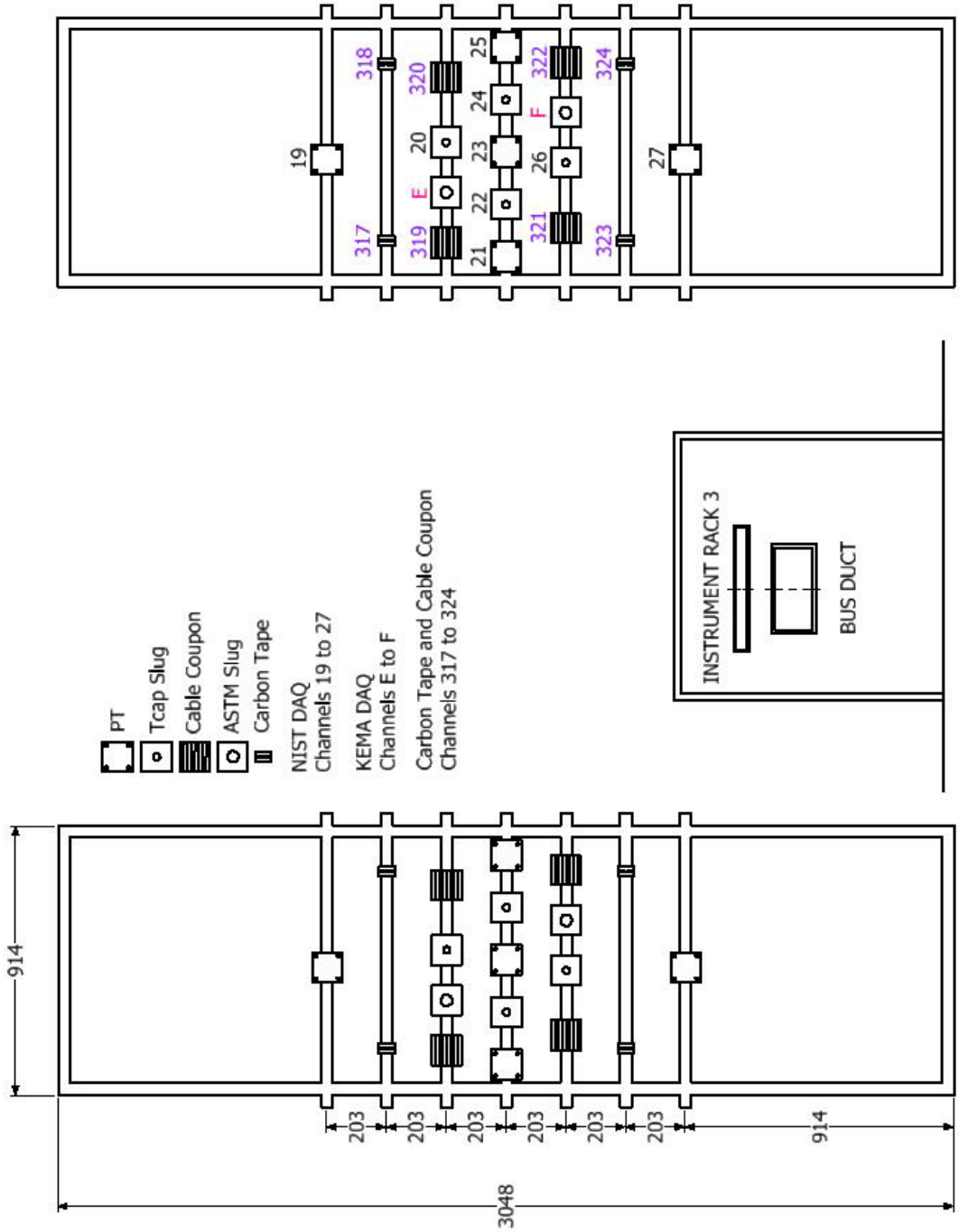


Fig. 94. Illustration of horizontal Instrumentation Rack 3 used in experiments 2-25 & 2-26, with data acquisition channels. Dimensions in mm ± 5mm.

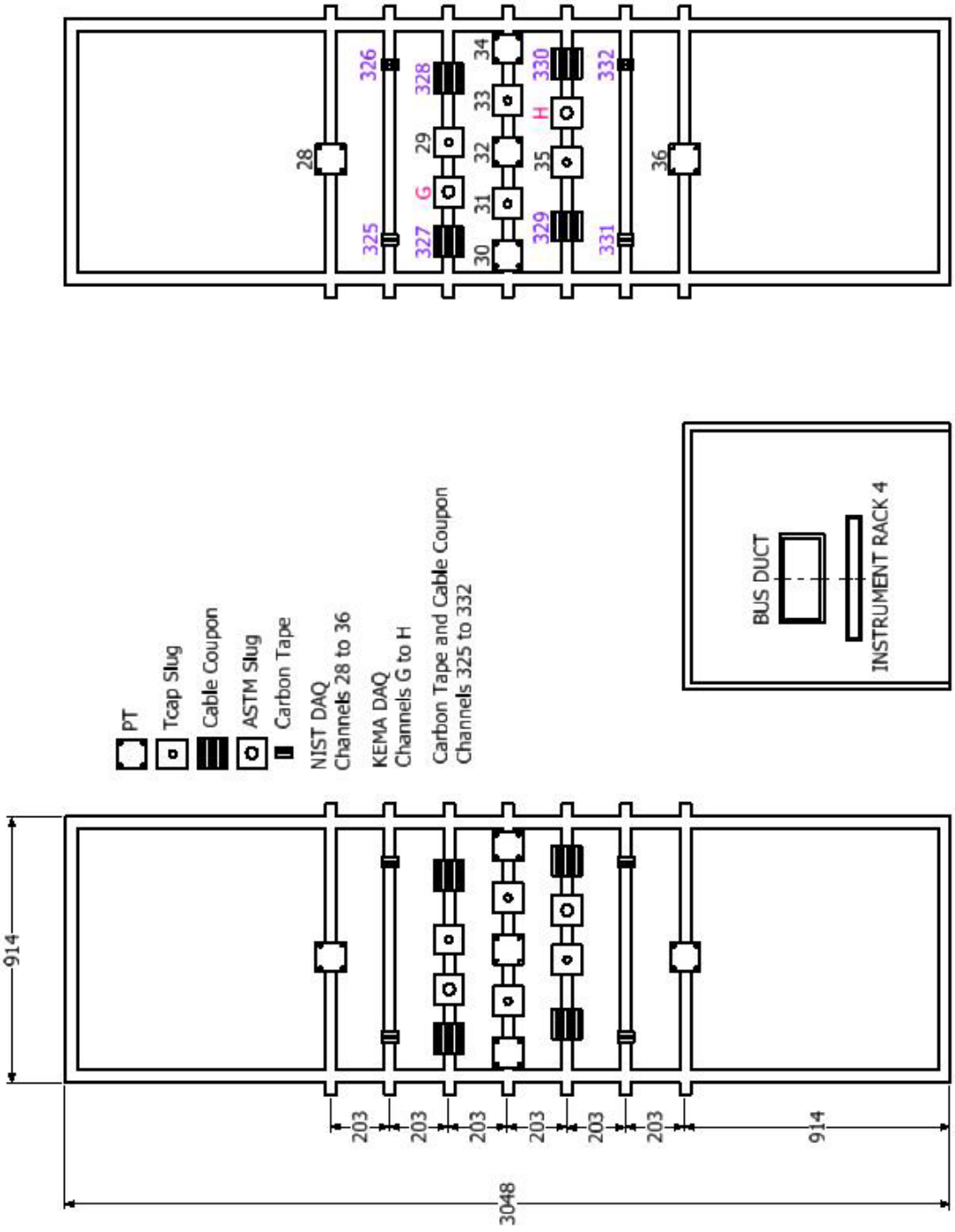


Fig. 95. Illustration of horizontal Instrumentation Rack 4 used in experiments 2-25 & 2-26, with data acquisition channels. Dimensions in mm ± 5mm.

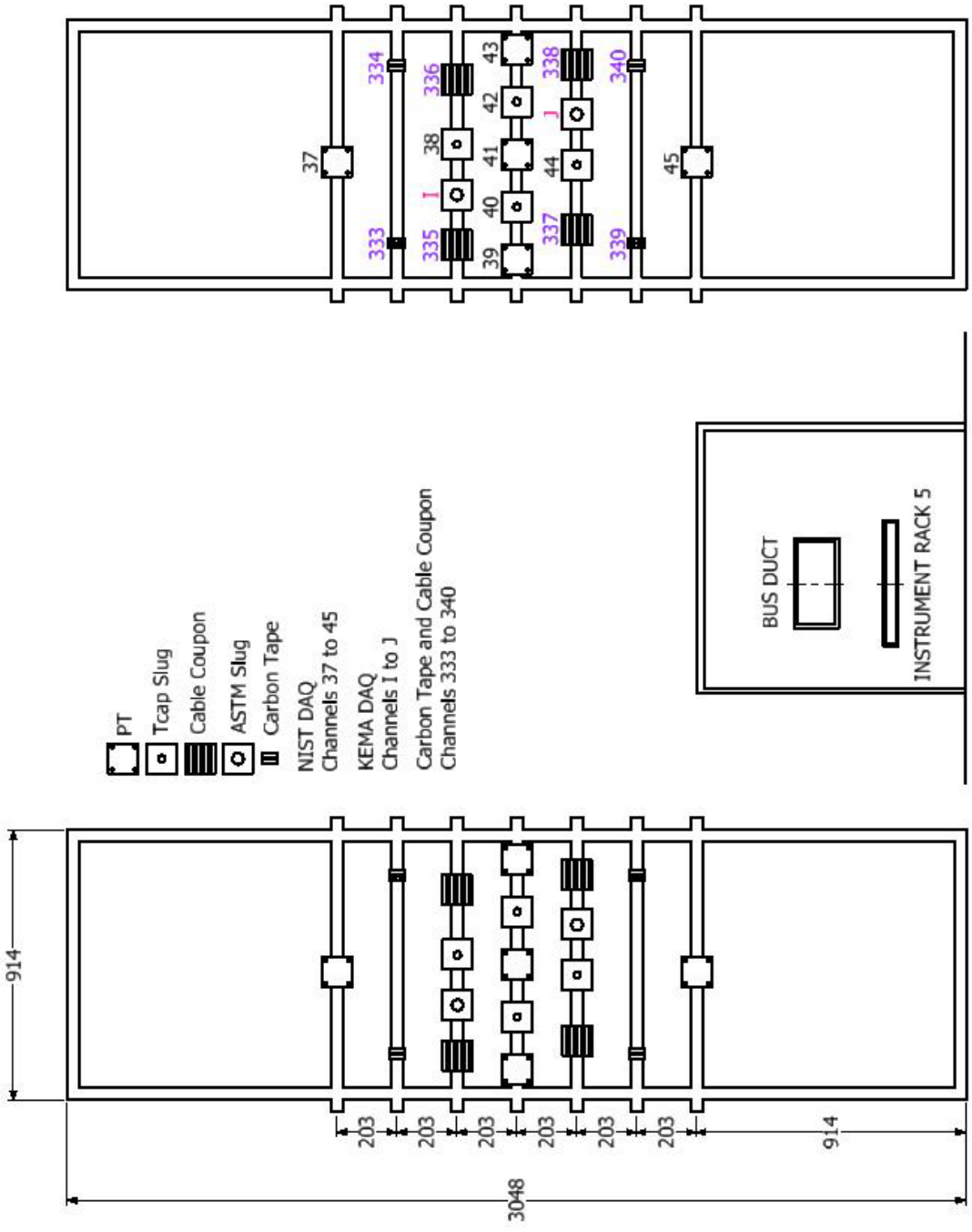


Fig. 96. Illustration of horizontal Instrumentation Rack 5 used in experiments 2-25 & 2-26, with data acquisition channels. Dimensions in mm ± 5mm.

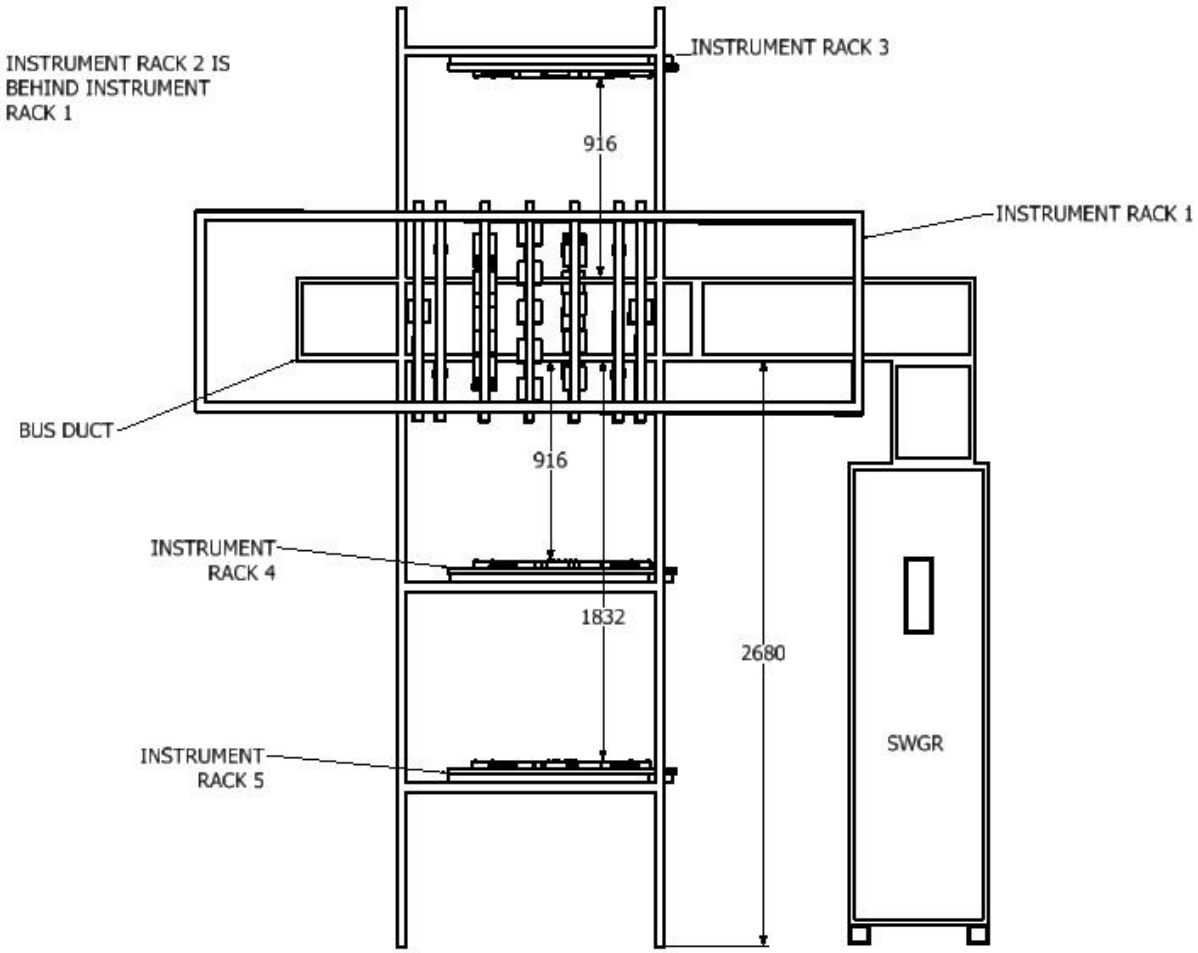


Fig. 97. Elevation view of instrument racks surrounding bus duct used in experiments 2-27, 2-28, 2-30, 2-30B, 2-31, and 2-32. (Note that Instrumentation Rack 2 is on the opposite side of the bus duct from Rack 1 and therefore not shown in this image.) Dimensions in mm ± 5mm.

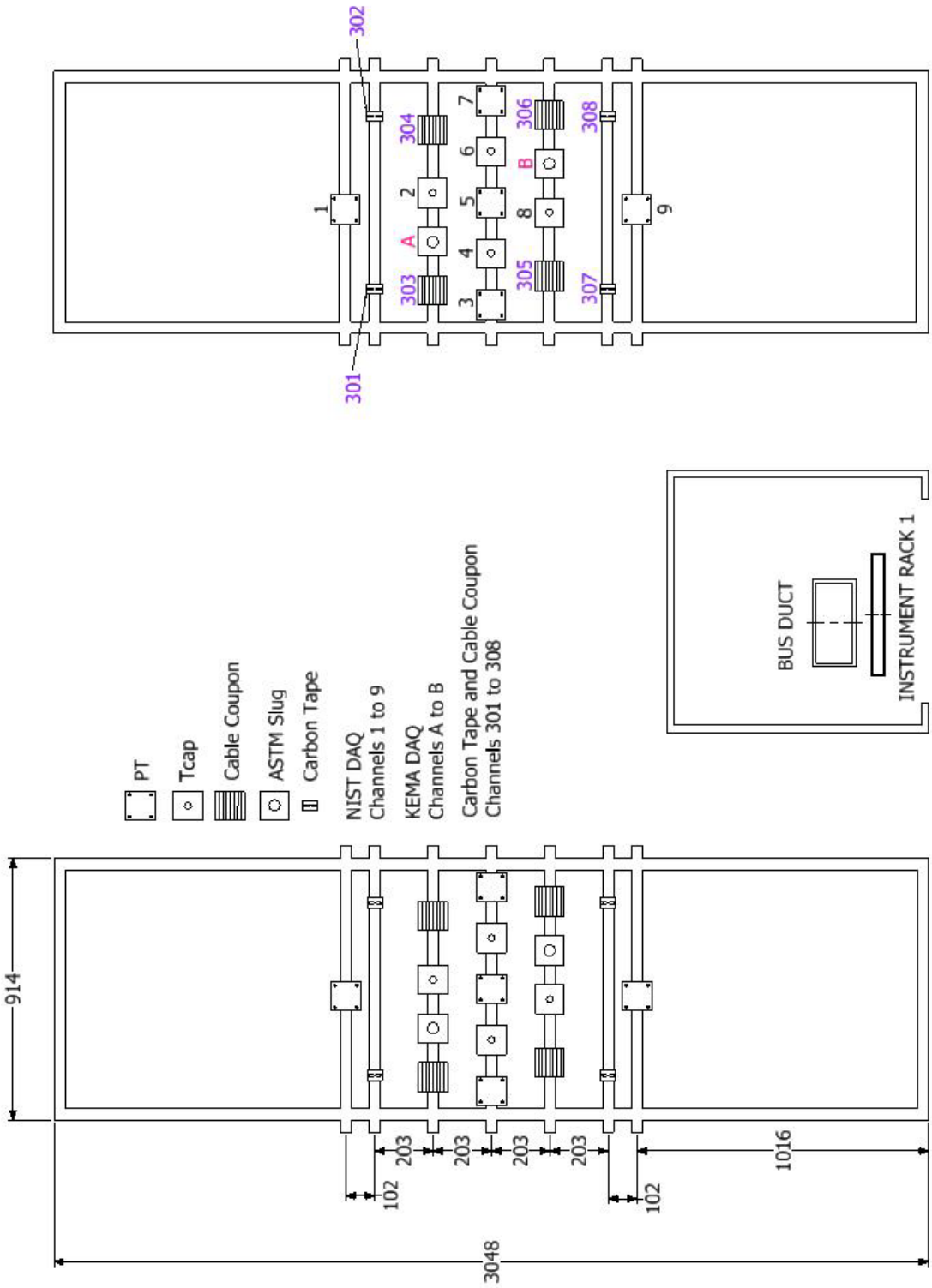


Fig. 98. Illustration of vertical Instrumentation Rack 1 used in experiments 2-27, 2-28, 2-30, 2-30B, 2-31 & 2-32, with data acquisition channels. Dimensions in mm ± 5mm.

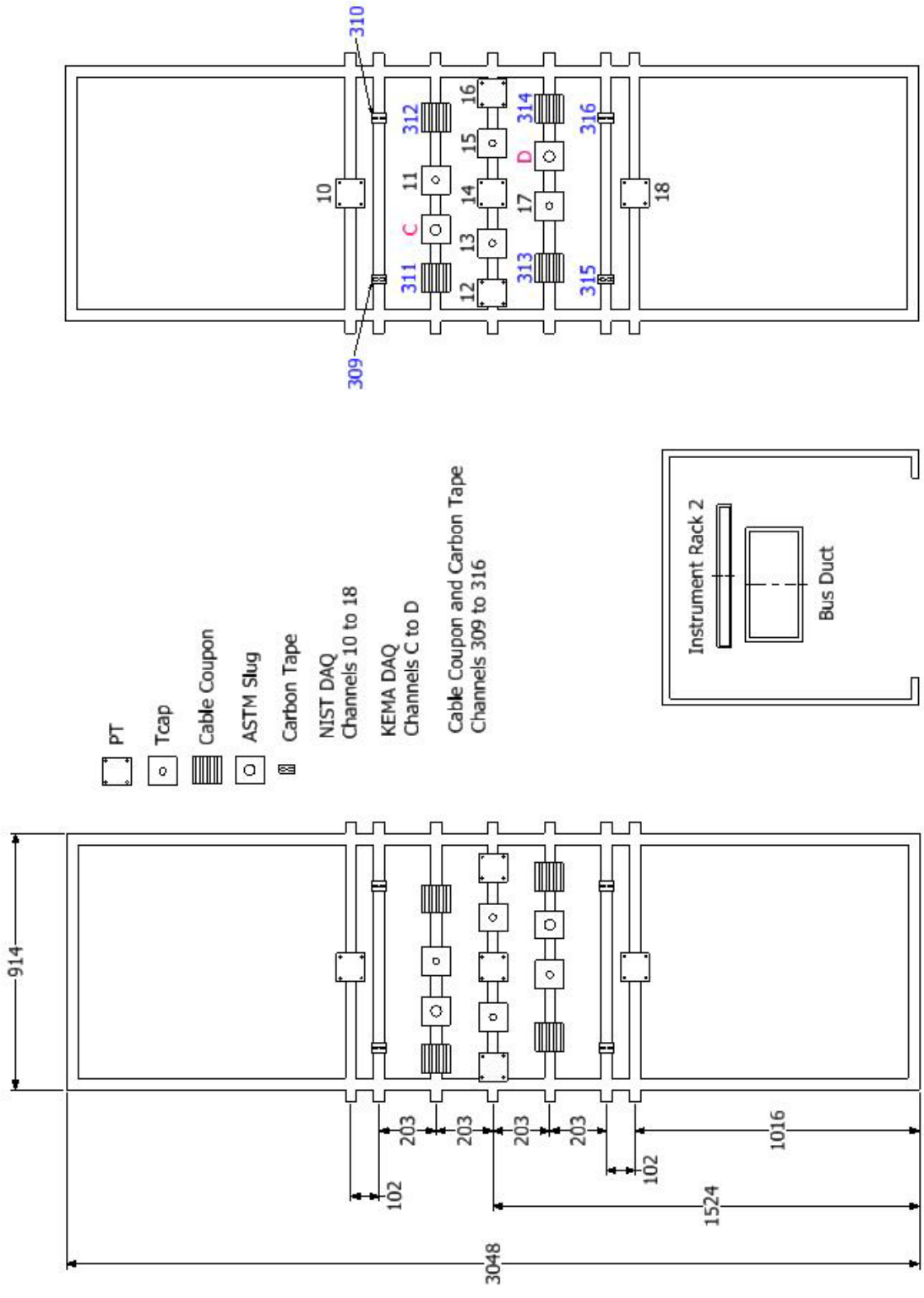


Fig. 99. Illustration of vertical Instrumentation Rack 2 used in experiments 2-27, 2-28, 2-30, 2-30B, 2-31 & 2-32, with data acquisition channels. Dimensions in mm ± 5mm.

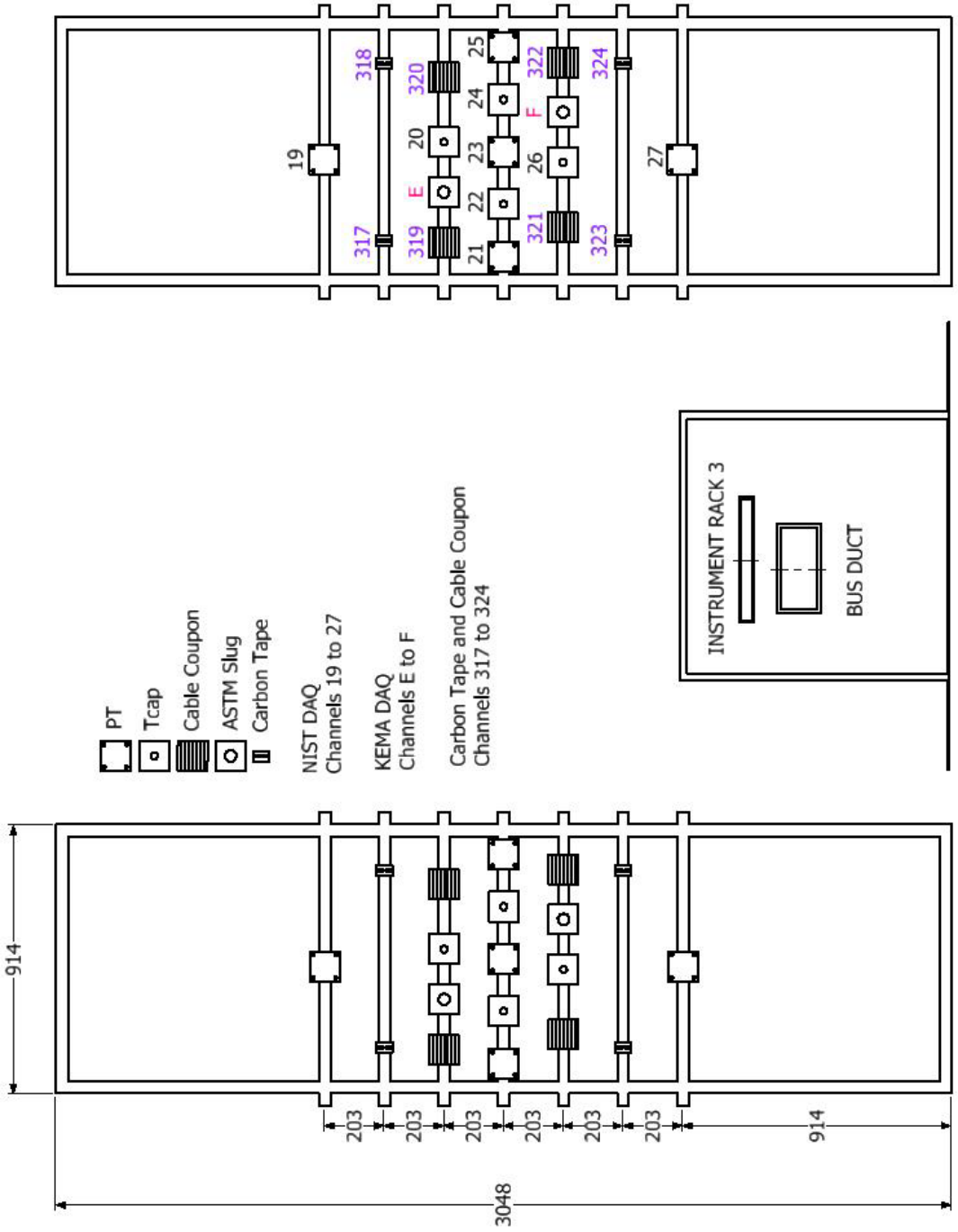


Fig. 100. Illustration of horizontal Instrumentation Rack 3 used in experiments 2-27, 2-28, 2-30, 2-30B, 2-31 & 2-32, with data acquisition channels. Dimensions in mm ± 5mm.

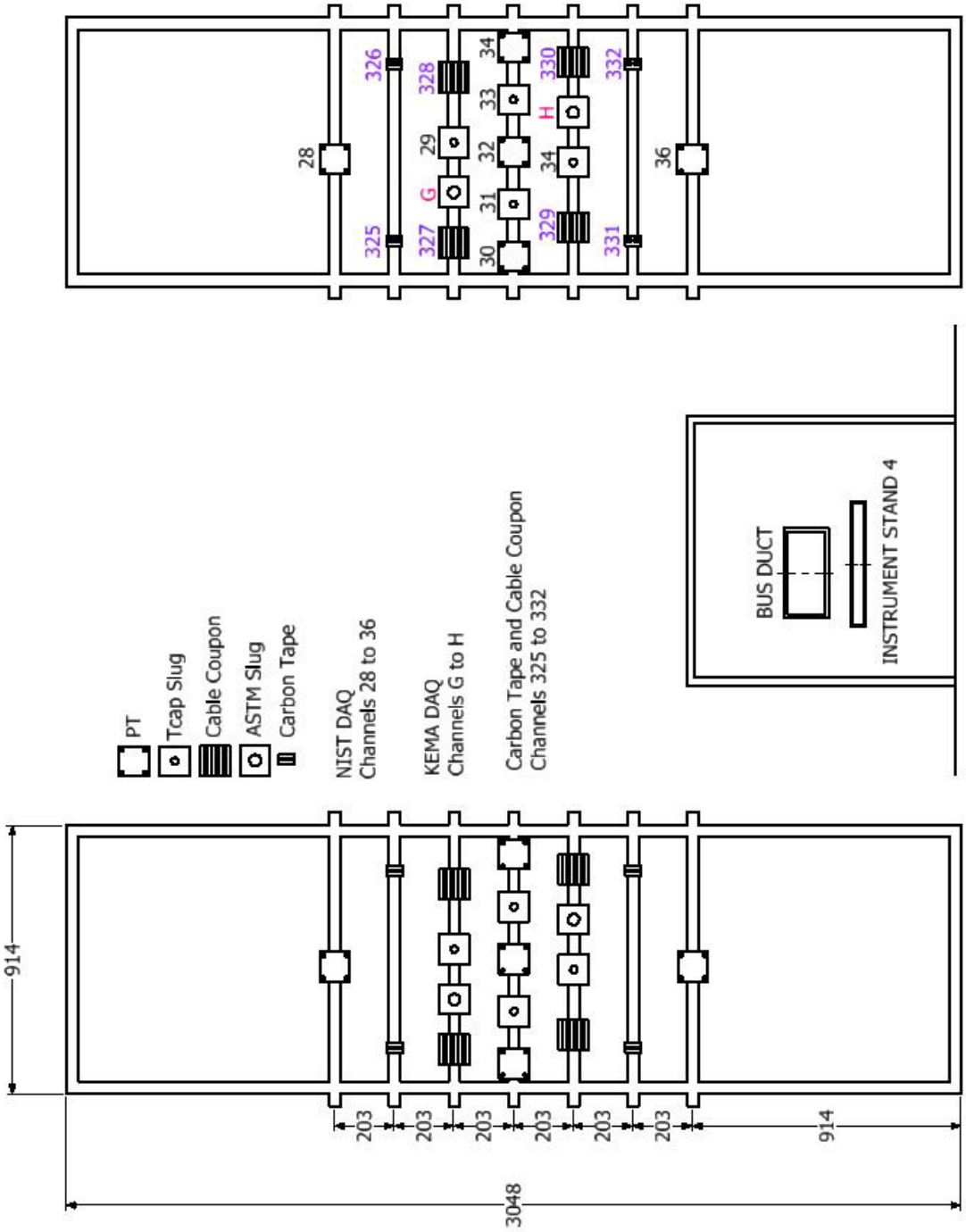


Fig. 101. Illustration of horizontal Instrumentation Rack 4 used in experiments 2-27, 2-28, 2-30, 2-30B, 2-31 & 2-32, with data acquisition channels. Dimensions in mm ± 5mm.

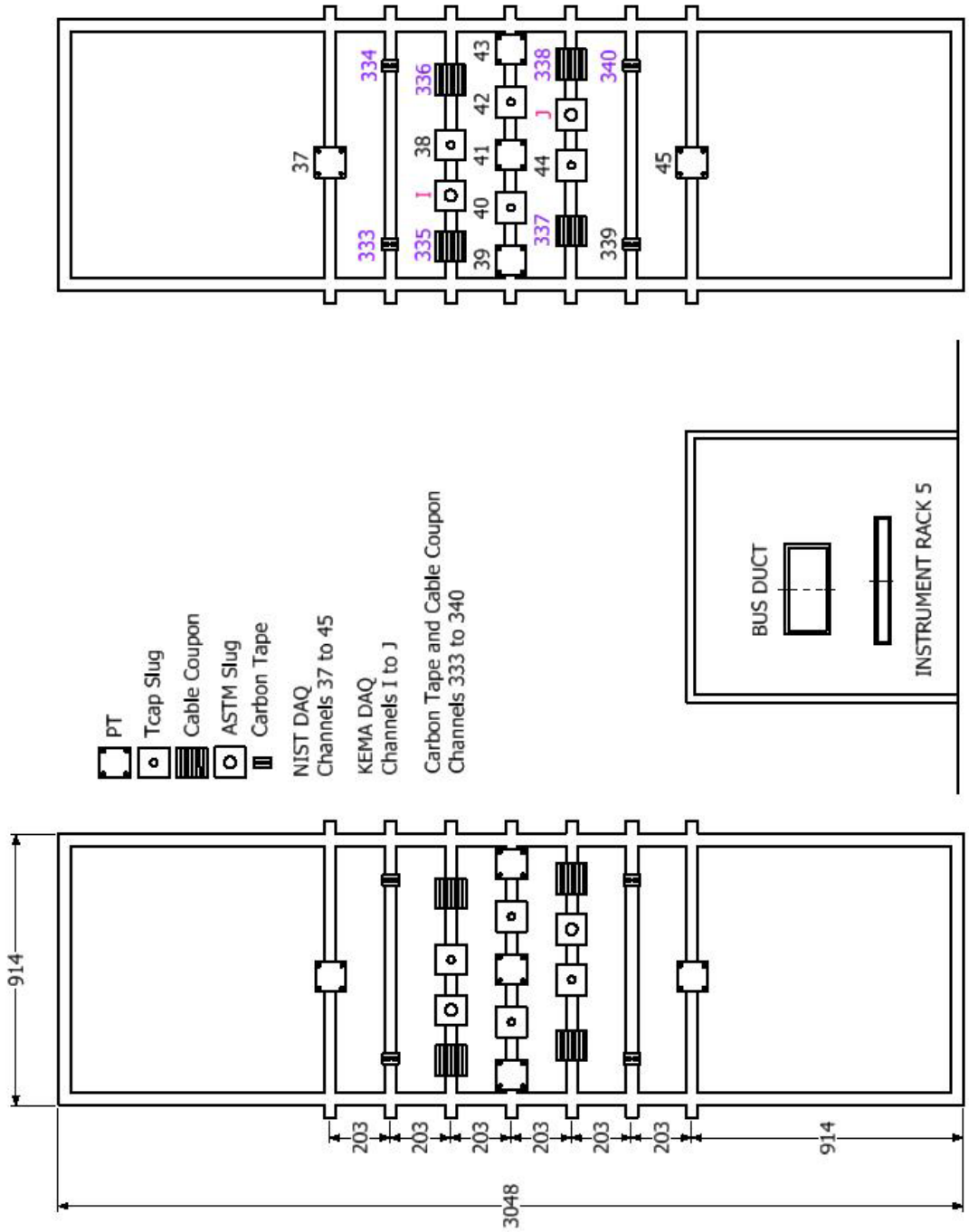


Fig. 102. Illustration of horizontal Instrumentation Rack 5 used in experiments 2-27, 2-28, 2-30, 2-30B, 2-31 & 2-32, with data acquisition channels. Dimensions in mm ± 5mm.

# Appendix B. Electrical Measurements

This appendix presents plots of the electrical measurements made during each experiment. The raw data files were converted to Matlab™ files using the KEMA labs' proprietary software. Once in Matlab,™ the data was processed and plotted.

## B.1. Experiment 2-10 (MV Switchgear, Copper Bus, Steel Enclosure, 6.9 kV, 32kA, 2 s)

The voltage and current profile for the entire duration of the experiment is shown in Fig. 103. The transient region for current phases is presented in Fig. 104. Energy and power profiles are presented in Fig. 105.

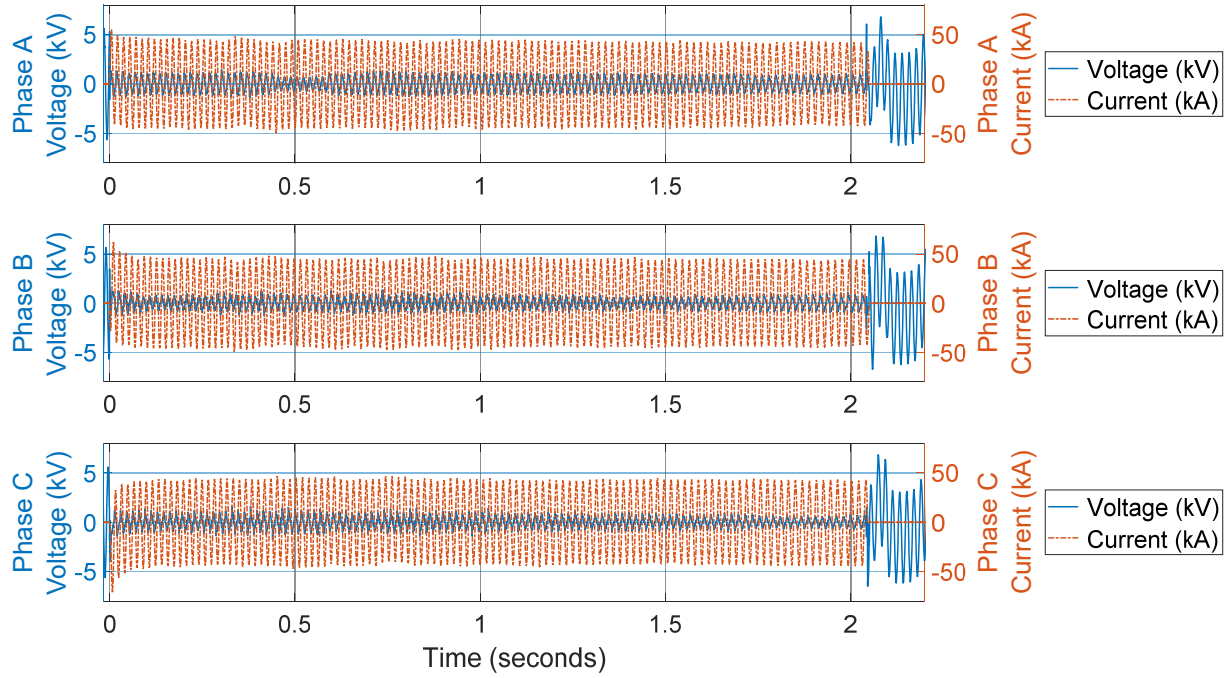


Fig. 103. Voltage and Current Profile during Experiment 2-10. Measurement uncertainty ±3 percent.

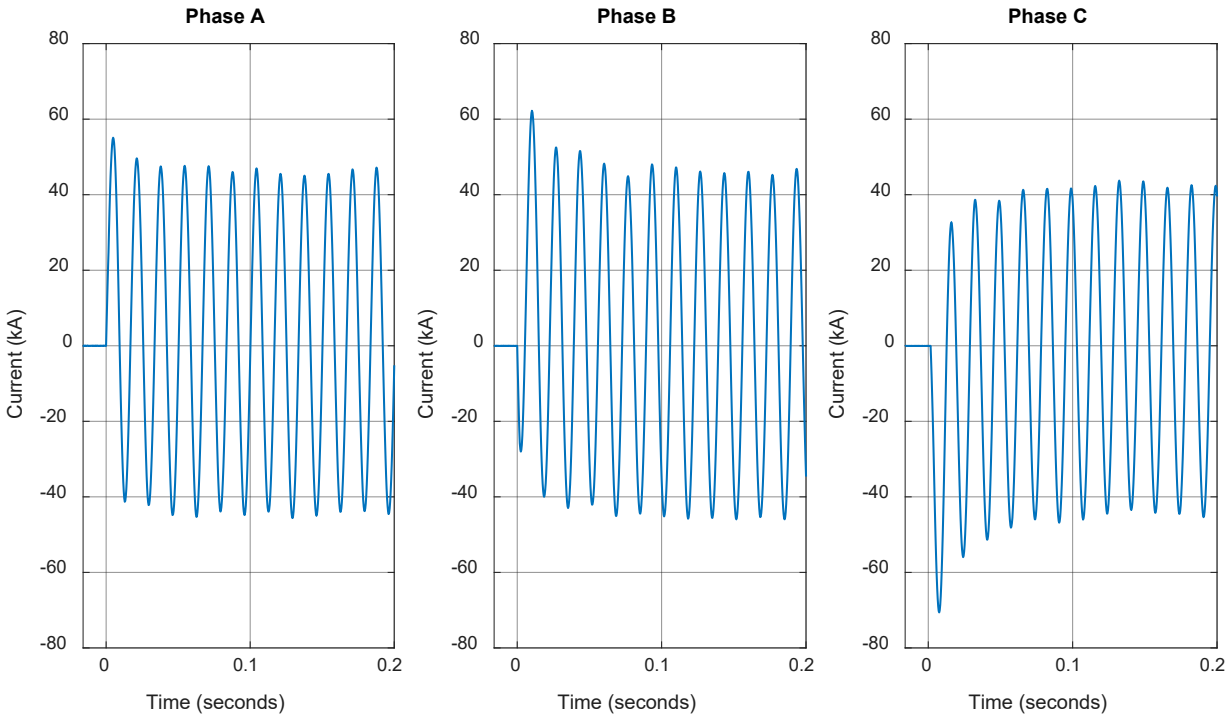


Fig. 104. Transient current profiles for Experiment 2-10. Measurement uncertainty ±3 percent.

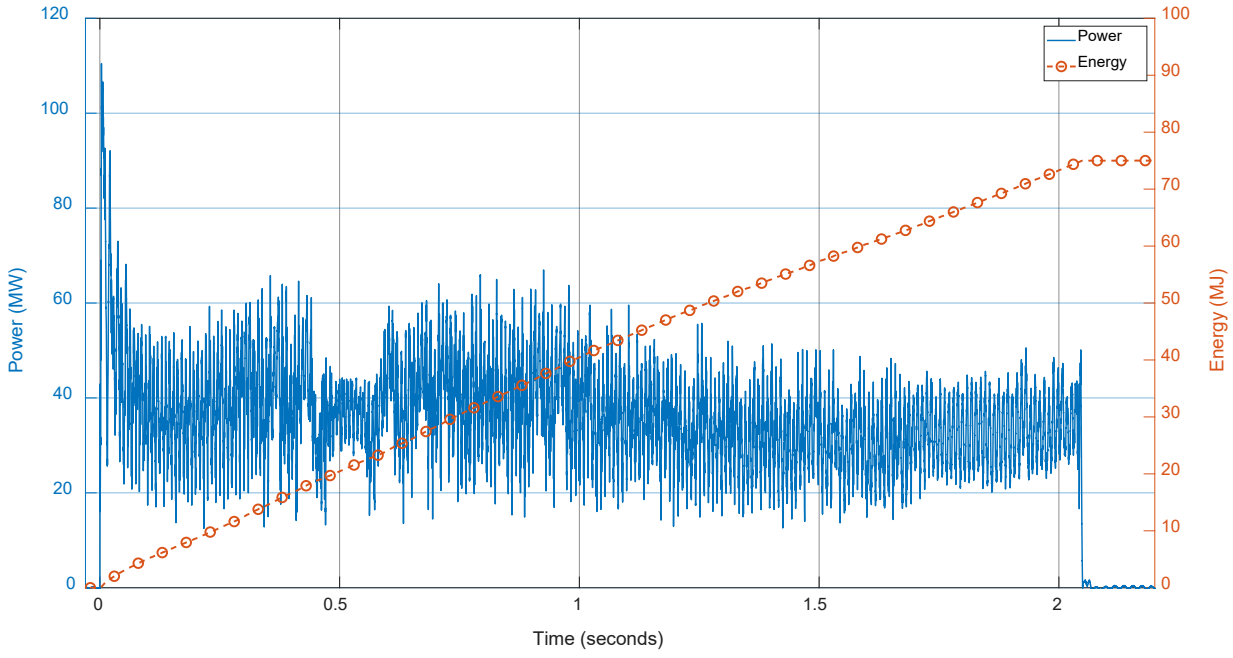


Fig. 105. Power and Energy for Experiment 2-10. Measurement uncertainty ±3 percent.

## B.2. Experiment 2-12 (MV Switchgear, Copper Bus, Steel Enclosure, 6.9 kV, 32kA, 4 s)

The voltage and current profile for the entire duration of the experiment is shown in Fig. 106. The transient region for current phases is presented in Fig. 107. Energy and power profiles are presented in Fig. 108.

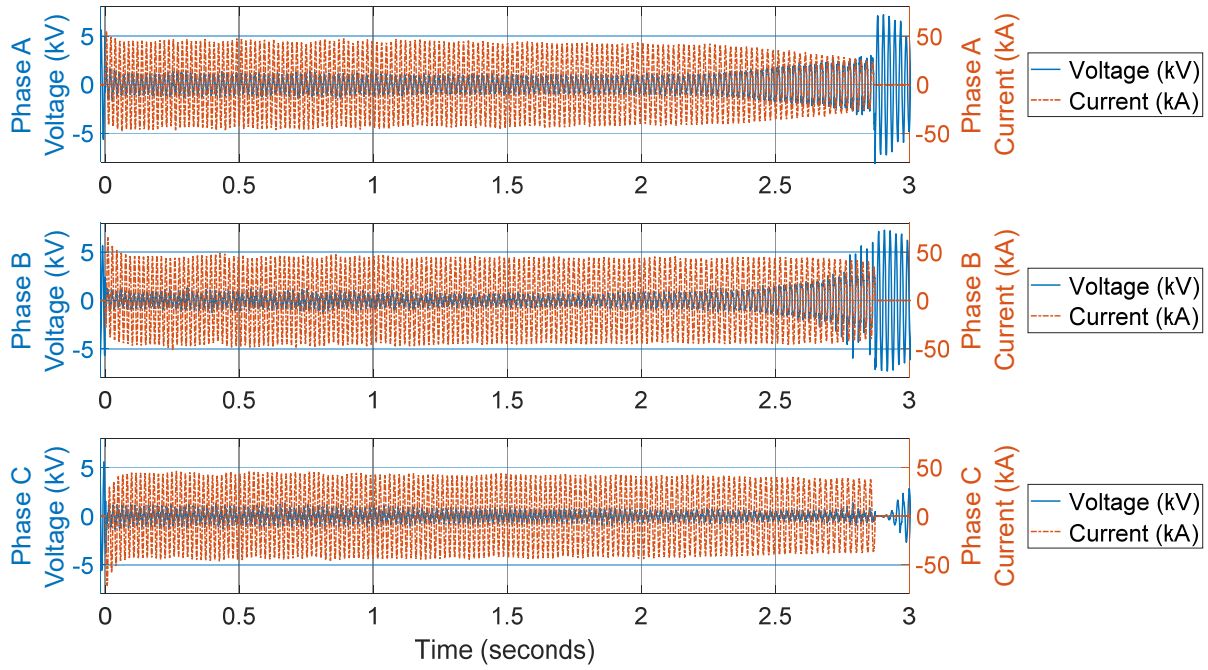


Fig. 106. Voltage and Current Profile during Experiment 2-12. Measurement uncertainty ±3 percent.

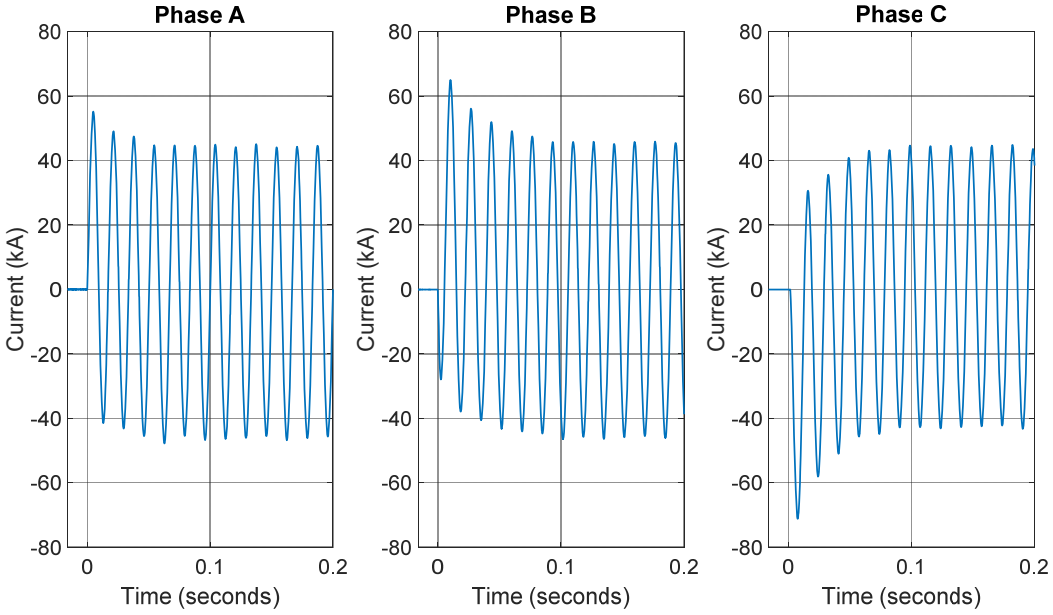


Fig. 107. Transient current profiles for Experiment 2-12. Measurement uncertainty ±3 percent.

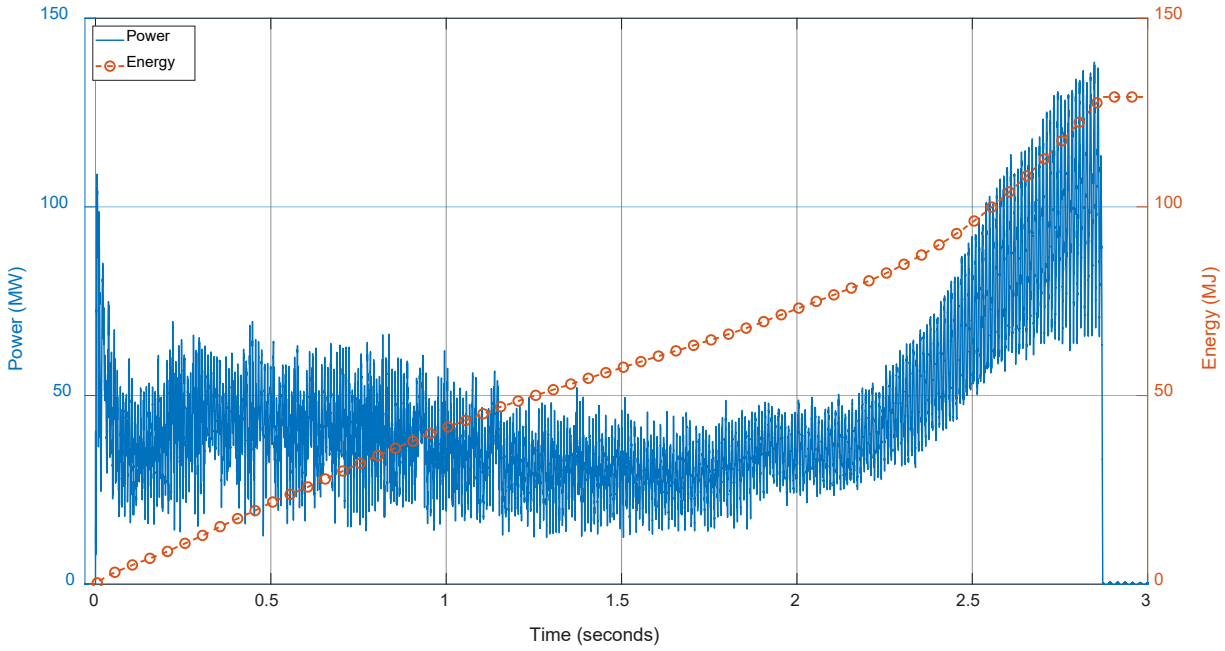


Fig. 108. Power and Energy for Experiment 2-12. Measurement uncertainty ±3 percent.

## B.3. Experiment 2-25 (MV Bus Duct, Copper Bus, Steel Enclosure, 4.16kV, 30kA, 2 s)

The voltage and current profile for the entire duration of the experiment is shown in Fig. 109. The transient region for current phases is presented in Fig. 110. Energy and power profiles are presented in Fig. 111.

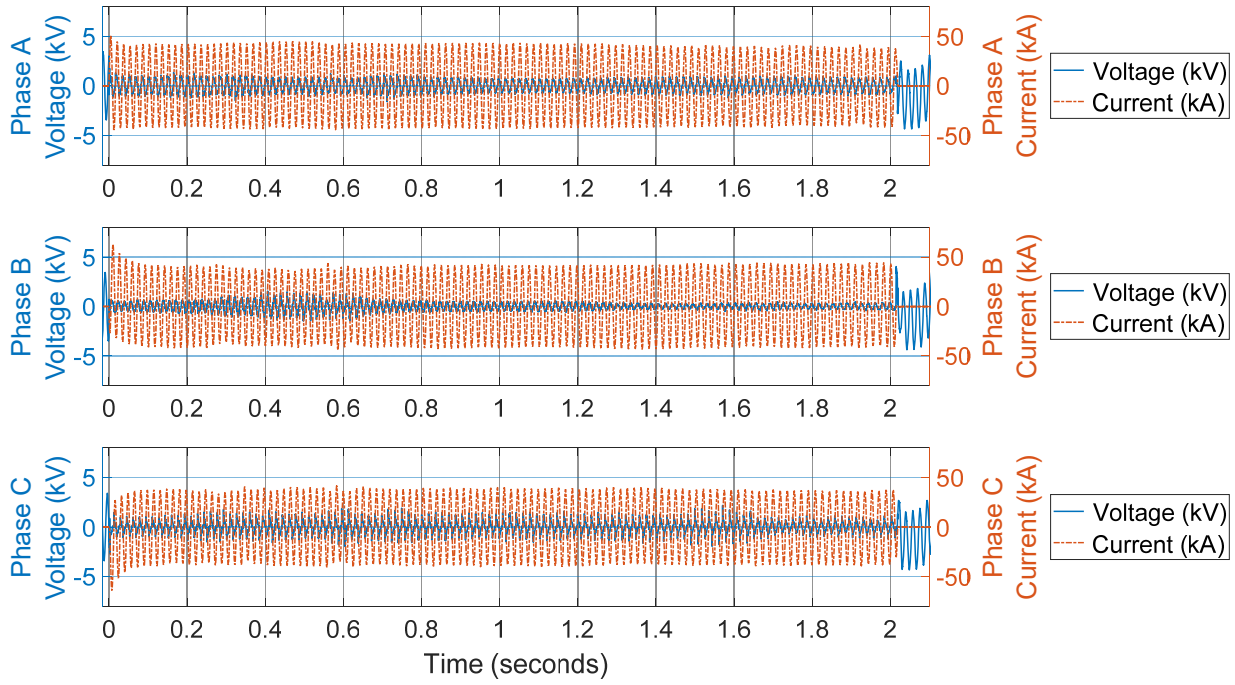


Fig. 109. Voltage and Current Profile during Experiment 2-25. Measurement uncertainty ±3 percent.

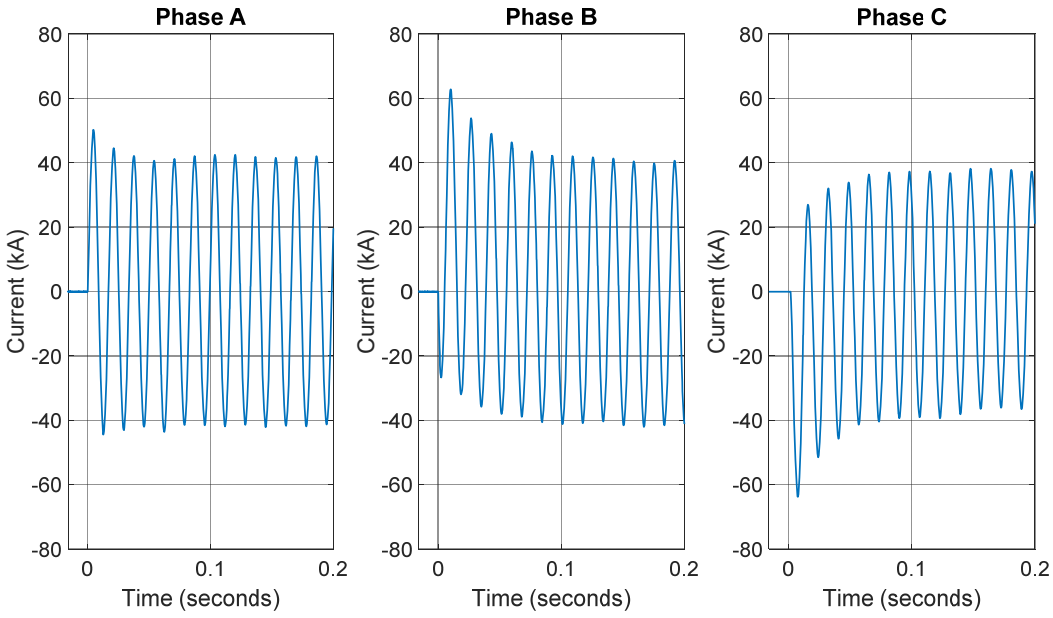


Fig. 110. Transient current profiles for Experiment 2-25. Measurement uncertainty ±3 percent.

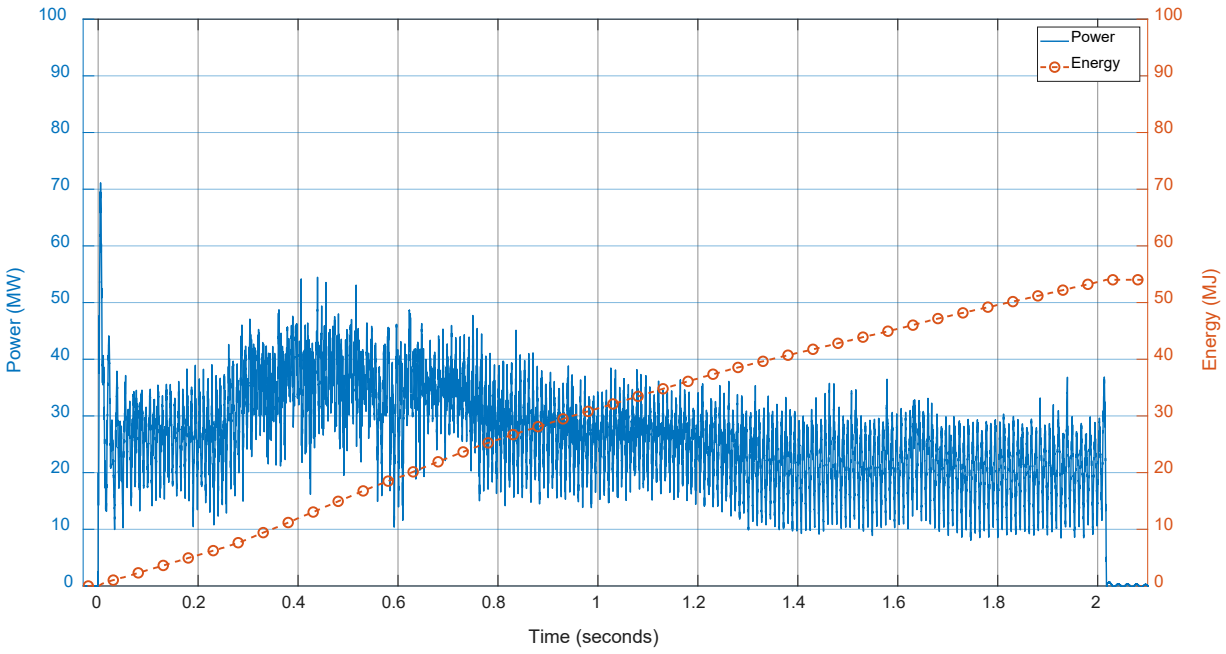


Fig. 111. Power and Energy for Experiment 2-25. Measurement uncertainty ±3 percent.

## B.4. Experiment 2-26 (MV Bus Duct, Copper Bus, Steel Enclosure, 4.16kV, 30kA, 4 s)

The voltage and current profile for the entire duration of the experiment is shown in Fig. 112. The transient region for current phases is presented in Fig. 113. Energy and power profiles are presented in Fig. 114.

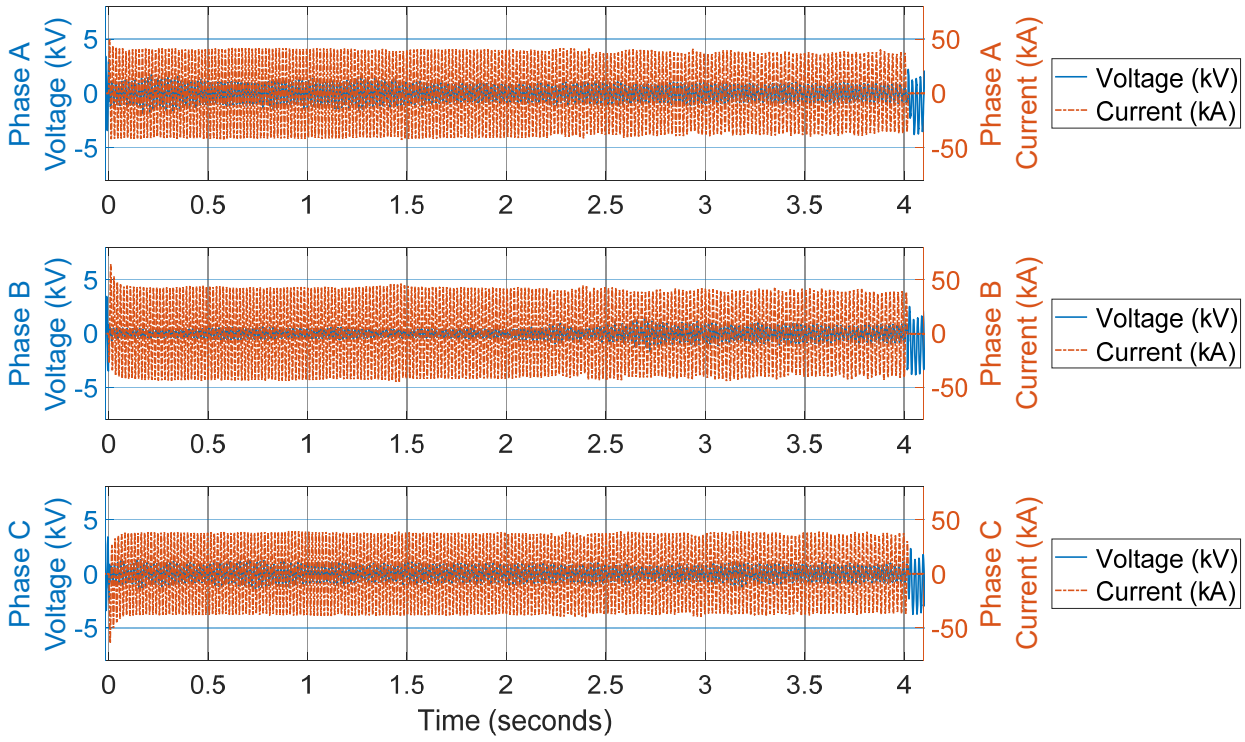


Fig. 112. Voltage and Current Profile during Experiment 2-26. Measurement uncertainty ±3 percent.

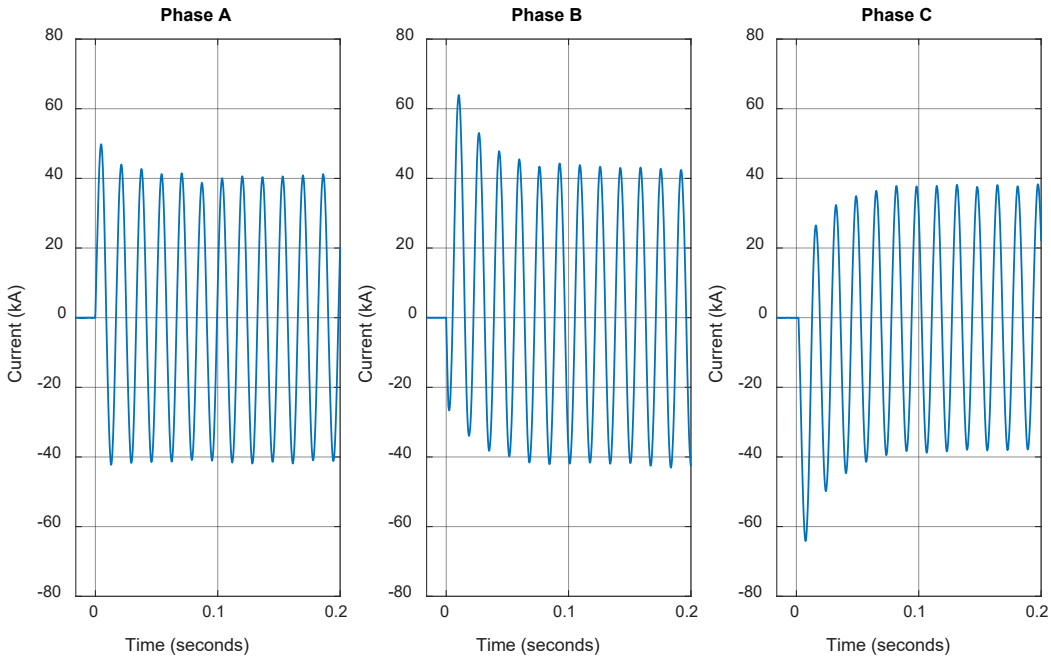


Fig. 113. Transient current profiles for Experiment 2-26. Measurement uncertainty ±3 percent.

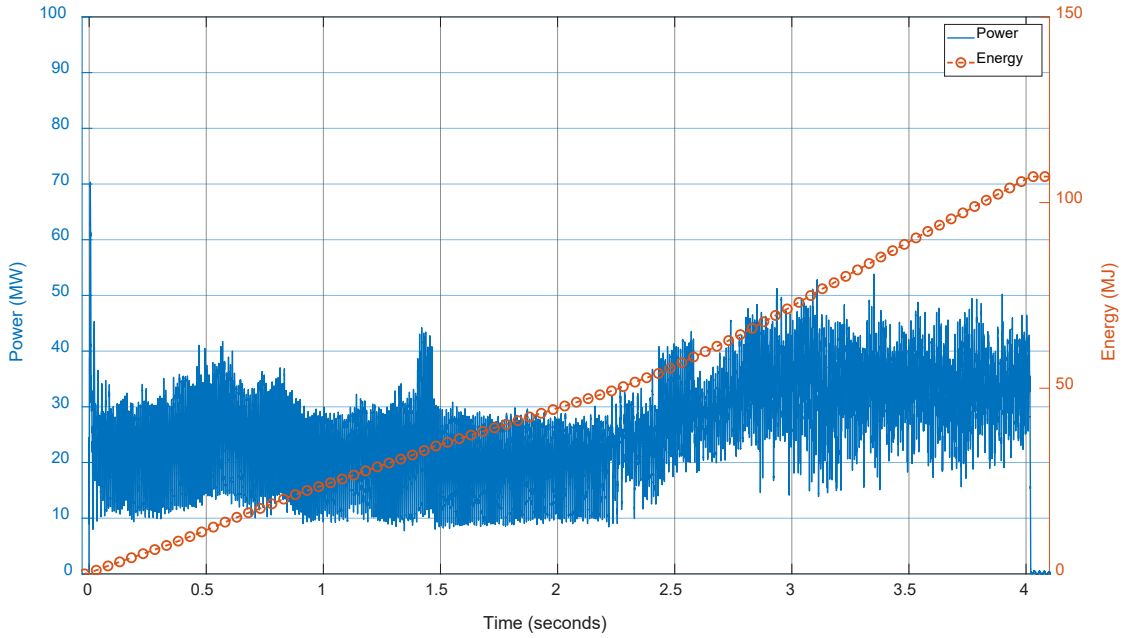


Fig. 114. Power and Energy for Experiment 2-26. Measurement uncertainty ±3 percent.

## B.5. Experiment 2-27 (MV Bus Duct, Copper Bus, Aluminum Enclosure, 4.16kV, 30kA, 2 s)

The voltage and current profile for the entire duration of the experiment is shown in Fig. 115. The transient region for current phases is presented in Fig. 116. Energy and power profiles are presented in Fig. 117.

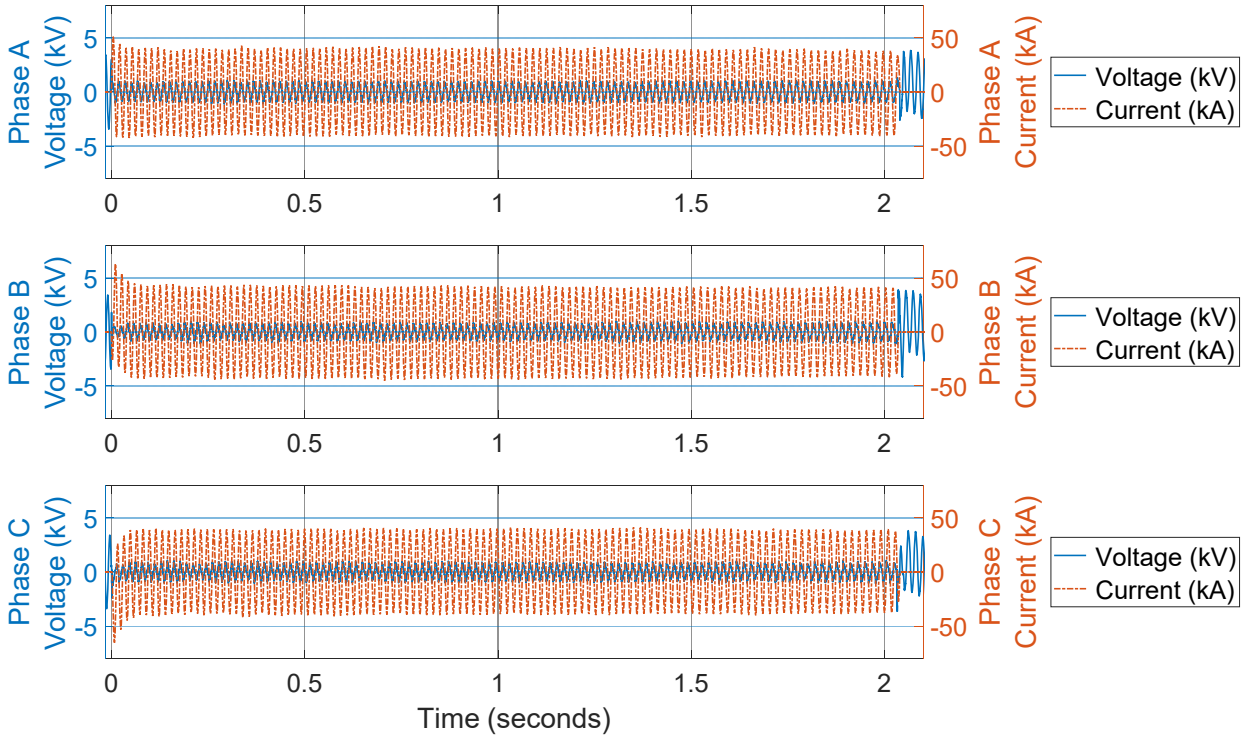


Fig. 115. Voltage and Current Profile during Experiment 2-27. Measurement uncertainty ±3 percent.

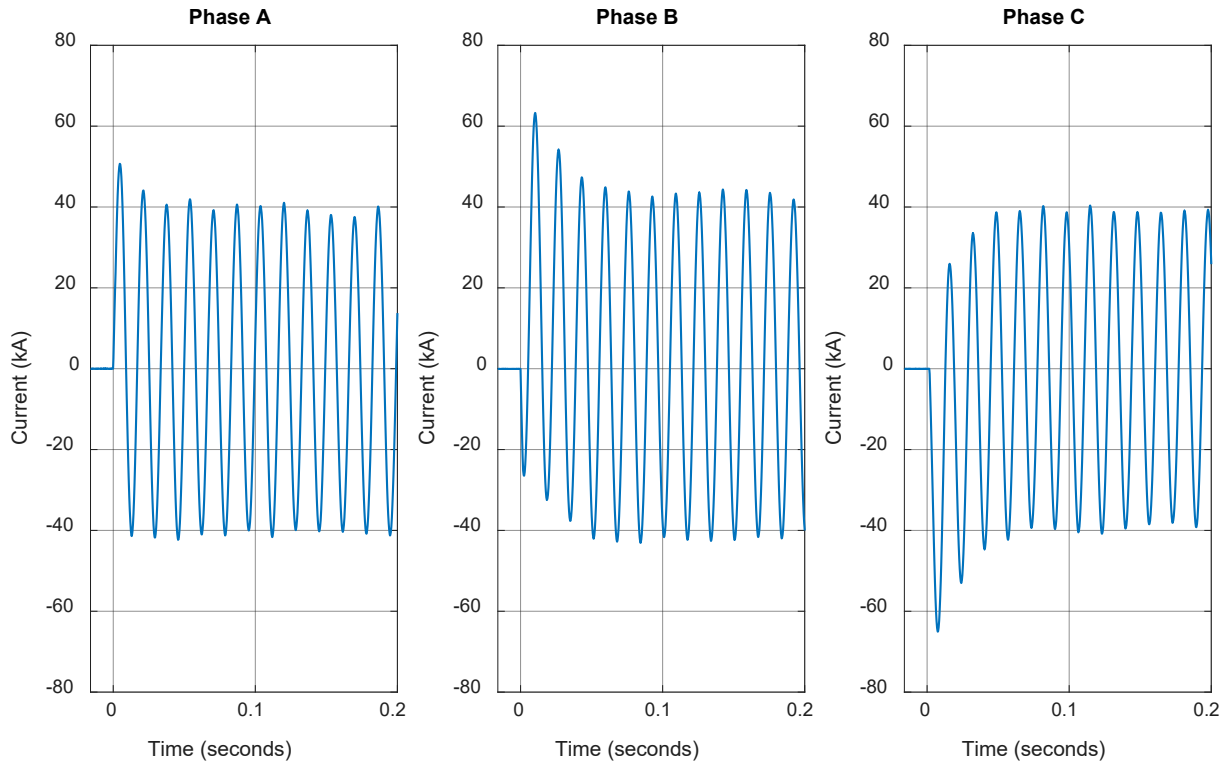


Fig. 116. Transient current profiles for Experiment 2-27. Measurement uncertainty ±3 percent.

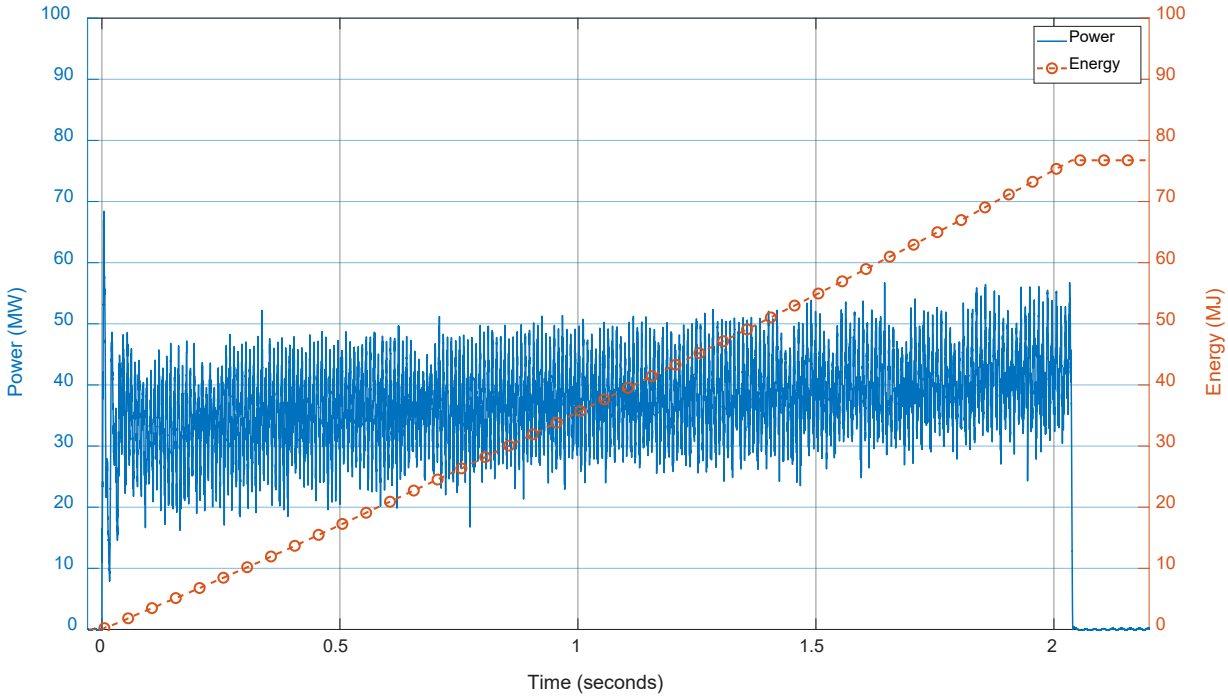


Fig. 117. Power and Energy for Experiment 2-27. Measurement uncertainty ±3 percent.

## B.6. Experiment 2-28 (MV Bus Duct, Copper Bus, Aluminum Enclosure, 4.16kV, 30kA, 4 s)

The voltage and current profile for the entire duration of the experiment is shown in Fig. 118. The transient region for current phases is presented in Fig. 119. Energy and power profiles are presented in Fig. 120.

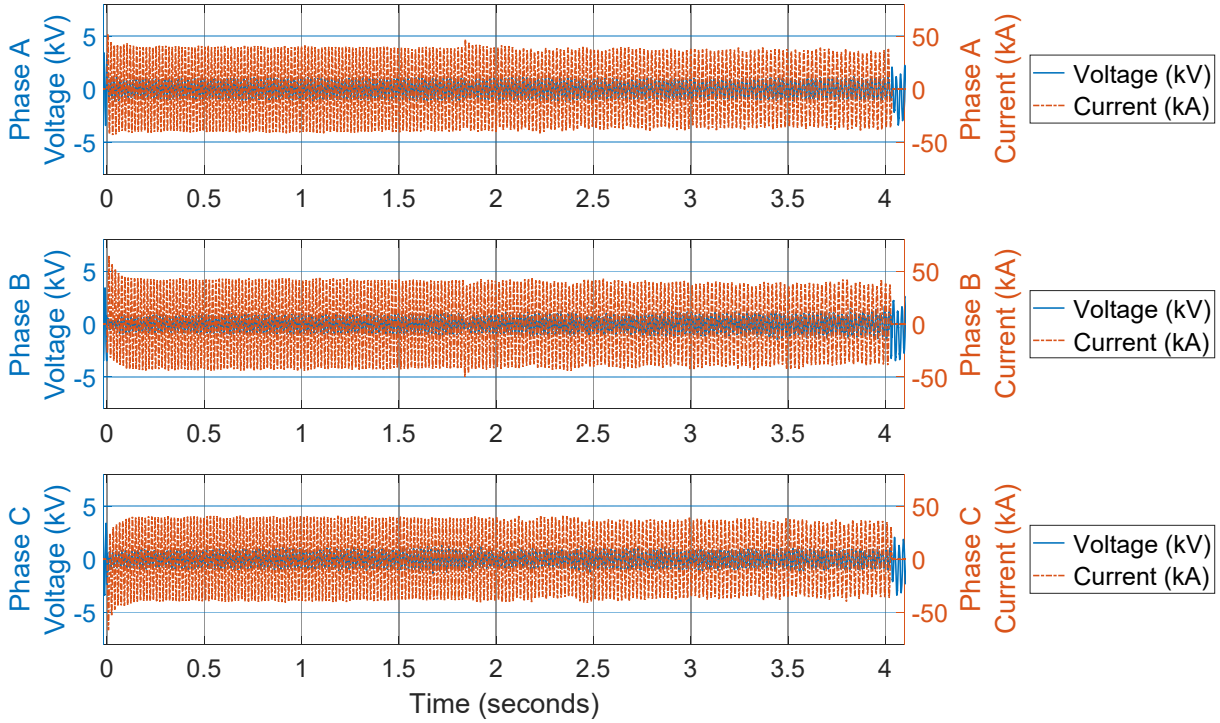


Fig. 118. Voltage and Current Profile during Experiment 2-28. Measurement uncertainty ±3 percent.

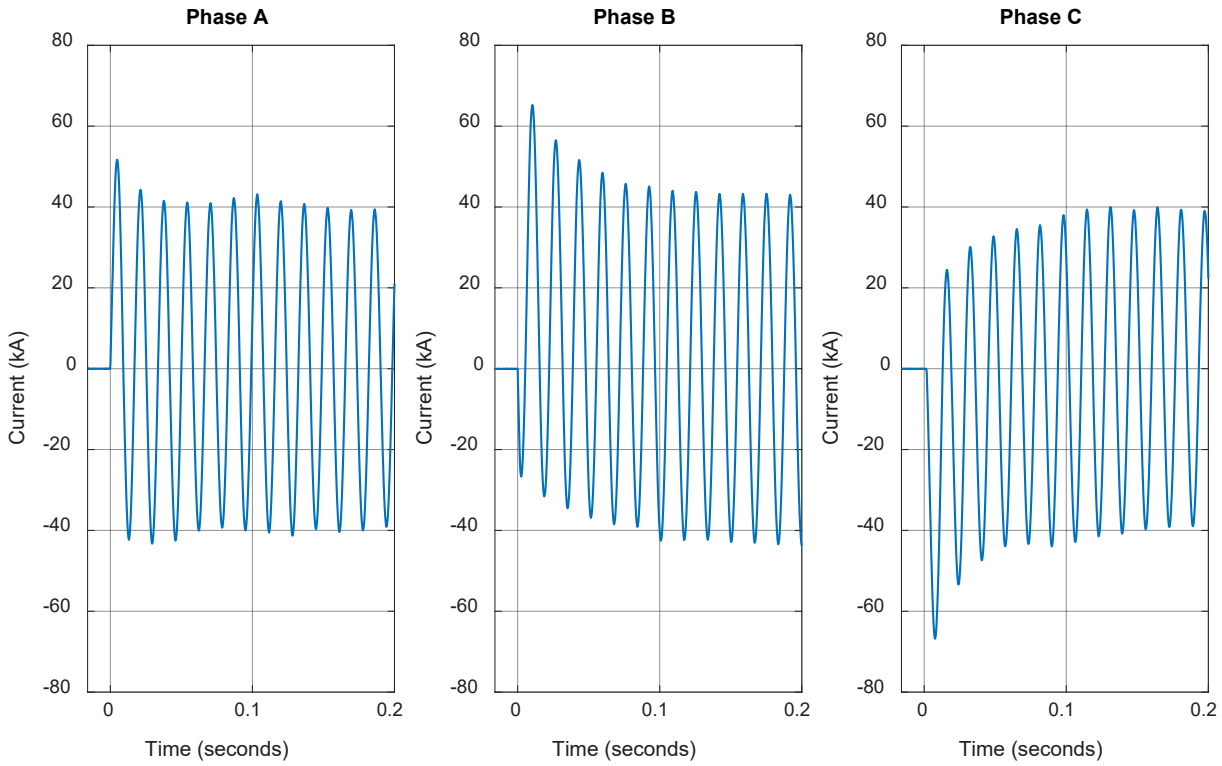


Fig. 119. Transient current profiles for Experiment 2-28. Measurement uncertainty ±3 percent.

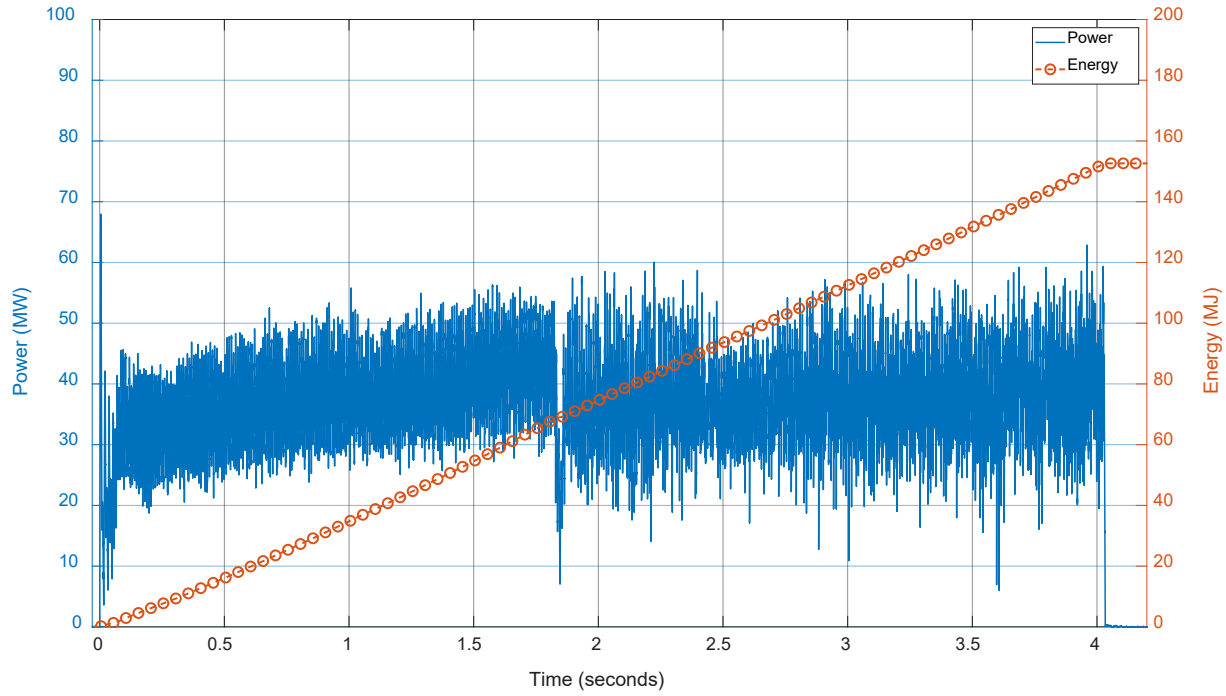


Fig. 120. Power and Energy for Experiment 2-28. Measurement uncertainty ±3 percent.

## B.7. Experiment 2-30 (MV Bus Duct, Aluminum Bus, Steel Enclosure, 4.16kV, 30kA, 4 s)

The voltage and current profile for the entire duration of the experiment is shown in Fig. 121. The transient region for current phases is presented in Fig. 122. Energy and power profiles are presented in Fig. 123.

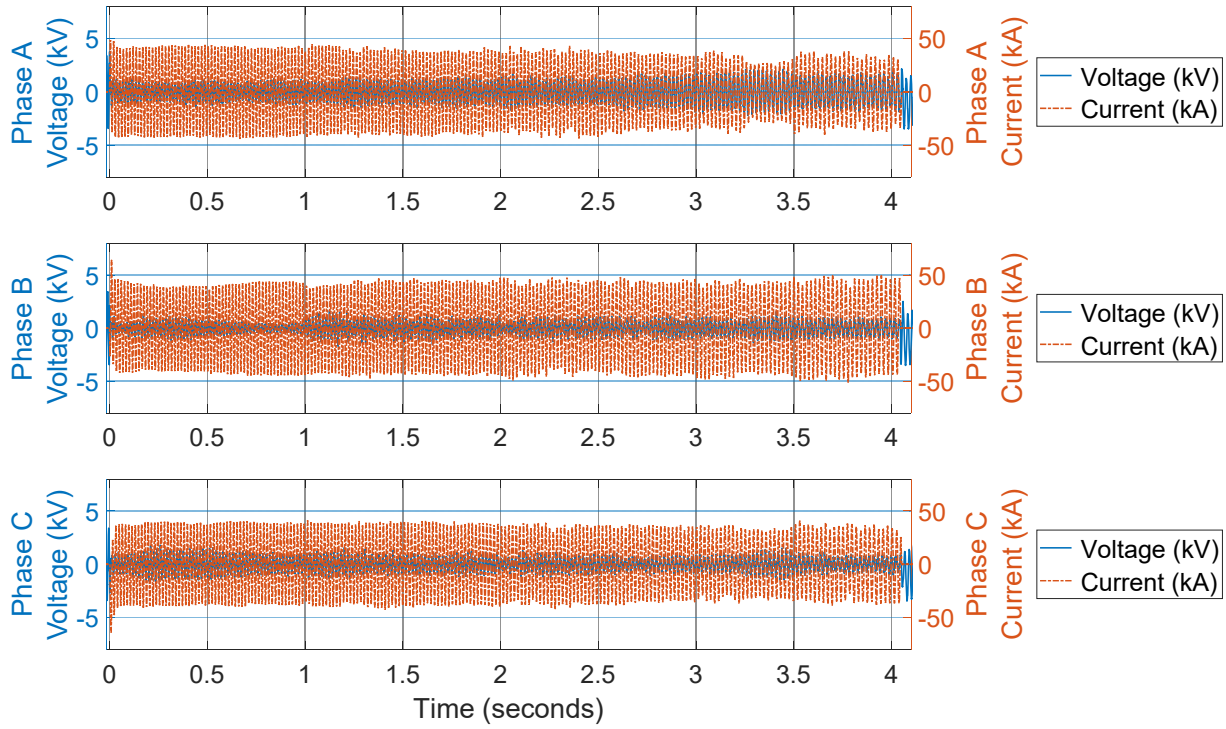


Fig. 121. Voltage and Current Profile during Experiment 2-30. Measurement uncertainty ±3 percent.

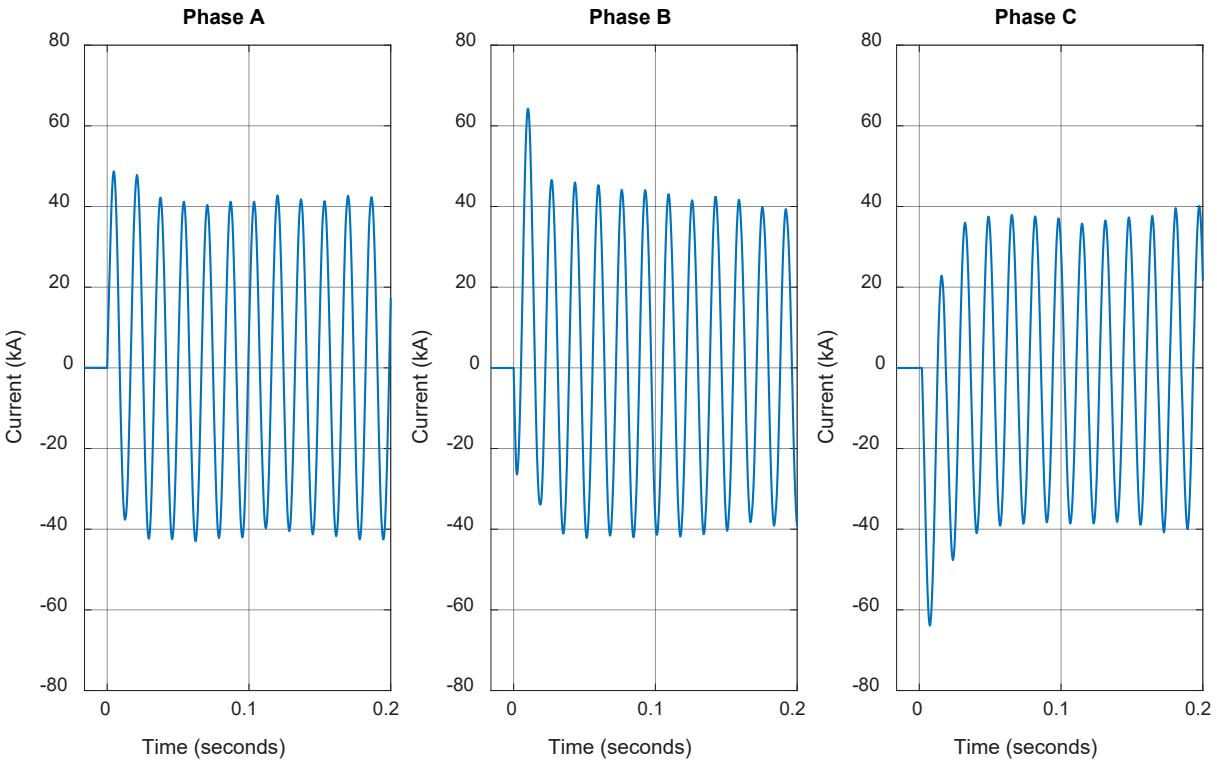


Fig. 122. Transient current profiles for Experiment 2-30. Measurement uncertainty ±3 percent.

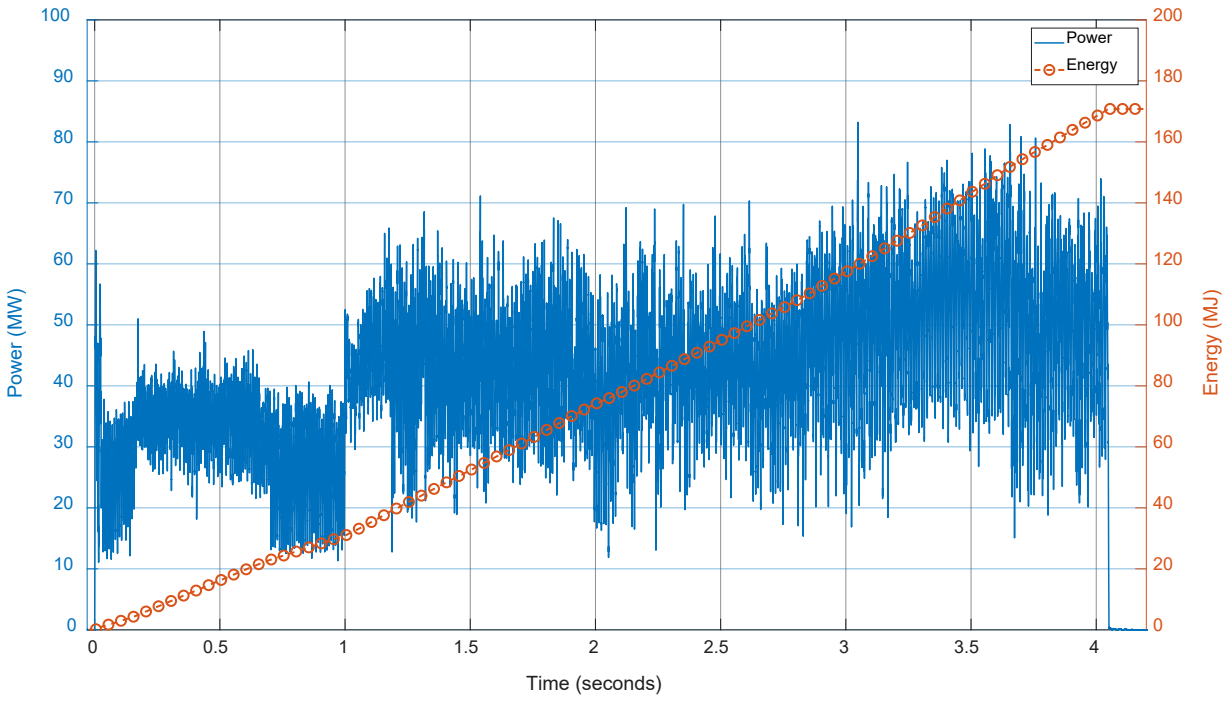


Fig. 123. Power and Energy for Experiment 2-30. Measurement uncertainty ±3 percent.

## B.8. Experiment 2-30B (MV Bus Duct, Aluminum Bus, Steel Enclosure, 4.16kV, 30kA, 4 s)

The voltage and current profile for the entire duration of the experiment is shown in Fig. 124. The transient region for current phases is presented in Fig. 125. Energy and power profiles are presented in Fig. 126.

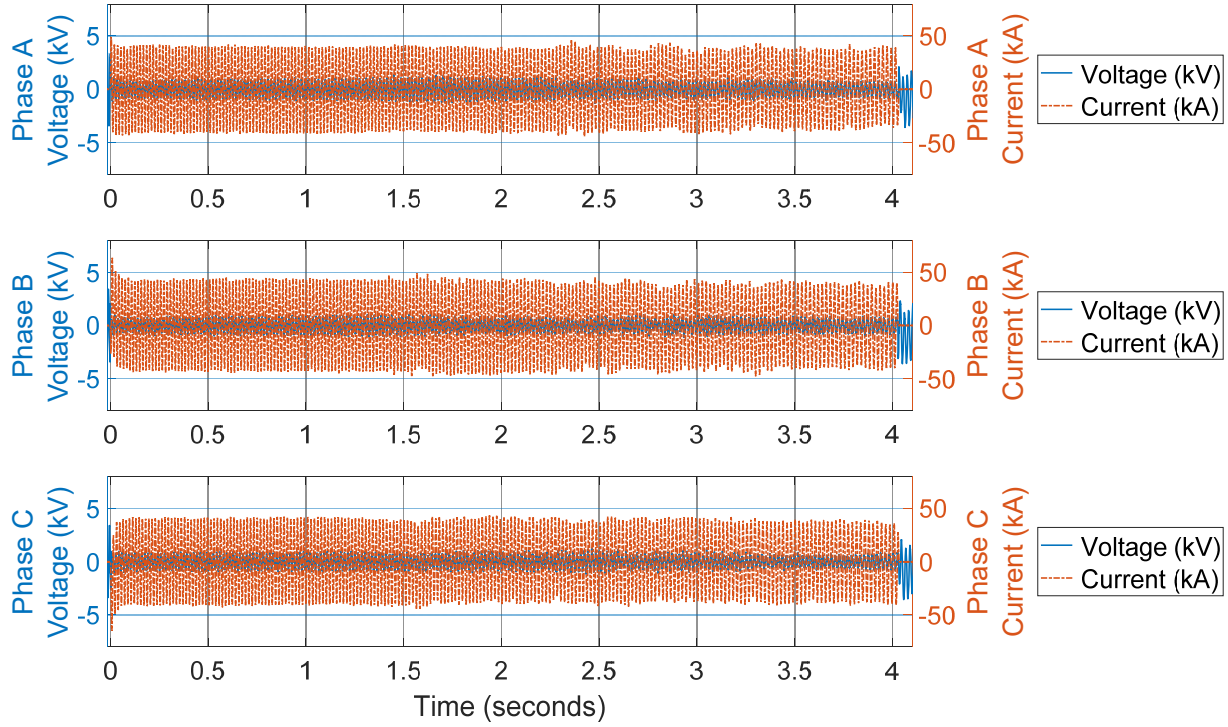


Fig. 124. Voltage and Current Profile during Experiment 2-30B. Measurement uncertainty ±3 percent.

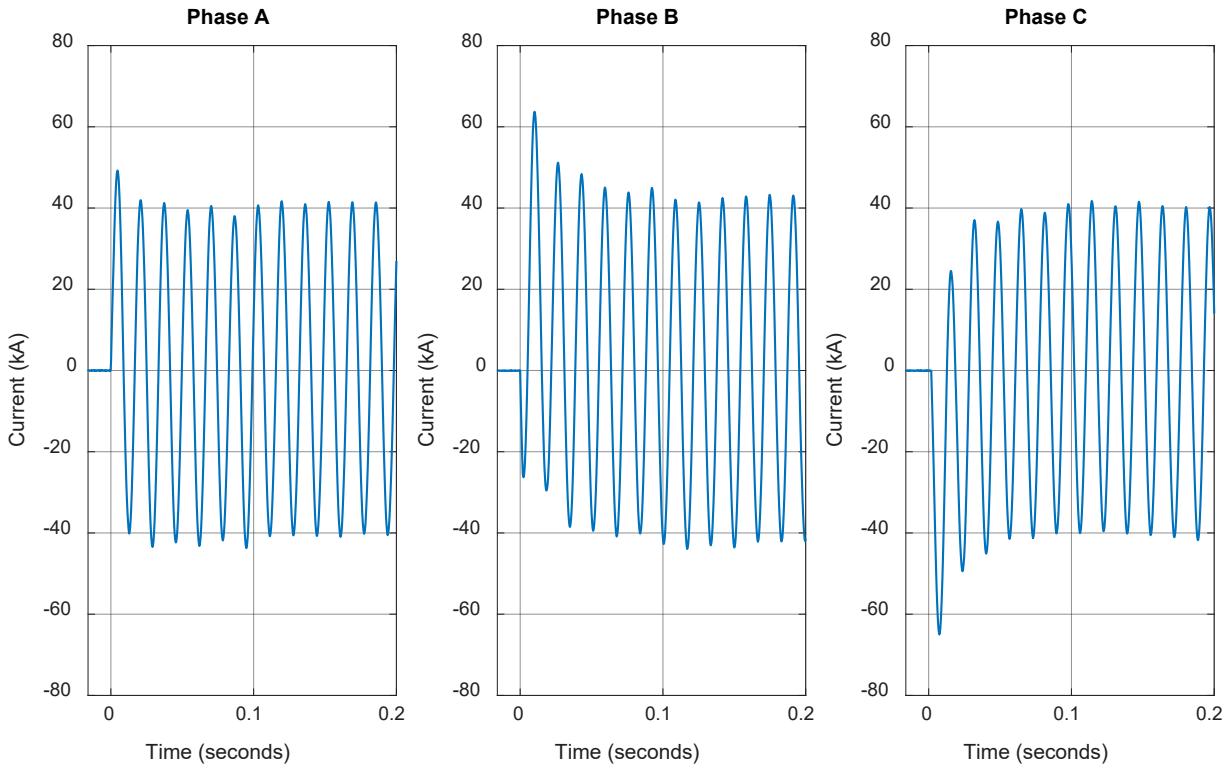


Fig. 125. Transient current profiles for Experiment 2-30B. Measurement uncertainty ±3 percent.

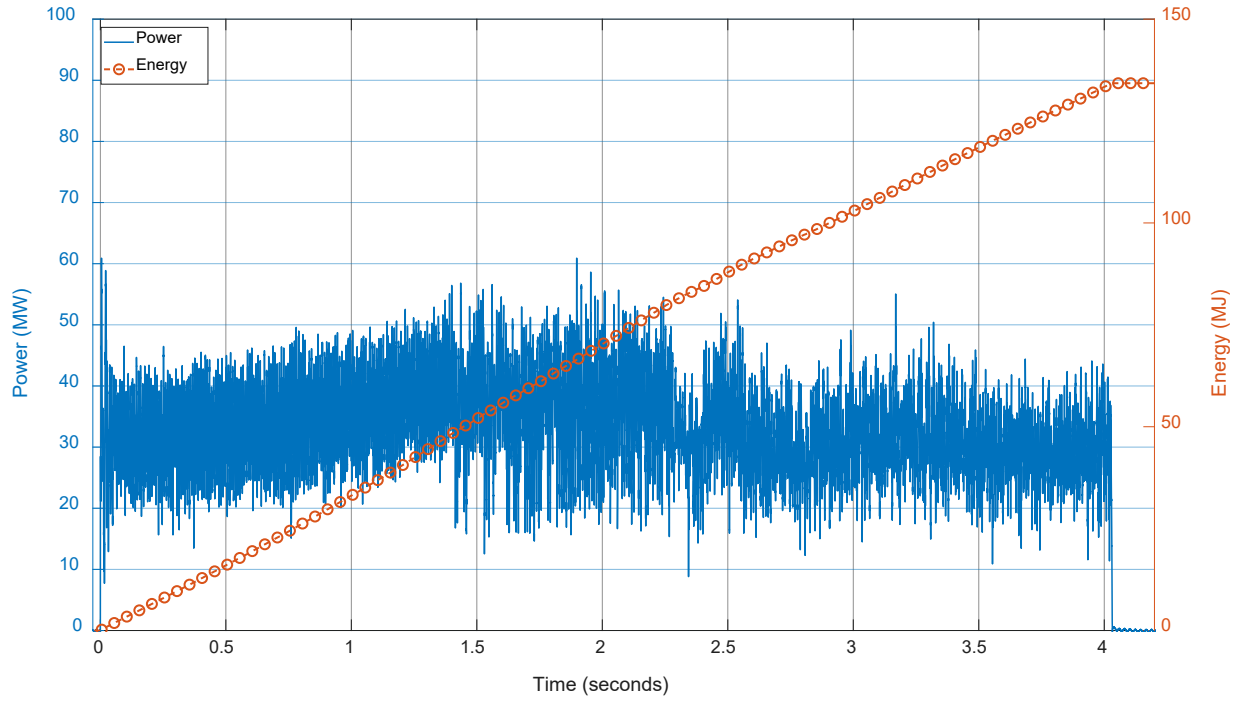


Fig. 126. Power and Energy for Experiment 2-30B. Measurement uncertainty ±3 percent.

## B.9. Experiment 2-31 (MV Bus Duct, Aluminum Bus, Aluminum Enclosure, 4.16kV, 30kA, 2 s)

The voltage and current profile for the entire duration of the experiment is shown in Fig. 127. The transient region for current phases is presented in Fig. 128. Energy and power profiles are presented in Fig. 129.

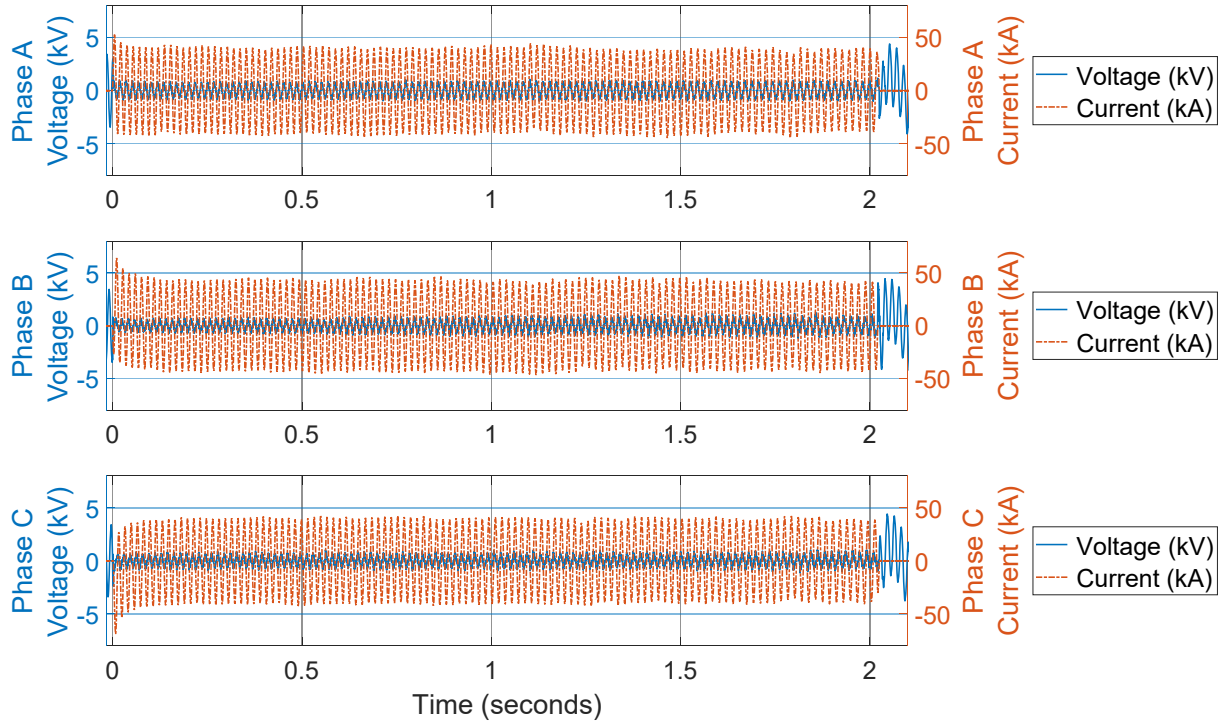


Fig. 127. Voltage and Current Profile during Experiment 2-31. Measurement uncertainty ±3 percent.

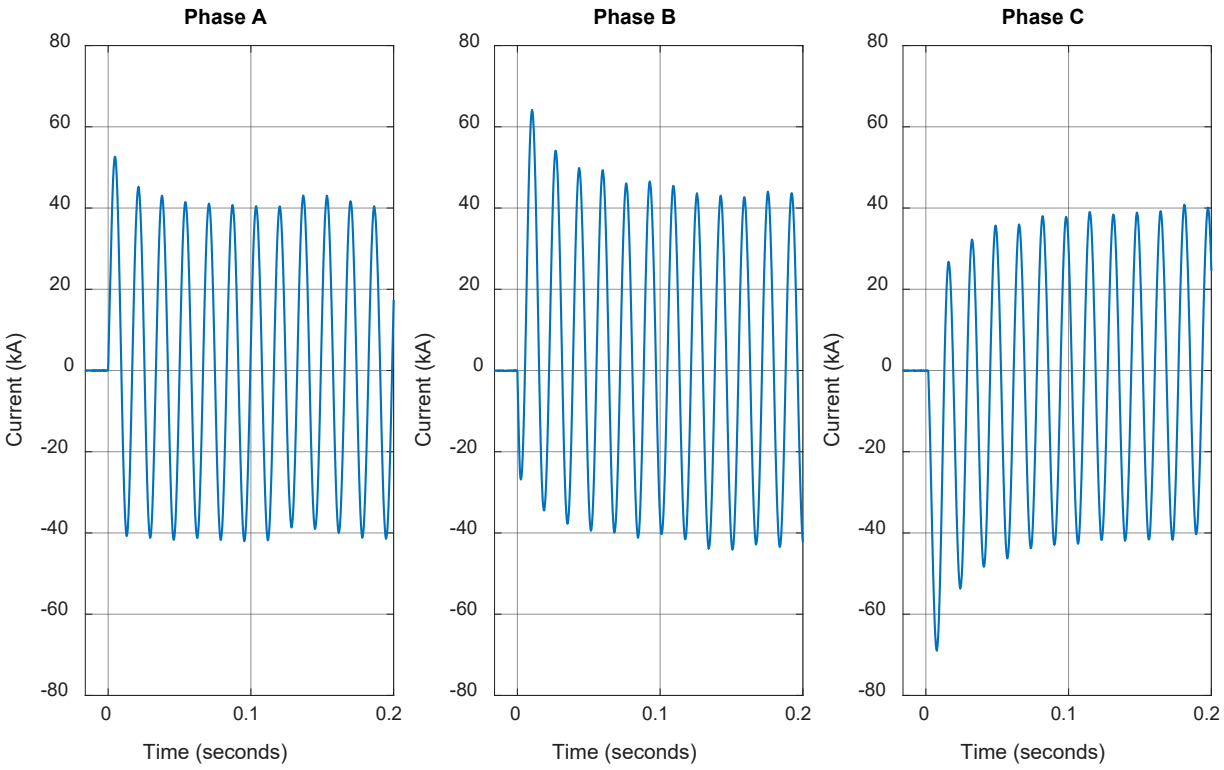


Fig. 128. Transient current profiles for Experiment 2-31. Measurement uncertainty ±3 percent.

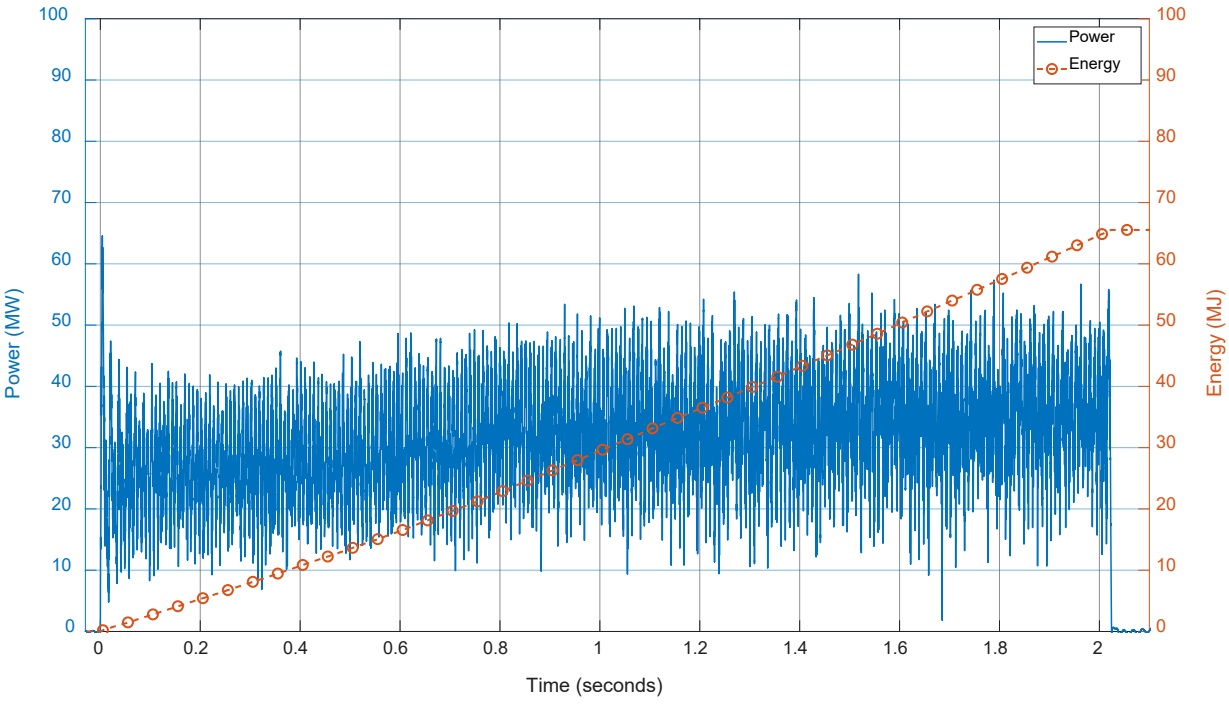


Fig. 129. Power and Energy for Experiment 2-31. Measurement uncertainty ±3 percent.

## B.10. Experiment 2-32 (MV Bus Duct, Aluminum Bus, Aluminum Enclosure, 4.16kV, 30kA, 4 s)

The voltage and current profile for the entire duration of the experiment is shown in Fig. 130. The transient region for current phases is presented in Fig. 131. Energy and power profiles are presented in Fig. 132.

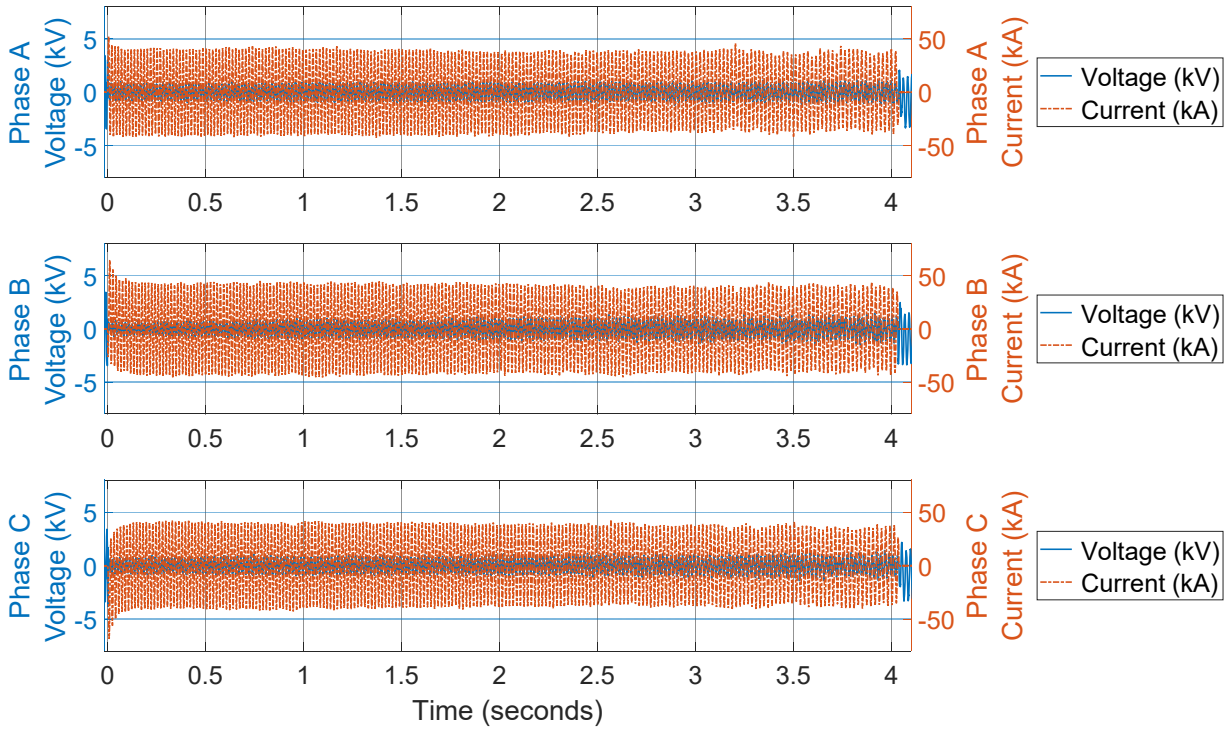


Fig. 130. Voltage and Current Profile during Experiment 2-32. Measurement uncertainty ±3 percent.

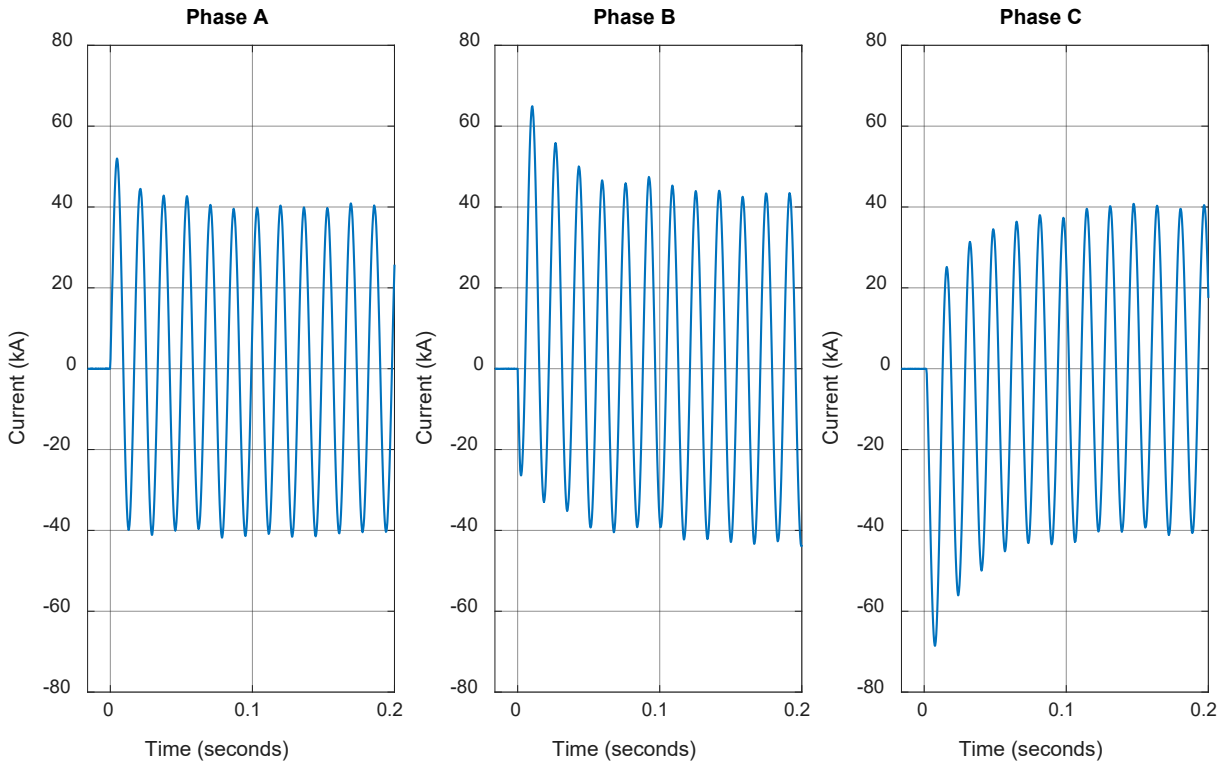


Fig. 131. Transient current profiles for Experiment 2-32. Measurement uncertainty ±3 percent.

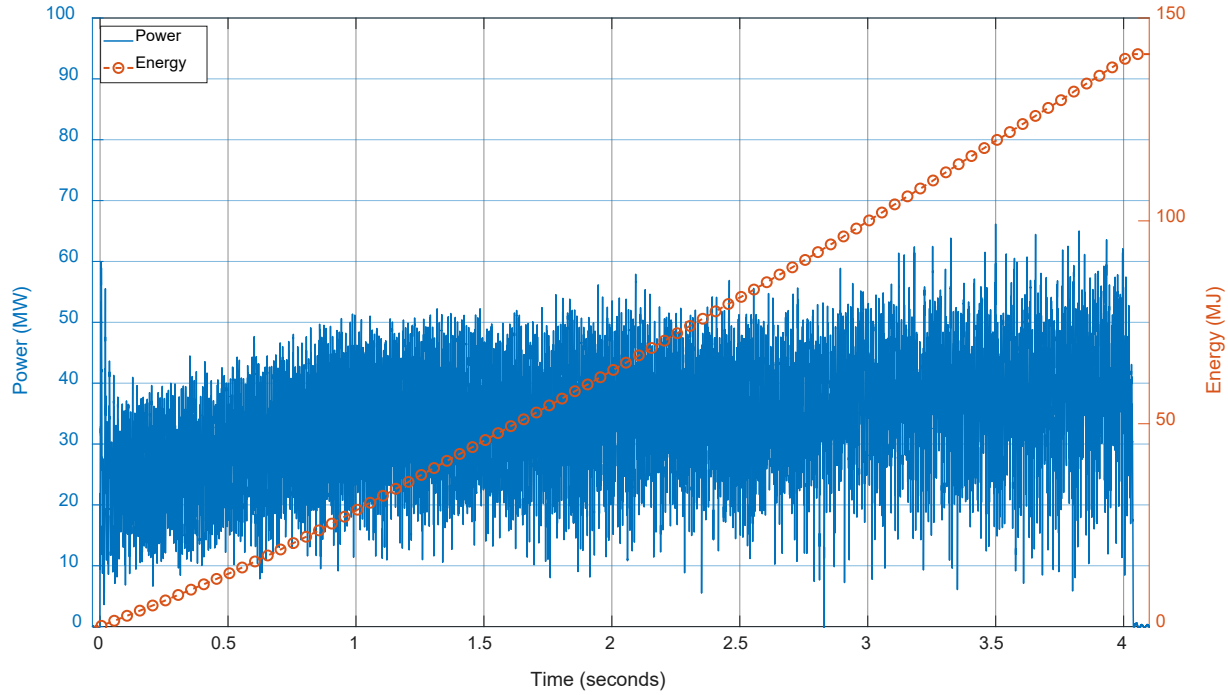


Fig. 132. Power and Energy for Experiment 2-32. Measurement uncertainty ±3 percent.

# Appendix C. Weights and Measurements

This appendix provides mass and dimension measurements of experiment object components.

## C.1. Switchgear Electrical Enclosure and Conductors

Prior to performing high energy arcing fault experiments on the experiment devices, the electrical contractor removed the metal cladding, and with the support from NRC and NIST staff, each removed panel was weighed using calibrated mass balances. The initial and final measurements for the metal cladding are presented below for each experiment device. The figures that follow (Fig. 130 through Fig. 135) have been annotated to identify the panels that were weighted. The figures include panel dimensions which are reported in centimeters (inches). The bus conductors in the primary cable connection compartment were removed and weighed before and after each experiment. Those measurements are also reported in this appendix.

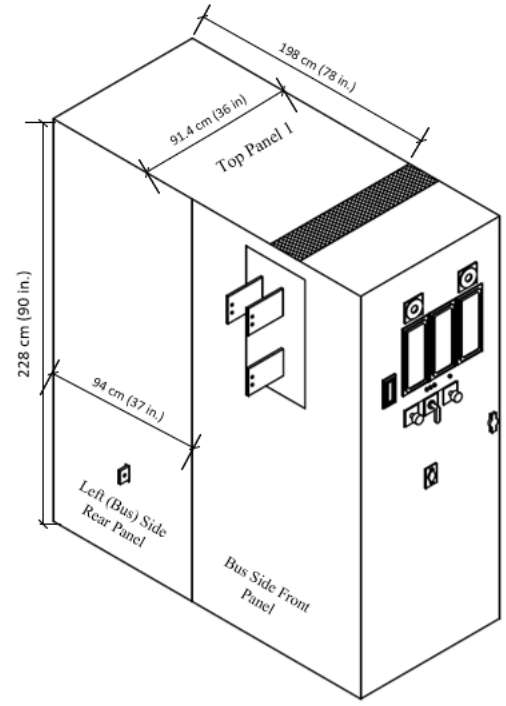


Fig. 133. Exterior Isometric. Dimensions ± 0.6 cm (± 0.25 in).

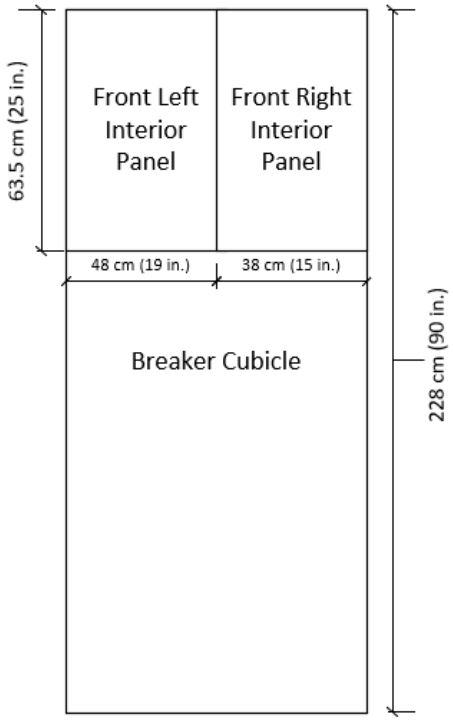


Fig. 134. Interior Front. Dimensions ± 0.6 cm (± 0.25 in).

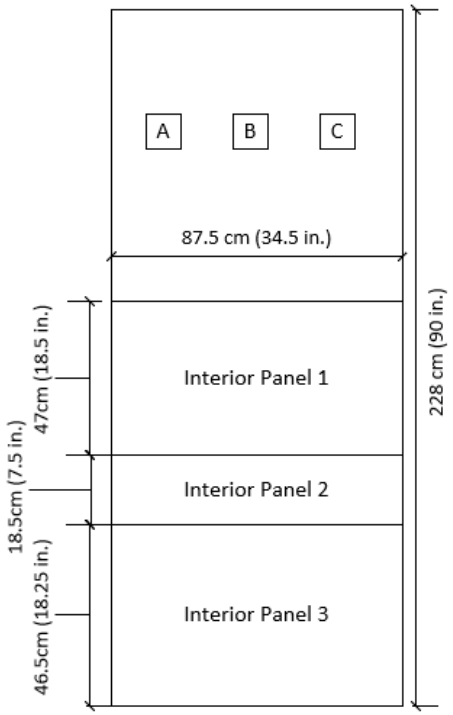


Fig. 135. Interior Rear. Dimensions ± 0.6 cm (± 0.25 in).

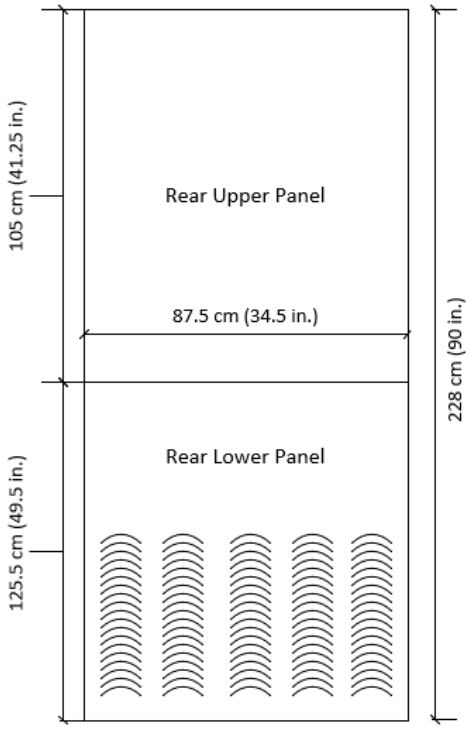


Fig. 136. Exterior Rear. Dimensions ± 0.6 cm (± 0.25 in).

### C.1.1. Switchgear Enclosure Weights

#### C.1.1.1. Experiment 2-10 Switchgear Medium-Voltage Copper Bus, 2s

The mass measurements from the electrical enclosure metal cladding are presented in Table 55. The masses recorded from the electrical conductors are presented in Table 56. Soot and other loose byproducts were removed from the electrical conductors prior to measurement. The expanded uncertainty in the scale 1 measurements, based on manufacturer specifications of similar scales, is ± 1 kg with a 95 percent confidence interval. The expanded uncertainty in the scale 2 measurements, derived from manufacturer specifications, is ± 1 g with a 95 percent confidence interval.

Table 57. Experiment Device Mass Measurements from Experiment 2-10 - Enclosure Metal-Cladding

| Figure | Description | Pre-Experiment | | Post-Experiment | | Δ mass (g) | Approximate Dimensions (in) |
|---|---|---|---|---|---|---|---|
| | | Scale 1 (kg) | Scale 2 (g) | Scale 1 (kg) | Scale 2 (g) | | |
| Fig. 133 | Right Side Rear Panel | 93.0 | | No observable enclosure breach noted during post-experiment inspection. Therefore, post-experiment enclosure mass measurements were not taken. | | | 37 L x 89.25 H |
| Fig. 133 | Left (Bus) Side Rear Panel | 43.1 | | | | | 37 L x 89.25 H |
| Fig. 134 | Front Left Interior Panel | | 6 115.0 | | | | 25 H x 19 W |
| Fig. 134 | Front Right Interior Panel | | 4 731.5 | | | | 25 H x 15 W |
| Fig. 133 | Top Panel 1 | 35.6 | | | | | 78 L x 36 W |
| Fig. 135 | Interior Panel 1 | | 9634.0 | | | | 34.5 L x 18.5 H |
| Fig. 135 | Interior Panel 2 | | 85914.5 | | | | 34.5 L x1 7.25 H |
| N/A | Interior Panel 2 steel connector | | 270.0 | | | | |
| Fig. 135 | Interior Panel 3 | | 10,201.5 | | | | 34.5 L x 18.25 H |
| N/A | Grounding Strap | | 1824.0 | | | | 34.5 L x 2 H x 0.25 W |
| N/A | Ground Connection | | | | | | 6 L x 2 H x 0.25 W |
| Fig. 136 | Rear Upper Panel | 16.1 | 15996.0 | | | | 36 W x 41.25 H |
| Fig. 136 | Rear Lower Panel | 24.5 | 24,392.0 | | | | 35.75 W x 49.5 H |

Table 58. Experiment Device Mass Measurements from Experiment 2-10 – Electrical Conductors [made using Scale 2 with uncertainty of ± 1 g]

| Description | Pre-Experiment (g) | Post-Experiment (g) | Mass Loss (g) |
|---|---|---|---|
| **Bus Phase A** | 5 093.5 | 5 093.5 | -524.5 |
| **Bus Phase B** | 5 087.5 | 5 087.5 | -985.0 |
| **Bus Phase C** | 5 108.5 | 5 108.5 | -525.5 |
| | | Total Mass Loss | 2 035.0 |

Bus bar dimensions: nominally 6.4 mm (0.25 in) by 76.2 mm (3 in), 635 mm (24 in) long, 152 mm (6 in) riser, 102 mm (4 in) connection to can (primary).

### C.1.1.2. Experiment 2-12 Switchgear Medium-Voltage Copper Bus, 4 s

The mass measurements from the electrical enclosure metal cladding are presented in Table 57. Lessons learned from the 2018 experimental series demonstrated that mass measurements using a calibrated scale were unreliable due to the HEAF experiment plating metal to the component being measured resulting in an inaccurate method to estimate mass loss. In RIL 2021-10, a graphical analysis method was used to estimate the breach area from a photograph with a measurement reference and then given the known approximate enclosure thickness (0.2381mm [0.0937 in]) and steel density (7.90g/cm$^3$) the breach mass loss can be estimated with reasonable accuracy. The analysis for this enclosure is presented in Fig. 137 and indicates a total of approximately 1287g of mass loss from the top of the enclosure. Note that the screen area was estimated to be 50 percent open and 50 percent steel. The masses recorded from the electrical conductors are presented in Table 58. Soot and other loose byproducts were removed from the electrical conductors prior to measurement.

Table 59. Experiment Device Mass Measurements from Experiment 2-12 - Enclosure Metal-Cladding

| Figure | Description | Pre-Experiment | | Δ mass (g) | Approx. Dimensions (in) |
|---|---|---|---|---|---|
| | | Scale 1 (kg) | Scale 2 (g) | | |
| Fig. 133 | Right Side Rear Panel | 43.4 | | | 37W x 89.25 H |
| Fig. 133 | Left (Bus) Side Rear Panel | 43.4 | | | 37W x 89.25 H |
| Fig. 134 | Front Left Interior Panel | | 6 188.0 | | 25H x 19 W |
| Fig. 134 | Front Right Interior Panel | | 4 791.0 | | 25 H x 15 W |
| Fig. 133 | Top Panel | 35.4 | 35 097.0 | 1 432.8[e] | 78 L x 36 W |
| Fig. 135 | Interior Panel 1 | | 9 391.0 | | 34.5 W x 18.5 H |
| Fig. 135 | Interior Panel 2 (middle) | | 14 005.0 | | 34.5 W x 27.7 H |
| N/A | Interior Panel 2 steel connector | | | | |
| Fig. 135 | Interior Panel 3 (bottom) | | 4 265.0 | | 34.5 W x 8.75H |
| N/A | Grounding Strap | | | | 34.5 W x 2 L x 0.25 H |
| N/A | Ground Connection | | | | 6 L x 2 W x 0.25 H |
| Fig. 136 | Rear Upper Panel | | 15 675.5 | | 36 W x 41.5 H |
| Fig. 136 | Rear Lower Panel | | 21 379.0 | | 35.75 W x 49.5 H |

[e] estimated vis graphical analysis

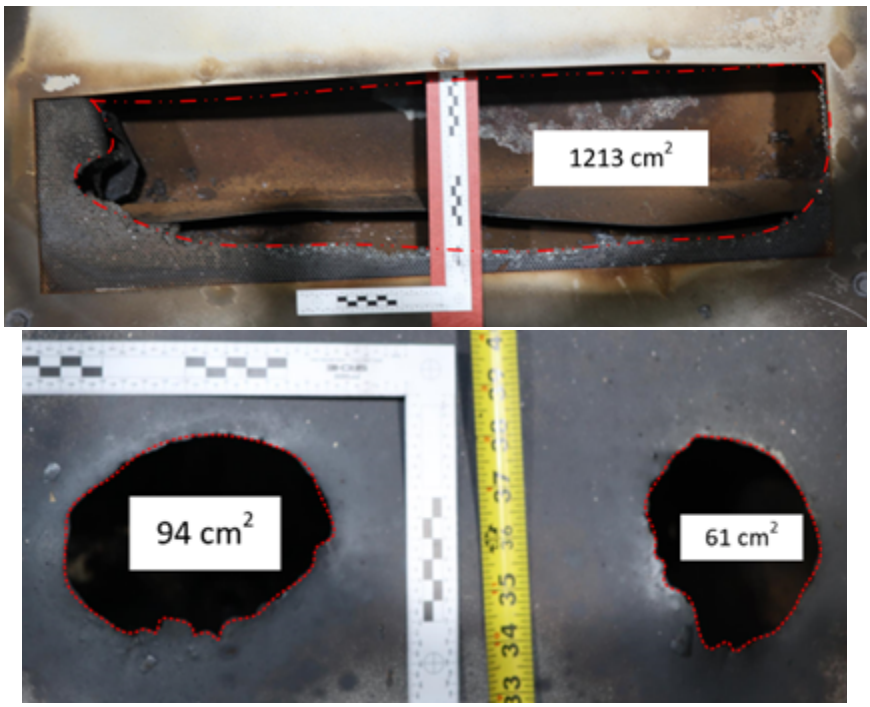


Fig. 137. Photos show breach opening with size estimate

Table 60. Experiment Device Mass Measurements from Experiment 2-12 – Electrical Conductors [made using Scale 2 with uncertainty of ± 1 g]

| Description | Pre-Experiment (g) | Post-Experiment (g) | Mass Loss (g) |
|---|---|---|---|
| **Bus Phase A** | 5 070.5 | 3 881.5 | -1 189.0 |
| **Bus Phase B** | 5 095.0 | 4 022.5 | -1 072.5 |
| **Bus Phase C** | 5 071.0 | 3 983.5 | -1 087.5 |
| | | Total Mass Loss | -3 349.0 |

Bus bar dimensions: nominally 6.4 mm (0.25 in) by 76.2 mm (3 in), 635 mm (24 in) long, 152 mm (6 in) riser, 102 mm (4 in) connection to can (primary).

## C.2. Non-Segregated Bus Duct Enclosure and Conductors

Similar to Section E.1, the enclosure panels, support members, and electrical conductors were measured and weighted. The initial and final measurements for the metal cladding are presented below for each experiment device. The figures that follow (Fig. 138 through Fig. 144) have been annotated to identify the panels that were weighted. The figures include panel dimensions which are reported in inches. The bus conductors were removed and weighed before and after each experiment. Those measurements are also reported in this appendix.

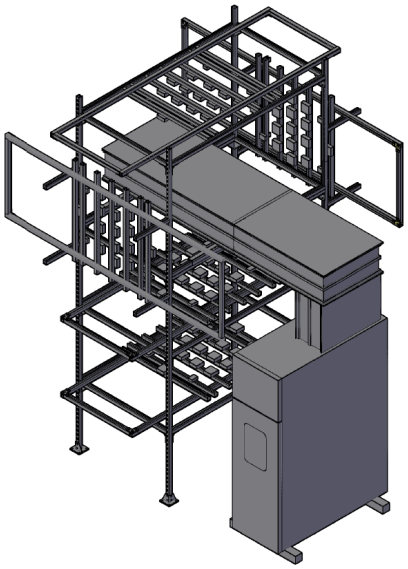

Fig. 138. Isometric drawing of general bus duct experiment configuration

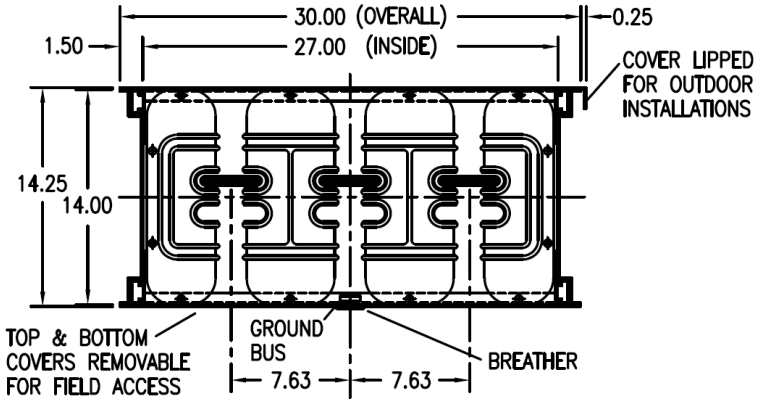


Fig. 139. Cross-section of bus duct (Note measurements in inches. Approximate from manufacturer.)

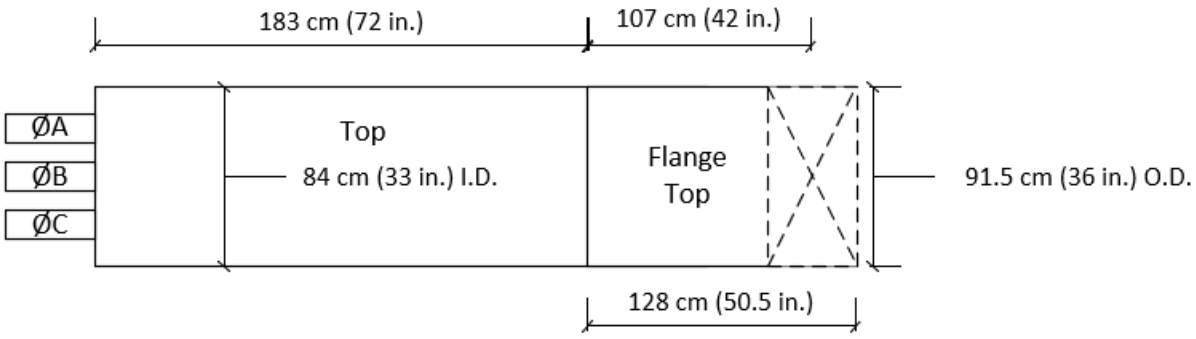


Fig. 140. Bus Duct Plan View (Aluminum bus bars) Dimensions ± 0.6 cm (± 0.25 in).

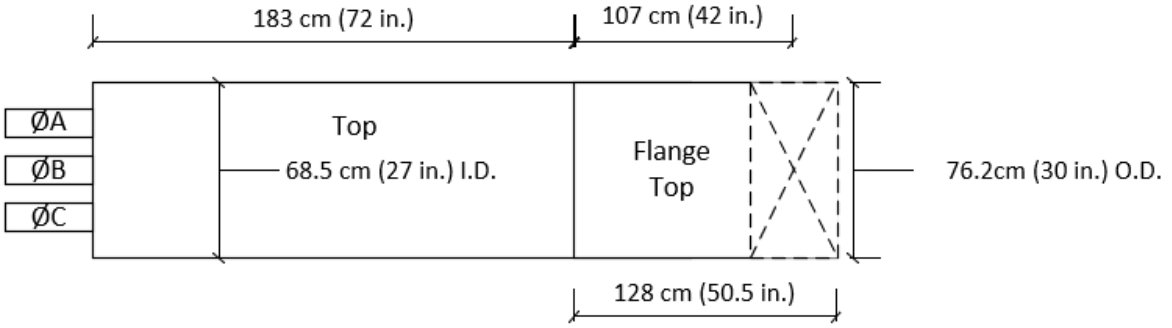


Fig. 141. Bus Duct Plan View (Copper bus bars) Dimensions ± 0.6 cm (± 0.25 in).

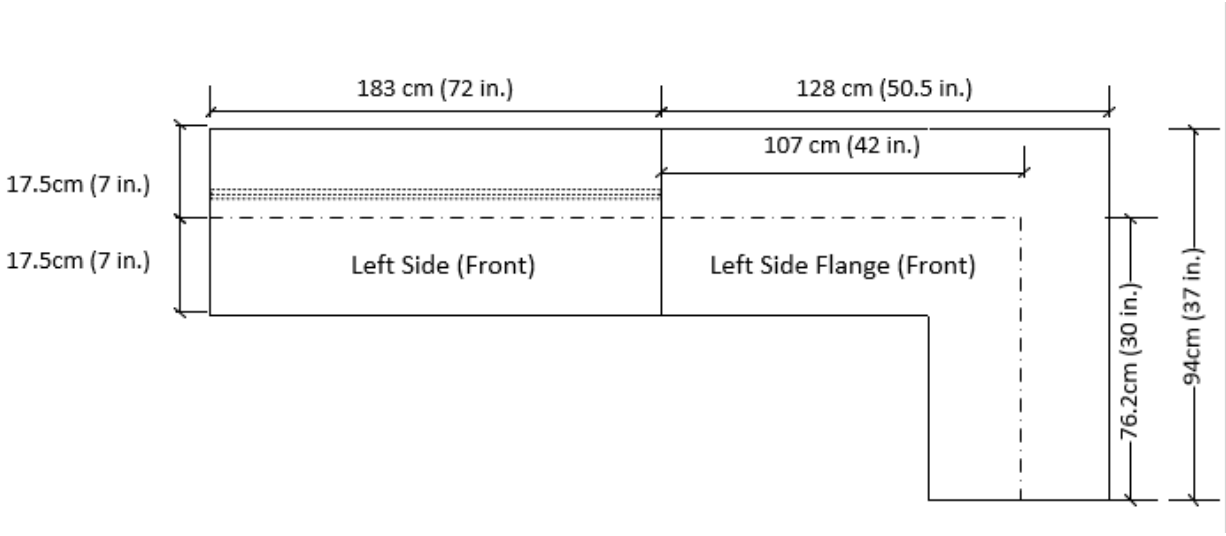


Fig. 142. Bus Duct Elevation View. Dimensions ± 0.6 cm (± 0.25 in).

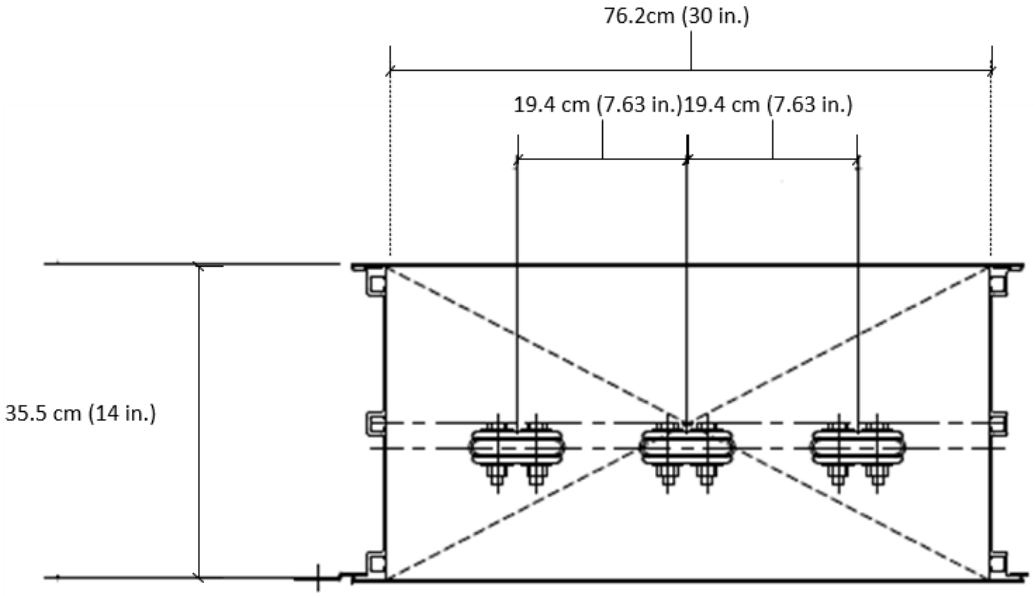


Fig. 143. Interior View (Copper Bus). Dimensions ± 0.6 cm (± 0.25 in).

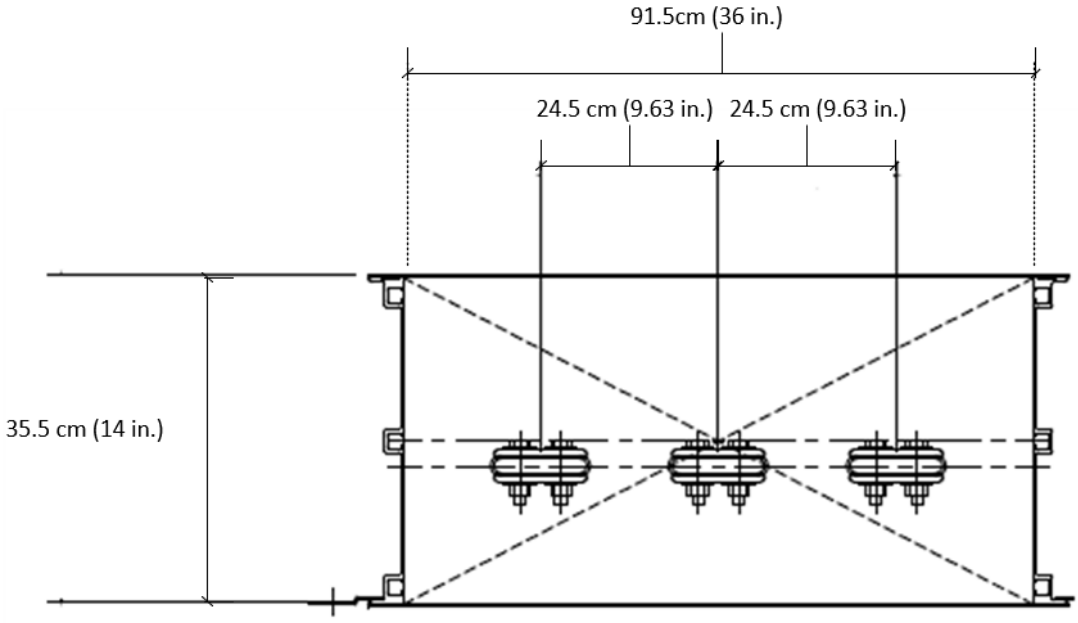


Fig. 144. Interior View (Aluminum Bus). Dimensions ± 0.6 cm (± 0.25 in).

### C.2.2. Experiment 2-25 NSBD Copper Bus, Steel Enclosure, 2s

The mass measurements from the electrical enclosure metal cladding are presented in Table 61. Mass loss was estimated using graphical analysis as discussed previously. Using the bus duct enclosure approximate thickness (0.29 mm [0.115 in]) and steel density (7.902081 g/cm3) the breach mass loss can be estimated with reasonable accuracy. The analysis for this enclosure is presented in Fig. 145 and indicates a total of approximately 726 g of mass loss from the top of the enclosure. The masses recorded from the electrical conductors are presented in Table 58. Soot and other loose byproducts were removed from the electrical conductors prior to measurement.

Table 61. Experiment Device Mass Measurements from Experiment 2-25 - Enclosure Metal-Cladding

| Figure | Description | Pre-Experiment Scale 2 (g) | Δ mass (g) | Notes |
|---|---|---|---|---|
| Fig. 141 | Top | 29962.0 | | |
| Fig. 142 | Left Side (front) | 23767.0 | | |
| Fig. 142 | Right Side (rear) | 22521.0 | | 71 in x 14 in |
| Fig. 141 | Bottom | 29940.0 | 726[e] | |
| N/A | Ground bar cross member | 3302.0 | | |
| N/A | Ground bar axial | 4122.0 | | |
| Fig. 141 | Flange Top | 5743.5 | | |
| Fig. 141 | Flange Bottom | 5611.0 | | |

[e] estimated via graphical analysis

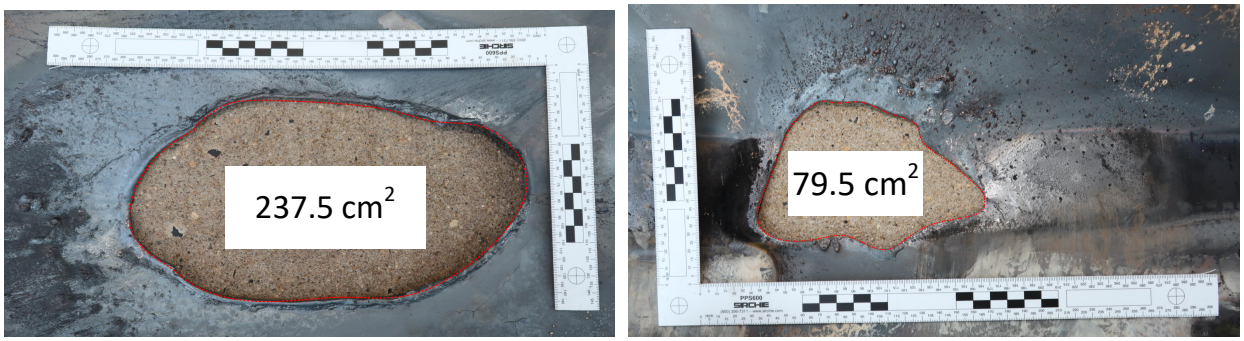


Fig. 145. Photos showing breach opening with size estimate.

Table 62. Experiment Device Mass Measurements from Experiment 2-25 – Electrical Conductors [made using Scale 2 with uncertainty of ± 1 g]

| Description | Pre-Experiment (g) | Pre-Experiment w/insulation (g) | Post-Experiment (g) | Mass Loss (g) |
|---|---|---|---|---|
| **Bus Phase A** | 26 374.0 | 26 393.0 | 25 025.0 | -1 349.0 |
| **Bus Phase B** | 26 037.5 | 26 057.0 | 24 478.5 | -1 559.0 |
| **Bus Phase C** | 26 499.0 | 26 518.0 | 25 558.5 | -940.5 |
| | | | Total Mass Loss | -3 848.5 |

## C.2.3. Experiment 2-26 NSBD Copper Bus, Steel Enclosure, 4s

The mass measurements from the electrical enclosure metal cladding are presented in Table 57. Mass loss was estimated using graphical analysis as discussed previously. Using the bus duct enclosure approximate thickness (0.29 mm [0.115 in]) and steel density (7.902081 g/cm3) the breach mass loss can be estimated with reasonable accuracy. The analysis for this enclosure is presented in Fig. 115 and indicates a total of approximately 1 287g of mass loss from the top of the enclosure. Note that the screen area was estimated to be 50 percent open and 50 percent steel. The masses recorded from the electrical conductors are presented in Table 58. Soot and other loose byproducts were removed from the electrical conductors prior to measurement.

Table 63. Experiment Device Mass Measurements from Experiment 2-26 - Enclosure Metal-Cladding

| Figure | Description | Pre-Experiment Scale 2 (g) | Δ mass (g) | Notes |
|---|---|---|---|---|
| Fig. 141 | Top | 29 962.0 | | Enclosure breach was not observed from thermal damage. |
| Fig. 142 | Left Side (front) | 23 767.0 | | |
| Fig. 142 | Right Side (rear) | 22 521.0 | | |
| Fig. 141 | Bottom | 29 940.0 | | |
| N/A | Ground bar cross member | 3 302.0 | | |
| N/A | Ground bar axial | 4 122.0 | | |
| Fig. 141 | Flange Top | 5 743.5 | | |
| Fig. 141 | Flange Bottom | 5 611.0 | | |

Table 64. Experiment Device Mass Measurements from Experiment 2-26 – Electrical Conductors [made using Scale 2 with uncertainty of ± 1 g]

| Description | Pre-Experiment w/o insulation (g) | Pre-Experiment w/insulation (g) | Post-Experiment (g) | Mass Loss (g) |
|---|---|---|---|---|
| **Bus Phase A** | 26 184.0 | 26 202.0 | 24 368.0 | -1 816.0 |
| **Bus Phase B** | 26 128.5 | 26 146.0 | 23 759.5 | -2 369.0 |
| **Bus Phase C** | 26 072.0 | 26 090.5 | 24 266.0 | -1 806.0 |
| | | | Total Mass Loss | -5 991.0 |

### C.2.4. Experiment 2-27 NSBD Copper Bus, Aluminum Enclosure, 2s

The mass measurements from the electrical enclosure metal cladding are presented in Table 60. Mass loss was estimated using graphical analysis as discussed previously. Using the bus duct enclosure approximate thickness (0.29 mm [0.115 in]) and steel density (7.902081 g/cm3) the breach mass loss can be estimated with reasonable accuracy. The analysis for this enclosure is presented in Fig. 115 and indicates a total of approximately 726 g of mass loss from the top of the enclosure. The masses recorded from the electrical conductors are presented in Table 58. Soot and other loose byproducts were removed from the electrical conductors prior to measurement.

Table 65. Experiment Device Mass Measurements from Experiment 2-27 - Enclosure Metal-Cladding

| Figure | Description | Pre-Experiment Scale 2 (g) | Δ mass (g) |
|---|---|---|---|
| Fig. 141 | Top | 9 978.0 | 3 059.0 |
| Fig. 142 | Top Flange 90 degree | 7 426.0 | 2 381.0 |
| Fig. 142 | Left Side (front) | 9 767.5 | 1 480.0 |
| Fig. 141 | Left side (front) 90 degree | 4 250.5 | 1 453.0 |
| N/A | Right Side (rear) | 9 782.0 | 1 564.0 |
| N/A | Right side (rear) 90 degree | 4 332.0 | 813.5 |
| Fig. 141 | Bottom | 9 990.0 | 3 620.0 |
| Fig. 141 | Bottom Flange 90 degree | 5 304.0 | 2 565.5 |
| | | Total Mass Loss | 16 936.0 |

Table 66. Experiment Device Mass Measurements from Experiment 2-27 – Electrical Conductors [made using Scale 2 with uncertainty of ± 1 g]

| Description | Pre-Experiment w/insulation (g) | Post-Experiment (g) | Mass Loss (g) |
|---|---|---|---|
| **Bus Phase A** | 18 428.5 | 17 671.0 | -757.5 |
| **Bus Phase B** | 18 420.5 | 17 510.5 | -910.0 |
| **Bus Phase C** | 18 307.0 | 17 515.5 | -791.5 |
| | | Total Mass Loss | -2 459.0 |

### C.2.5. Experiment 2-28 NSBD Copper Bus, Aluminum Enclosure, 4s

The mass measurements from the electrical enclosure metal cladding are presented in Table 67. Mass loss was estimated using graphical analysis as discussed previously. Using the bus duct enclosure approximate thickness (0.29 mm [0.115 in]) and steel density (2.9 g/cm$^3$) the breach mass loss can be estimated with reasonable accuracy. The analysis for this enclosure is presented in Fig. 115 and indicates a total of 25 023 g mass loss from the top of the enclosure. The masses recorded from the electrical conductors are presented in Table 68. Soot and other loose byproducts were removed from the electrical conductors prior to measurement.

Table 67. Experiment Device Mass Measurements from Experiment 2-28 - Enclosure Metal-Cladding

| Figure | Description | Pre-Experiment Scale 2 (g) | Δ mass (g) |
|---|---|---|---|
| Fig. 141 | Top straight | 9 978.0 | 3 275.5 |
| Fig. 142 | Top Flange 90 degree | 7 426.0 | 6 683.5 |
| Fig. 142 | Left Side (front) straight | 9 767.5 | 1 437.5 |
| Fig. 141 | Left side (front) 90 degree | 4 250.5 | 2 061.0 |
| N/A | Right Side (rear) | 9 782.0 | 1 750.0 |
| N/A | Right Side (rear) 90 degree | 4 332.0 | 2 122.0 |
| Fig. 141 | Bottom | 9 990.0 | 2 921.0 |
| Fig. 141 | Bottom Flange 90 degree | 5 304.0 | 4 773.0 |
| | | Total Mass Loss | 25 023.0 |

Table 68. Experiment Device Mass Measurements from Experiment 2-28 – Electrical Conductors [made using Scale 2 with uncertainty of ± 1 g]

| Description | Pre-experiment w/insulation (g) | Post-Experiment (g) | Mass Loss (g) |
|---|---|---|---|
| **Bus Phase A** | 18 408.0 | 16 802.5 | -1 605.5 |
| **Bus Phase B** | 18 462.5 | 16 652.5 | -1 810.0 |
| **Bus Phase C** | 18 694.5 | 17 013.5 | -1 681.0 |
| | | Total Mass Loss | -5 096.5 |

### C.2.6. Experiment 2-30 NSBD Aluminum Bus, Steel Enclosure, 4s

The mass measurements from the electrical enclosure metal cladding are presented in Table 69. Mass loss was estimated using graphical analysis as discussed previously. Using the bus duct enclosure approximate thickness (0.29 mm [0.115 in]) and steel density (7.902081 g/cm3) the breach mass loss can be estimated with reasonable accuracy. The analysis for this enclosure indicates a total of approximately 8 664 g of mass loss from the top of the enclosure. The masses recorded from the electrical conductors are presented in Table 70. Soot and other loose byproducts were removed from the electrical conductors prior to measurement.

Table 69. Experiment Device Mass Measurements from Experiment 2-30 - Enclosure Metal-Cladding

| Figure | Description | Pre-Experiment Scale 2 (g) | Δ mass (g) |
|---|---|---|---|
| Fig. 140 | Top | 33 106.0 | 3 488.0 |
| Fig. 142 | Left Side (front) | 22 405.0 | 1 047.0 |
| Fig. 142 | Right Side (rear) | 22 181.0 | 818.0 |
| Fig. 140 | Bottom | 33 057.0 | 3 311.0 |
| | | Total Mass Loss | 8 664.0 |

Table 70. Experiment Device Mass Measurements from Experiment 2-30 – Electrical Conductors [made using Scale 2 with uncertainty of ± 1 g]

| Description | Pre-Experiment w/insulation (g) | Post-Experiment (g) | Mass Loss (g) |
|---|---|---|---|
| **Bus Phase A** | 12 849.5 | 11 377.5 | -1 472.0 |
| **Bus Phase B** | 12 913.5 | 11 294.5 | -1 619.0 |
| **Bus Phase C** | 12 872.0 | 11 517.5 | -1 354.5 |
| | | Total Mass Loss | -4 445.5 |

### C.2.7. Experiment 2-30B NSBD Aluminum Bus, Steel Enclosure, 4s

The mass measurements from the electrical enclosure metal cladding are presented in Table 71. Mass loss was estimated using graphical analysis as discussed previously. Using the bus duct enclosure approximate thickness (0.29 mm [0.115 in]) and steel density (7.9 g/cm$^3$) the breach mass loss can be estimated with reasonable accuracy. The analysis for this enclosure indicates a total of approximately 8 954.0 g of mass loss from the top of the enclosure. The masses recorded from the electrical conductors are presented in Table 72. Soot and other loose byproducts were removed from the electrical conductors prior to measurement.

Table 71. Experiment Device Mass Measurements from Experiment 2-30B - Enclosure Metal-Cladding

| Figure | Description | Pre-Experiment Scale 2 (g) | ∆ mass (g) |
|---|---|---|---|
| Fig. 140 | Top | 33 106.0 | 760.5 |
| Fig. 142 | Left Side (front) | 22 405.0 | 2 921.5 |
| Fig. 142 | Right Side (rear) | 22 181.0 | 2 291.5 |
| Fig. 140 | Bottom | 33 057.0 | 3 980.5 |
| | | Total Mass Loss | 8 954.0 |

Table 72. Experiment Device Mass Measurements from Experiment 2-30B – Electrical Conductors [made using Scale 2 with uncertainty of ± 1 g]

| Description | Pre-Experiment (g) | Post-Experiment (g) | Mass Loss (g) |
|---|---|---|---|
| **Bus Phase A** | 9 047.0 | 7 922.5 | -1 124.5 |
| **Bus Phase B** | 9 012.5 | 7 800.5 | -1 212.0 |
| **Bus Phase C** | 9 127.0 | 7 858.5 | -1 268.5 |
| | | Total Mass Loss | -3 605.0 |

## C.2.8. Experiment 2-31 NSBD Aluminum Bus, Aluminum Enclosure, 2 s

The mass measurements from the electrical enclosure metal cladding are presented in Table 73. Mass loss was estimated using graphical analysis as discussed previously. The bus duct enclosure thickness varied. Using the approximate thickness of the bottoms and tops (0.29 cm [0.115 in]), the sides (0.36 cm [ 0.14 in]), and the aluminum density (2.9 g/cm$^3$), the breach mass loss can be estimated with reasonable accuracy. The analysis indicates a total of approximately 9 770.5 g of mass loss from the enclosure. The masses recorded from the electrical conductors are presented in Table 74. Soot and other loose byproducts were removed from the electrical conductors prior to measurement.

Table 73. Experiment Device Mass Measurements from Experiment 2-31 CR - Enclosure Metal-Cladding

| Figure | Description | Pre-Experiment Scale 2 (g) | Δ mass (g) |
|---|---|---|---|
| Fig. 140 | Bottom and sides – Straight Section | 22 164.0 | 3 376.0 |
| Fig. 142 | Top Panel – Straight Section | 8 696.0 | 3 330.0 |
| Fig. 142 | 90 degree Flange duct | Not Measured | 3 064.5 |
| | | Total mass loss | 9 770.5 |

Table 74. Experiment Device Mass Measurements from Experiment 2-31 CR– Electrical Conductors [made using Scale 2 with uncertainty of ± 1 g]

| Description | Pre-experiment w/insulation (g) | Post-Experiment (g) | Mass Loss (g) |
|---|---|---|---|
| **Bus Phase A Top** | 5 305.5 | 5 034.0 | -271.5 |
| **Bus Phase A Middle** | 5 461.0 | 5 174.5 | -286.5 |
| **Bus Phase A Bottom** | 5 227.0 | 4 976.0 | -251.0 |
| **Bus Phase B Top** | 5 425.5 | 4 705.0 | -720.5 |
| **Bus Phase B Middle** | 5 291.0 | 4 992.5 | -298.5 |
| **Bus Phase B Bottom** | 5 264.5 | 4 967.5 | -297.0 |
| **Bus Phase C Top** | 5 262.5 | 4 979.0 | -283.5 |
| **Bus Phase C Middle** | 5 232.5 | 4 951.5 | -281.0 |
| **Bus Phase C Bottom** | 5 296.0 | 5 000.5 | -295.5 |
| | | Total Mass Loss | -2 985.0 |

## C.2.9. Experiment 2-32 NSBD Aluminum Bus, Aluminum Enclosure, 4s

The mass measurements from the electrical enclosure metal cladding are presented in Table 75. Mass loss was estimated using graphical analysis as discussed previously. The bus duct enclosure thickness varied. Using the approximate thicknesses of the bottoms and tops (0.29 cm [0.115 in]), the sides (0.36 cm [ 0.14 in]) and the aluminum density (2.9 g/cm$^3$) the breach mass loss can be estimated with reasonable accuracy. The analysis for this enclosure estimated a total of 10 865 g mass loss from the enclosure. The masses recorded from the electrical conductors are presented in Table 76. Soot and other loose byproducts were removed from the electrical conductors prior to measurement.

Table 75. Experiment Device Mass Measurements from Experiment 2-32 CR - Enclosure Metal-Cladding

| Figure | Description | Pre-Experiment Scale 2 (g) | Δ mass (g) |
|---|---|---|---|
| Fig. 140 | Bottom and both sides | 22 537.5 | -7 204.5 |
| Fig. 142 | Top | 8 750.5 | -3 660.5 |
| | | Total mass Loss | -10 865.0 |

Table 76. Experiment Device Mass Measurements from Experiment 2-32 CR – Electrical Conductors [made using Scale 2 with uncertainty of ± 1 g]

| Description | Pre-experiment w/insulation (g) | Post-Experiment (g) | Mass Loss (g) |
|---|---|---|---|
| **Bus Phase A Top** | 5 256.5 | 4 799.0 | -457.5 |
| **Bus Phase A Middle** | 5 257.0 | 4 774.0 | -483.0 |
| **Bus Phase A Bottom** | 5 325.0 | 4 763.5 | -561.5 |
| **Bus Phase B Top** | 5 255.5 | 4 770.0 | -485.5 |
| **Bus Phase B Middle** | 5 272.5 | 4 676.0 | -596.5 |
| **Bus Phase B Bottom** | 5 193.5 | 4 636.0 | -557.5 |
| **Bus Phase C Top** | 5 271.0 | 4 819.0 | -452.0 |
| **Bus Phase C Middle** | 5 228.0 | 4 656.5 | -571.5 |
| **Bus Phase C Bottom** | 5 207.0 | 4 579.0 | -628.0 |
| | | Total Mass Loss | -4 793.0 |

Note : The mass of the nominally 25.4 mm (1 in) insulation removed from single bus bar was 21.0 g

# Appendix D. Photographs from Experiments

This appendix presents select photographs for each experiment. Additional photographs are presented in the KEMA Report of Test (Appendix E).

## D.1. Experiment 2-10

Fig. 146. Pre-Experiment 2-10 (as procured by the NRC). Top left (Front door showing relays and controls), Top center (Front instrumentation and breaker compartment with door open), Top right (top of enclsoure showing vent, vent located over main bus and near front door), Bottom left (power supply side with main bus extensions covered with foam for personal protection), Bottom center (opposite side from power supply side), Bottom right (rear panel showing louver vents).

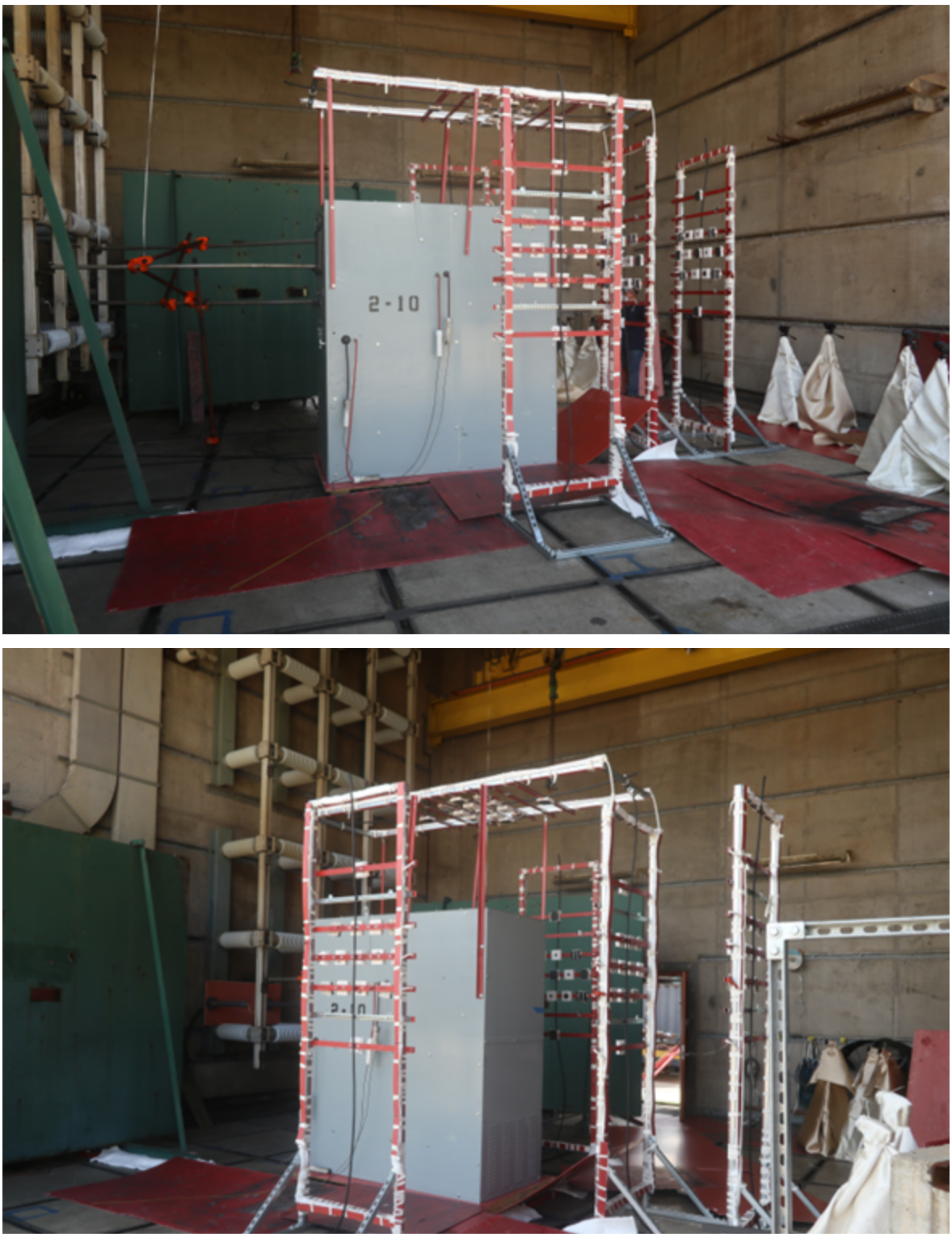


Fig. 147. Pre-Experiment in test cell. Top (front from Cell opening), bottom (rear from cell opening)


Fig. 148. Post-Experiment 2-10. Top (side view from cell opening), Bottom (off angle rear view)

Fig. 149. Post-Experiment Conductors. Top (Plan view of primary cable connection bus bars; top – Phase C, middle – Phase B, bottom – Phase C), Bottom (elevation view of primary cable connection bus bars; left – Phase A, center – Phase B, right – Phase C)

## D.2. Experiment 2-12

The experiment device used in Experiment 2-12 is identical to that used in Experiment 2-10.

Fig. 150. Pre-Experiment 2-12 (as procured by the NRC). Top left (Front door showing relays and controls), Top right (Front instrumentation and breaker compartment with door open) Bottom (Rear off-angle view showing louver ventialtion on the rear bottom panel).

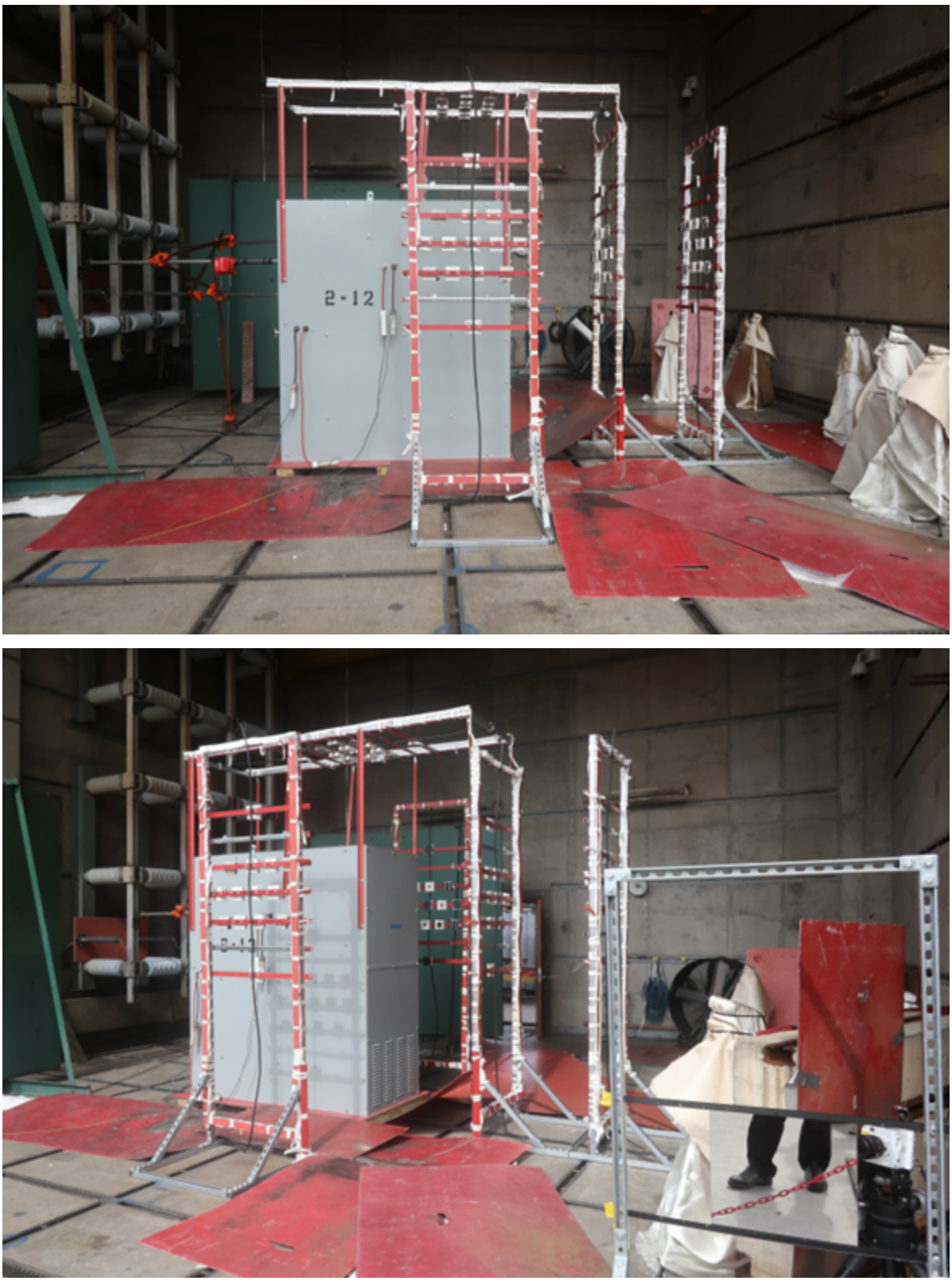


Fig. 151. Pre-Experiment 2-12 in test cell. Top (Side from cell opening), Bottom (rear from cell opening)


Fig. 152. Post-Experiment 2-12 Top (side view from cell opening), Bottom (off angle rear view)


Fig. 153. Post-Experiment Conductors

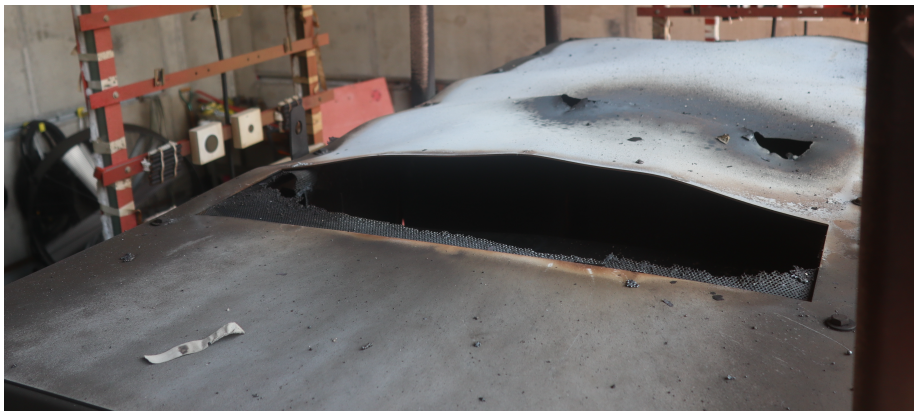

Fig. 154. Post-Experiment Enclosure Breach

## D.3. Experiment 2-25

Fig. 155. Pre-Experiment Experiment 2-25 (left – front angle; right – rear angle)


Fig. 156. Post-Experiment Experiment 2-25 (clockwise from top-left, Front angle; rear angle; front showing panel damage; front showing splice joint with breather)

Fig. 157. Post-Experiment 2-25 Conductors

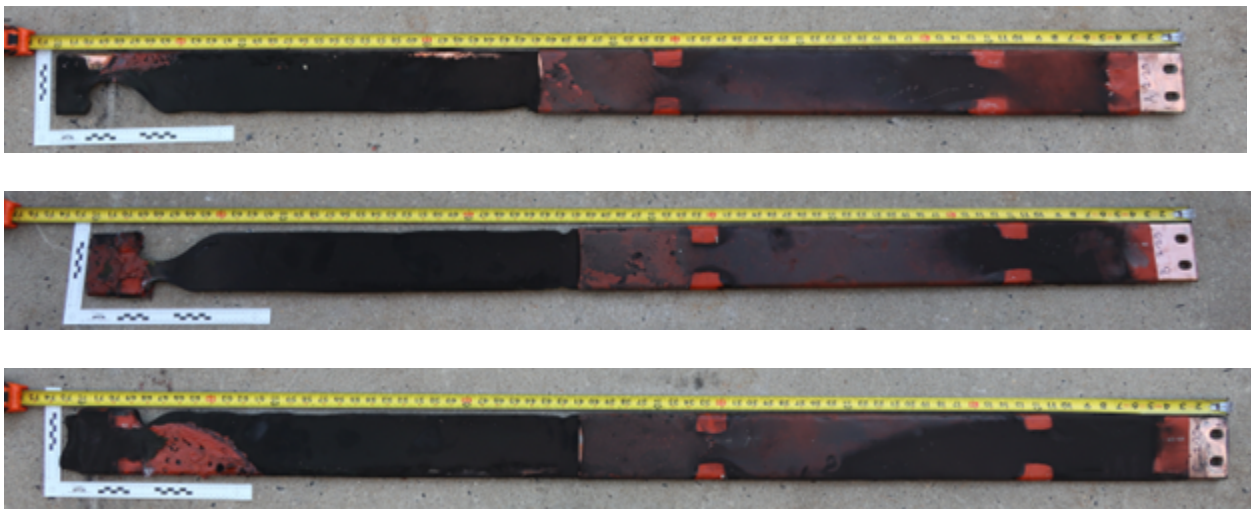

Fig. 158. Additional conductor photos – Post-Experiment Experiment 2-25 (Top – Phase A; Middle – Phase B; Bottom – Phase C)

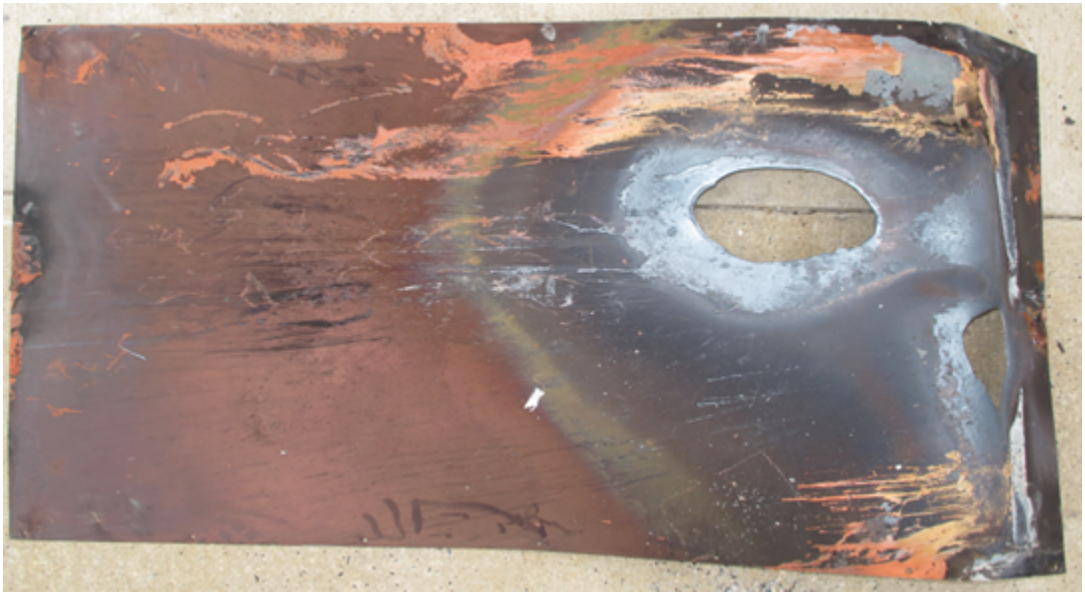

Fig. 159. Post-Experiment Experiment 2-25 Enclosure Breach (note panel is not lying flat on ground near right side, there is a bend downward near the right breach).

## D.4. Experiment 2-26


Fig. 160. Pre-Experiment 2-26 (left – front; right – rear angle)

Fig. 161. Post-Experiment 2-26 (top-left – front; top-right – rear; bottom-left – rear looking up at bus duct; bottom-right – lower splice panel found lying on ground, breather screen missing)

Fig. 162. Post-Experiment 2-26 Conductors (top – with conductors in duct; Bottom conductor ends A-B-C left to right)

## D.5. Experiment 2-27


Fig. 163. Pre-Experiment 2-27 (left – front; right – rear)

Fig. 164. Post-Experiment 2-27 (Top left – below bus duct front; Top-right – front; bottom-left (directly below duct; bottom-right (end of duct at 90 degree bend))

Fig. 165. Post-Experiment 2-27 Conductors (top – conductors in duct at end of experiment; bottom – conductors removed A-B-C: top to bottom)

Fig. 166. Post-Experiment 2-27 Enclosure Breach (Top-left – top cover; Top-right – front side; Bottom-left – bottom cover; Bottom-right – rear side)

## D.6. Experiment 2-28

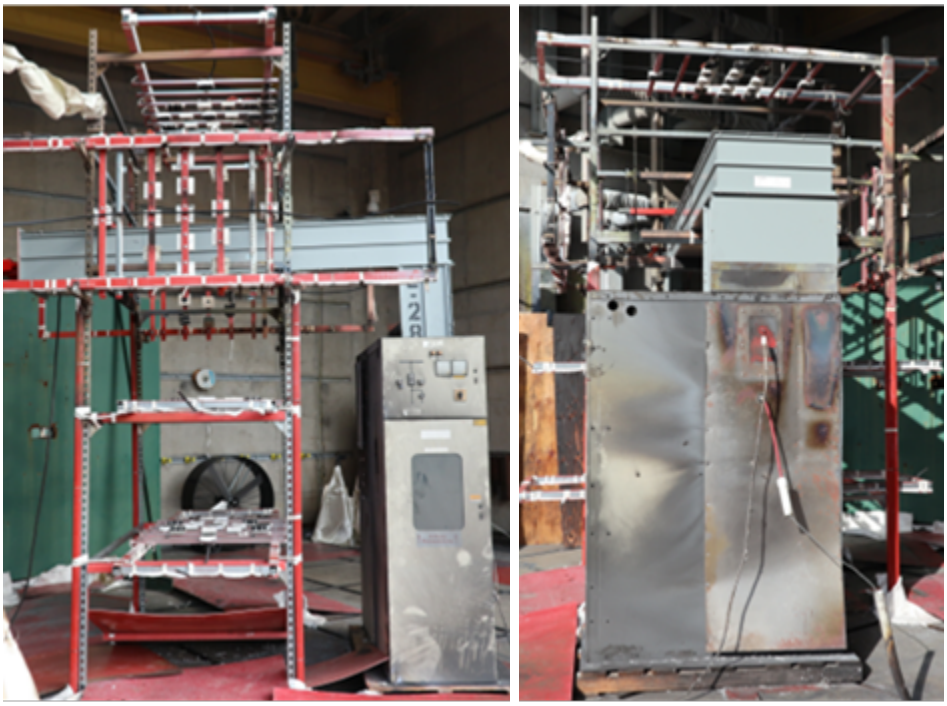

Fig. 167. Pre-Experiment 2-28 (left – front view; right – 90 degree bend view)

Fig. 168. Post-Experiment 2-28 (Top – front angle view; Bottom – rear angle view)

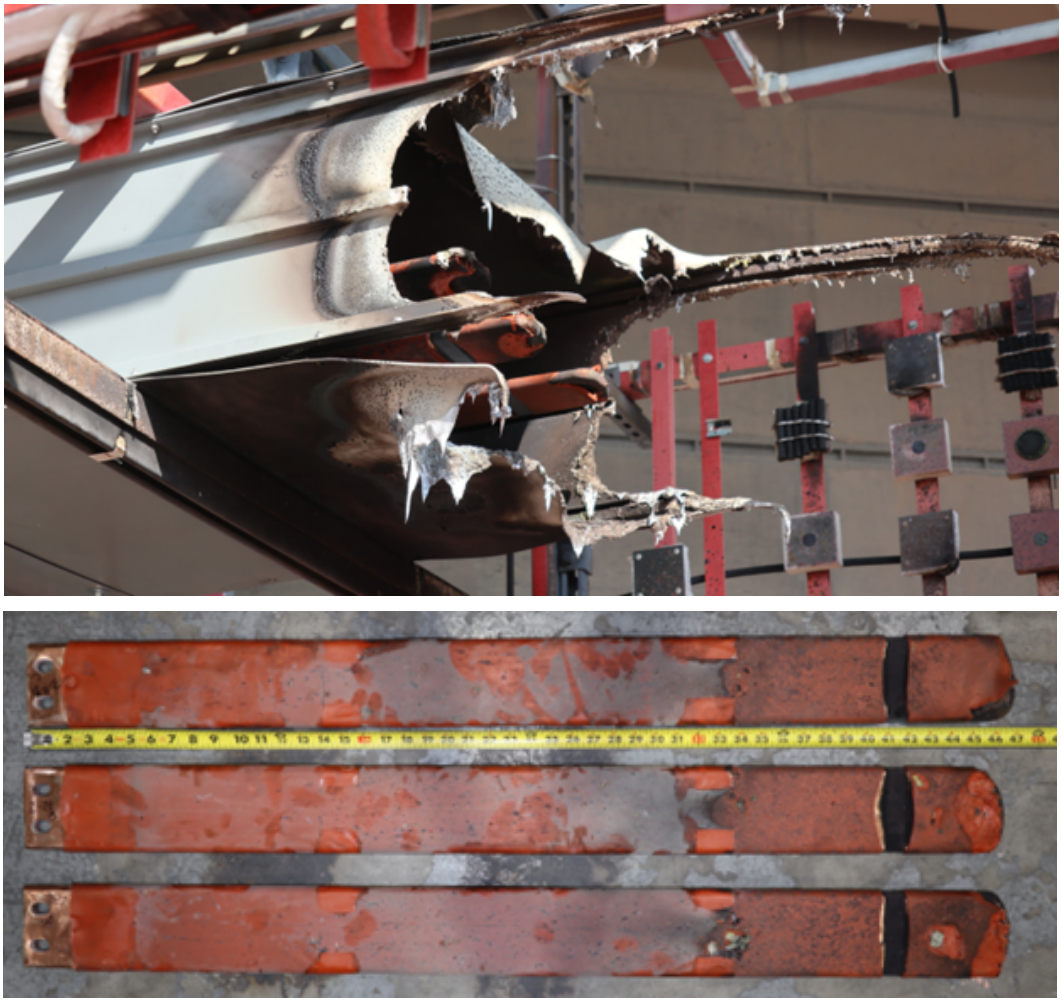

Fig. 169. Post-Experiment 2-28 Conductors (Top – within duct after experiment; Bottom – removed from enclosure [Phase A-B-C top to bottom])

Fig. 170. Post-Experiment 2-28 insulated conductor Rack 2 at 90 degree bend end

Fig. 171. Post-Experiment 2-28 Enclosure Breach

## D.7. Experiment 2-30


Fig. 172. Pre-Experiment


Fig. 173. Post-Experiment 2-30 (Top – Front view; Bottom-left – view looking up at bottom cover; Bottom-right – rear view)

Fig. 174. Post-Experiment 2-30 Conductors


Fig. 175. Post-Experiment 2-30 Enclosure Breach (Top – front; Upper-Mid-left – front breach; Upper-Mid-right – rear breach; Lower-Mid – top breach; Bottom-left – lower cover front; Bottom-right – lower cover rear)

## D.8. Experiment 2-30B


Fig. 176. Pre-Experiment 2-30B


Fig. 177. Post-Experiment 2-30B (Top – front view; Bottom – front view zoomed to breach)

Fig. 178. Post-Experiment 2-30B Conductors (C-B-A, top to bottom)

Fig. 179. Post-Experiment 2-30B Enclosure Breach (Top – view from below duct front; Bottom – view from below duct rear)

## D.9. Experiment 2-31

Fig. 180. Pre-Experiment 2-31

Fig. 181. Post-Experiment 2-31 (Top - front; Bottom - front zoomed)

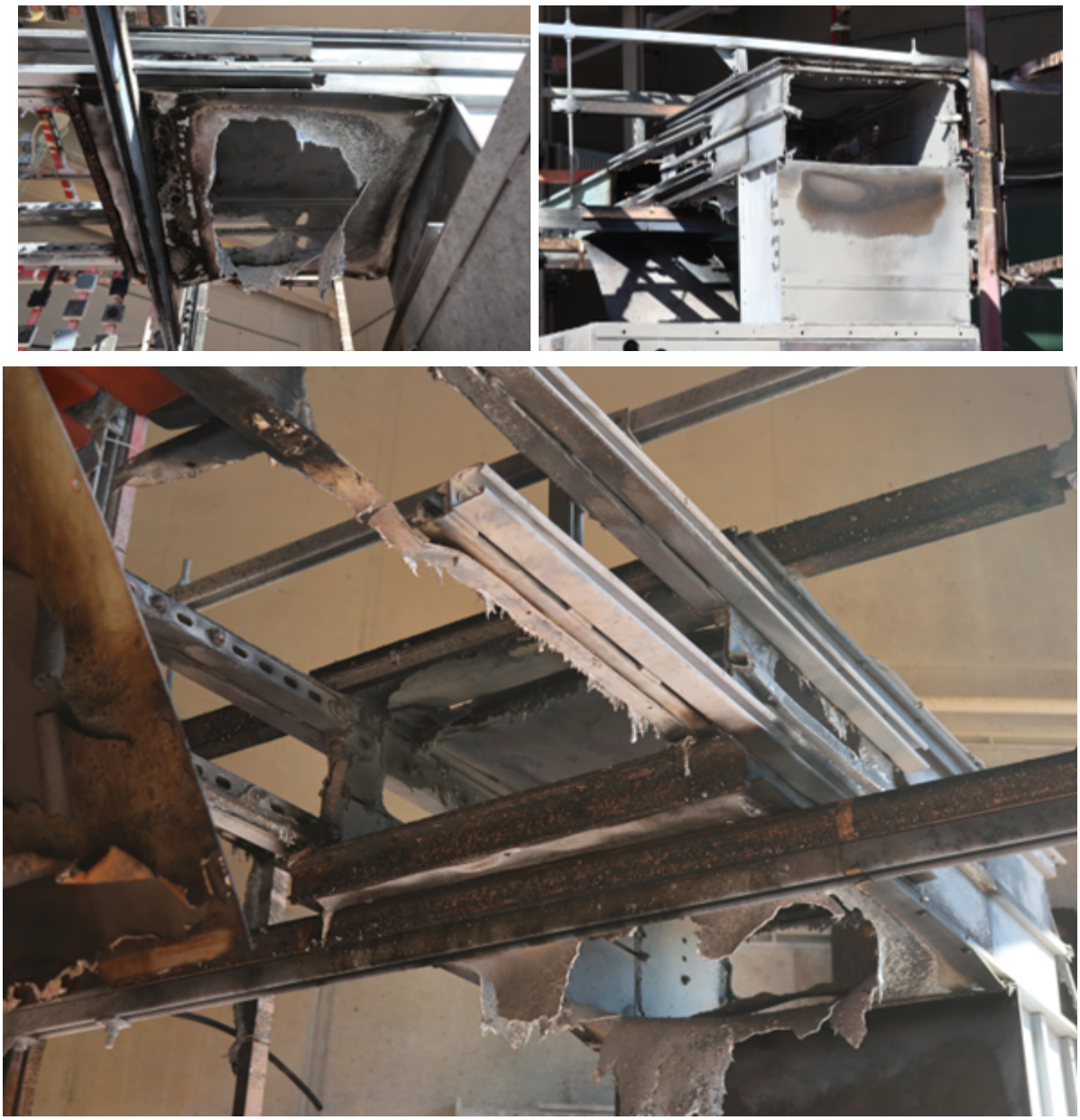

Fig. 182. Post-Experiment 2-31 (Top-left – bottom horizontal duct cover on 90 degree; top-right – end view of 90 degree; bottom – view from below duct in front)

Fig. 183. Post-Experiment 2-31 Conductors

Fig. 184. Post-Experiment 2-31 Enclosure Breach (Top-left – 90 degree front; Top-right – 90 degree end; Bottom-left – 90 degree rear; Bottom-right – 90 degree lower cover)

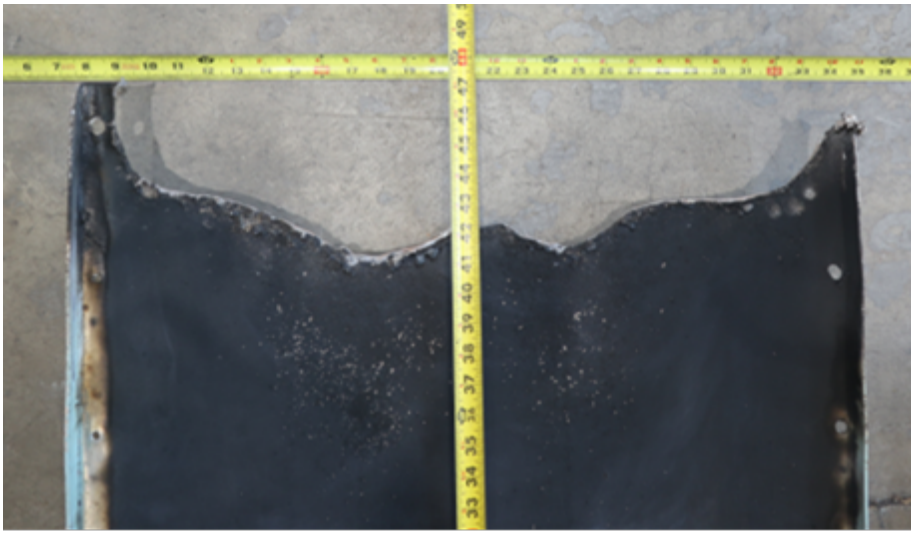

Fig. 185. Post-Experiment 2-31 (Straight section top cover), note bottom cover did not experience damage.

## D.10. Experiment 2-32


Fig. 186. Pre-Experiment 2-32 (Left – front view; Right – rear angle)

Fig. 187. Post-Experiment 2-32 (Top – rear view of enclosure breach and conductors; Bottom – Front view)

Fig. 188. Post-Experiment 2-32 Conductors (Top – Conductor ends; Bottom – overhead view of top conductors with enclosure top removed)

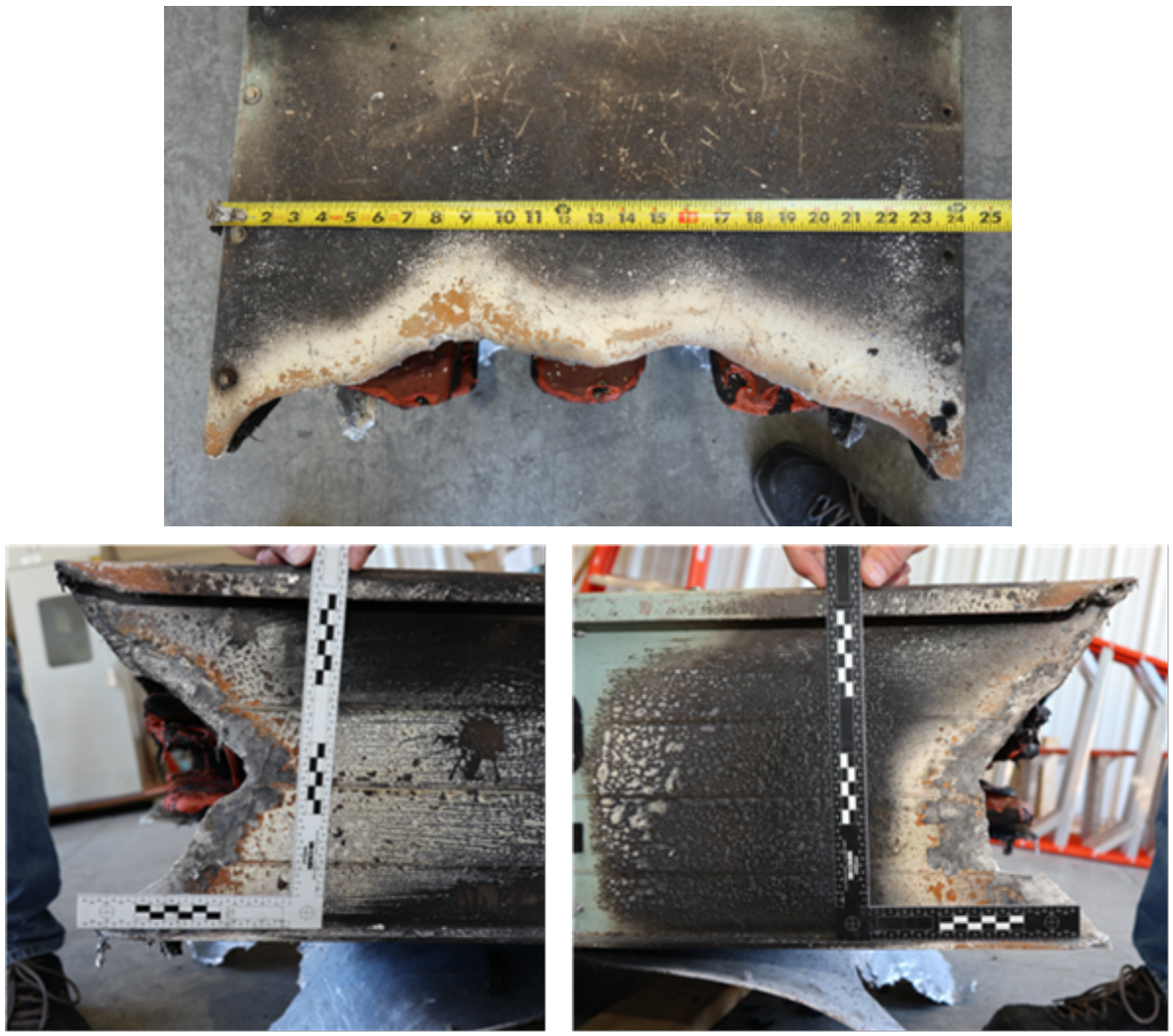

Fig. 189. Post-Experiment 2-32 Enclosure Breach Straight Aluminum duct (Top – Overhead view; Bottom-left – Rear; Bottom-right – front)

Fig. 190. Post-Experiment 2-32 Enclosure Breach 90 degree steel duct (Top – overhead view; Bottom-left – rear; Bottom-right – front)

## Appendix E. KEMA Experiment Report

Appendix E is attached and contains a copy of the KEMA Lab experimental report.

# KEMA TEST REPORT

**24512713**

| | | | |
|---|---|---|---|
| **Object** | Switchgears and bus ducts | | |
| **Type** | MV bus ducts and switchgears<br><br>6.9 kV – 32 kA – 60 Hz<br>4.16 kV – 30kA – 60Hz | **Serial No.** | 2-10, 2-12, 2-25, 2-26, 2-30, 2-27, 2-28, 2-30B, 2-31, 2-32 |
| **Client** | U.S. Nuclear Regulatory Commission<br>CSB-4A07m<br>Washington DC, 2055-0001 | | |
| **Manufacturer** | U.S. Nuclear Regulatory Commission<br>CSB-4A07m<br>Washington DC, 2055-0001 | | |
| **Tested by** | KEMA-Powertest LLC<br>4379 County Line Road<br>Chalfont, PA 18914, USA | | |
| **Date of tests** | 22, 23, 24, 25, 26, 29, 30 and 31 August 2022 and 1 September 2022 | | |
| **Test specification** | All arc tests have been carried out in accordance with the client's instructions. | | |

**Disclaimers**

This report applies only to the individual object tested. KEMA-Powertest LLC ("KEMA") makes no representations or warranties with respect to any device other than the object tested. It is the responsibility of the applicable device manufacturer to ensure that any other devices or units having the same name and descriptions as the test object are identical.

No certificate of performance or other report issued by KEMA for the purpose of confirming the performance of a test object in relation to the testing requirements of a national or international standard, or in relation to any other testing specification, shall constitute a warranty as to the adequacy or quality of the design or construction of the test object. No other document issued by KEMA for the purpose of reporting, explaining or describing any engineering or consulting services performed by KEMA shall constitute a warranty as to the adequacy or quality of the design or construction of any apparatus or system that is the subject of the document.

This report consists of 267 pages in total.

November 29, 2022

Frank Cielo
Director
KEMA-Powertest, LLC

## INFORMATION SHEET

**1 KEMA Type Test Certificate**

A KEMA Type Test Certificate contains a record of a series of (type) tests carried out in accordance with a recognized standard. The object tested has fulfilled the requirements of this standard and the relevant ratings assigned by the manufacturer are endorsed by KEMA Labs. In addition, the object's technical drawings have been verified and the condition of the object after the tests is assessed and recorded. The Certificate contains the essential drawings and a description of the object tested. A KEMA Type Test Certificate signifies that the object meets all the requirements of the named subclauses of the standard. It can be identified by gold-embossed lettering on the cover and a gold seal on its front sheet.
The Certificate is applicable to the object tested only. KEMA Labs is responsible for the validity and the contents of the Certificate. The responsibility for conformity of any object having the same type references as the one tested rests with the manufacturer.
Detailed rules on types of certification are given in KEMA Labs' Certification procedure applicable to KEMA Labs.

**2 KEMA Report of Performance**

A KEMA Report of Performance is issued when an object has successfully completed and passed a subset (but not all) of test programmes in accordance with a recognized standard. In addition, the object's technical drawings have been verified and the condition of the object after the tests is assessed and recorded. The report is applicable to the object tested only. A KEMA Report of Performance signifies that the object meets the requirements of the named subclauses of the standard. It can be identified by silver-embossed lettering on the cover and a silver seal on its front sheet.
The sentence on the front sheet of a KEMA Report of Performance will state that the tests have been carried out in accordance with …… The object has complied with the relevant requirements.

**3 KEMA Test Report**

A KEMA Test Report is issued in all other cases.

**4 Official and uncontrolled test documents**

The official test documents of KEMA Labs are issued in bound form. Uncontrolled copies may be provided as a digital file for convenience of reproduction by the client. The copyright has to be respected at all times.

**5 Accreditation of KEMA Labs**

KEMA Labs is accredited in accordance with ISO/IEC 17025 by the respective national accreditation bodies. KEMA Labs Arnhem, the Netherlands, is accredited by RvA under nos. L020, L218, K006 and K009. KEMA Labs Chalfont, United States, is accredited by A2LA under no. 0553.01. KEMA Labs Prague, the Czech Republic, is accredited by CAI as testing laboratory no. 1035.

## REVISION OVERVIEW

| Rev. No | Date of issue | Reason for issue |
|---|---|---|
| 0 | 11/29/2022 | Final issue |

## TABLE OF CONTENTS

End of Document [1 PAGE]

# 1 IDENTIFICATION OF THE OBJECT TESTED

## 1.1 Ratings/characteristics of the object tested

**Switchgear Arc Test Ratings**

| | |
|---|---|
| Voltage | 6.9 kV |
| Number of phases | 3 |
| Frequency | 60 Hz |
| Main circuit | |
| • peak withstand current | 83.2 kApeak |
| • short-time withstand current | 32 kA |

**Bus Ducts Arc Test Ratings**

| | |
|---|---|
| Voltage | 4.16 kV |
| Number of phases | 3 |
| Frequency | 60 Hz |
| Main circuit | |
| • peak withstand current | 78 kApeak |
| • short-time withstand current | 30 kA |

## 1.2 Description of the object tested

Client tested various type of bus materials and enclosure materials throughout the program to acquire energy and thermal data.

## 1.3 List of drawings

No drawings were provided by the client.

# 2 GENERAL INFORMATION

## 2.1 The tests were witnessed by

The following persons witnessed the tests at the KEMA premises:

| Name | Company |
|---|---|
| John Tappert (August 29th) | |
| Mike Franovich (August 29th) | |
| Christian Araguas (August 29th) | U.S. Nuclear Regulatory Commission |
| Mark Henry Salley (August 29th, August 30th) | CSB-4A07m |
| Kenneth A. Hamburger | Washington DC, 2055-0001 |
| Nicholas B. Melly | |
| Gabriel J. Taylor | |
| Kenn Miller | |
| Austin Glover | Sandia National Laboratories, New Mexico |
| Jamal Mohmand | 1515 Eubank SE |
| Alvaro Cruz-Cabrera | Albuquerque, NM 8785 |
| Ryan Flanagan | |
| Joannie Chin (August 30th) | |
| A. Kirk Dohne (August 30th) | |
| Albert J. Wavering (August 30th) | |
| Laslo Varadi (August 30th) | National Institute of Standards Technology |
| Scott Bareham | 100 Bureau Dr. |
| Christopher U. Brown | Gaithersburg, MD 20899 |
| Ryan Falkenstein-Smith | |
| Stephen Fink | |
| Michael Heck | |
| Anthony D. Putorti Jr. | |
| Charles Fourneau | BelV, Belgium |
| Abderrazzaq Bounagui | CNSC, Canada |
| Frantisek Stvan | UJV, Czec Republic |
| Joëlle Fleurot | IRSN, France |
| Sylvain Suard | |
| Marina Röwekamp | GRS, Germany |
| Christian Northe | BASE, Germany |
| Tsukasa Miyagi | |
| Koji Shirai | |
| Tomoaki Sakurai | CRIEPI, Japan |
| Kosuke Matsuda | |
| Yong Hun Jung | KAERI, Korea |

| | |
|---|---|
| Sung Hyun Kim | KEPCO, Korea |
| Sangkyu Lee<br>Young Seob Moon | KINS, Korea |
| Laima Kuriene | ANVS, Netherlands |
| Eunate Armañanzas Albaizar | CSN, Spain |
| Henrik Hellberg | SSM, Sweden |
| Dominik Hermann | ENSI, Switzerland |
| Markus Beilmann | NEA, France |

## 2.2 The tests were carried out by

| **Name** | **Company** |
|---|---|
| Samuel Andris | KEMA-Powertest LLC,<br>Chalfont, PA, USA |

## 2.3 Accuracy of measurement

The guaranteed uncertainty in the figures mentioned, taking into account the total measuring system, is less than 3%, unless mentioned otherwise. Measurement uncertainty can be verified by reviewing the instrument calibration records. The instruments used are calibrated on a regular basis and are traceable to the National Institute of Standards and Technology.

## 2.4 Notes

KEMA Labs recorded data from calorimeters, for each arc test. Calorimeters were calibrated before they were sent to the customer. Only the functionality of the calorimeters was checked before each arc test. Therefore, the calorimeters are not included in the instrument list.

For each arc test, the client provided additional calorimeters. Data from the additional calorimeters was recorded by the client. The client also recorded each test on hi-speed cameras, and on thermal imaging cameras.

The attached procedure was written by and has been included in the report at the behest of the client. KEMA Labs has not verified the attached procedure's compliance with any recognized testing standard. Interpretation of the data presented within this test report against the requirements of the attached procedure, or a recognized testing standard is the responsibility of the reader. KEMA MAKES NO REPRESENTATIONS OR WARRANTIES REGARDING THE ACCURACY OF THE PROCEDURE OR THAT THE PROCEDURE MEETS ANY APPLICABLE INDUSTRY STANDARDS OR LEGAL OR REGULATORY REQUIREMENTS.

1. HEAF_Test_Plan OECDNEA 2022 r1 [33 pages]

## 3 LEGEND

**Phase indications**

If more than one phase is recorded on oscillogram, the phases are indicated by the digits 1, 2 and 3. These phases 1, 2 and 3 correspond to the phase values in the columns of the accompanying table, respectively from left to right.

**Explanation of the letter symbols and abbreviations on the oscillograms**

| | |
|---|---|
| pu | Per unit (the reference length of one unit is represented by the black bar on the oscillogram) |
| I1TO | Current through test object |
| I2TO | Current through test object |
| I3TO | Current through test object |
| PT#1 | Pressure transducer |
| PT#2 | Pressure transducer |
| PT#3 | Pressure transducer |
| PT#4 | Pressure transducer |
| U1TO | Voltage across test object |
| U2TO | Voltage across test object |
| U3TO | Voltage across test object |

# 4 CHECKING CIRCUIT PARAMETERS

**Standard and date**

| | |
|---|---|
| Standard | Client's instructions |
| Test date | 22 August 2022 |

**Serial No.**

N/A

## 4.1 Condition before test

Shorting bar connected to input terminals of test device.

## 4.2 Test results and oscillograms

**Overview of test numbers**
220822-9002

**Remarks**
-

**Checking circuit parameters**

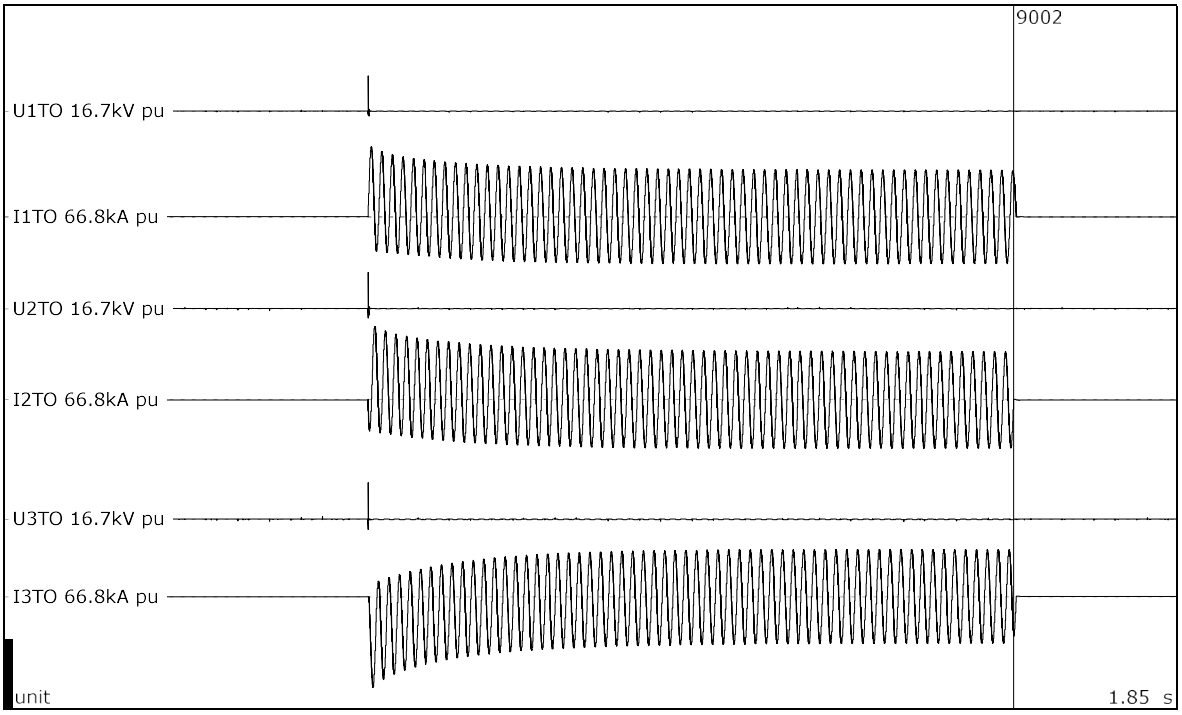


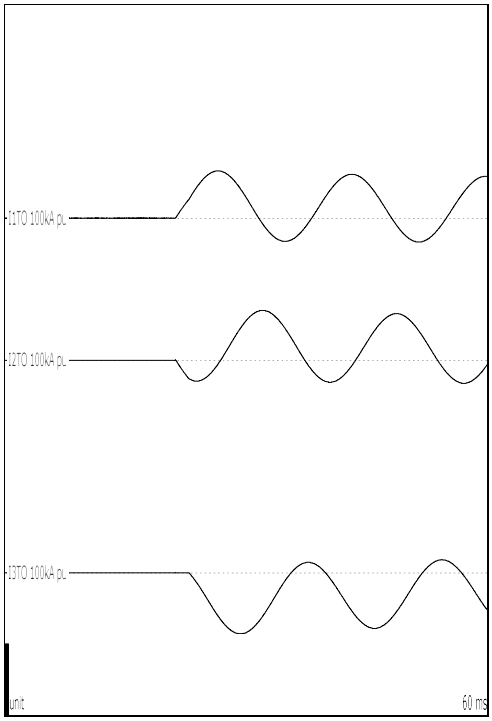


**Test number:** **220822-9002**

| Phase | | AØ | BØ | CØ |
|---|---|---|---|---|
| Current | $kA_{peak}$ | 66.7 | 70.0 | -86.3 |
| Current, a.c. component, beginning | $kA_{RMS}$ | 32.9 | 34.0 | 32.9 |
| Current, a.c. component, middle | $kA_{RMS}$ | 31.7 | 32.7 | 31.7 |
| Current, a.c. component, end | $kA_{RMS}$ | 31.4 | 32.4 | 31.4 |
| Current, a.c. component, average | $kA_{RMS}$ | 32.2 | 33.3 | 32.2 |
| Current, a.c. component, three-phase average | $kA_{RMS}$ | 32.6 | | |
| Duration, current | s | 1.02 | 1.02 | 1.02 |

Gas pressure at 20 °C - MPa

Observations: No visible disturbance. Circuit parameters are 6900 V open circuit voltage, with an average current of 32.6kA. Current duration will be adjusted for each arc test.

## 4.3 Condition / inspection after test

See observations for test details.

# 5 ARC TEST: 32KA, 2S, CU

**Standard and date**

| | |
|---|---|
| Standard | Client's instructions |
| Test date | 22 August 2022 |

**Serial No.**

2-10

## 5.1 Condition before test

Enclosure grounded.
Test sample new.
Arc to be initiated by #24 AWG wire on the load side of the breaker, on the backside of the cabinet.
PT#1: 30PSI transducer in the secondary cabinet on the left side.
PT#2: 50PSI transducer in the secondary cabinet on the left side.
PT#3: 30PSI transducer in the arc cabinet.
PT#4 50PSI transducer in the arc cabinet.

## 5.2 Test circuit S01

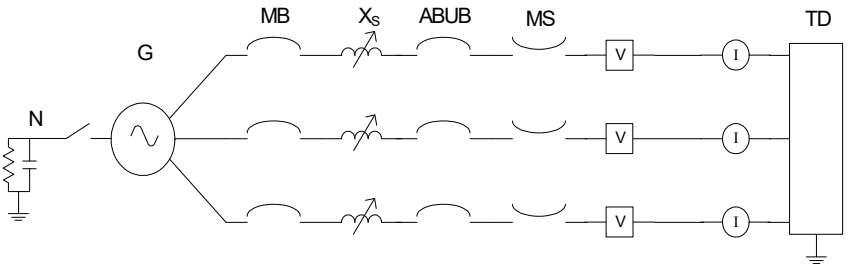


| | | | | | |
|---|---|---|---|---|---|
| G | = Generator | ABUB | = Aux. Breaker | R | = Resistance |
| N | = Neutral | XFMR | = Transformer | V | = Voltage Measurement |
| MB | = Main Breaker | TD | = Test Device | I | = Current Measurement |
| MS | = Make Switch | X | = Inductance | | |

| **Supply** | | |
|---|---|---|
| Power | MVA | 390 |
| Frequency | Hz | 60 |
| Phase(s) | | 3 |
| Voltage | V | 6900 |
| Current | kA | 32.6 |
| Impedance | Ω | 0.1222 |
| Power factor | | < 0.1 |
| Neutral | | not earthed |

Remarks: -

## 5.3 Photograph before test


08/22/2022


08/22/2022


08/22/2022


2-10
08/22/2022

## 5.4 Test results and oscillograms

**Overview of test numbers**
220822-9003

**Remarks**

| Calorimeter Slug # | Average Start Temp. | Initial Heat Capacity | Max. Temp. | Final Heat Capacity | Total Heat Energy |
|---|---|---|---|---|---|
| | °C | cal/(g°C) | °C | cal/(g°C) | J/(cm$^2$) |
| 1 | 29.23 | 0.092165 | 95.75 | 0.094205 | 37.161 |
| 2 | 29.07 | 0.092160 | 86.16 | 0.093915 | 31.851 |
| 3 | 28.66 | 0.092148 | 125.33 | 0.095079 | 54.260 |
| 4 | 28.56 | 0.092145 | 134.32 | 0.095337 | 59.439 |
| 5 | 28.90 | 0.092155 | 28.96 | 0.092157 | 0.029 |
| 6 | 29.19 | 0.092164 | 58.14 | 0.093054 | 16.071 |
| 7 | 28.93 | 0.092156 | 83.99 | 0.093849 | 30.703 |
| 8 | 28.44 | 0.092141 | 88.89 | 0.093998 | 33.734 |
| 9 | 28.86 | 0.092154 | 104.20 | 0.094459 | 42.146 |
| 10 | 27.40 | 0.092109 | 91.40 | 0.094074 | 35.722 |

PT#1: 1.84 psi above atmospheric
PT#2: 2.47 psi above atmospheric
PT#3: 5.87 psi above atmospheric
PT#4: 7.08 psi above atmospheric

**Arc Test: 32kA, 2s, CU**

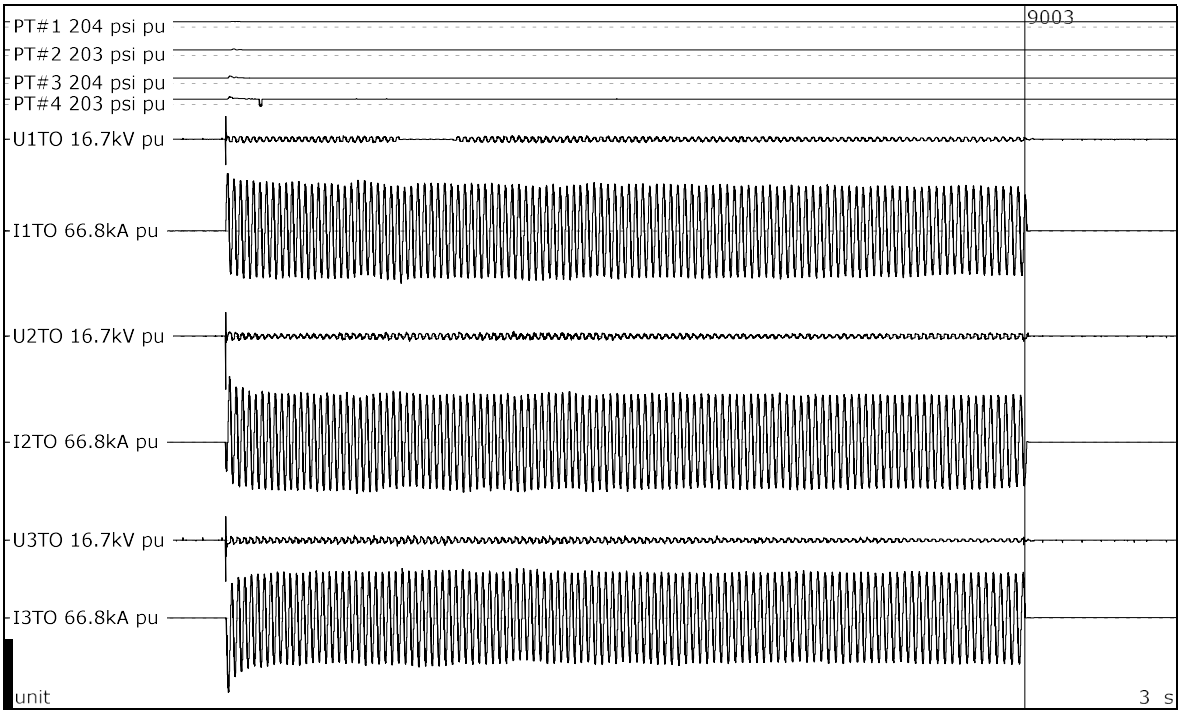


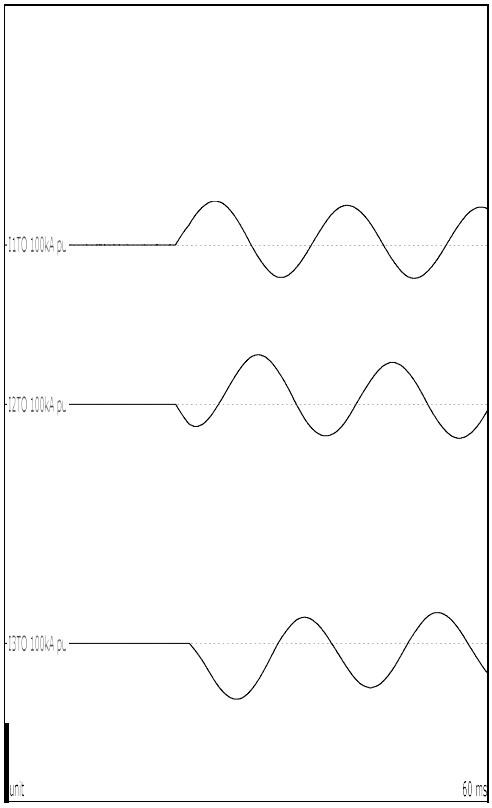


**Test number:** **220822-9003**

| Phase | | AØ | BØ | CØ |
|---|---|---|---|---|
| Applied voltage, phase-to-ground | $kV_{RMS}$ | 3.99 | 3.99 | 3.99 |
| Applied voltage, phase-to-phase | $kV_{RMS}$ | 6.91 | | |
| Making current | $kA_{peak}$ | 55.1 | 62.2 | -70.6 |
| Current, a.c. component, beginning | $kA_{RMS}$ | 33.1 | 33.9 | 33.9 |
| Current, a.c. component, middle | $kA_{RMS}$ | 31.4 | 32.1 | 30.5 |
| Current, a.c. component, end | $kA_{RMS}$ | 29.7 | 31.0 | 30.4 |
| Current, a.c. component, average | $kA_{RMS}$ | 31.6 | 32.1 | 31.1 |
| Current, a.c. component, three-phase average | $kA_{RMS}$ | 31.6 | | |
| Duration | s | 2.05 | 2.05 | 2.04 |
| Arc energy | MJ | 71.5 | | |
| Equivalent RMS value and duration | | 32.5 kA during 2.00 s | | |

Observations: Emission of flames and gas observed.

**Test number:** **220822-9003**

## 5.5 Condition / inspection after test

Cabinet door blew open during test and touched A phase bus. Signs of arcing between lab station bus extensions and the door of the switchgear.
Interior and sides of the sample exterior were heavily burned.

## 5.6 Photograph after test


08/22/2022


08/22/2022


R
Front
08/22/2022


2-10
08/22/2022


08/22/2022

# 6 ARC TEST: 32KA, 4S, CU

**Standard and date**

| | |
|---|---|
| Standard | Client's instructions |
| Test date | 23 August 2022 |

**Serial No.**

2-12

## 6.1 Condition before test

Enclosure grounded.
Test sample new.
Arc to be initiated by #24 AWG wire on the load side of the breaker, on the backside of the cabinet.
PT#1: 30PSI transducer in the secondary cabinet on the left side.
PT#2: 50PSI transducer in the secondary cabinet on the left side.
PT#3: 30PSI transducer in the arc cabinet.
PT#4: 50PSI transducer in the arc cabinet.

## 6.2 Test circuit S01

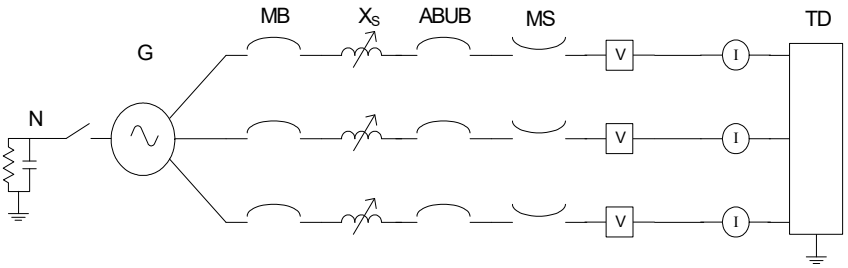


| | | | | | |
|---|---|---|---|---|---|
| G | = Generator | ABUB | = Aux. Breaker | R | = Resistance |
| N | = Neutral | XFMR | = Transformer | V | = Voltage Measurement |
| MB | = Main Breaker | TD | = Test Device | I | = Current Measurement |
| MS | = Make Switch | X | = Inductance | | |

| **Supply** | | |
|---|---|---|
| Power | MVA | 390 |
| Frequency | Hz | 60 |
| Phase(s) | | 3 |
| Voltage | V | 6900 |
| Current | kA | 32.6 |
| Impedance | Ω | 0.1222 |
| Power factor | | < 0.1 |
| Neutral | | not earthed |

Remarks: -

## 6.3 Photograph before test


2-12
08/23/2022

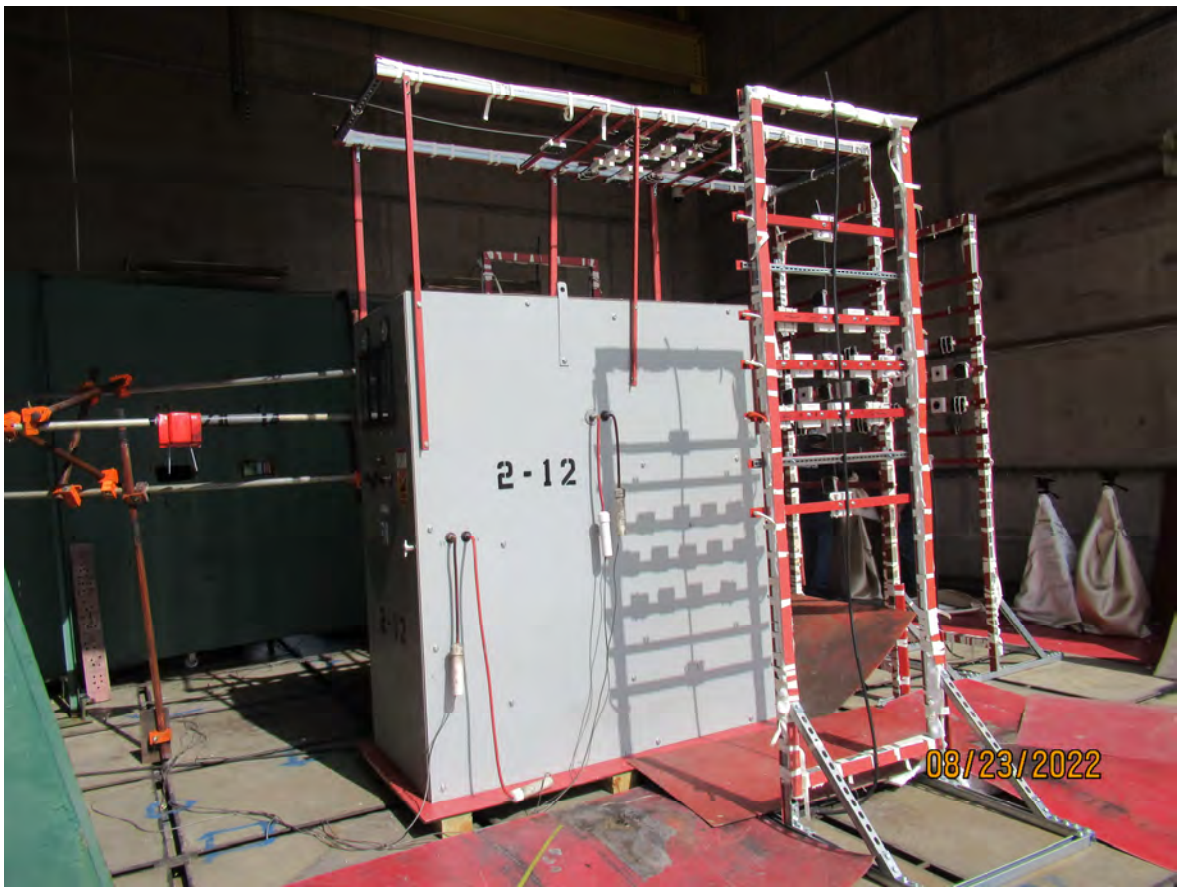
2-12
08/23/2022

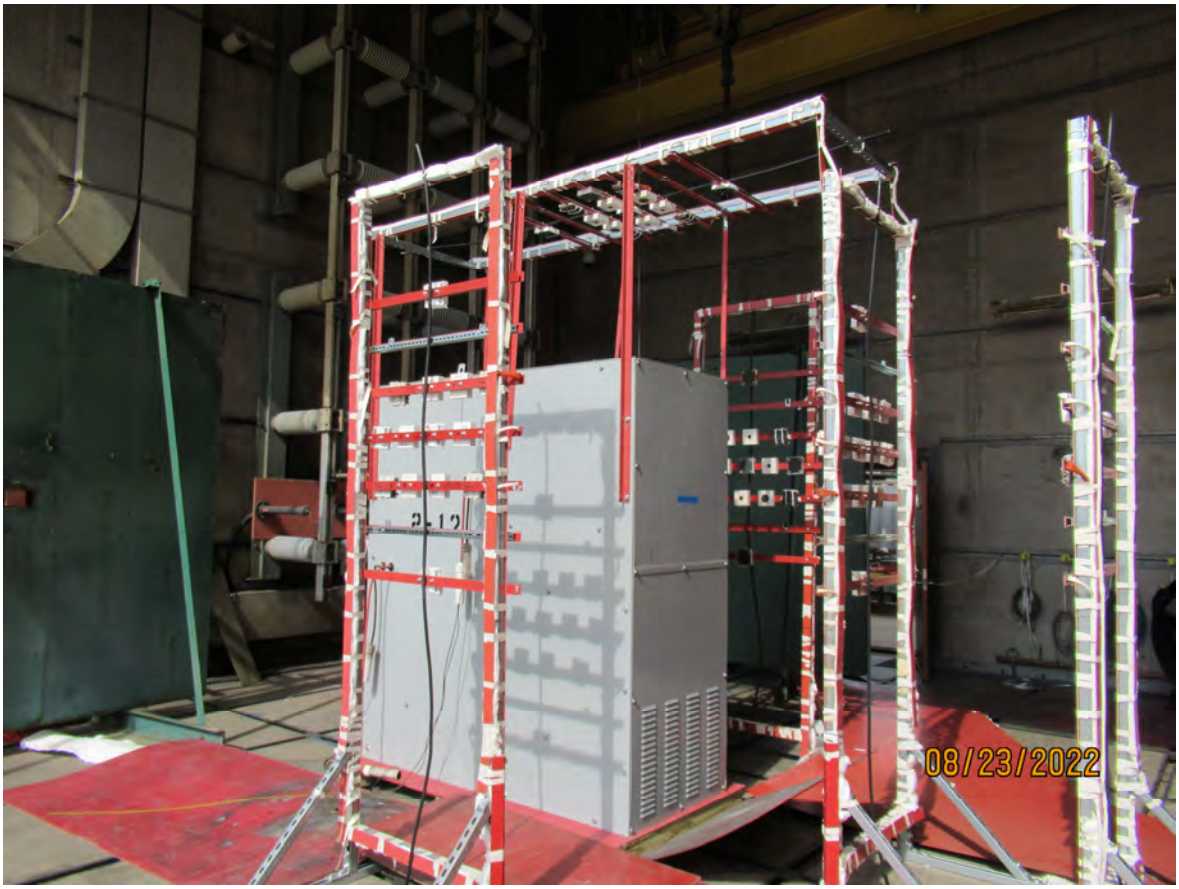
08/23/2022


08/23/2022

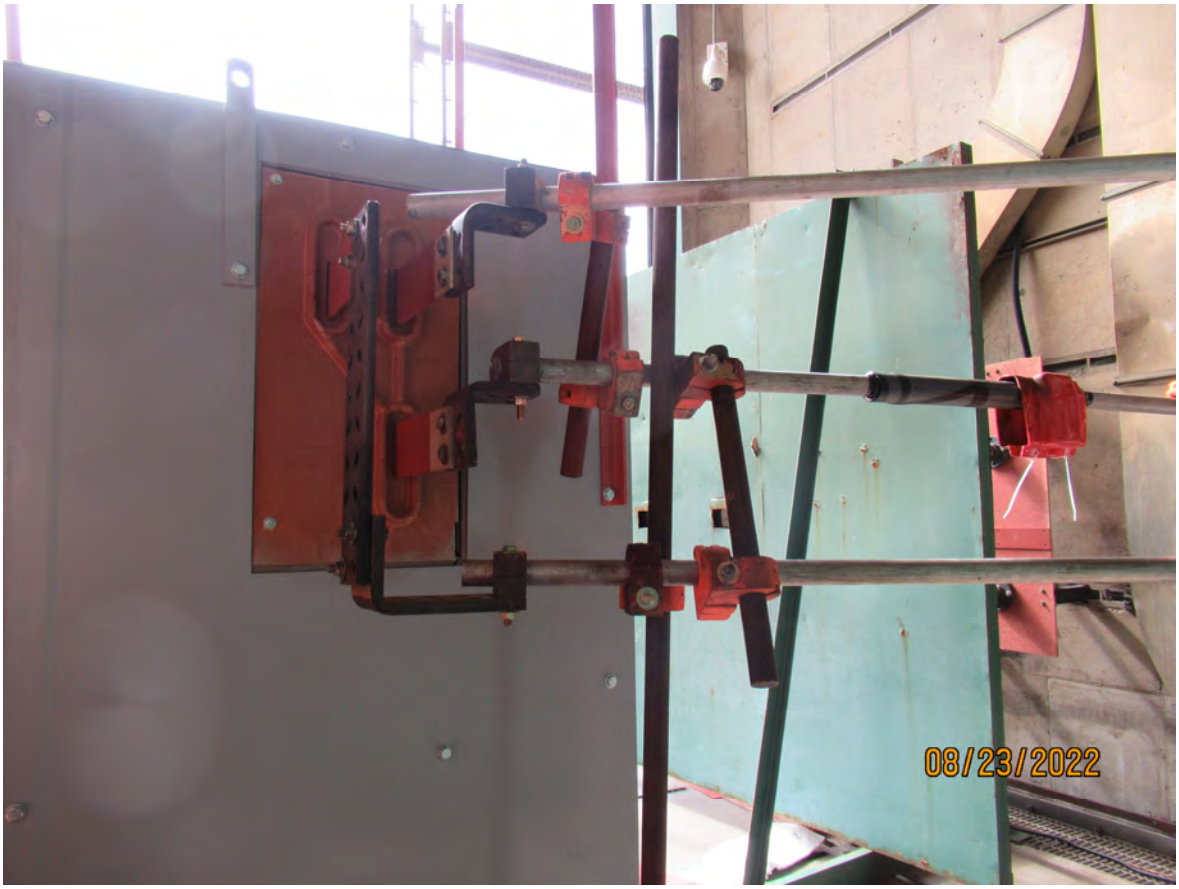
08/23/2022

## 6.4 Test results and oscillograms

**Overview of test numbers**
220823-9001

**Remarks**

| Calorimeter Slug # | Average Start Temp. | Initial Heat Capacity | Max. Temp. | Final Heat Capacity | Total Heat Energy |
|---|---|---|---|---|---|
| | °C | cal/(g°C) | °C | cal/(g°C) | J/( $cm^2$) |
| 1 | 30.53 | 0.092205 | 134.06 | 0.095330 | 58.203 |
| 2 | 31.71 | 0.092241 | 118.55 | 0.094882 | 48.709 |
| 3 | 28.43 | 0.092141 | 170.66 | 0.096335 | 80.359 |
| 4 | 28.24 | 0.092135 | 189.51 | 0.096825 | 91.353 |
| 5 | 27.18 | 0.092103 | 69.50 | 0.093405 | 23.535 |
| 6 | 26.49 | 0.092082 | 75.68 | 0.093594 | 27.377 |
| 7 | 31.02 | 0.092219 | 127.33 | 0.095137 | 54.094 |
| 8 | 32.86 | 0.092275 | 127.22 | 0.095134 | 53.014 |
| 9 | 29.94 | 0.092187 | 149.88 | 0.095773 | 67.581 |
| 10 | 29.55 | 0.092175 | 167.71 | 0.096257 | 78.044 |

PT#1: 1.91 psi above atmospheric
PT#2: 1.81 psi above atmospheric
PT#3: 5.89 psi above atmospheric
PT#4: 7.45 psi above atmospheric

**Arc Test: 32kA, 4s, CU**

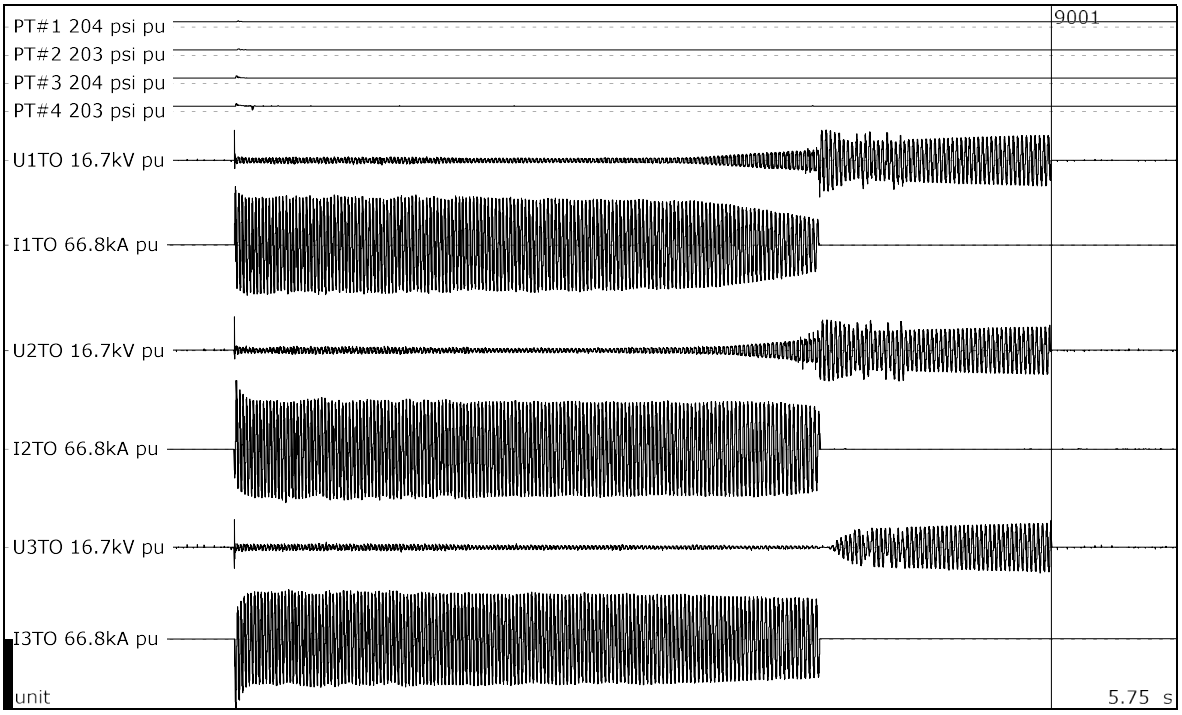


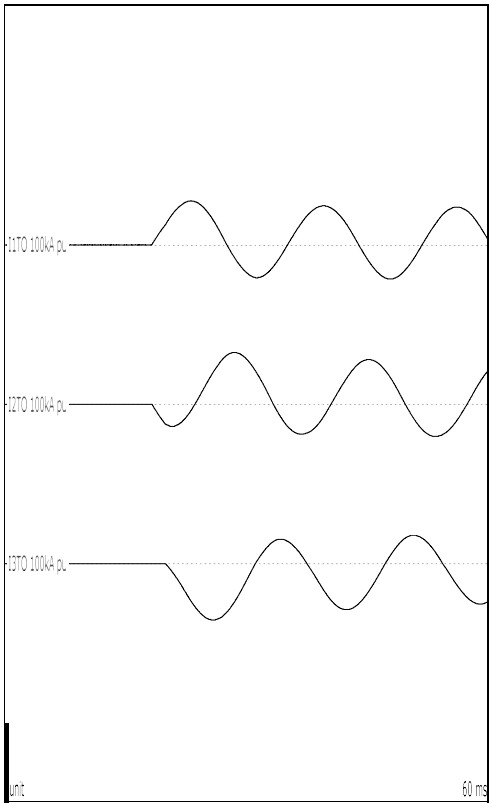


**Test number:** **220823-9001**

| Phase | | AØ | BØ | CØ |
|---|---|---|---|---|
| Applied voltage, phase-to-ground | $kV_{RMS}$ | 3.98 | 3.99 | 3.98 |
| Applied voltage, phase-to-phase | $kV_{RMS}$ | 6.90 | | |
| Making current | $kA_{peak}$ | 55.2 | 65.0 | -71.2 |
| Current, a.c. component, beginning | $kA_{RMS}$ | 33.1 | 34.6 | 33.7 |
| Current, a.c. component, middle | $kA_{RMS}$ | 29.4 | 31.4 | 29.8 |
| Current, a.c. component, end | $kA_{RMS}$ | 0.000 | 0.000 | 0.000 |
| Current, a.c. component, average | $kA_{RMS}$ | 30.8 | 32.2 | 30.7 |
| Current, a.c. component, three-phase average | $kA_{RMS}$ | 31.23 | | |
| Duration | s | 2.87 | 2.87 | 2.87 |
| Arc energy | MJ | 125 | | |
| Equivalent RMS value and duration | | 31.23 kA during 2.87 s | | |

Observations: Emission of flames and gas observed. Arc self-extinguished after 2.87 seconds. Fire inside the unit was put out with fire extinguisher.

## 6.5 Condition / inspection after test

Heavy damage to the test device. Signs of arcing and burn through on each side of the switchgear.
Fire inside of the switchgear was put out.

## 6.6 Photograph after test


08/23/2022


08/23/2022


2-12
08/23/2022


08/23/2022


08/23/2022


08/23/2022


08/23/2022

# 7 CHECKING CIRCUIT PARAMETERS

**Standard and date**

| | |
|---|---|
| Standard | Client's instructions |
| Test date | 24 August 2022 |

**Serial No.**

N/A

## 7.1 Condition before test

Shorting bar connected to input terminals of test device.

## 7.2 Test results and oscillograms

**Overview of test numbers**
220824-9002

**Remarks**
-

**Checking circuit parameters**

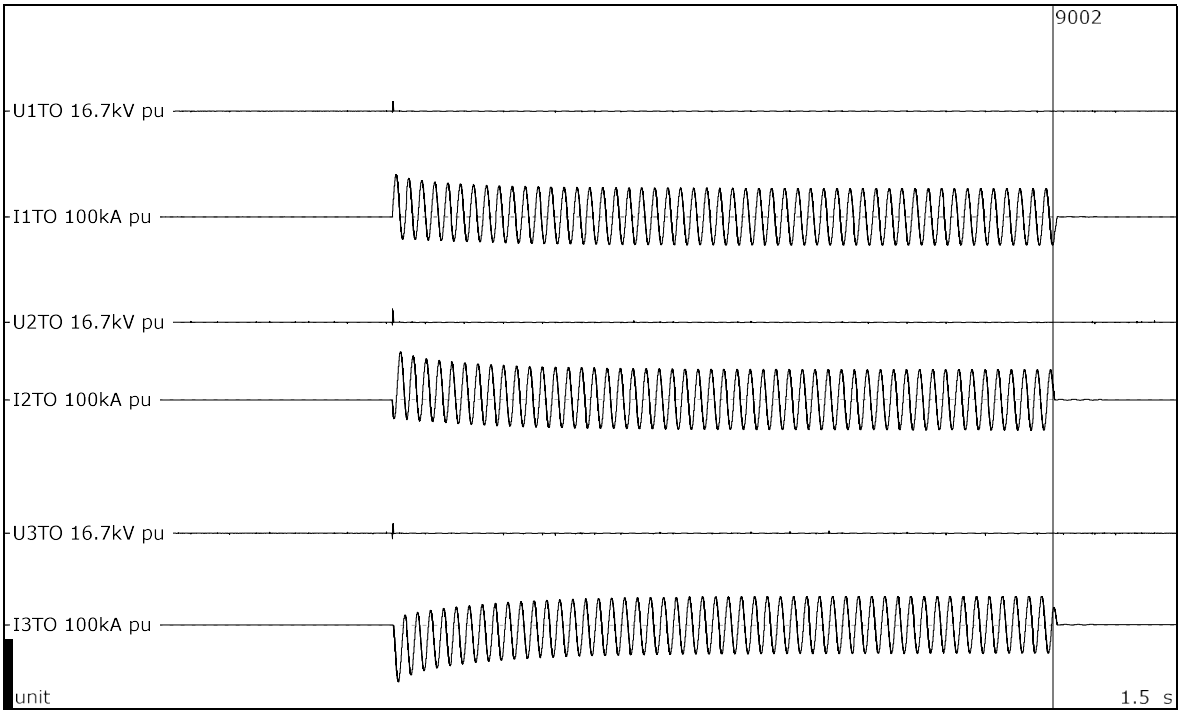


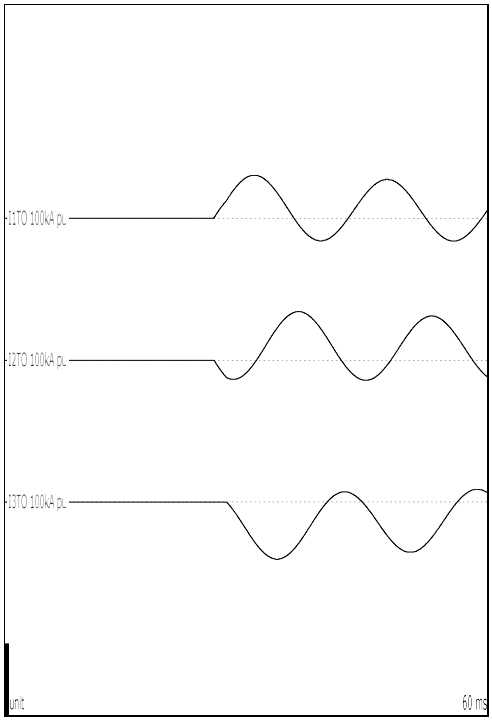


**Test number:** **220824-9002**

| Phase | | AØ | BØ | CØ |
|---|---|---|---|---|
| Current | $kA_{peak}$ | 60.7 | 68.4 | -81.1 |
| Current, a.c. component, beginning | $kA_{RMS}$ | 31.8 | 34.1 | 31.9 |
| Current, a.c. component, middle | $kA_{RMS}$ | 28.7 | 30.5 | 28.9 |
| Current, a.c. component, end | $kA_{RMS}$ | 28.7 | 30.5 | 28.9 |
| Current, a.c. component, average | $kA_{RMS}$ | 29.2 | 31.1 | 29.4 |
| Current, a.c. component, three-phase average | $kA_{RMS}$ | 29.9 | | |
| Duration, current | s | 0.845 | 0.845 | 0.844 |

Gas pressure at 20 °C - MPa

Observations: Circuit parameters are 4160 V open circuit voltage with an average current of 29.9kA. Circuit will be pro-rated to be 4174 V open circuit voltage with average current of 30kA.

## 7.3 Condition / inspection after test

See observations for test details.

# 8 ARC TEST: 30KA, 2S, CU BUS BARS

**Standard and date**

| | |
|---|---|
| Standard | Client's instructions |
| Test date | 24 August 2022 |

**Serial No.**

2-25

## 8.1 Condition before test

Enclosure grounded.
Bus duct enclosure is steel.
Copper bus in the bus duct.
New bus duct attached to the source.
Switchgear new.
Arc to be initiated by #24 AWG wire located in the bus duct.
PT#1: 30PSI transducer on the right side of the switchgear.

## 8.2 Test circuit S02

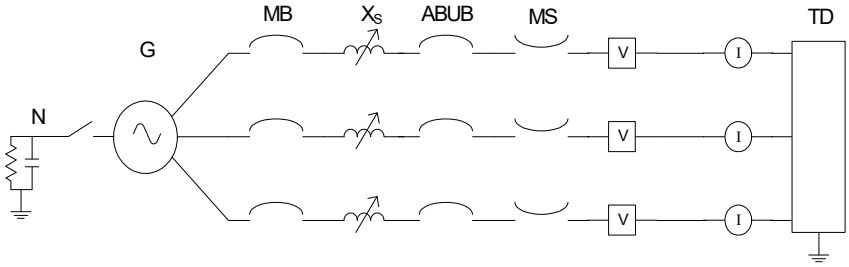


| | | | | | |
|---|---|---|---|---|---|
| G | = Generator | ABUB | = Aux. Breaker | R | = Resistance |
| N | = Neutral | XFMR | = Transformer | V | = Voltage Measurement |
| MB | = Main Breaker | TD | = Test Device | I | = Current Measurement |
| MS | = Make Switch | X | = Inductance | | |

| **Supply** | | |
|---|---|---|
| Power | MVA | 217 |
| Frequency | Hz | 60 |
| Phase(s) | | 3 |
| Voltage | kV | 4.174 |
| Current | kA | 30 |
| Impedance | Ω | 0.0803 |
| Power factor | | < 0.1 |
| Neutral | | not earthed |

Remarks: -

## 8.3 Photograph before test

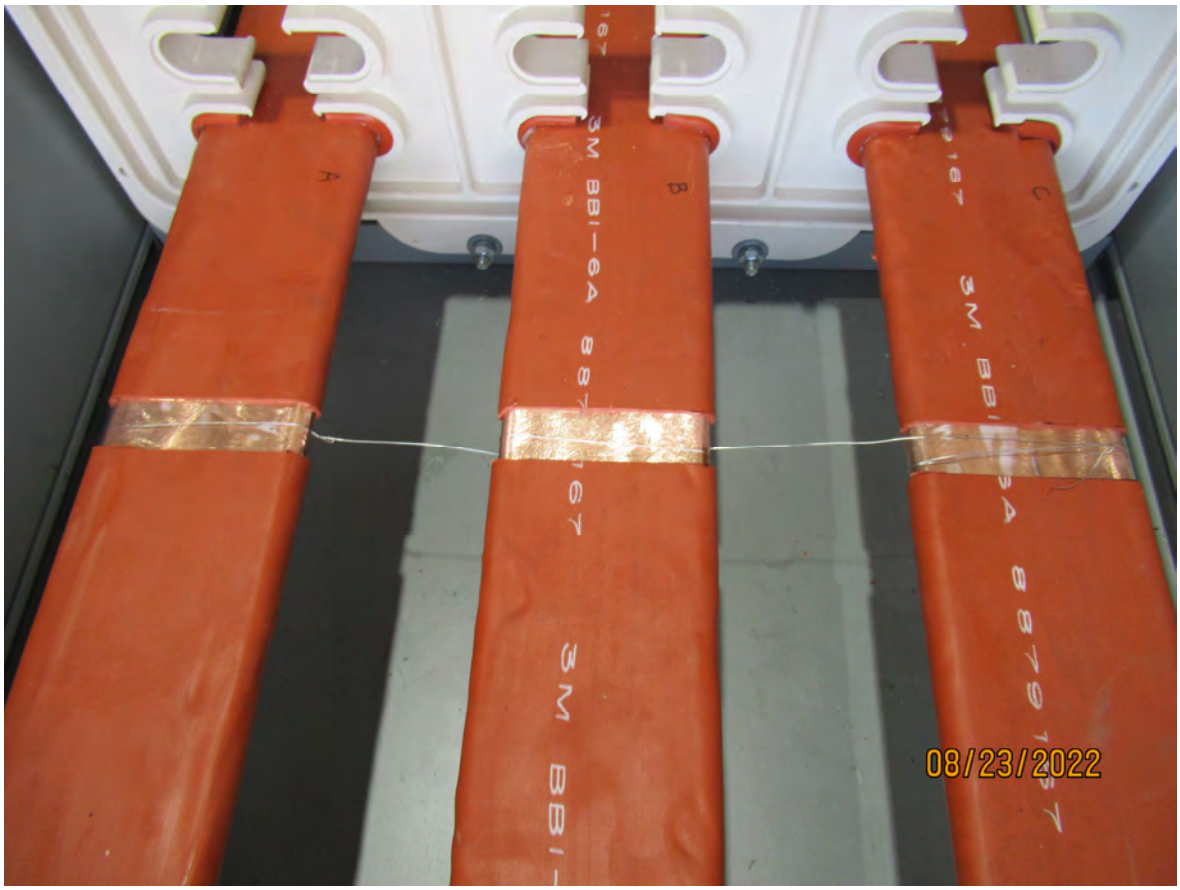


08/24/2022


08/24/2022


08/24/2022


08/24/2022


08/24/2022

## 8.4 Test results and oscillograms

**Overview of test numbers**
220824-9003

**Remarks**

| Calorimeter Slug # | Average Start Temp. | Initial Heat Capacity | Max. Temp. | Final Heat Capacity | Total Heat Energy |
|---|---|---|---|---|---|
| | °C | cal/(g°C) | °C | cal/(g°C) | J/( $cm^2$) |
| 1 | 31.07 | 0.092221 | 232.59 | 0.097871 | 114.834 |
| 2 | 31.18 | 0.092224 | 154.18 | 0.095891 | 69.363 |
| 3 | 34.59 | 0.092328 | 140.92 | 0.095523 | 59.874 |
| 4 | 34.63 | 0.092330 | 170.00 | 0.096318 | 76.553 |
| 5 | 35.40 | 0.092353 | 96.35 | 0.094224 | 34.089 |
| 6 | 34.51 | 0.092326 | 91.18 | 0.094067 | 31.664 |
| 7 | 31.33 | 0.092229 | 111.03 | 0.094661 | 44.648 |
| 8 | 31.10 | 0.092222 | 114.38 | 0.094760 | 46.678 |
| 9 | 31.20 | 0.092225 | 74.41 | 0.093555 | 24.064 |
| 10 | 30.58 | 0.092206 | 74.82 | 0.093568 | 24.639 |

PT#1: 4.85 psi above atmospheric

**Arc Test: 30kA, 2s, CU Bus bars**

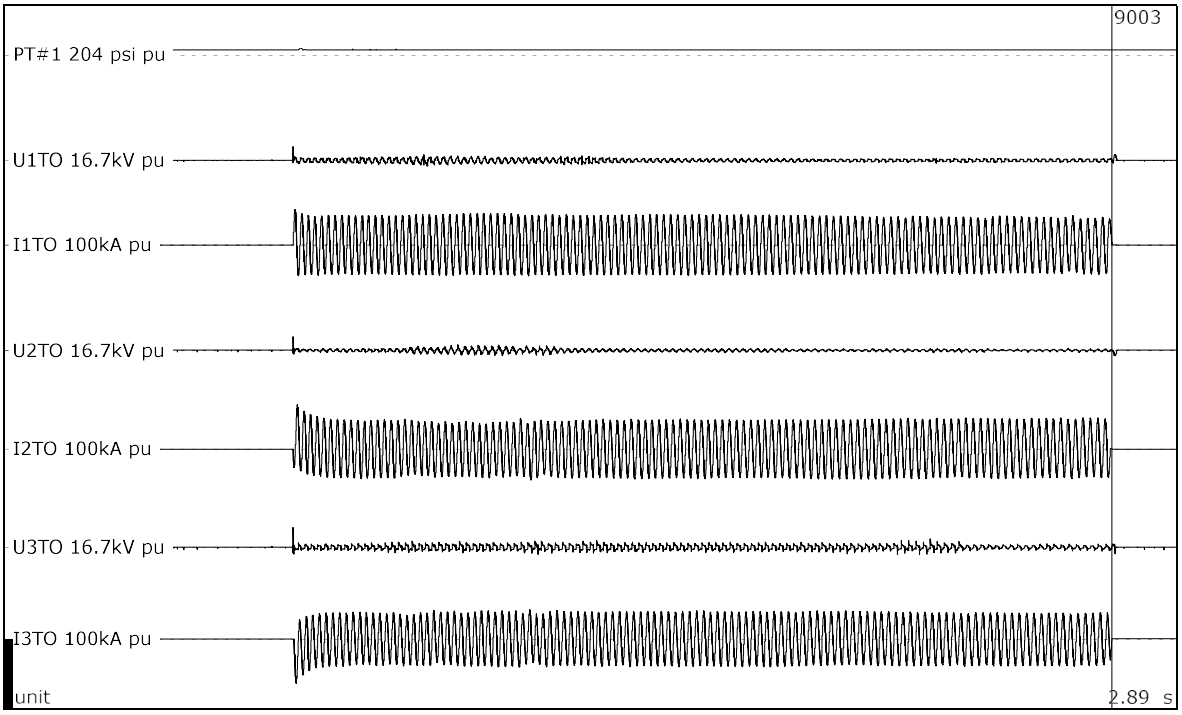


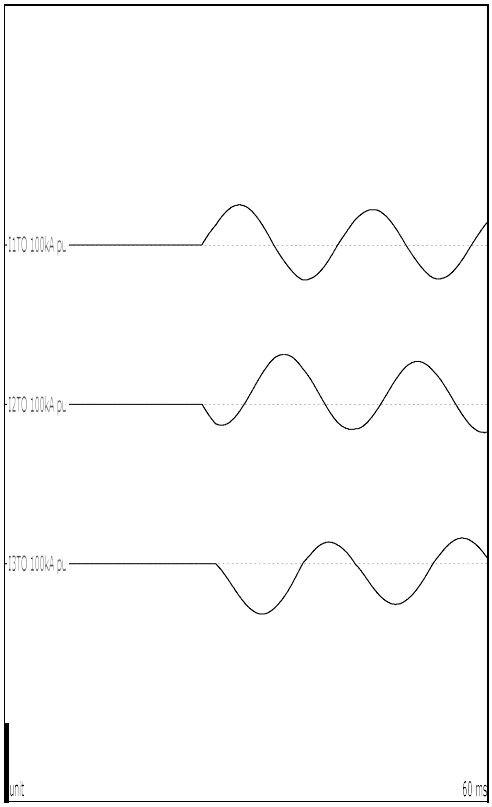


**Test number:** **220824-9003**

| Phase | | AØ | BØ | CØ |
|---|---|---|---|---|
| Applied voltage, phase-to-ground | $kV_{RMS}$ | 2.41 | 2.41 | 2.41 |
| Applied voltage, phase-to-phase | $kV_{RMS}$ | 4.17 | | |
| Making current | $kA_{peak}$ | 50.3 | 62.8 | -63.7 |
| Current, a.c. component, beginning | $kA_{RMS}$ | 32.5 | 32.5 | 29.9 |
| Current, a.c. component, middle | $kA_{RMS}$ | 30.2 | 29.3 | 27.2 |
| Current, a.c. component, end | $kA_{RMS}$ | 28.1 | 29.7 | 26.4 |
| Current, a.c. component, average | $kA_{RMS}$ | 30.2 | 29.7 | 27.3 |
| Current, a.c. component, three-phase average | $kA_{RMS}$ | 29.1 | | |
| Duration | s | 2.02 | 2.02 | 2.02 |
| Arc energy | MJ | 51.4 | | |
| Equivalent RMS value and duration | | 30.0 kA during 2.00 s | | |

Observations: Emission of flames and gas observed.

## 8.5 Condition / inspection after test

Heavy damage to the test device. Signs of arcing and burn through on each side of the bus duct.
After test, fire on the instrumentation racks were put out.

## 8.6 Photograph after test

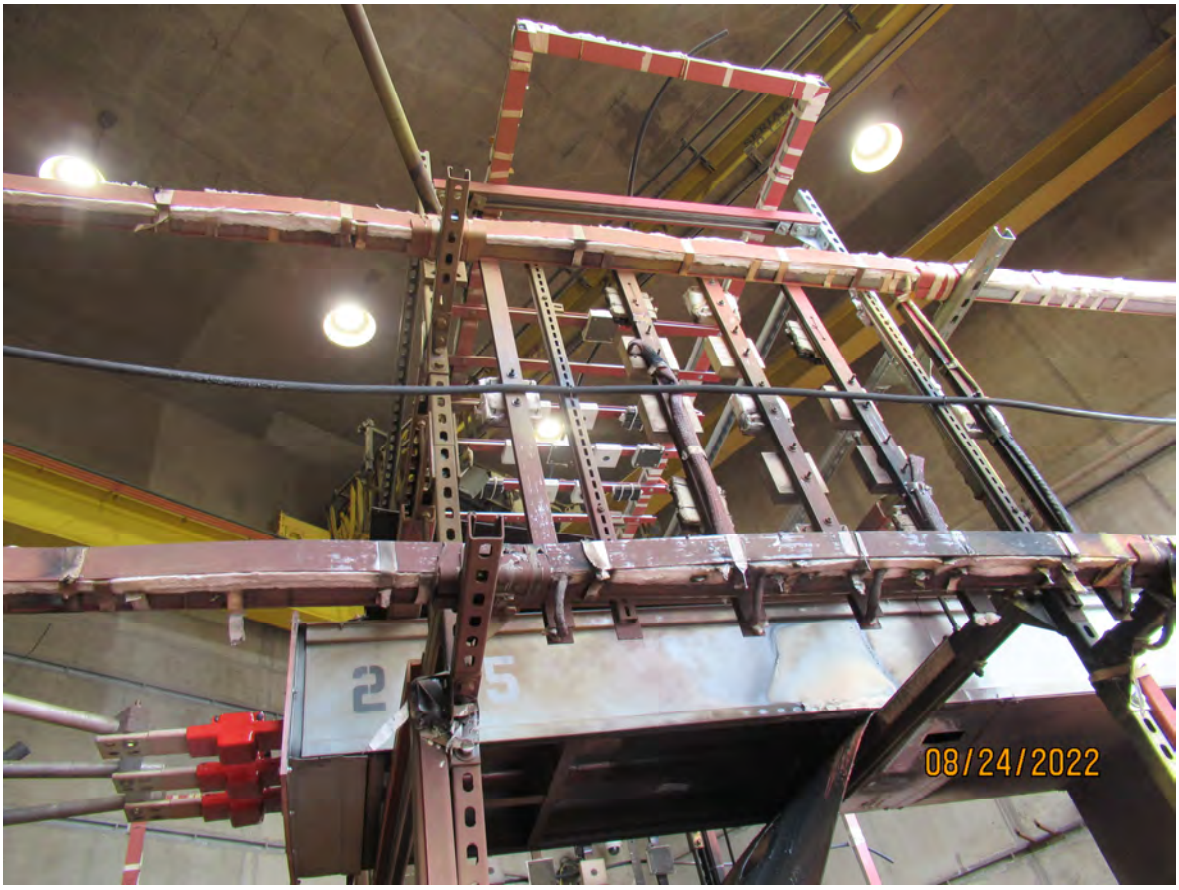
08/24/2022


08/24/2022


08/24/2022

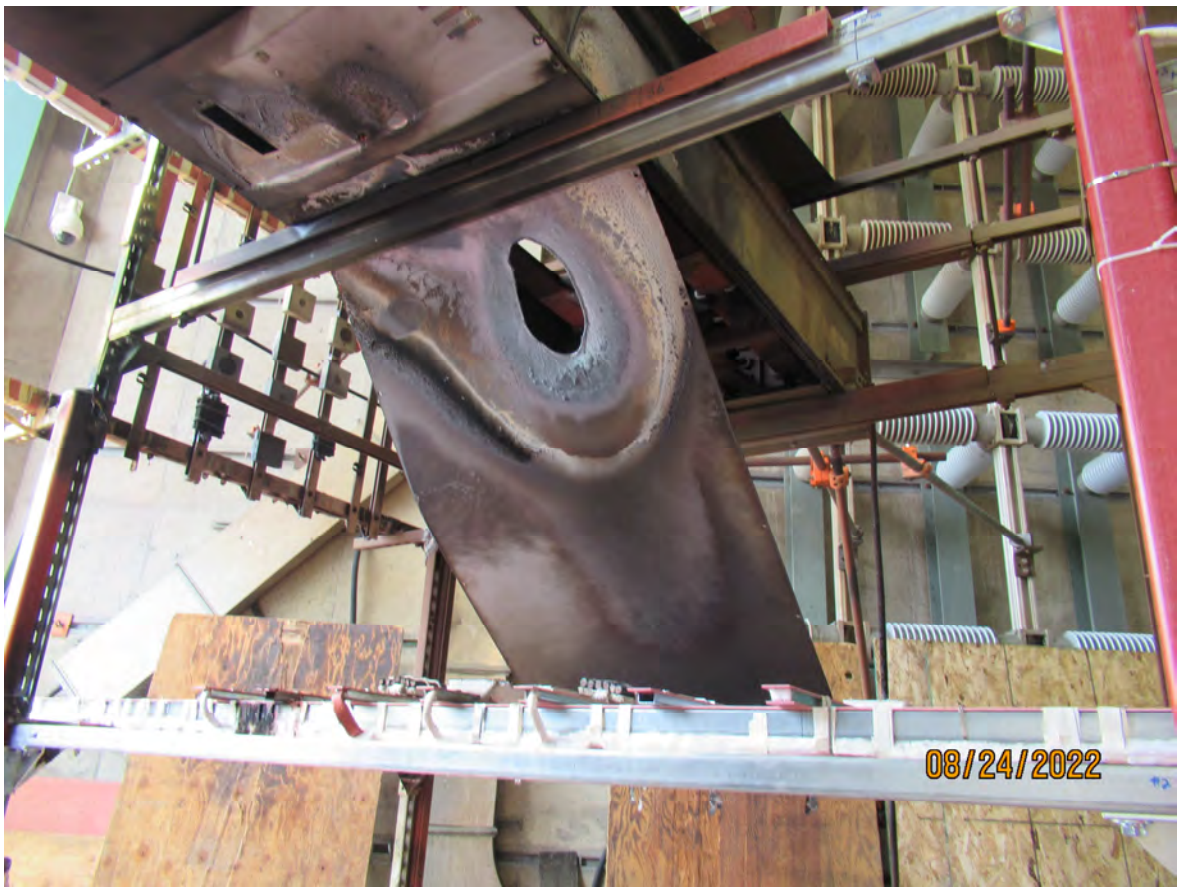
08/24/2022


08/24/2022


08/24/2022


08/24/2022


08/24/2022

# 9 ARC TEST: 30KA, 4S, CU BUS BARS

**Standard and date**

| | |
|---|---|
| Standard | Client's instructions |
| Test date | 25 August 2022 |

**Serial No.**

2-26

## 9.1 Condition before test

Enclosure grounded.
Bus duct enclosure is steel.
Copper bus in the bus duct.
New bus duct attached to the source.
Switchgear same as previous test.
Arc to be initiated by #24 AWG wire located in the bus duct.
PT#1: 30PSI transducer on the right side of the switchgear.

## 9.2 Test circuit S02

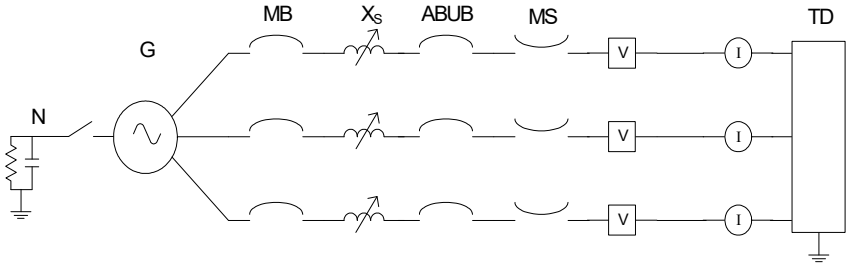


| | | | | | |
|---|---|---|---|---|---|
| G | = Generator | ABUB | = Aux. Breaker | R | = Resistance |
| N | = Neutral | XFMR | = Transformer | V | = Voltage Measurement |
| MB | = Main Breaker | TD | = Test Device | I | = Current Measurement |
| MS | = Make Switch | X | = Inductance | | |

| **Supply** | | |
|---|---|---|
| Power | MVA | 217 |
| Frequency | Hz | 60 |
| Phase(s) | | 3 |
| Voltage | kV | 4.174 |
| Current | kA | 30 |
| Impedance | Ω | 0.0803 |
| Power factor | | < 0.1 |
| Neutral | | not earthed |

Remarks: -

## 9.3 Photograph before test


08/25/2022


08/25/2022


08/25/2022


08/25/2022

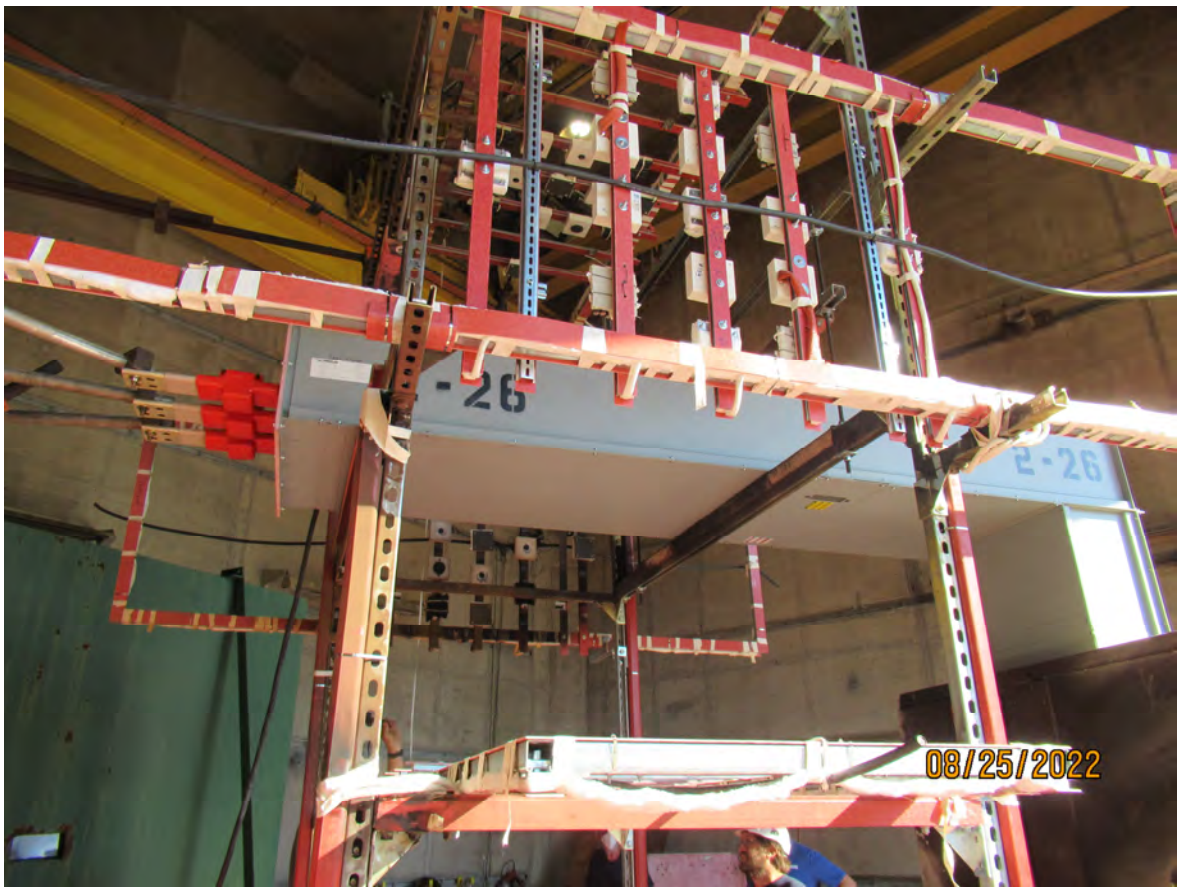
-26
2-26
08/25/2022


2-26
08/25/2022
Achtung
Rückspannung


2
2-26
08/25/2022


08/25/2022


08/23/2022

## 9.4 Test results and oscillograms

**Overview of test numbers**
220825-9001

**Remarks**

| Calorimeter Slug # | Average Start Temp. | Initial Heat Capacity | Max. Temp. | Final Heat Capacity | Total Heat Energy |
|---|---|---|---|---|---|
| | °C | cal/(g°C) | °C | cal/(g°C) | J/( $cm^2$) |
| 1 | 30.43 | 0.092202 | 188.92 | 0.096810 | 89.800 |
| 2 | 29.81 | 0.092182 | 176.93 | 0.096501 | 83.218 |
| 3 | 32.31 | 0.092259 | 198.05 | 0.097040 | 94.053 |
| 4 | 32.15 | 0.092254 | 179.78 | 0.096575 | 83.566 |
| 5 | 31.99 | 0.092249 | 110.42 | 0.094643 | 43.939 |
| 6 | 30.69 | 0.092209 | 116.29 | 0.094816 | 47.990 |
| 7 | 44.69 | 0.092638 | 115.93 | 0.094806 | 40.028 |
| 8 | 41.68 | 0.092546 | 83.90 | 0.093846 | 23.588 |
| 9 | 43.40 | 0.092599 | 81.75 | 0.093780 | 21.423 |
| 10 | 40.14 | 0.092498 | 75.78 | 0.093598 | 19.883 |

PT#1: 5.47 psi above atmospheric

**Arc Test: 30kA, 4s, CU Bus bars**

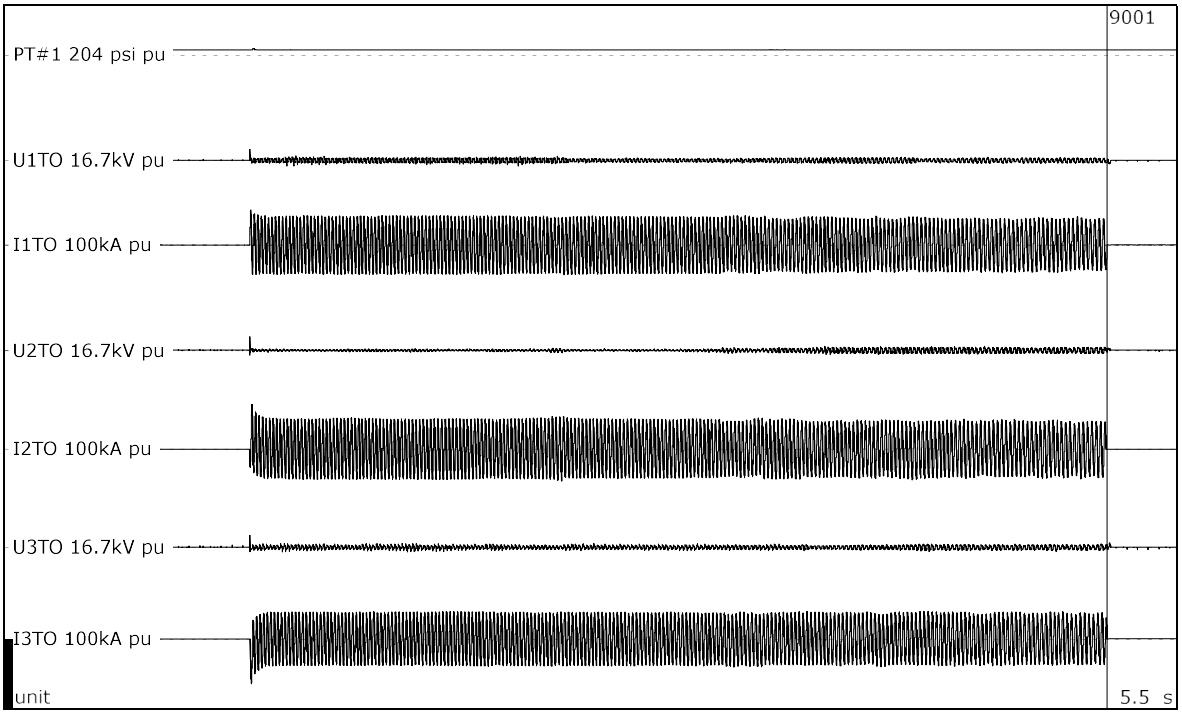


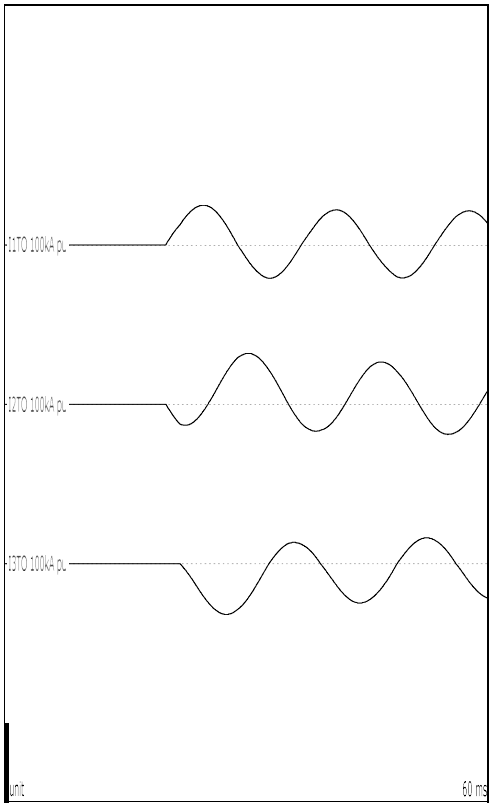


**Test number:** **220825-9001**

| Phase | | AØ | BØ | CØ |
|---|---|---|---|---|
| Applied voltage, phase-to-ground | $kV_{RMS}$ | 2.41 | 2.41 | 2.41 |
| Applied voltage, phase-to-phase | $kV_{RMS}$ | 4.17 | | |
| Making current | $kA_{peak}$ | 49.8 | 63.9 | -64.2 |
| Current, a.c. component, beginning | $kA_{RMS}$ | 31.5 | 33.3 | 29.5 |
| Current, a.c. component, middle | $kA_{RMS}$ | 28.6 | 29.7 | 26.6 |
| Current, a.c. component, end | $kA_{RMS}$ | 26.1 | 27.7 | 25.3 |
| Current, a.c. component, average | $kA_{RMS}$ | 28.8 | 30.1 | 27.1 |
| Current, a.c. component, three-phase average | $kA_{RMS}$ | 28.7 | | |
| Duration | s | 4.02 | 4.02 | 4.02 |
| Arc energy | MJ | 101 | | |
| Equivalent RMS value and duration | | 30.0 kA during 4.00 s | | |

Observations: Emission of flames and gas observed.

## 9.5 Condition / inspection after test

Heavy damage to the test device. Signs of arcing and burn through on each side of the bus duct.
After test, fire on the instrumentation racks were put out.

## 9.6 Photograph after test


26
08/25/2022


08/25/2022


08/25/2022


08/25/2022


08/25/2022


08/25/2022


08/25/2022


08/25/2022


08/25/2022


2-26
08/25/2022

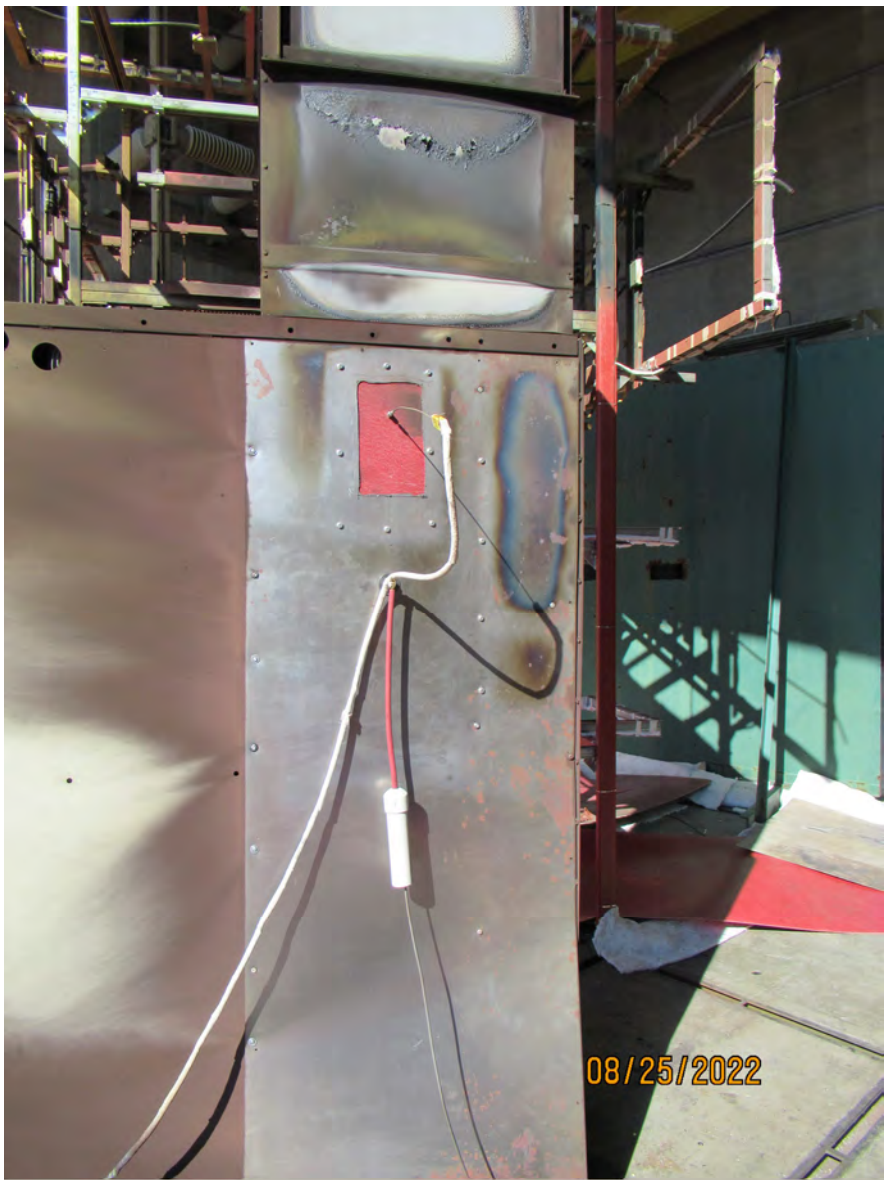
08/25/2022

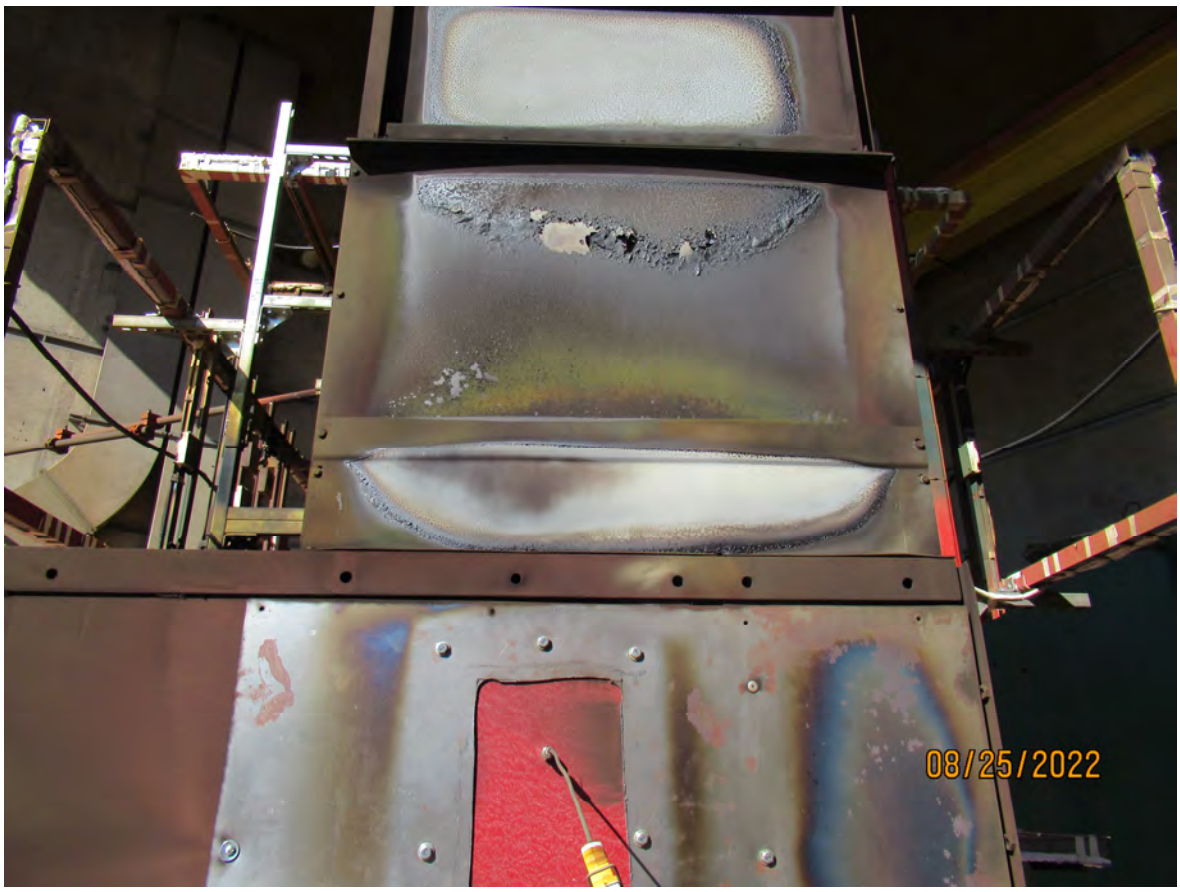
08/25/2022


08/25/2022

## 10 ARC TEST: 30KA, 4S, AL BUS BARS

**Standard and date**

| | |
|---|---|
| Standard | Client's instructions |
| Test date | 26 August 2022 |

**Serial No.**
2-30

### 10.1 Condition before test

Enclosure grounded.
Bus duct enclosure is steel.
Aluminum bus in the bus duct.
New bus duct attached to the source.
Switchgear same as previous test.
Arc to be initiated by #24 AWG wire located in the bus duct.
PT#1: 30PSI transducer on the right side of the switchgear.
PT#2: 30PSI transducer on the back side of the switchgear.

## 10.2 Test circuit S02

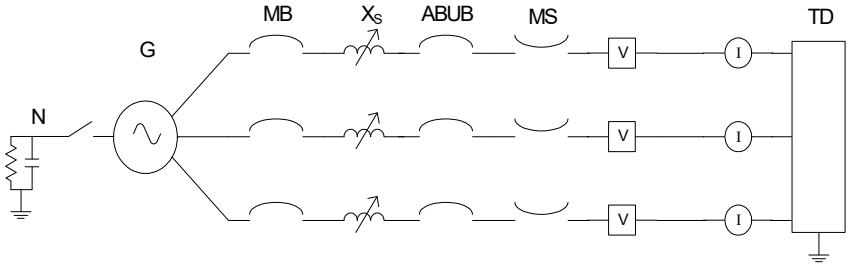


| | | | | | |
|---|---|---|---|---|---|
| G | = Generator | ABUB | = Aux. Breaker | R | = Resistance |
| N | = Neutral | XFMR | = Transformer | V | = Voltage Measurement |
| MB | = Main Breaker | TD | = Test Device | I | = Current Measurement |
| MS | = Make Switch | X | = Inductance | | |

| **Supply** | | |
|---|---|---|
| Power | MVA | 217 |
| Frequency | Hz | 60 |
| Phase(s) | | 3 |
| Voltage | kV | 4.174 |
| Current | kA | 30 |
| Impedance | Ω | 0.0803 |
| Power factor | | < 0.1 |
| Neutral | | not earthed |

Remarks: -

## 10.3 Photograph before test

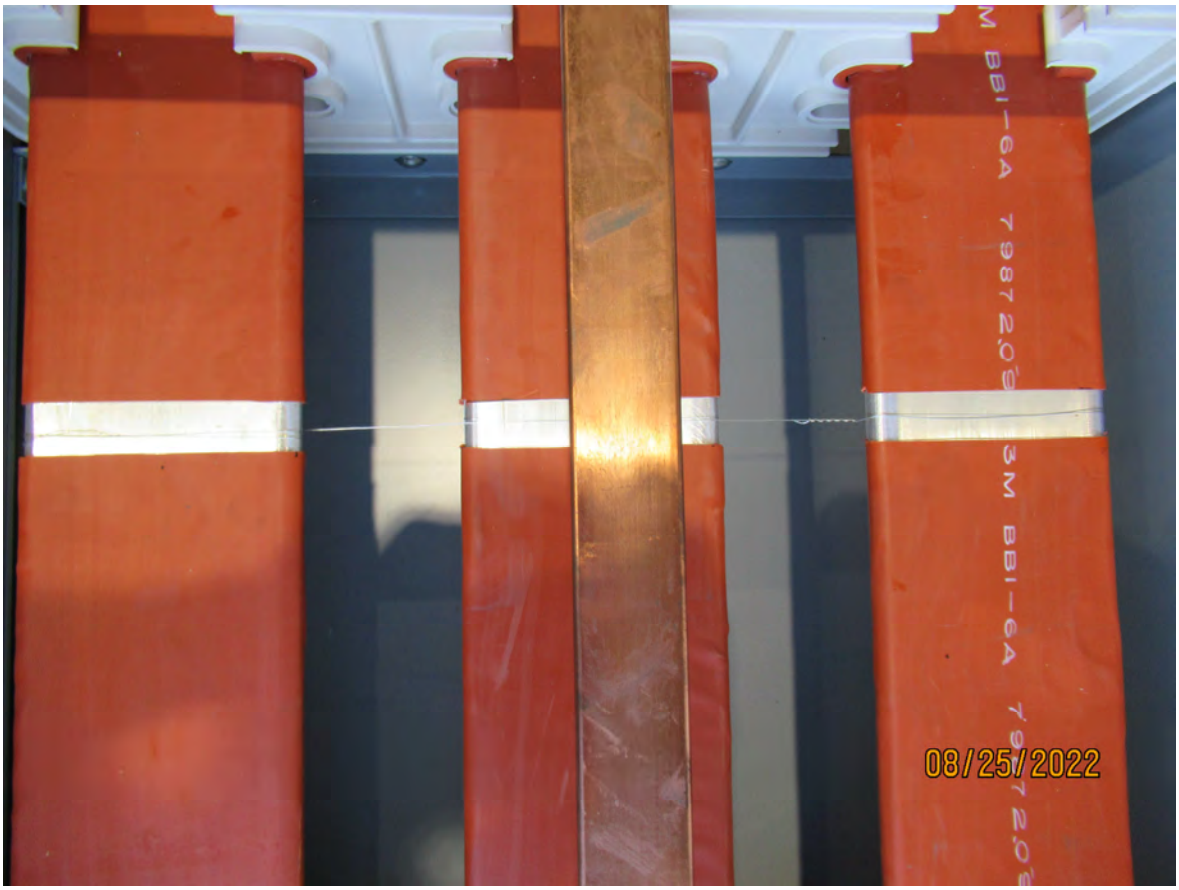


2-30
08/26/2022


08/26/2022

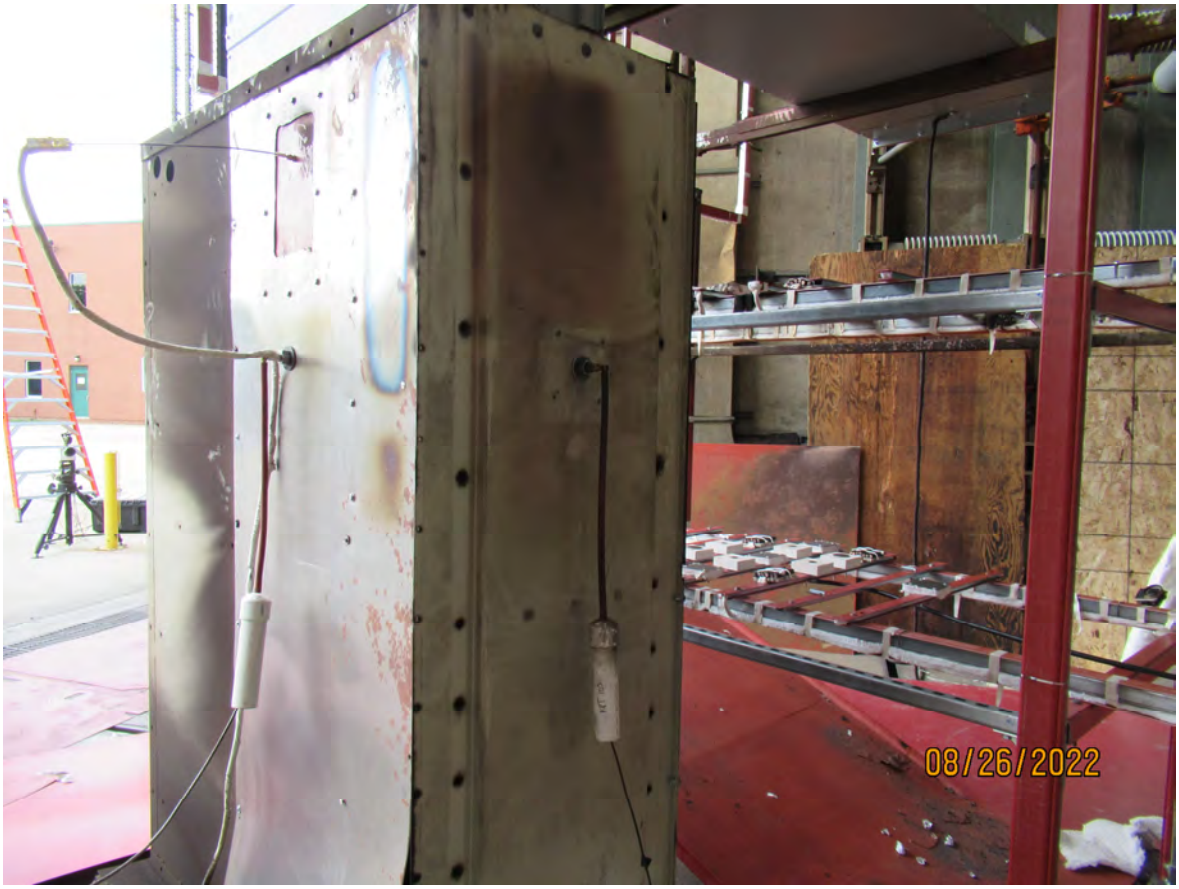
08/26/2022


08/26/2022


08/26/2022


08/26/2022

## 10.4 Test results and oscillograms

**Overview of test numbers**
220826-9001

**Remarks**

| Calorimeter Slug # | Average Start Temp. | Initial Heat Capacity | Max. Temp. | Final Heat Capacity | Total Heat Energy |
|---|---|---|---|---|---|
| | °C | cal/(g°C) | °C | cal/(g°C) | J/( $cm^2$) |
| 1 | 29.28 | 0.092167 | 144.60 | 0.095627 | 64.922 |
| 2 | 29.50 | 0.092173 | 103.52 | 0.094439 | 41.407 |
| 3 | 30.29 | 0.092197 | 196.72 | 0.097007 | 94.399 |
| 4 | 34.17 | 0.092315 | 189.60 | 0.096827 | 88.131 |
| 5 | 30.47 | 0.092203 | 127.64 | 0.095146 | 54.572 |
| 6 | 30.06 | 0.092190 | 165.86 | 0.096208 | 76.695 |
| 7 | 34.12 | 0.092314 | 205.85 | 0.097234 | 97.583 |
| 8 | 34.10 | 0.092313 | 157.92 | 0.095994 | 69.896 |
| 9 | 29.05 | 0.092159 | 99.95 | 0.094332 | 39.641 |
| 10 | 28.49 | 0.092143 | 85.57 | 0.093897 | 31.831 |

PT#1: 4.09 psi above atmospheric
PT#2: 2.29 psi above atmospheric

**Arc Test: 30kA, 4s, Al Bus bars**

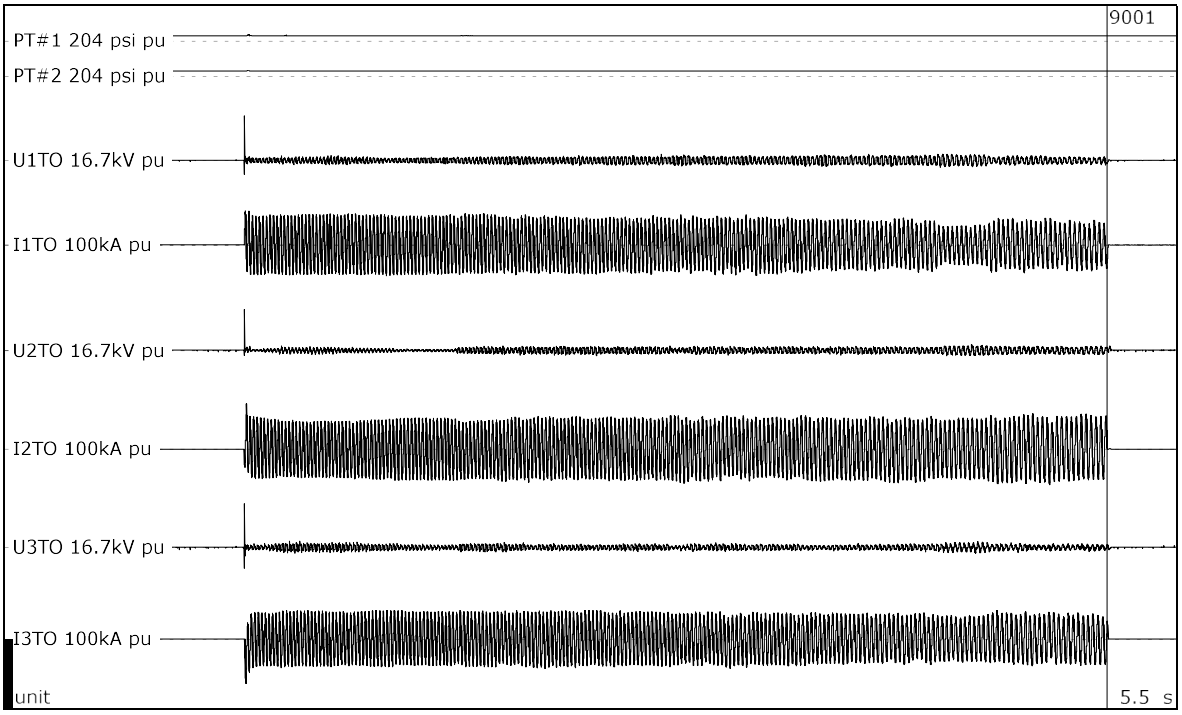


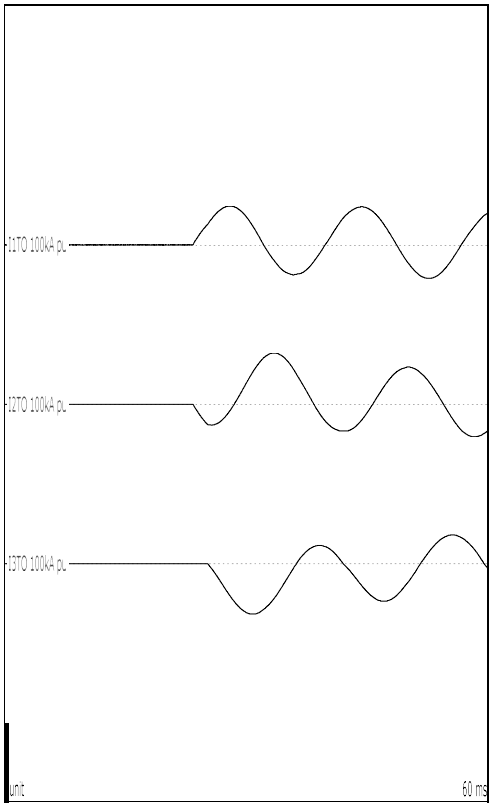


**Test number:** **220826-9001**

| Phase | | AØ | BØ | CØ |
|---|---|---|---|---|
| Applied voltage, phase-to-ground | $kV_{RMS}$ | 2.41 | 2.41 | 2.41 |
| Applied voltage, phase-to-phase | $kV_{RMS}$ | 4.17 | | |
| Making current | $kA_{peak}$ | 48.7 | 64.2 | -63.9 |
| Current, a.c. component, beginning | $kA_{RMS}$ | 30.4 | 33.3 | 27.7 |
| Current, a.c. component, middle | $kA_{RMS}$ | 27.6 | 33.2 | 25.7 |
| Current, a.c. component, end | $kA_{RMS}$ | 24.2 | 31.6 | 25.2 |
| Current, a.c. component, average | $kA_{RMS}$ | 28.0 | 31.0 | 26.4 |
| Current, a.c. component, three-phase average | $kA_{RMS}$ | 28.4 | | |
| Duration | s | 4.05 | 4.05 | 4.04 |
| Arc energy | MJ | 158 | | |
| Equivalent RMS value and duration | | 30.0 kA during 4.00 s | | |

Observations: Emission of flames and gas observed.

## 10.5 Condition / inspection after test

Heavy damage to the test device. Signs of arcing and burn through on each side of the bus duct.
After test, fire on the instrumentation racks and bus duct were put out.
Heavy signs of arcing on the supply bus.
A phase voltage divider measurement is arc voltage across test device plus the arc voltage across the break in the source on A phase bus.

## 10.6 Photograph after test


08/26/2022


30
08/26/2022


2-30
08/26/2022

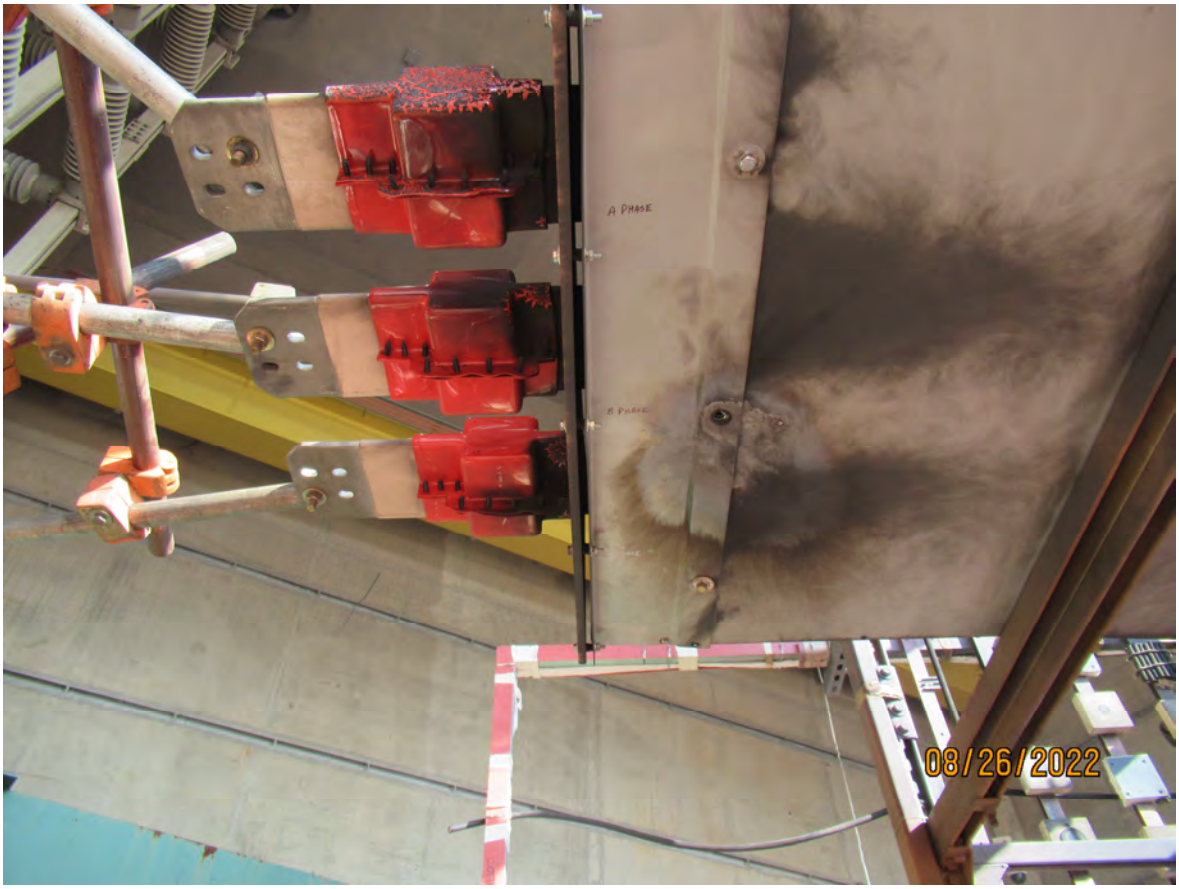
A PHASE
08/26/2022


08/26/2022


08/26/2022

## 11 ARC TEST: 30KA, 2S, CU BUS BARS

**Standard and date**

| | |
|---|---|
| Standard | Client's instructions |
| Test date | 29 August 2022 |

**Serial No.**
2-27

### 11.1 Condition before test

Enclosure grounded.
Bus duct enclosure is aluminum.
Copper bus in the bus duct.
New bus duct attached to the source.
Switchgear same as previous test.
Arc to be initiated by #24 AWG wire located in the bus duct.
PT#1: 30PSI transducer on the right side of the switchgear.
PT#2: 30PSI transducer on the back side of the switchgear.

## 11.2 Test circuit S02

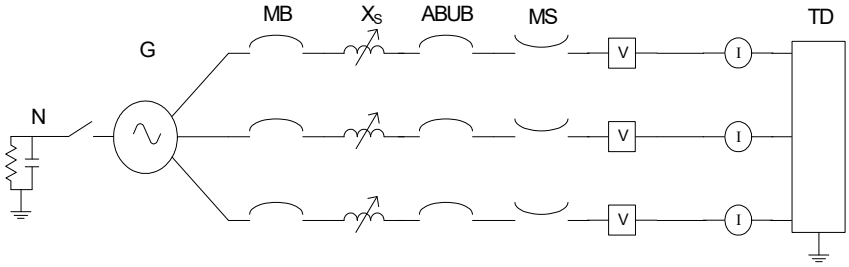


| | | | | | |
|---|---|---|---|---|---|
| G | = Generator | ABUB | = Aux. Breaker | R | = Resistance |
| N | = Neutral | XFMR | = Transformer | V | = Voltage Measurement |
| MB | = Main Breaker | TD | = Test Device | I | = Current Measurement |
| MS | = Make Switch | X | = Inductance | | |

| **Supply** | | |
|---|---|---|
| Power | MVA | 217 |
| Frequency | Hz | 60 |
| Phase(s) | | 3 |
| Voltage | kV | 4.174 |
| Current | kA | 30 |
| Impedance | Ω | 0.0803 |
| Power factor | | < 0.1 |
| Neutral | | not earthed |

Remarks: -

## 11.3 Photograph before test


08/29/2022


08/29/2022


08/29/2022


2-2
08/29/2022


08/29/2022

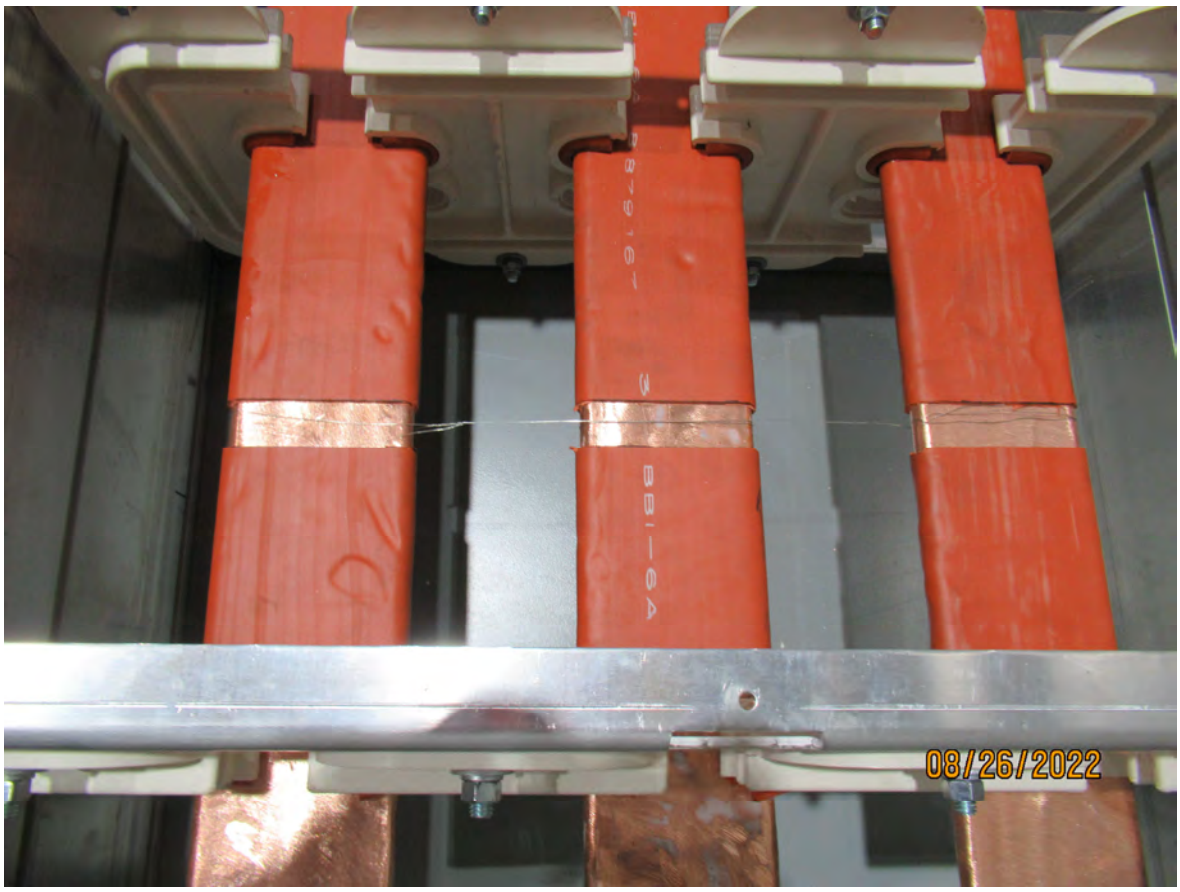
08/26/2022

## 11.4 Test results and oscillograms

**Overview of test numbers**
220829-9001

**Remarks**

| Calorimeter Slug # | Average Start Temp. | Initial Heat Capacity | Max. Temp. | Final Heat Capacity | Total Heat Energy |
|---|---|---|---|---|---|
| | °C | cal/(g°C) | °C | cal/(g°C) | J/( $cm^2$) |
| 1 | 32.27 | 0.092258 | 38.42 | 0.092446 | 3.404 |
| 2 | 29.78 | 0.092182 | 143.26 | 0.095589 | 63.881 |
| 3 | 32.37 | 0.092261 | 141.05 | 0.095527 | 61.182 |
| 4 | 31.56 | 0.092236 | 125.02 | 0.095070 | 52.479 |
| 5 | 31.40 | 0.092231 | 124.32 | 0.095050 | 52.165 |
| 6 | 31.09 | 0.092221 | 105.19 | 0.094488 | 41.474 |
| 7 | 30.12 | 0.092192 | 192.54 | 0.096902 | 92.070 |
| 8 | 30.06 | 0.092190 | 313.82 | 0.099592 | 163.135 |
| 9 | 30.53 | 0.092205 | 125.63 | 0.095088 | 53.391 |

PT#1: 3.52 psi above atmospheric
PT#2: 2.23 psi above atmospheric

**Arc Test: 30kA, 2s, CU Bus bars**

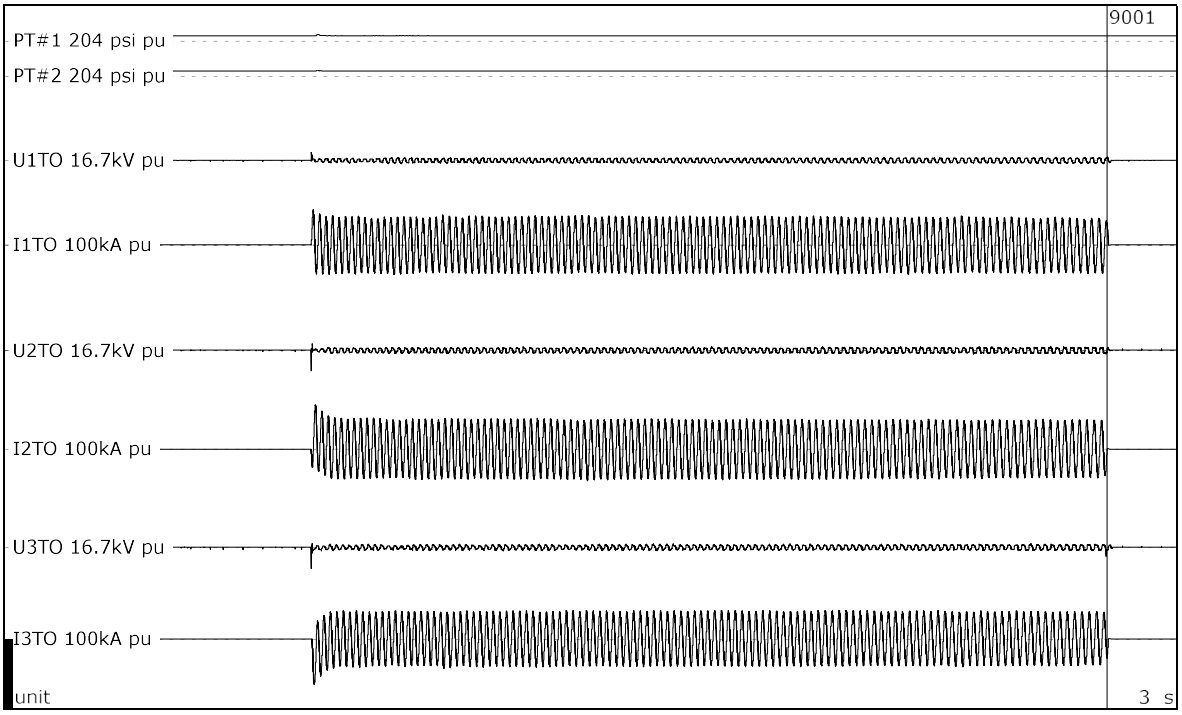


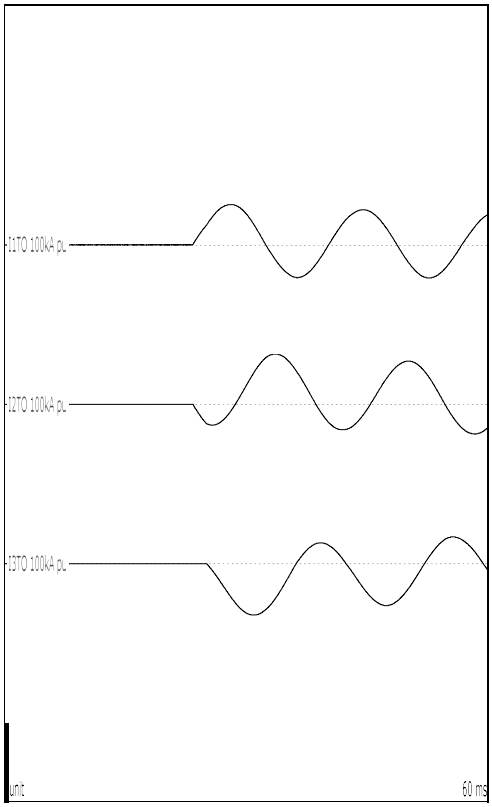


**Test number:** **220829-9001**

| Phase | | AØ | BØ | CØ |
|---|---|---|---|---|
| Applied voltage, phase-to-ground | $kV_{RMS}$ | 2.41 | 2.41 | 2.41 |
| Applied voltage, phase-to-phase | $kV_{RMS}$ | 4.17 | | |
| Making current | $kA_{peak}$ | 50.7 | 63.3 | -65.0 |
| Current, a.c. component, beginning | $kA_{RMS}$ | 31.4 | 32.8 | 30.0 |
| Current, a.c. component, middle | $kA_{RMS}$ | 28.9 | 29.9 | 28.1 |
| Current, a.c. component, end | $kA_{RMS}$ | 27.6 | 29.1 | 27.0 |
| Current, a.c. component, average | $kA_{RMS}$ | 29.0 | 30.4 | 28.1 |
| Current, a.c. component, three-phase average | $kA_{RMS}$ | 29.1 | | |
| Duration | s | 2.04 | 2.04 | 2.03 |
| Arc energy | MJ | 73.3 | | |
| Equivalent RMS value and duration | | 30.0 kA during 2.00 s | | |

Observations: Emission of flames and gas observed.

## 11.5 Condition / inspection after test

Heavy damage to the test device. Majority of bus duct enclosure has vaporized.
Pressure transducer #1 found on the ground after the test.

## 11.6 Photograph after test


08/29/2022


08/29/2022


08/29/2022


08/29/2022


08/29/2022


08/29/2022


08/29/2022

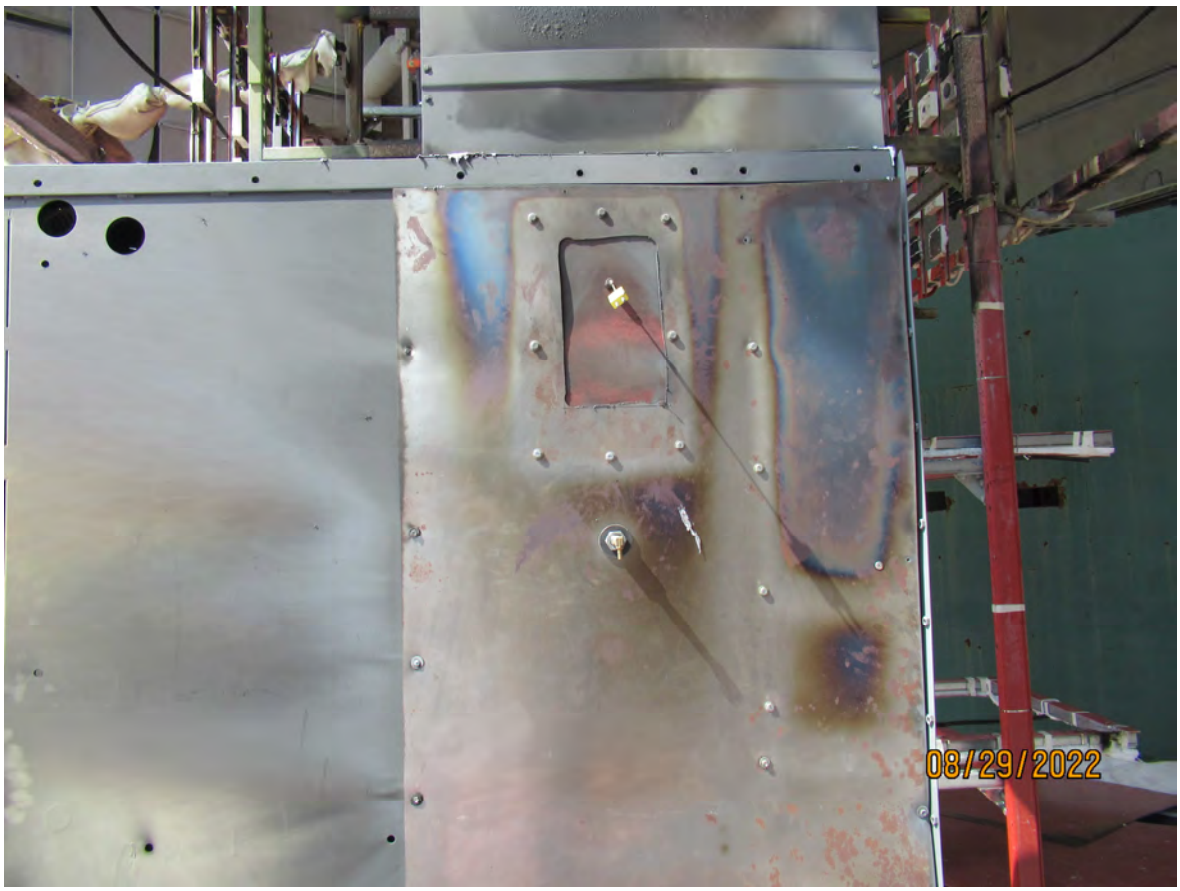
08/29/2022


BD 57
08/29/2022


08/29/2022


08/29/2022

## 12 ARC TEST: 30KA, 4S, CU BUS BARS

**Standard and date**

| | |
|---|---|
| Standard | Client's instructions |
| Test date | 30 August 2022 |

**Serial No.**
2-28

### 12.1 Condition before test

Enclosure grounded.
Bus duct enclosure is aluminum.
Copper bus in the bus duct.
New bus duct attached to the source.
Switchgear same as previous test.
Arc to be initiated by #24 AWG wire located in the bus duct.
PT#1: 30PSI transducer on the right side of the switchgear.
PT#2: 30PSI transducer on the back side of the switchgear.
Calorimeter "1" not used.

## 12.2 Test circuit S02

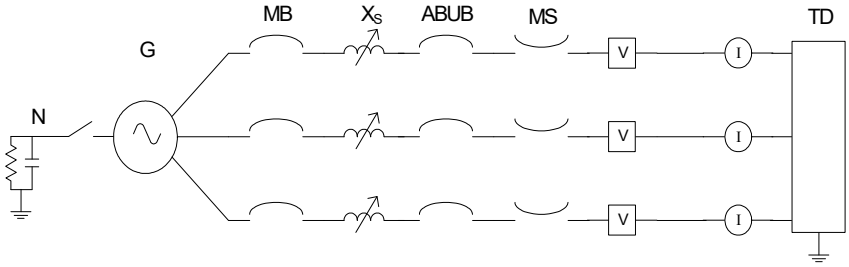


| | | | | | |
|---|---|---|---|---|---|
| G | = Generator | ABUB | = Aux. Breaker | R | = Resistance |
| N | = Neutral | XFMR | = Transformer | V | = Voltage Measurement |
| MB | = Main Breaker | TD | = Test Device | I | = Current Measurement |
| MS | = Make Switch | X | = Inductance | | |

| **Supply** | | |
|---|---|---|
| Power | MVA | 217 |
| Frequency | Hz | 60 |
| Phase(s) | | 3 |
| Voltage | kV | 4.174 |
| Current | kA | 30 |
| Impedance | Ω | 0.0803 |
| Power factor | | < 0.1 |
| Neutral | | not earthed |

Remarks: -

## 12.3 Photograph before test

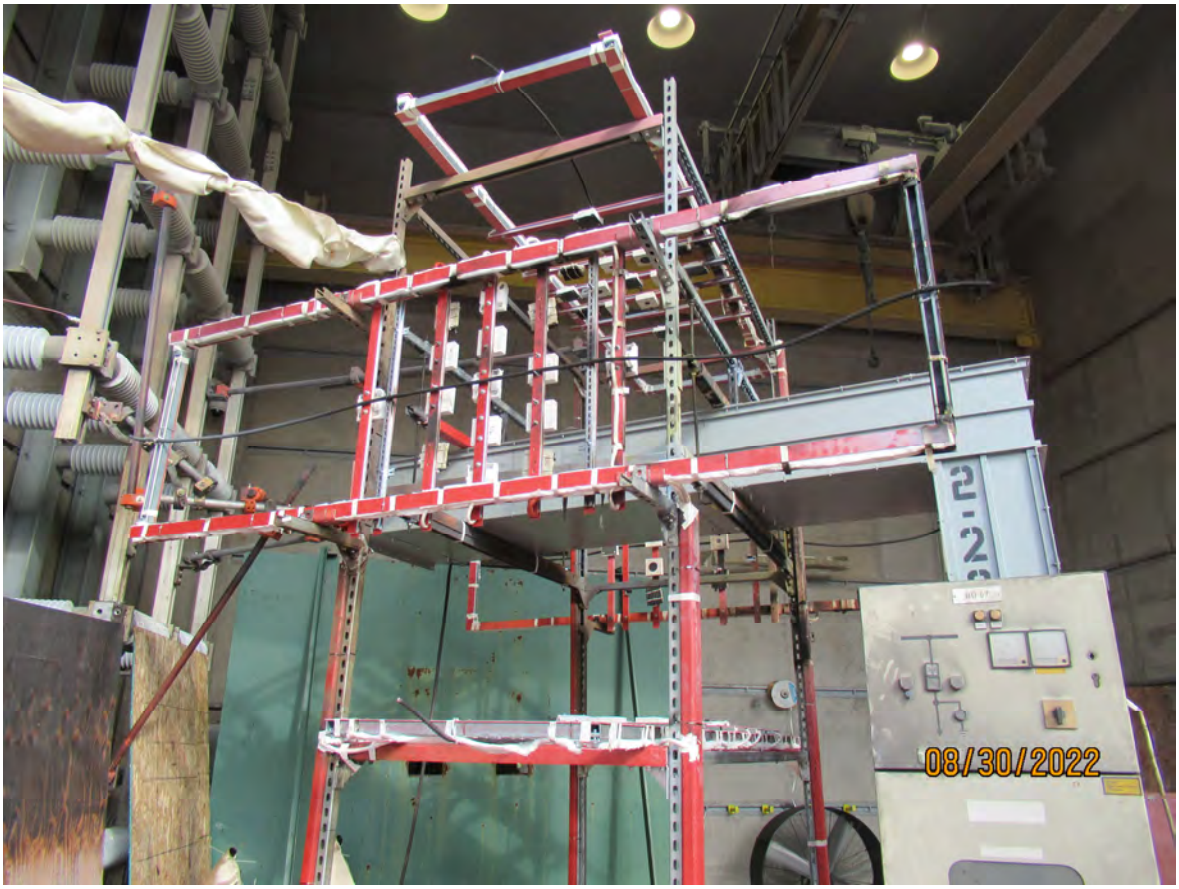
08/30/2022


08/30/2022


08/30/2022


08/30/2022


08/30/2022

## 12.4 Test results and oscillograms

**Overview of test numbers**
220830-9001

**Remarks**

| Calorimeter Slug # | Average Start Temp. | Initial Heat Capacity | Max. Temp. | Final Heat Capacity | Total Heat Energy |
|---|---|---|---|---|---|
| | °C | cal/(g°C) | °C | cal/(g°C) | J/( $cm^2$) |
| 1 | N/A | N/A | N/A | N/A | N/A |
| 2 | 30.81 | 0.092213 | 353.34 | 0.100334 | 186.166 |
| 3 | 34.45 | 0.092324 | 359.14 | 0.100439 | 187.627 |
| 4 | 34.51 | 0.092326 | 263.91 | 0.098570 | 131.276 |
| 5 | 32.32 | 0.092259 | 292.10 | 0.099160 | 149.071 |
| 6 | 31.54 | 0.092235 | 269.41 | 0.098688 | 136.143 |
| 7 | 34.71 | 0.092332 | 300.36 | 0.099327 | 152.630 |
| 8 | 34.31 | 0.092320 | 360.39 | 0.100462 | 188.449 |
| 9 | 30.55 | 0.092205 | 144.73 | 0.095630 | 64.296 |
| 10 | 30.24 | 0.092196 | 194.55 | 0.096953 | 93.168 |

PT#1: 2.87 psi above atmospheric
PT#2: 1.99 psi above atmospheric

**Arc Test: 30kA, 4s, CU Bus bars**

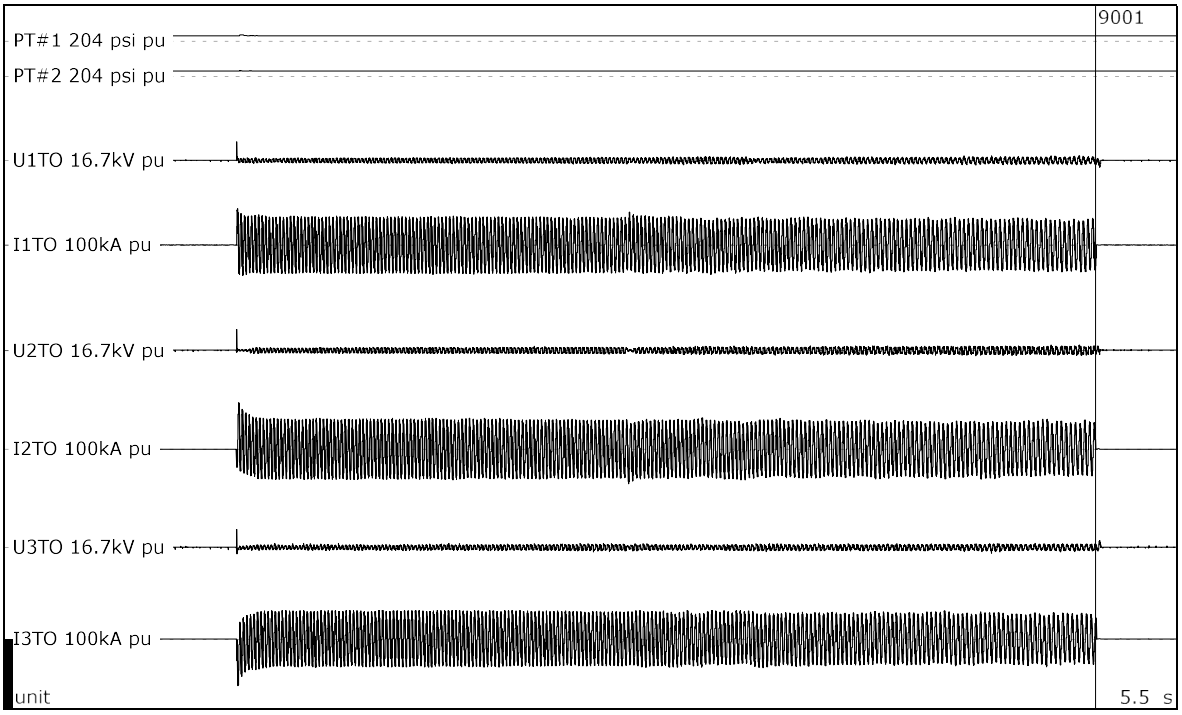


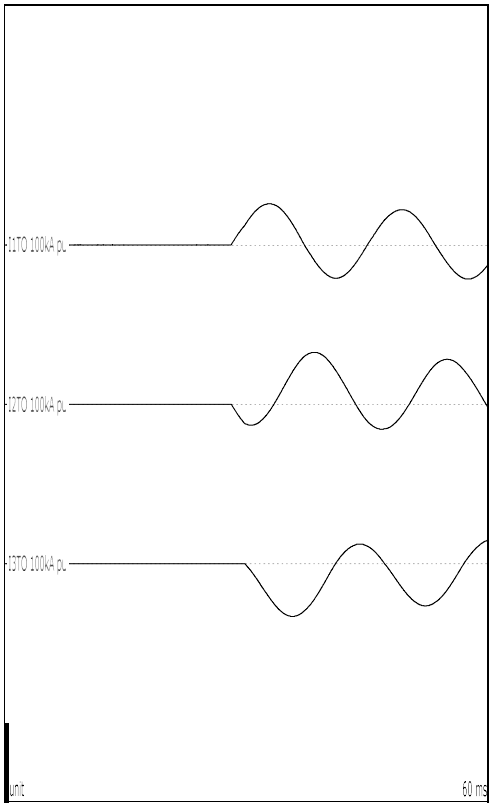


**Test number:** **220830-9001**

| Phase | | AØ | BØ | CØ |
|---|---|---|---|---|
| Applied voltage, phase-to-ground | $kV_{RMS}$ | 2.41 | 2.41 | 2.41 |
| Applied voltage, phase-to-phase | $kV_{RMS}$ | 4.17 | | |
| Making current | $kA_{peak}$ | 51.7 | 65.2 | -66.8 |
| Current, a.c. component, beginning | $kA_{RMS}$ | 31.9 | 33.3 | 29.8 |
| Current, a.c. component, middle | $kA_{RMS}$ | 27.6 | 29.3 | 27.4 |
| Current, a.c. component, end | $kA_{RMS}$ | 26.0 | 27.9 | 25.4 |
| Current, a.c. component, average | $kA_{RMS}$ | 28.1 | 29.7 | 27.5 |
| Current, a.c. component, three-phase average | $kA_{RMS}$ | 28.4 | | |
| Duration | s | 4.03 | 4.03 | 4.03 |
| Arc energy | MJ | 147 | | |
| Equivalent RMS value and duration | | 30.0 kA during 4.00 s | | |

Observations: Emission of flames and gas observed.

## 12.5 Condition / inspection after test

Heavy damage to the test device. Majority of bus duct enclosure has vaporized.

## 12.6 Photograph after test

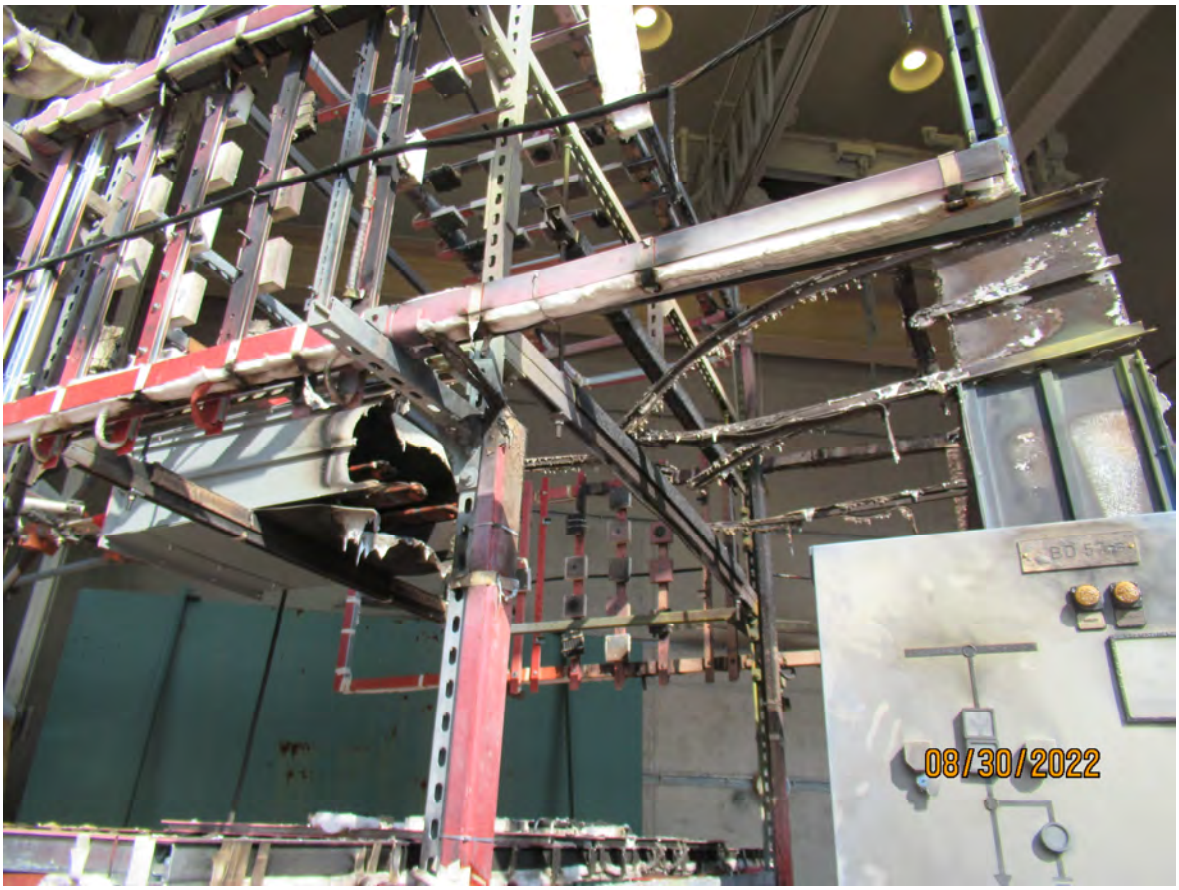

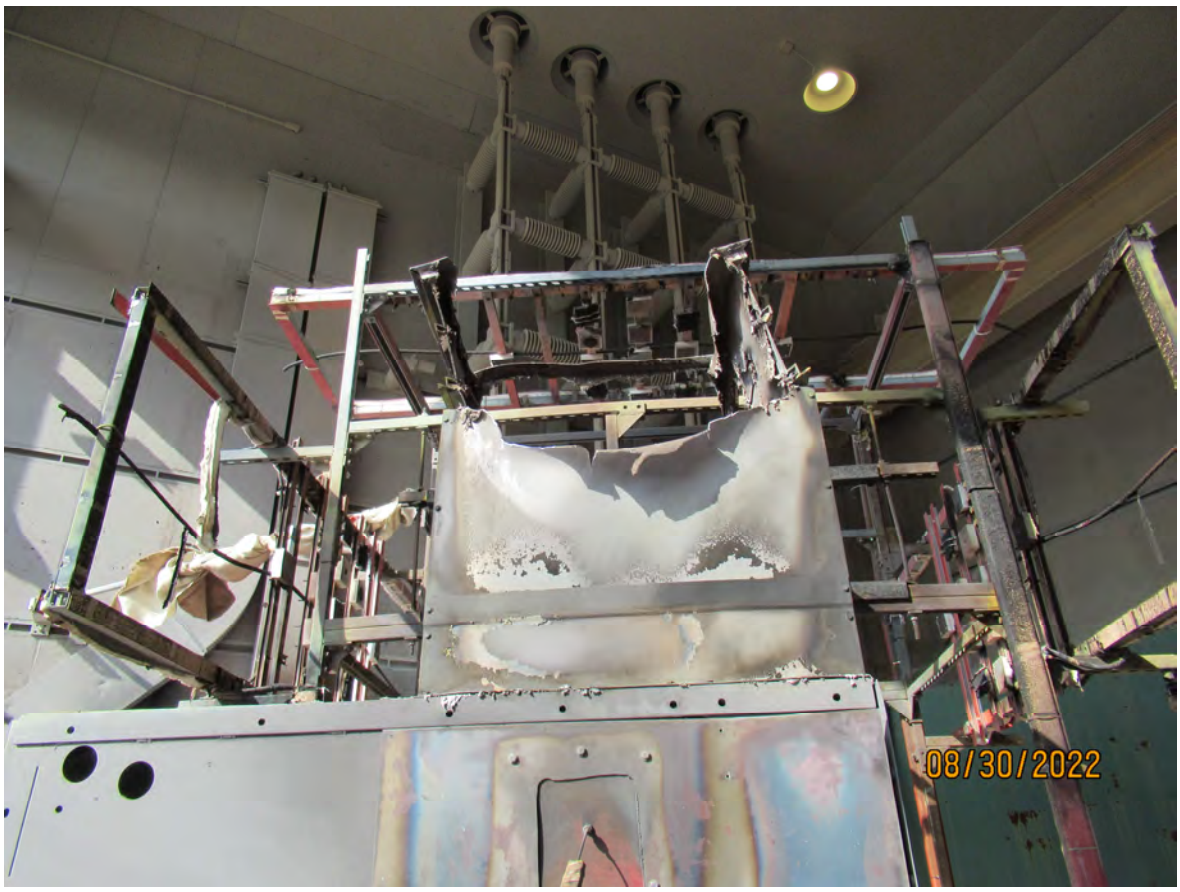
08/30/2022

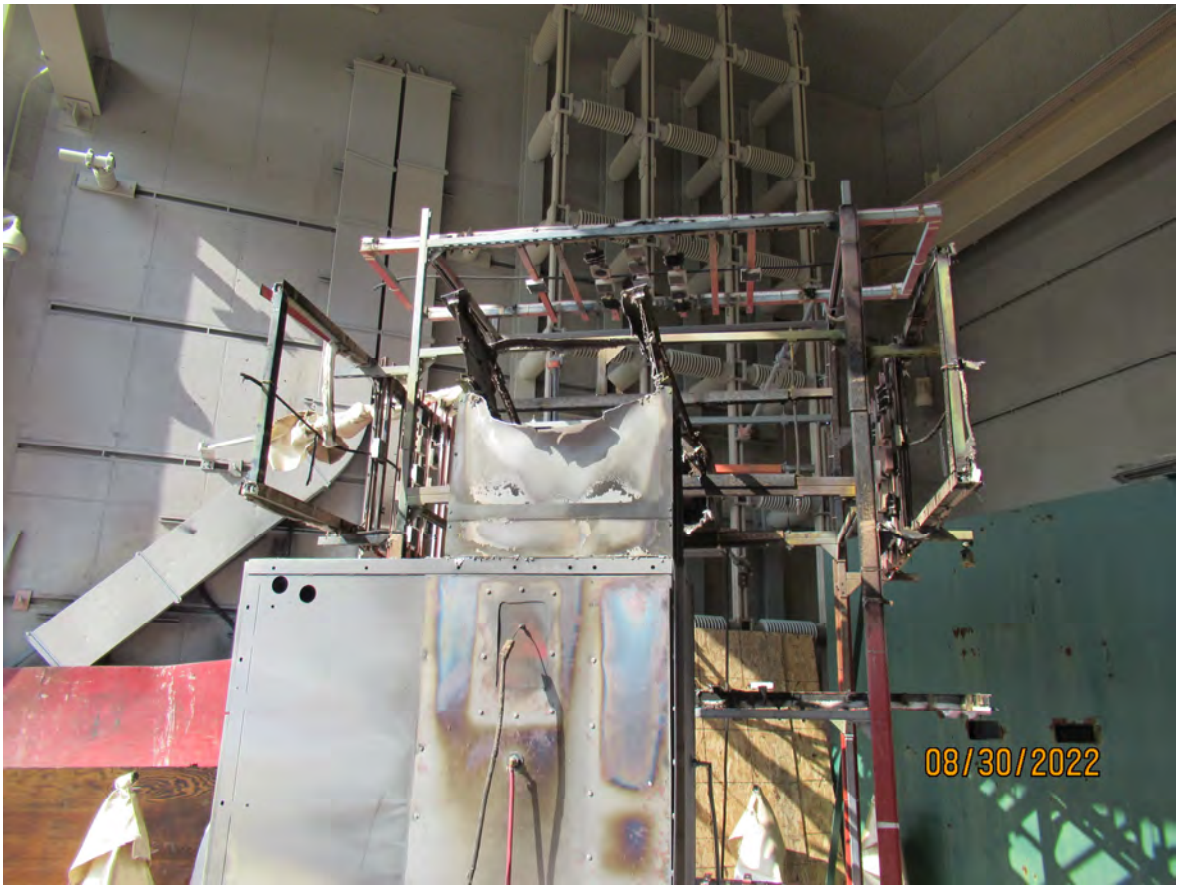
08/30/2022


08/30/2022


08/30/2022


08/30/2022

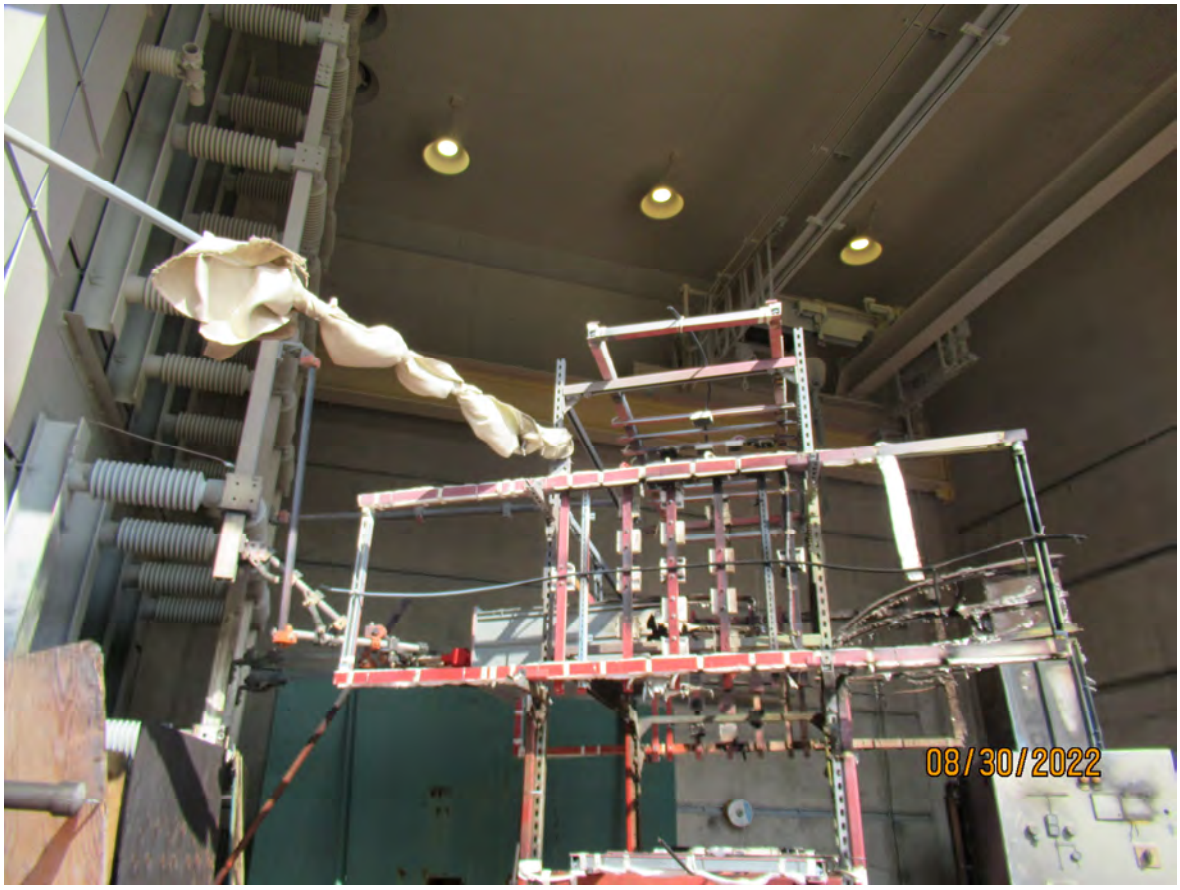
08/30/2022


08/30/2022


08/30/2022

# 13 ARC TEST: 30KA, 4S, AL BUS BARS

**Standard and date**

| | |
|---|---|
| Standard | Client's instructions |
| Test date | 31 August 2022 |

**Serial No.**
2-30B

## 13.1 Condition before test

Enclosure grounded.
Bus duct enclosure is steel.
Aluminum bus in the bus duct.
New bus duct attached to the source.
Switchgear same as previous test.
Arc to be initiated by #24 AWG wire located in the bus duct.
PT#1: 30PSI transducer on the right side of the switchgear.
PT#2: 30PSI transducer on the back side of the switchgear.

## 13.2 Test circuit S02

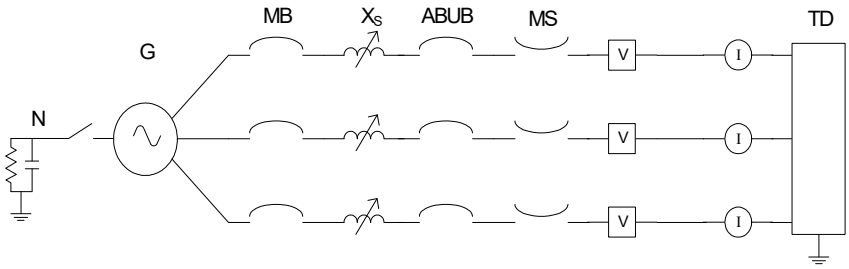


| | | | | | |
|---|---|---|---|---|---|
| G | = Generator | ABUB | = Aux. Breaker | R | = Resistance |
| N | = Neutral | XFMR | = Transformer | V | = Voltage Measurement |
| MB | = Main Breaker | TD | = Test Device | I | = Current Measurement |
| MS | = Make Switch | X | = Inductance | | |

| **Supply** | | |
|---|---|---|
| Power | MVA | 217 |
| Frequency | Hz | 60 |
| Phase(s) | | 3 |
| Voltage | kV | 4.174 |
| Current | kA | 30 |
| Impedance | Ω | 0.0803 |
| Power factor | | < 0.1 |
| Neutral | | not earthed |

Remarks: -

## 13.3 Photograph before test

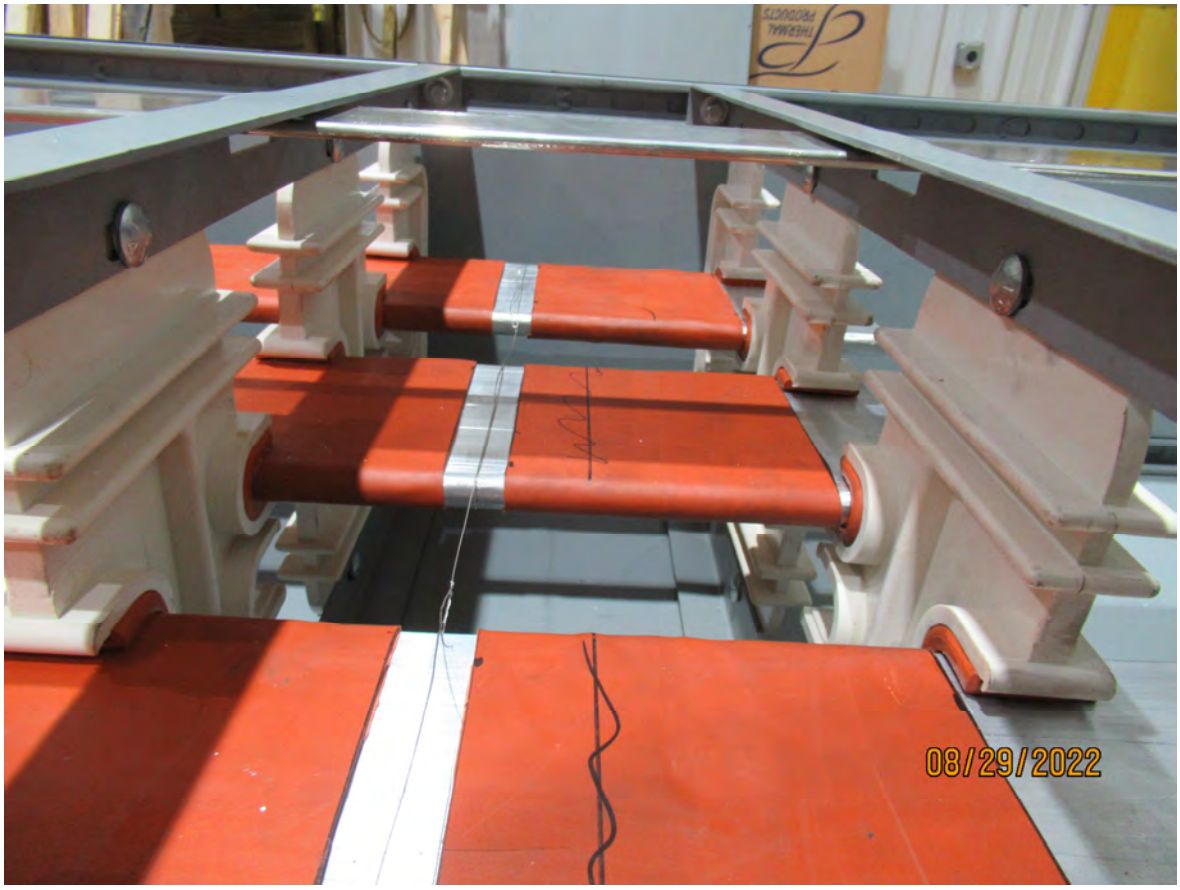
08/29/2022


08/31/2022


08/31/2022


2-30B
08/31/2022


2-30B
08/31/2022


08/31/2022


08/31/2022


08/31/2022


08/31/2022

## 13.4 Test results and oscillograms

**Overview of test numbers**
220831-9002

**Remarks**

| Calorimeter Slug # | Average Start Temp. | Initial Heat Capacity | Max. Temp. | Final Heat Capacity | Total Heat Energy |
|---|---|---|---|---|---|
| | °C | cal/(g°C) | °C | cal/(g°C) | J/( $cm^2$) |
| 1 | 32.82 | 0.092274 | 225.19 | 0.097698 | 109.555 |
| 2 | 32.97 | 0.092279 | 217.84 | 0.097524 | 105.191 |
| 3 | 31.95 | 0.092248 | 216.75 | 0.097498 | 105.115 |
| 4 | 32.02 | 0.092250 | 174.14 | 0.096427 | 80.383 |
| 5 | 33.99 | 0.092310 | 246.61 | 0.098190 | 121.424 |
| 6 | 34.00 | 0.092310 | 286.35 | 0.099043 | 144.759 |
| 7 | 49.23 | 0.092778 | 483.75 | 0.102569 | 254.459 |
| 8 | 39.87 | 0.092490 | 295.26 | 0.099224 | 146.778 |
| 9 | 49.84 | 0.092797 | 156.14 | 0.095945 | 60.143 |
| 10 | 36.25 | 0.092379 | 123.01 | 0.095012 | 48.739 |

PT#1: 3.47 psi above atmospheric
PT#2: 1.5 psi above atmospheric

**Arc Test: 30kA, 4s, Al Bus bars**

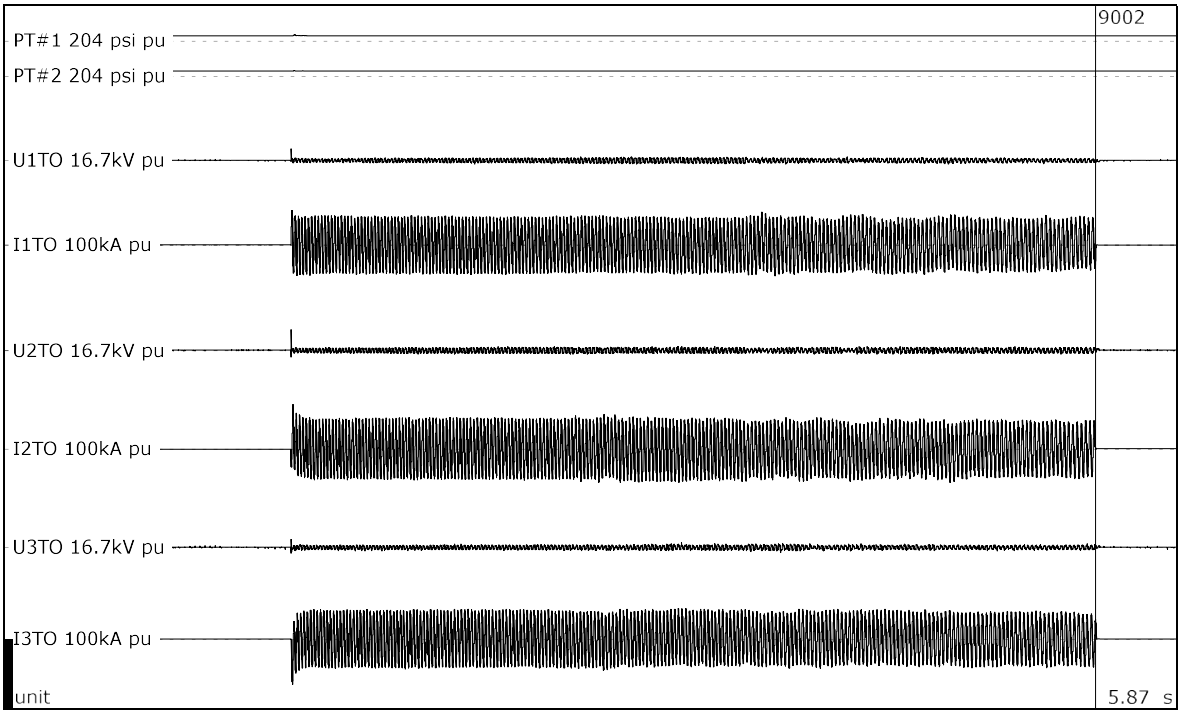


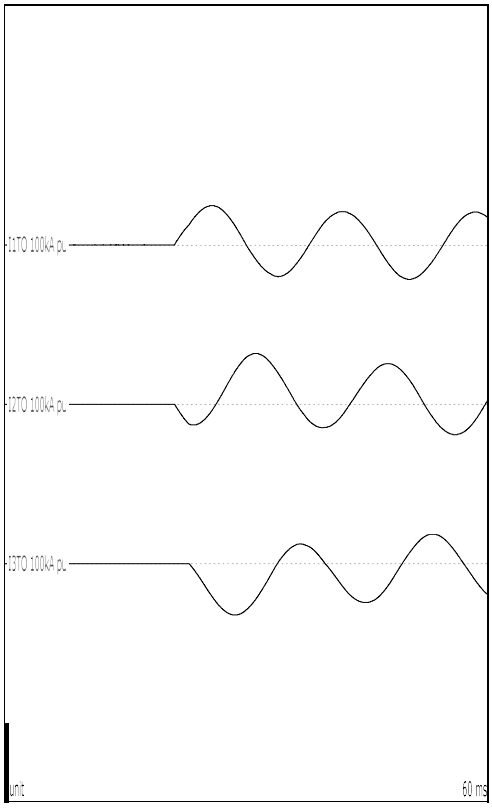


**Test number:** **220831-9002**

| Phase | | AØ | BØ | CØ |
|---|---|---|---|---|
| Applied voltage, phase-to-ground | $kV_{RMS}$ | 2.41 | 2.41 | 2.41 |
| Applied voltage, phase-to-phase | $kV_{RMS}$ | 4.17 | | |
| Making current | $kA_{peak}$ | 49.2 | 63.7 | -65.0 |
| Current, a.c. component, beginning | $kA_{RMS}$ | 30.3 | 32.4 | 28.9 |
| Current, a.c. component, middle | $kA_{RMS}$ | 27.3 | 30.9 | 27.6 |
| Current, a.c. component, end | $kA_{RMS}$ | 25.7 | 28.6 | 26.5 |
| Current, a.c. component, average | $kA_{RMS}$ | 28.4 | 30.0 | 27.9 |
| Current, a.c. component, three-phase average | $kA_{RMS}$ | 28.8 | | |
| Duration | s | 4.03 | 4.03 | 4.03 |
| Arc energy | MJ | 128 | | |
| Equivalent RMS value and duration | | 30.0 kA during 4.00 s | | |

Observations: Emission of flames and gas observed.

## 13.5 Condition / inspection after test

Heavy damage to the test device. Signs of arcing and burn through on each side of the bus duct.
After test, fire on the instrumentation racks and bus duct were put out.

## 13.6 Photograph after test

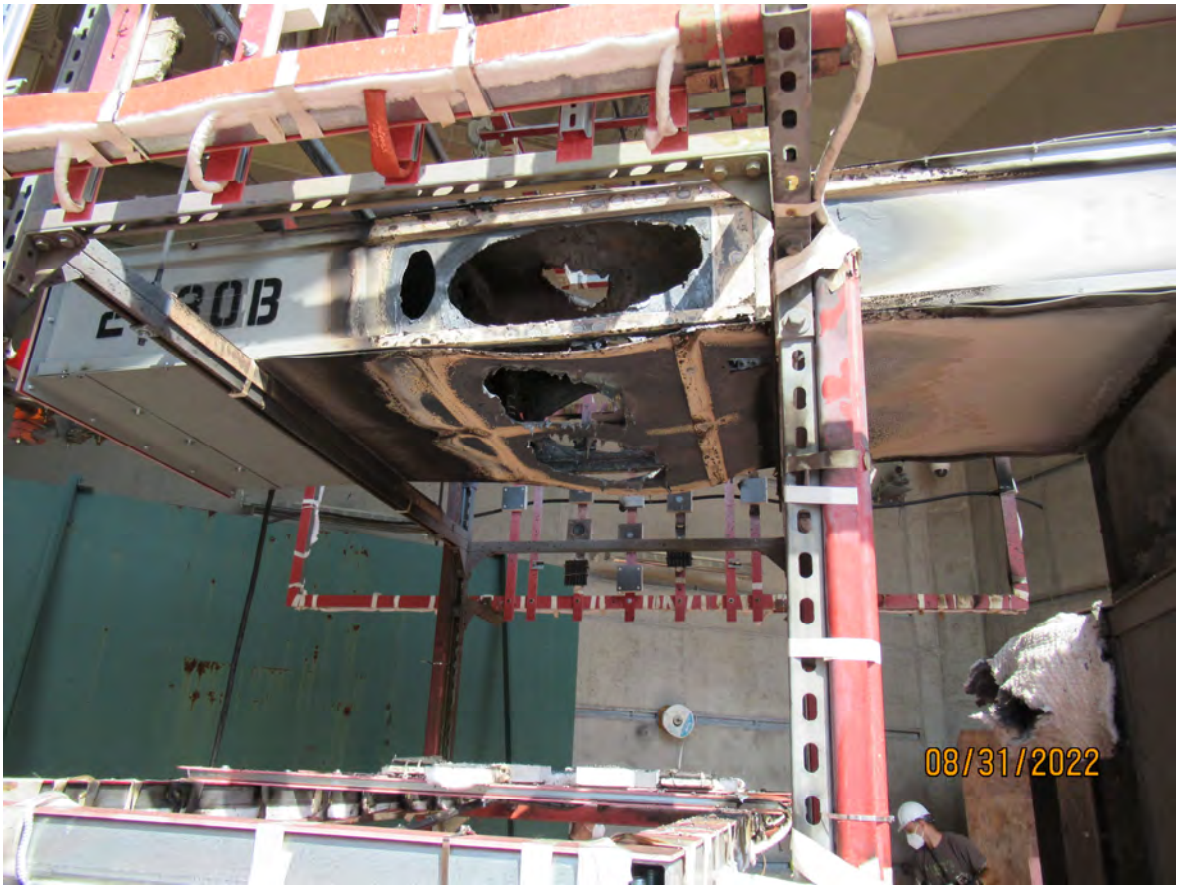
08/31/2022


08/31/2022


08/31/2022


08/31/2022

## 14 ARC TEST: 30KA, 2S, AL BUS BARS

**Standard and date**

| | |
|---|---|
| Standard | Client's instructions |
| Test date | 1 September 2022 |

**Serial No.**
2-31

### 14.1 Condition before test

Enclosure grounded.
Bus duct enclosure is aluminum.
Aluminum bus in the bus duct.
New bus duct attached to the source.
Switchgear same as previous test.
Arc to be initiated by #24 AWG wire located in the bus duct.
PT#1: 30PSI transducer on the right side of the switchgear.
PT#2: 30PSI transducer on the back side of the switchgear.
Calorimeter "6" not reading accurate values. Client requested to continue.

## 14.2 Test circuit S02

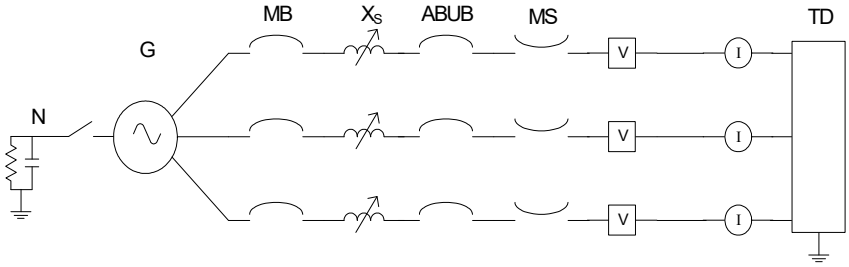


| | | | | | |
|---|---|---|---|---|---|
| G | = Generator | ABUB | = Aux. Breaker | R | = Resistance |
| N | = Neutral | XFMR | = Transformer | V | = Voltage Measurement |
| MB | = Main Breaker | TD | = Test Device | I | = Current Measurement |
| MS | = Make Switch | X | = Inductance | | |

| **Supply** | | |
|---|---|---|
| Power | MVA | 217 |
| Frequency | Hz | 60 |
| Phase(s) | | 3 |
| Voltage | kV | 4.174 |
| Current | kA | 30 |
| Impedance | Ω | 0.0803 |
| Power factor | | < 0.1 |
| Neutral | | not earthed |

Remarks: -

## 14.3 Photograph before test

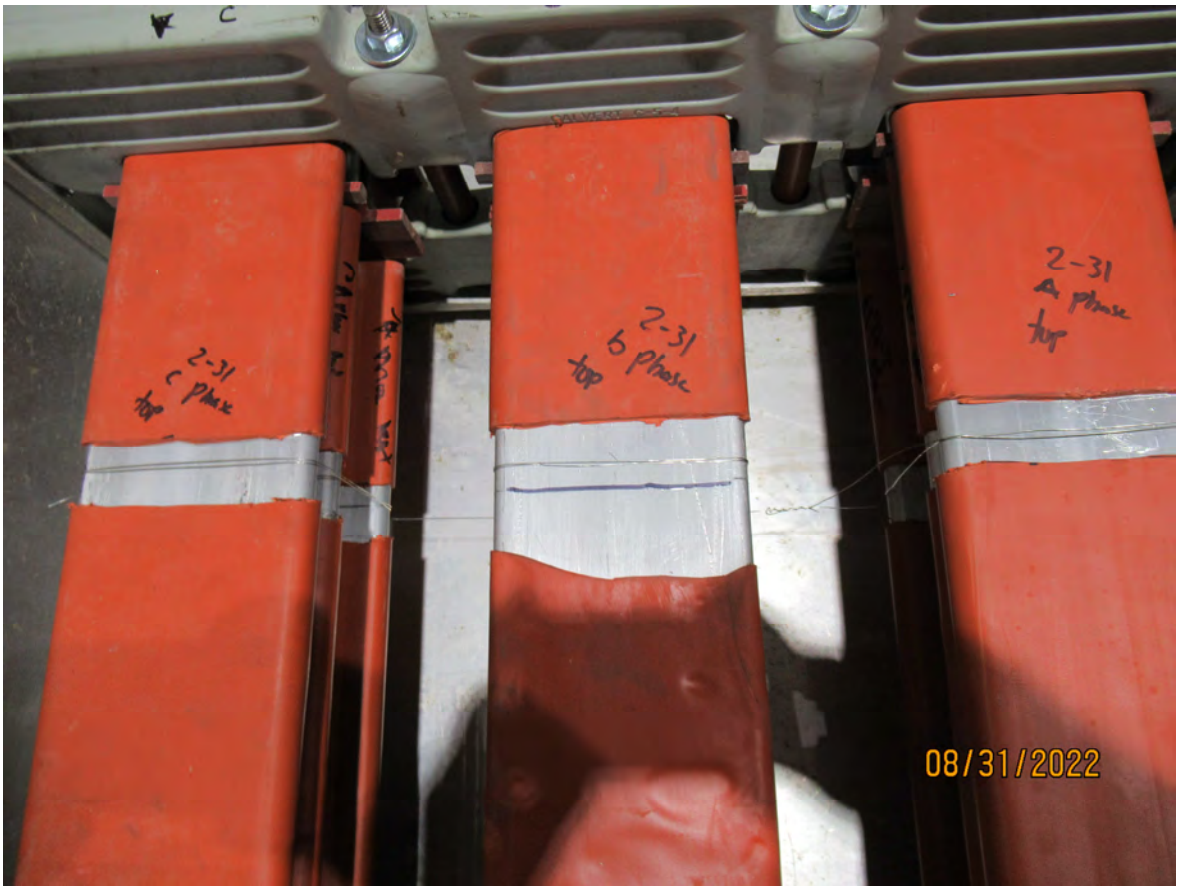


09/01/2022


09/01/2022


09/01/2022

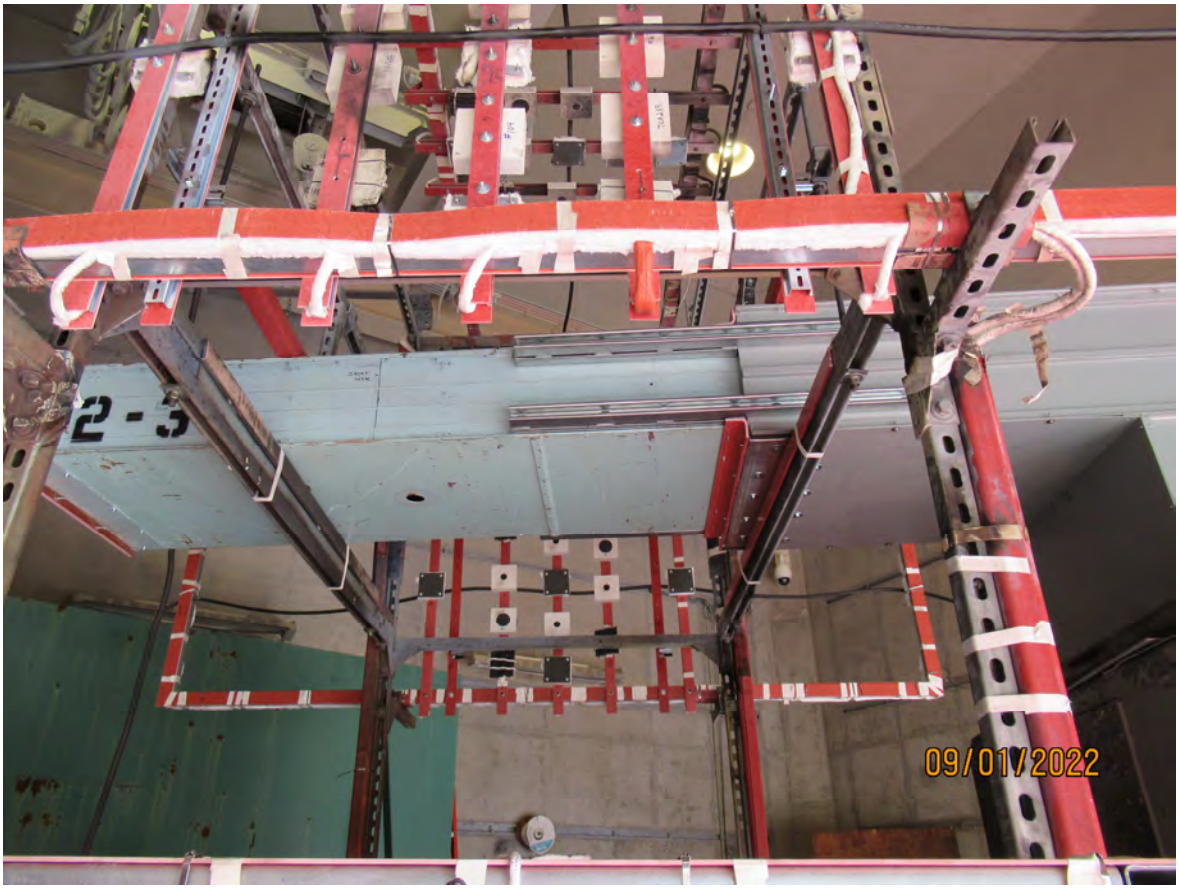
2 - 3
09/01/2022

## 14.4 Test results and oscillograms

**Overview of test numbers**
220901-9001

**Remarks**

| Calorimeter Slug # | Average Start Temp. | Initial Heat Capacity | Max. Temp. | Final Heat Capacity | Total Heat Energy |
|---|---|---|---|---|---|
| | °C | cal/(g°C) | °C | cal/(g°C) | J/( $cm^2$) |
| 1 | 31.07 | 0.092221 | 290.20 | 0.099122 | 148.638 |
| 2 | 31.43 | 0.092232 | 225.86 | 0.097714 | 110.708 |
| 3 | 34.59 | 0.092328 | 228.66 | 0.097780 | 110.599 |
| 4 | 36.56 | 0.092389 | 195.06 | 0.096966 | 89.972 |
| 5 | 37.60 | 0.092420 | 223.04 | 0.097648 | 105.661 |
| 6 | 17.27 | 0.091806 | -129.04 | 0.092053 | -80.643 |
| 7 | 43.50 | 0.092602 | 278.12 | 0.098872 | 134.669 |
| 8 | 42.85 | 0.092582 | 249.77 | 0.098260 | 118.378 |
| 9 | 29.42 | 0.092171 | 91.55 | 0.094079 | 34.692 |
| 10 | 29.44 | 0.092171 | 197.82 | 0.097035 | 95.509 |

PT#1: 3.37 psi above atmospheric
PT#2: 2.25 psi above atmospheric

**Arc Test: 30kA, 2s, Al Bus bars**

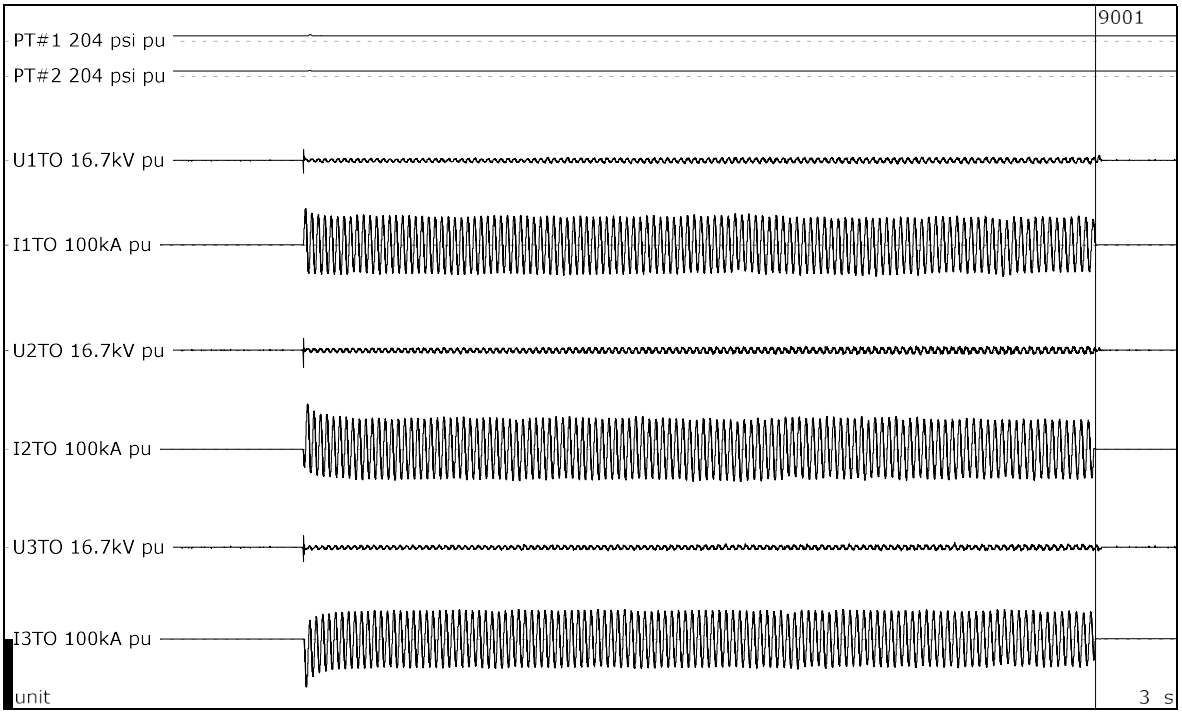


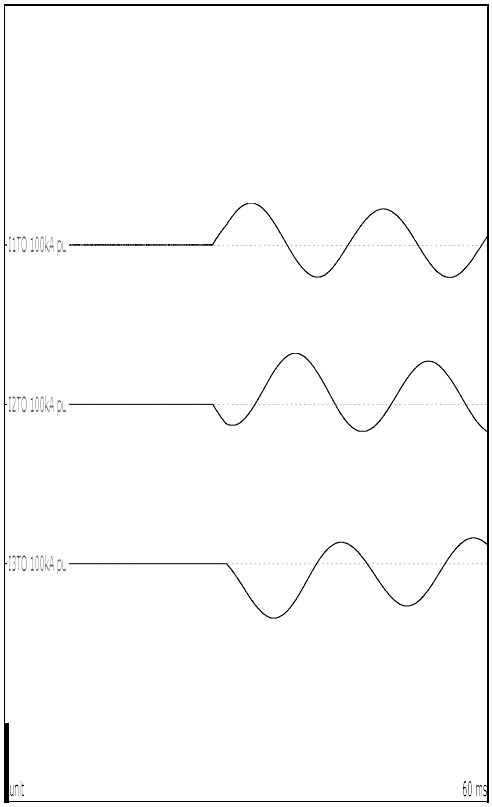


**Test number:** **220901-9001**

| Phase | | AØ | BØ | CØ |
|---|---|---|---|---|
| Applied voltage, phase-to-ground | $kV_{RMS}$ | 2.41 | 2.41 | 2.41 |
| Applied voltage, phase-to-phase | $kV_{RMS}$ | 4.17 | | |
| Making current | $kA_{peak}$ | 52.6 | 64.1 | -68.9 |
| Current, a.c. component, beginning | $kA_{RMS}$ | 31.7 | 33.5 | 31.1 |
| Current, a.c. component, middle | $kA_{RMS}$ | 28.8 | 31.2 | 28.8 |
| Current, a.c. component, end | $kA_{RMS}$ | 28.0 | 30.0 | 27.8 |
| Current, a.c. component, average | $kA_{RMS}$ | 29.2 | 31.1 | 29.0 |
| Current, a.c. component, three-phase average | $kA_{RMS}$ | 29.7 | | |
| Duration | s | 2.03 | 2.03 | 2.02 |
| Arc energy | MJ | 62.8 | | |
| Equivalent RMS value and duration | | 30.0 kA during 2.00 s | | |

Observations: Emission of flames and gas observed.

## 14.5 Condition / inspection after test

Heavy damage to the test device. Majority of bus duct enclosure has vaporized.

## 14.6 Photograph after test

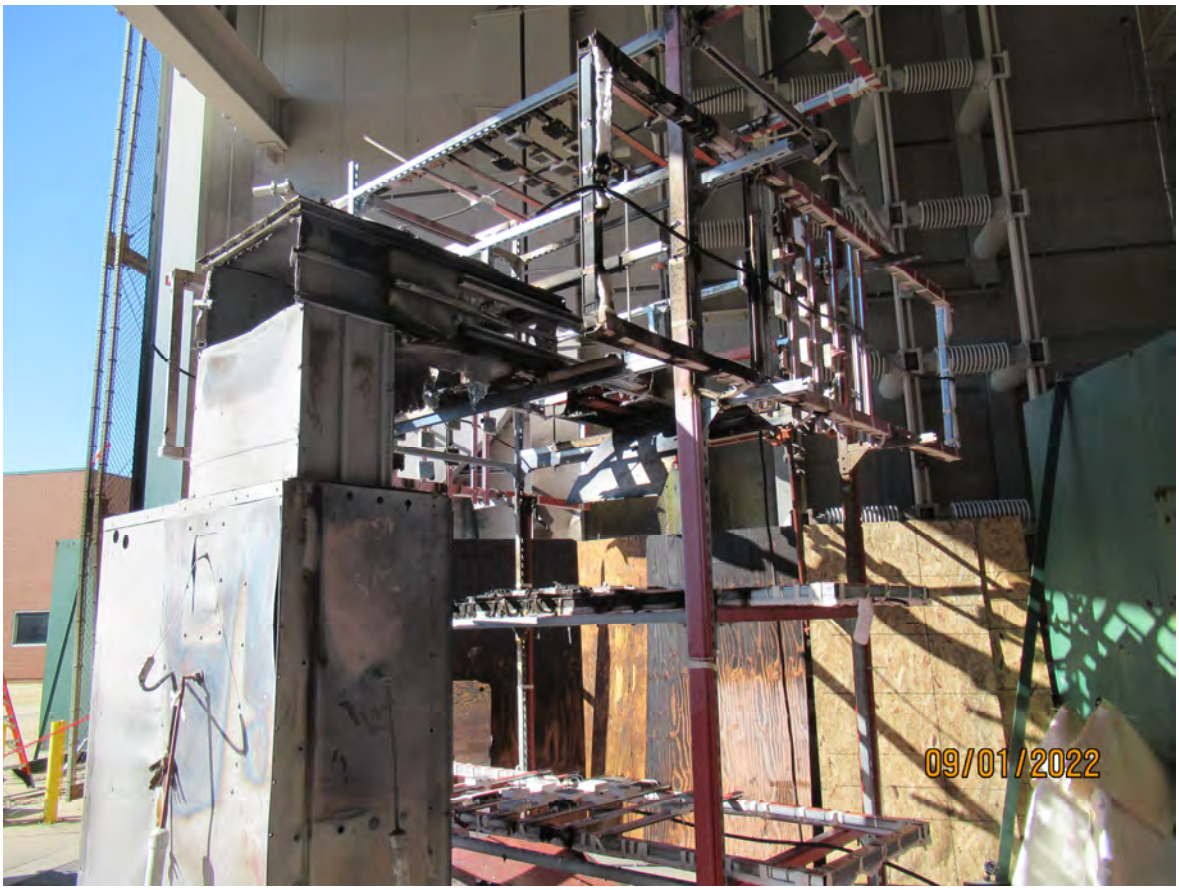


09/01/2022


09/01/2022


09/01/2022


09/01/2022


09/01/2022


09/01/2022

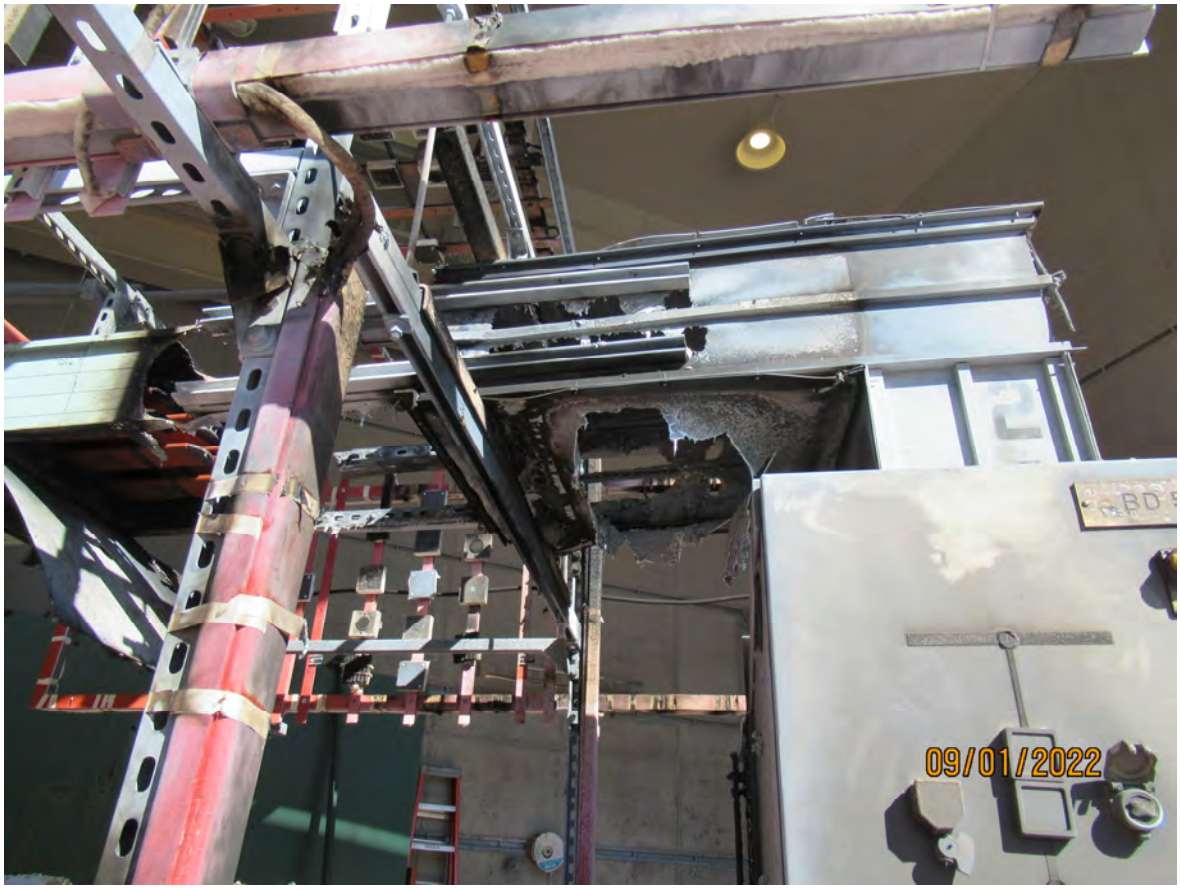
09/01/2022

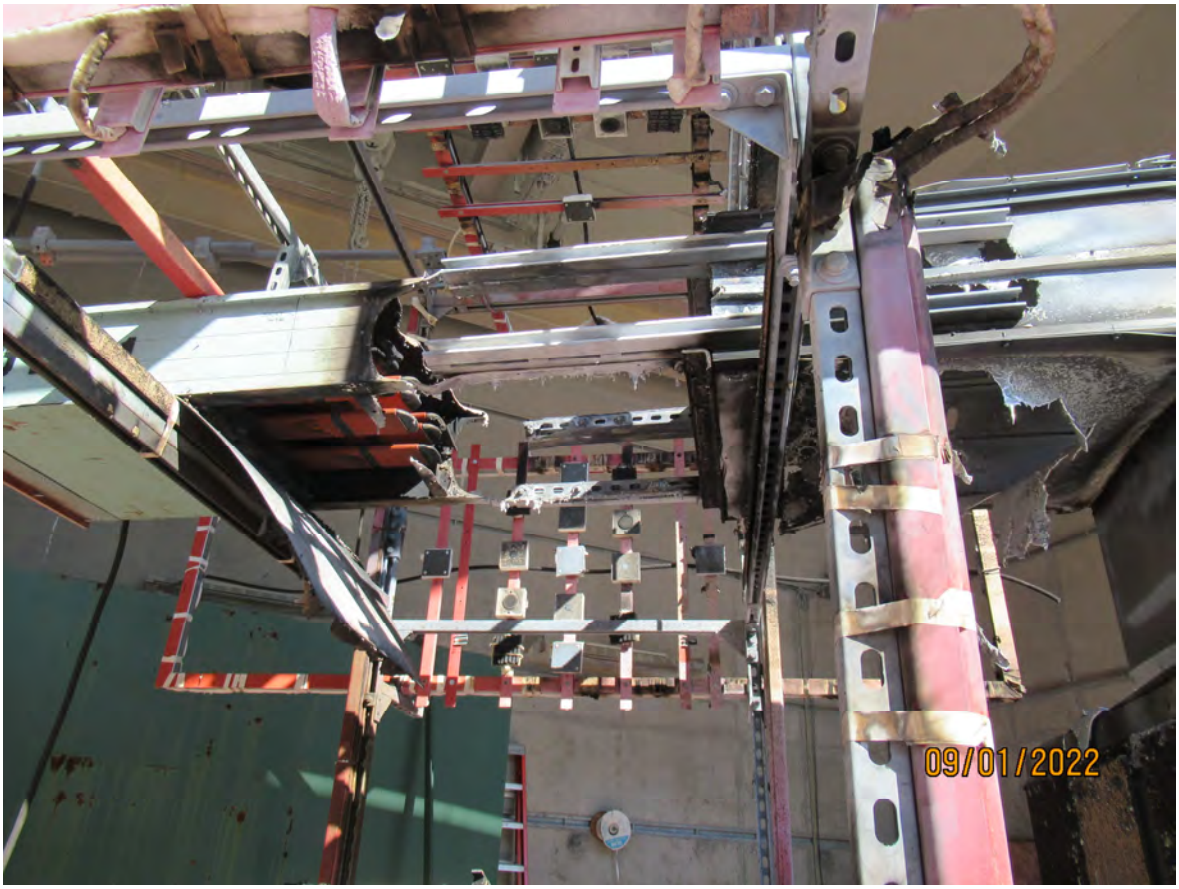
09/01/2022


09/01/2022

# 15 ARC TEST: 30KA, 4S, AL BUS BARS

**Standard and date**

| | |
|---|---|
| Standard | Client's instructions |
| Test date | 1 September 2022 |

**Serial No.**
2-32

## 15.1 Condition before test

Enclosure grounded.
Bus duct enclosure is aluminum.
Aluminum bus in the bus duct.
New bus duct attached to the source.
Switchgear same as previous test.
Arc to be initiated by #24 AWG wire located in the bus duct.
PT#1: 30PSI transducer on the right side of the switchgear.
PT#2: 30PSI transducer on the back side of the switchgear.

## 15.2 Test circuit S02

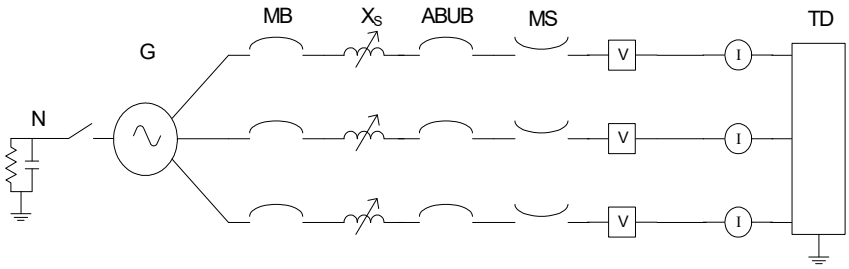


| | | | | | |
|---|---|---|---|---|---|
| G | = Generator | ABUB | = Aux. Breaker | R | = Resistance |
| N | = Neutral | XFMR | = Transformer | V | = Voltage Measurement |
| MB | = Main Breaker | TD | = Test Device | I | = Current Measurement |
| MS | = Make Switch | X | = Inductance | | |

| **Supply** | | |
|---|---|---|
| Power | MVA | 217 |
| Frequency | Hz | 60 |
| Phase(s) | | 3 |
| Voltage | kV | 4.174 |
| Current | kA | 30 |
| Impedance | Ω | 0.0803 |
| Power factor | | < 0.1 |
| Neutral | | not earthed |

Remarks: -

## 15.3 Photograph before test


C Top
2-32
B Top
2-32
A Top
2-32
09/01/2022


09/01/2022


09/01/2022


2-32
09/01/2022


2-32
09/01/2022


09/01/2022


09/01/2022


09/01/2022

## 15.4 Test results and oscillograms

**Overview of test numbers**
220901-9002

**Remarks**

| Calorimeter Slug # | Average Start Temp. | Initial Heat Capacity | Max. Temp. | Final Heat Capacity | Total Heat Energy |
|---|---|---|---|---|---|
| | °C | cal/(g°C) | °C | cal/(g°C) | J/( $cm^2$) |
| 1 | 31.94 | 0.092247 | 628.92 | 0.105256 | 353.450 |
| 2 | 31.75 | 0.092241 | 484.44 | 0.102581 | 264.387 |
| 3 | 31.42 | 0.092232 | 488.95 | 0.102657 | 267.299 |
| 4 | 31.55 | 0.092235 | 306.92 | 0.099457 | 158.241 |
| 5 | 31.99 | 0.092249 | 515.80 | 0.103116 | 283.348 |
| 6 | 32.45 | 0.092263 | 495.13 | 0.102762 | 270.501 |
| 7 | 31.20 | 0.092225 | 627.47 | 0.105225 | 352.934 |
| 8 | 30.97 | 0.092218 | 609.99 | 0.104864 | 342.088 |
| 9 | 30.91 | 0.092216 | 211.66 | 0.097375 | 102.725 |
| 10 | 30.52 | 0.092204 | 202.01 | 0.097139 | 97.335 |

PT#1: 3.76 psi above atmospheric
PT#2: 2.47 psi above atmospheric

**Arc Test: 30kA, 4s, Al Bus bars**

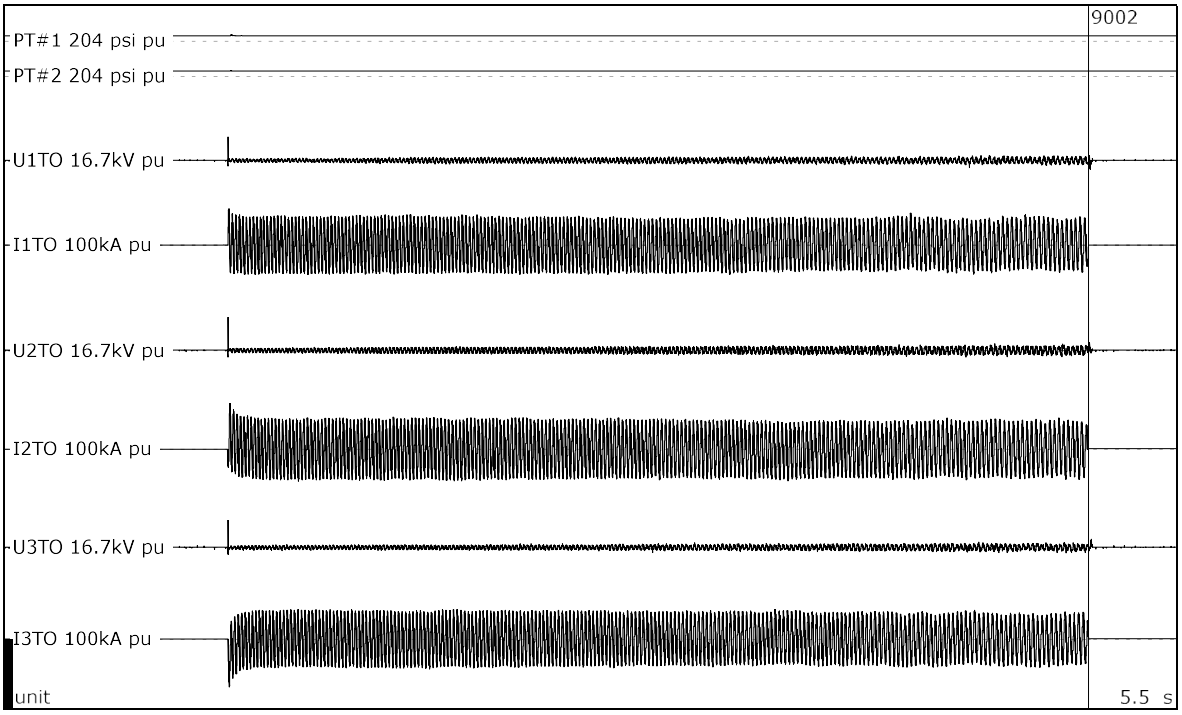


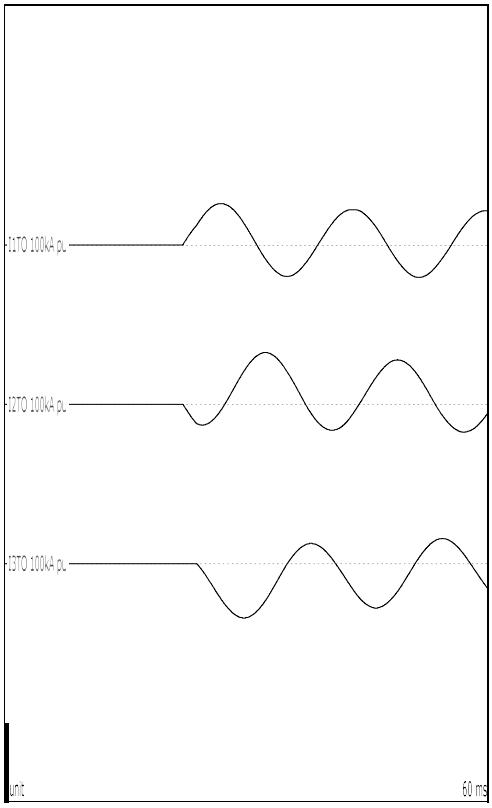


**Test number:** **220901-9002**

| Phase | | AØ | BØ | CØ |
|---|---|---|---|---|
| Applied voltage, phase-to-ground | $kV_{RMS}$ | 2.41 | 2.41 | 2.41 |
| Applied voltage, phase-to-phase | $kV_{RMS}$ | 4.17 | | |
| Making current | $kA_{peak}$ | 52.0 | 64.9 | -68.5 |
| Current, a.c. component, beginning | $kA_{RMS}$ | 31.2 | 33.4 | 30.9 |
| Current, a.c. component, middle | $kA_{RMS}$ | 27.4 | 30.1 | 27.2 |
| Current, a.c. component, end | $kA_{RMS}$ | 26.7 | 28.4 | 26.3 |
| Current, a.c. component, average | $kA_{RMS}$ | 28.1 | 30.0 | 28.1 |
| Current, a.c. component, three-phase average | $kA_{RMS}$ | 28.7 | | |
| Duration | s | 4.04 | 4.04 | 4.04 |
| Arc energy | MJ | 136 | | |
| Equivalent RMS value and duration | | 30.0 kA during 4.00 s | | |

Observations: Emission of flames and gas observed.

## 15.5 Condition / inspection after test

Heavy damage to the test device. Majority of bus duct enclosure has vaporized.

## 15.6 Photograph after test


32
09/01/2022


09/01/2022


09/01/2022


3
09/01/2022

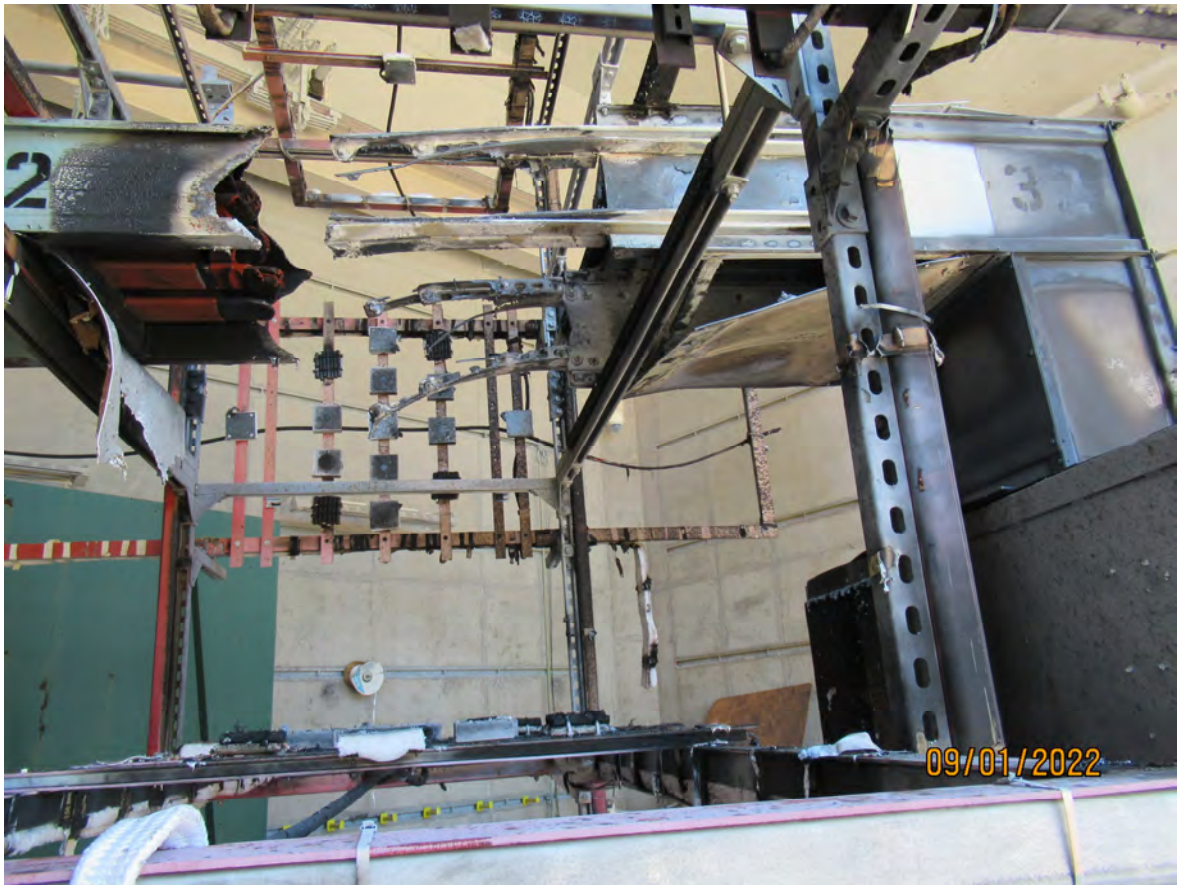
2
3
09/01/2022


09/01/2022


09/01/2022


09/01/2022


09/01/2022


09/01/2022


09/01/2022

## 16 INSTRUMENTATION INFORMATION SHEET

| CODE# | TYPE | MANUFACTURER | MODEL# | SERIAL# | CALIBRATION LAST | CALIBRATION DUE |
|---|---|---|---|---|---|---|
| DAS17 | DAS | NI/DEWETRON | DEWE-30-16 | 0195BB69 | 5/20/2022 | 12/6/2022 |
| PAV37 | PNL.VOLTMTR | SIMPSON | F45-1-34 | N/A | 2/23/2022 | 9/11/2022 |
| ISO108 | ISO AMP | DEWETRON | HIS-LV | 437702 | 5/20/2022 | 12/6/2022 |
| ISO109 | ISO AMP | DEWETRON | HIS-LV | 437703 | 5/20/2022 | 12/6/2022 |
| ISO110 | ISO AMP | DEWETRON | HIS-LV | 437704 | 5/20/2022 | 12/6/2022 |
| ISO111 | ISO AMP | DEWETRON | HIS-LV | 437705 | 5/20/2022 | 12/6/2022 |
| KPT103 | PRESS.TRANS | OMEGA | PX329 | 121317I013 | 8/5/2022 | 2/21/2023 |
| KPT111 | PRESS.TRANS | OMEGA | PX329 | 082216I08 | 8/5/2022 | 2/21/2023 |
| KPT104 | PRESS.TRANS | OMEGA | PX329 | 030318I127 | 8/5/2022 | 2/21/2023 |
| KPT117 | PRESS.TRANS | OMEGA | PX329 | 040218I028 | 5/16/2022 | 12/2/2022 |
| AMP41 | FO ISO AMP | AAA LAB SYST | AFL-300 | 1 | 3/25/2022 | 10/11/2022 |
| AMP42 | FO ISO AMP | AAA LAB SYST | AFL-300 | 2 | 3/25/2022 | 10/11/2022 |
| AMP43 | FO ISO AMP | AAA LAB SYST | AFL-300 | 3 | 3/25/2022 | 10/11/2022 |
| AMP44 | FO ISO AMP | AAA LAB SYST | AFL-300 | 4 | 3/25/2022 | 10/11/2022 |
| ISO132 | ISO AMP | DEWETRON | HIS-LV | 437726 | 5/20/2022 | 12/6/2022 |
| ISO117 | ISO AMP | DEWETRON | HIS-LV | 437711 | 5/20/2022 | 12/6/2022 |
| ISO118 | ISO AMP | DEWETRON | HIS-LV | 437712 | 5/20/2022 | 12/6/2022 |
| ISO124 | ISO AMP | DEWETRON | HIS-LV | 437718 | 5/20/2022 | 12/6/2022 |
| ISO125 | ISO AMP | DEWETRON | HIS-LV | 437719 | 5/20/2022 | 12/6/2022 |
| ISO126 | ISO AMP | DEWETRON | HIS-LV | 437720 | 5/20/2022 | 12/6/2022 |
| ISO136 | ISO AMP | DEWETRON | HIS-LV | 437730 | 5/20/2022 | 12/6/2022 |
| ISO137 | ISO AMP | DEWETRON | HIS-LV | 437731 | 5/20/2022 | 12/6/2022 |
| ISO138 | ISO AMP | DEWETRON | HIS-LV | 437732 | 5/20/2022 | 12/6/2022 |
| CTX172 | ROGOWSKI CT | PEM | SDS0680 | 0002-0100A | 5/20/2022 | 12/6/2022 |
| CTX173 | ROGOWSKI CT | PEM | SDS0680 | 0002-0100B | 5/20/2022 | 12/6/2022 |
| CTX174 | ROGOWSKI CT | PEM | SDS0680 | 0002-0100C | 5/20/2022 | 12/6/2022 |
| VDR84 | V.DIVIDER | NORTH STAR | VD-150 | 1 | 8/17/2022 | 3/5/2023 |
| VDR86 | V.DIVIDER | NORTH STAR | VD-150 | 3 | 8/17/2022 | 3/5/2023 |
| VDR88 | V.DIVIDER | NORTH STAR | VD-150 | 5 | 8/17/2022 | 3/5/2023 |
| PTX06 | P.T. | GE | JVM5 | 3737435 | 9/30/2020 | 9/30/2022 |
| PTX07 | P.T. | GE | JVM5 | 3737433 | 9/30/2020 | 9/30/2022 |
| PTX08 | P.T. | GE | JVM5 | 3737432 | 9/30/2020 | 9/30/2022 |
| VTD10 | VOLT.TRANSD | LEM | CV3-200 | 1141194044549 | 2/2022 | 3/21/2023 |
| VTD11 | VOLT.TRANSD | LEM | CV3-200 | 1141194044569 | 2/2022 | 3/21/2023 |
| VTD12 | VOLT.TRANSD | LEM | CV3-200 | 1141194044579 | 2/2022 | 3/21/2023 |
| TEM89 | TEMP.LOGGER | DEWESoft | KRYPTONi | D05980d869 | 8/18/2022 | 3/6/2023 |
| TEM91 | TEMP.LOGGER | DEWESoft | KRYPTONi | D05980F2EA | 8/18/2022 | 3/6/2023 |

## 17 ATTACHMENTS

The attached procedure was written by and has been included in the report at the behest of the client. KEMA Labs has not verified the attached procedure's compliance with any recognized testing standard. Interpretation of the data presented within this test report against the requirements of the attached procedure, or a recognized testing standard is the responsibility of the reader. KEMA MAKES NO REPRESENTATIONS OR WARRANTIES REGARDING THE ACCURACY OF THE PROCEDURE OR THAT THE PROCEDURE MEETS ANY APPLICABLE INDUSTRY STANDARDS OR LEGAL OR REGULATORY REQUIREMENTS.

1. HEAF_Test_Plan OECDNEA 2022 r1 [33 pages]

## OECD HEAF PHASE II TESTING – Rev 1 Changes

- Test Matrix change- Test 2-26 (Copper Bus/Steel Enclosure) will be assigned priority over test 2-31 (Aluminum Bus/Aluminum Enclosure)
    - This will assign priority to the copper bus ducts which were discussed to be of a greater interest to the international members to align with component population

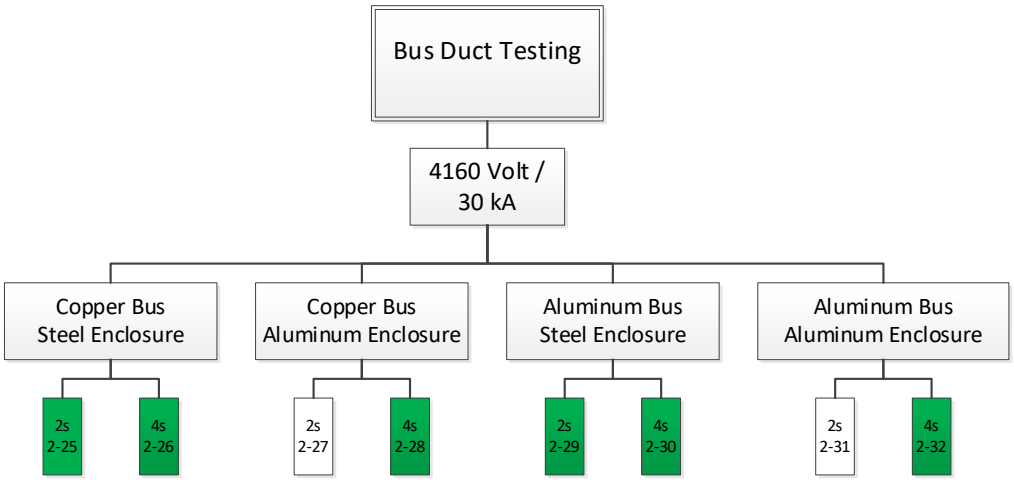

# OECD HEAF Phase II Testing
# August 2022 Campaign

Prepared by
Nicholas Melly, Gabriel Taylor, Kenneth Hamburger

US Nuclear Regulatory Commission
Office of Nuclear Regulatory Research
Washington, DC 20555-0001

July 2022

Prepared for:
U.S. Nuclear Regulatory Commission (NRC), Office of Nuclear Reactor Regulation (NRR)
OECD/NEA HEAF Phase II Management Board & Members

# TABLE OF CONTENTS

# LIST OF FIGURES

# LIST OF TABLES

# OVERVIEW OF EXPERIMENTAL PLAN

This experimental plan covers high energy arcing fault (HEAF) experiments to be conducted by the U.S. Nuclear Regulatory Commission (NRC) Office of Nuclear Regulatory Research (RES) as the operating agent for the Nuclear Energy Agency (NEA) High Energy Arcing Fault Events (HEAF) Phase 2 Project. These experiments will be performed at the CESI (KEMA Labs) facility in Chalfont, PA USA. The experiments are designed to collect data and information to evaluate the performance of models developed to estimate the electrical HEAF hazard. These confirmatory experiments will include six medium-voltage electrical non-segregated bus ducts and two medium-voltage electrical switchgear enclosures. The selection of this equipment is focused to address gaps in existing data used to develop HEAF hazard models. Namely, the lack of instrumented bus duct experiments, and switchgear experiments with copper bus bars that complement testing performed in 2018 [1]. These experiments will quantitatively characterize the thermal conditions, pressure conditions, and byproduct deposits on surfaces created by HEAFs. The results and measurements techniques from this investigation will be used as sources of model validation for a computational fluid dynamic model known as Fire Dynamics Simulator [2] and a modified arc flash model [3]. Presuming that the model validation is reasonable, the models will be used in conjunction with fire PRA target fragility criteria to predict HEAF zones of influence (ZOI) to assess the adequacy of existing HEAF ZOIs in NUREG/CR-6850 Chapter M and draft ZOI developed by a joint working group sponsored by the NRC-RES and the Electric Power Research Institute. The experimental setup is developed based on prior work by NRC and OECD partners. This experimental campaign will focus on two main areas of interest; medium-voltage non-segregated bus ducts and medium-voltage electrical switchgear enclosures.

The experimental campaign will take place in August of 2022 with two full testing weeks August 22$^{nd}$- 26$^{th}$ and August 29$^{th}$ – September 2$^{nd}$. The week of August 15$^{th}$ – 19$^{th}$ will be for instrumentation assembly and preparation. The final tear down of equipment used will take place the week of September 6$^{th}$ – 9$^{th}$.

The scope of this Investigation is to:

- Provide measurement and information of HEAF experiment evolution to support subsequent research efforts (model validation and zone of influence development).
- Explore how the different parameters (e.g. current, material properties, duration, equipment configuration, etc.) impact HEAF phenomena and zone of influence.

# ACRONYMS AND ABBREVIATIONS

| | |
|---|---|
| AC | alternating current |
| ACD | Advanced Components Development |
| AWG | American wire gage |
| CPT | control power transformer |
| CVT | current-voltage transformer |
| DC | direct current |
| DP | distribution panel |
| EMI | electromagnetic interference |
| FOV | field of view |
| HEAF | high energy arc fault |
| HRR | heat release rate |
| ICCD | intensified charged coupled device |
| IR | infrared |
| IEEE | Institute of Electrical and Electronics Engineers |
| MCCB | molded case circuit breaker |
| NPP | nuclear power plant |
| NRC | Nuclear Regulatory Commission |
| PMMA | Polymethyl methacrylate |
| RES | NRC Office of Nuclear Regulatory Research |
| SEM | scanning electron microscopy |
| SNL | Sandia National Laboratories |
| TC | thermocouple |
| TTL | transistor–transistor logic |
| XPS | X-ray photoelectron spectroscopy |
| ZOI | zone of influence |

# 1 OBJECTIVES, TECHNICAL BACKGROUND AND APPROACH

## 1.1 Objectives

This experimental plan reflects the upcoming HEAF experimental campaign to take place in August 2022 at the KEMA Labs Chalfont, PA facility. Figure 1 presents a graphical experimental matrix for electrical switchgear enclosures, while Figure 2 presents the graphical matrix for medium-voltage non-segregated bus duct. The cells highlighted in "green" represent the experiments that will be performed as part of this experimental campaign. Cells highlighted in "red" are experiments that have been previously completed [1], while unhighlighted cells are experiments that have not been completed. The objective of this study is to quantitatively characterize the thermal conditions, pressure conditions, and deposits on nearby surfaces created by HEAFs occurring in medium-voltage electrical non-segregated phase bus ducts and medium-voltage electrical switchgear enclosures. The collection of data and information will be used to evaluate the performance of models developed to estimate the electrical HEAF hazard. That evaluation will be documented in a separate report.

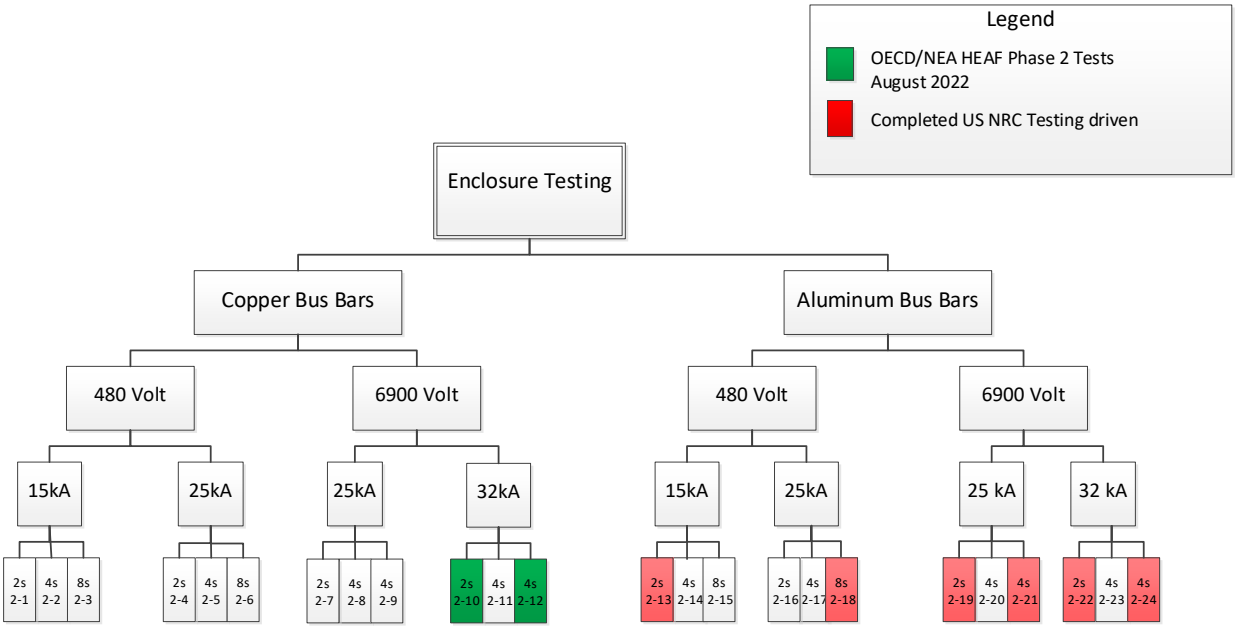


**Figure 1. Electrical enclosure matrix**

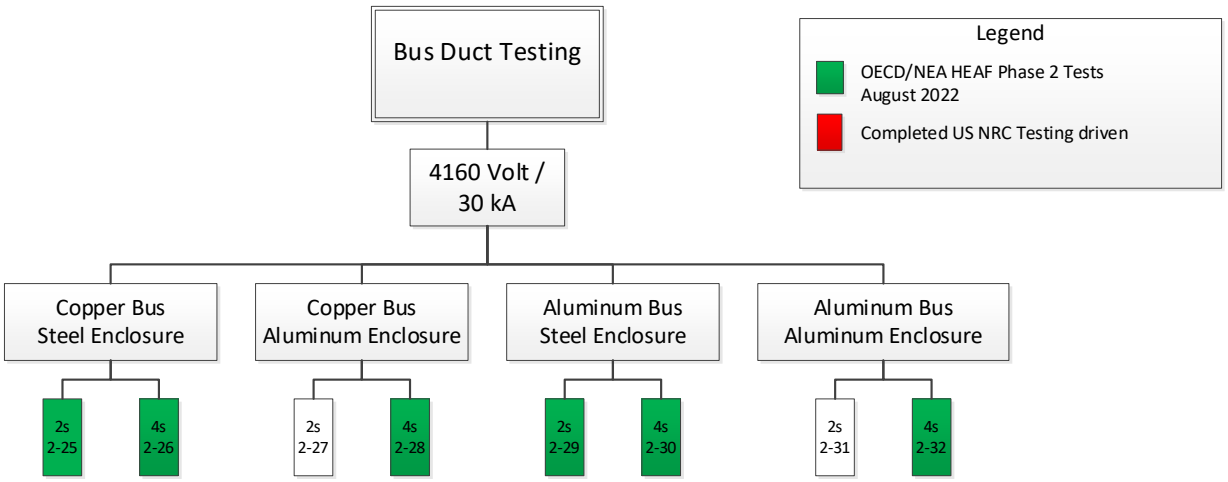


**Figure 2. Bus duct matrix**

## 1.2 General Approach

Previous work in OECD/NEA HEAF Phase I experiments examined a variety of electrical cabinets encompassing several manufacturers, manufacture dates, materials, and configurations [4]. While the Phase I experiments provided an important understanding of the performance of available equipment, there are many HEAF parameters that influence the severity, which are important, but not well understood [5].

To better understand the importance of variables such as bus bar material, enclosure material, operating voltage, arc current, arc duration and equipment configuration on the conditions produced by the HEAF, electrical switchgear enclosures similar to those used in 2018 [1] and non-segregated bus ducts will be used so that repetitive and repeatable tests can be performed. The switchgear/bus duct configuration will be chosen based on typical plant design and preliminary experiments will be performed to ensure the arc will not extinguish until the power supply to the test object is turned off. The bus bar configuration will be chosen based on the desire for a known and repeatable arc location and plasma ejection direction. Real-time measurements of voltage and current during the arc will provide data for calculation of arc energy and arc power for comparison to thermal and pressure measurements as well as an input to modeling needs. The use of a common electrical cabinet and bus duct should increase repeatability between experiments. Experiments will be performed that would subject any equipment to conditions exceeding the equipment ratings (e.g., voltage higher than equipment ratings).

## 1.3 Experiment Facility

The full-scale experiments will be performed at KEMA Labs (referred to in the remainder of this report as “KEMA”), located in Chalfont, Pennsylvania USA. The experiments will be performed in August 2022. KEMA was chosen for its ability to meet the requirements of the program, specifically the required voltage and current to sustain an electrical arc within the test enclosure, as well as the ability to allow for post-HEAF ensuing fire for a period of time after the HEAF

duration, unless the fire places the laboratory in an unsafe condition, at which time the laboratory will extinguish the fire.

The test cells were approximately 8.7 m by 8.5 m by 8 m high, open on one side. The open side of the test cell faces the operator control room which is equipped with impact resistant glazing. Test Cell #9 will be used for the medium-voltage experiments. The test cell is shown in Figure 3 through Figure 5.

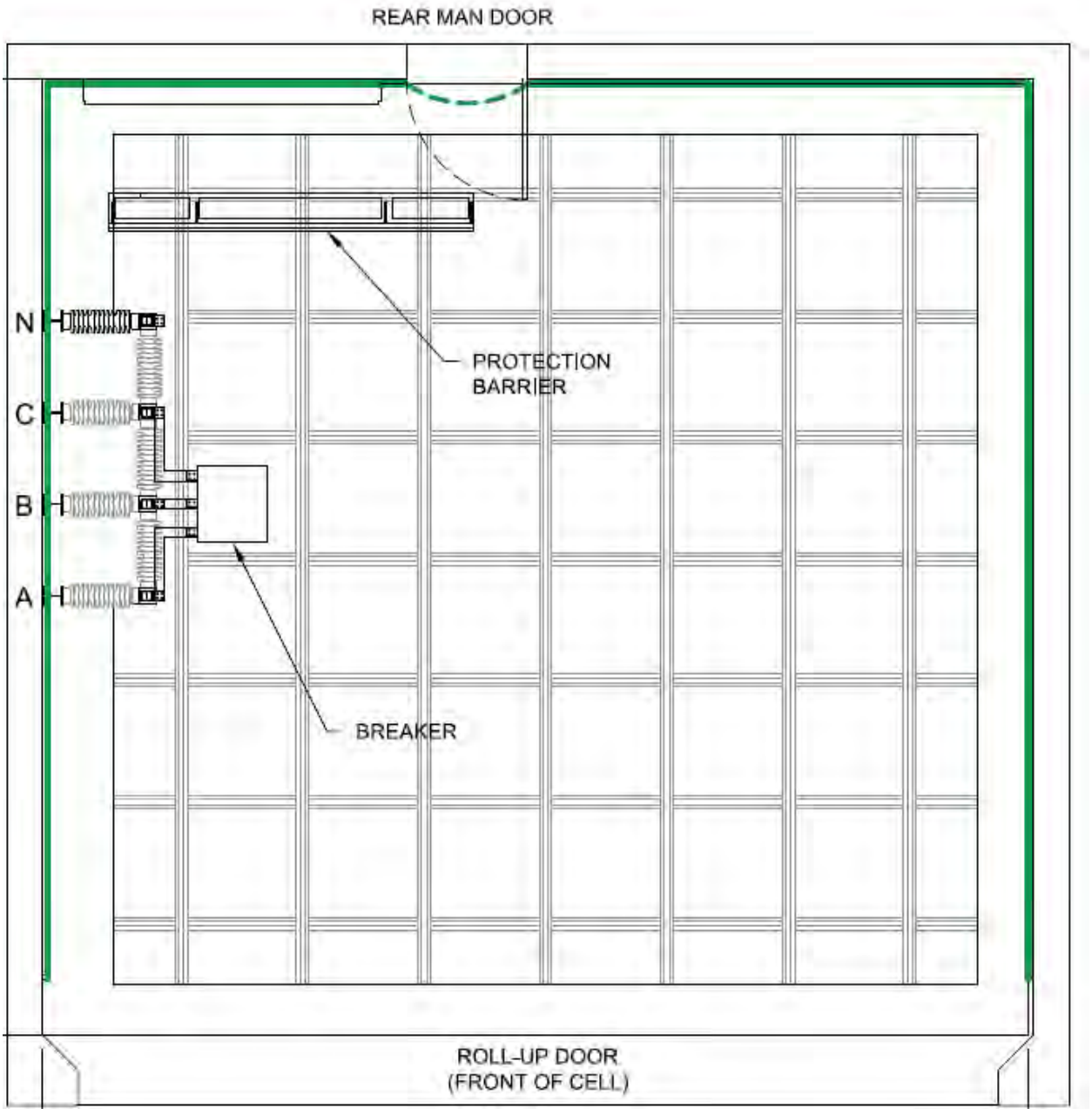


**Figure 3. Plan view of KEMA Labs Cell #9.**

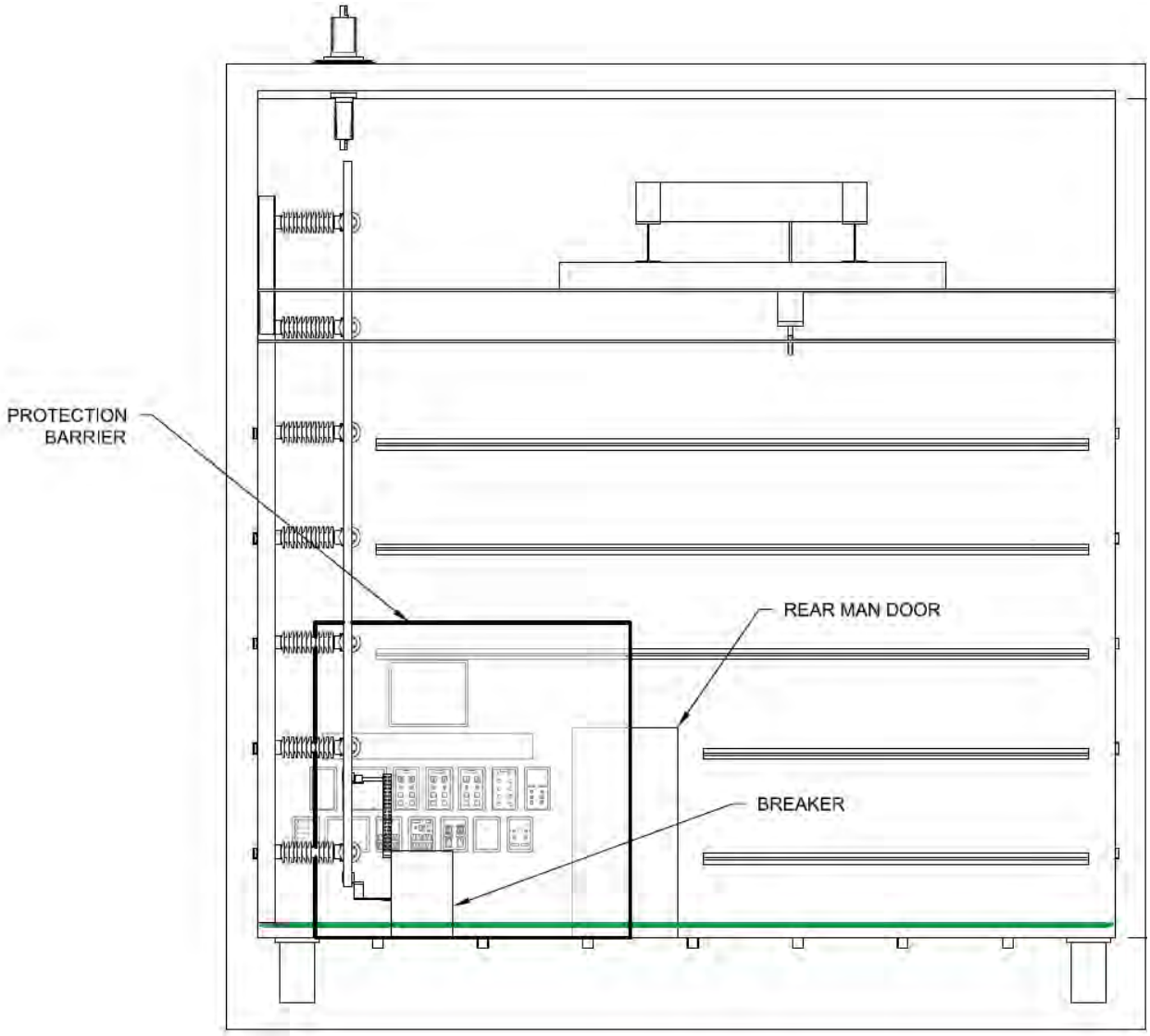


**Figure 4. Elevation view of KEMA Labs Cell #9 (note 'breaker' shown is make-break breaker and not the test device under evaluation.)**

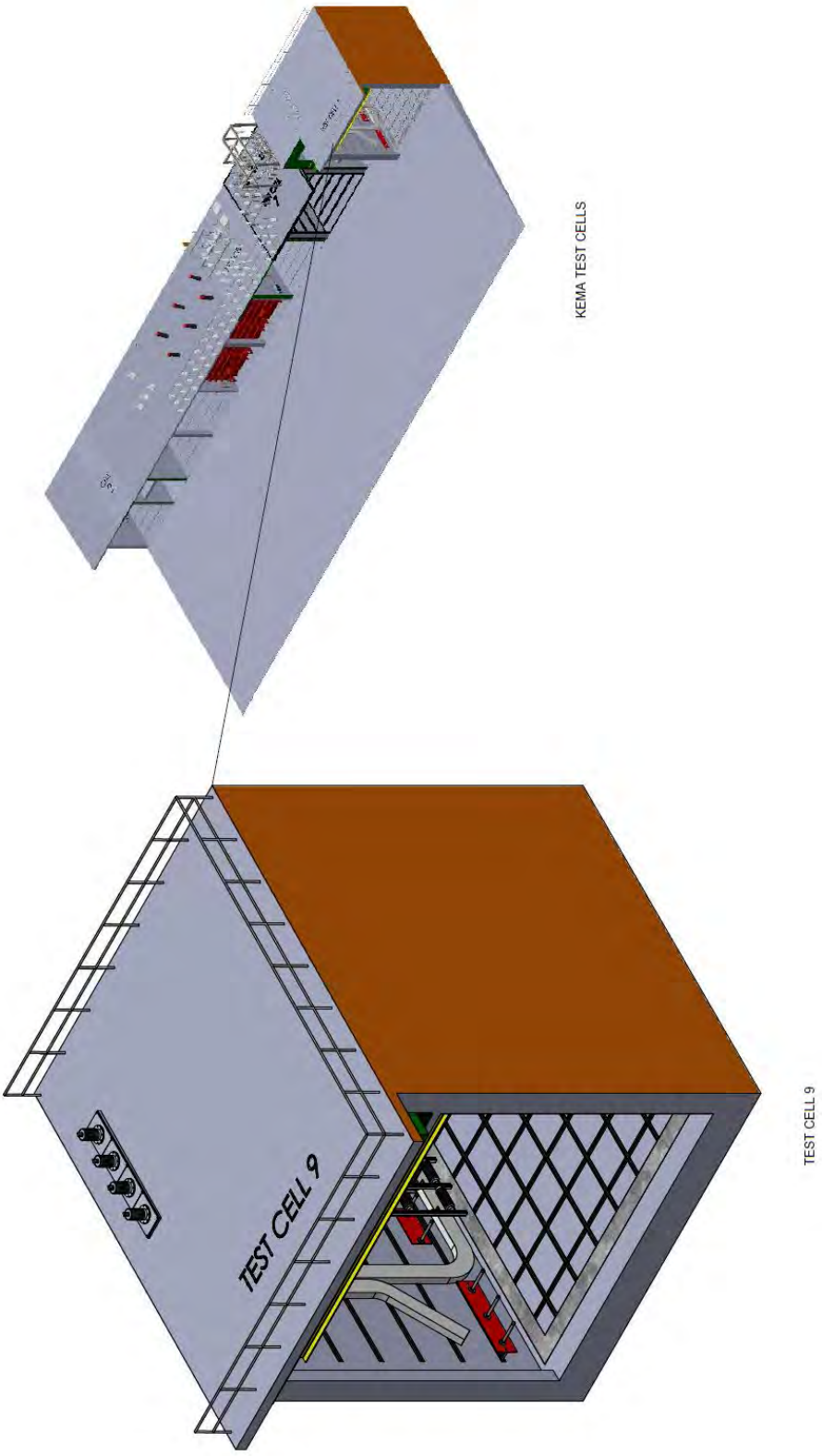


**Figure 5. Isometric drawing of KEMA Labs Cell # 9 with respect to KEMA Facility**

## 1.4 Test Objects

Medium-voltage non-segregated bus ducts and medium-voltage electrical switchgear are included in this experimental campaign. Descriptions of the individual test objects are presented next.

### 1.4.1 Medium-voltage Electrical Switchgear

Two metal-clad switchgear units were procured for these experiments. Both units are Type M-36 manufactured by General Electric, used and refurbished from an ISO 9001 certified medium-voltage circuit breaker and electrical power distribution supplier. The units are approximately 92 cm (36 in) wide by 202 cm (79.5 in) long and 229 cm (90 in) high. Main buses will be extended outside of the enclosure approximately 30 cm (12 in) to allow for connection to the test laboratory's power supply. A shorter grounding stab also extended outside the enclosure. Figure 6 provides a drawing of the enclosure. The metal-clad switchgear ratings are presented in Table 1. Each unit contained one medium voltage circuit breaker. All breakers were GE Magne-blast Type AM-7.2-500 circuit breakers.

**Table 1. Type M-36 Switchgear Ratings**

| RATING | VALUE |
|---|---|
| **Power** | 500 MVA |
| **Nominal operating voltage** | 6.9 kVAC |
| **Rated maximum voltage** | 8.25 kVAC |
| **Main bus continuous rating** | 1,200 A |
| **Short Circuit** | > 33,000 A |
| **Impulse Withstand** | 95,000 Volts |
| **Close / Latch Capability** | 111,000 A Peak |
| **System Frequency** | 60 Hz |
| **Approx. Weight w/out breaker** | 2,000 Lbs |
| **Approx. Breaker Weight** | 1,500 Lbs |

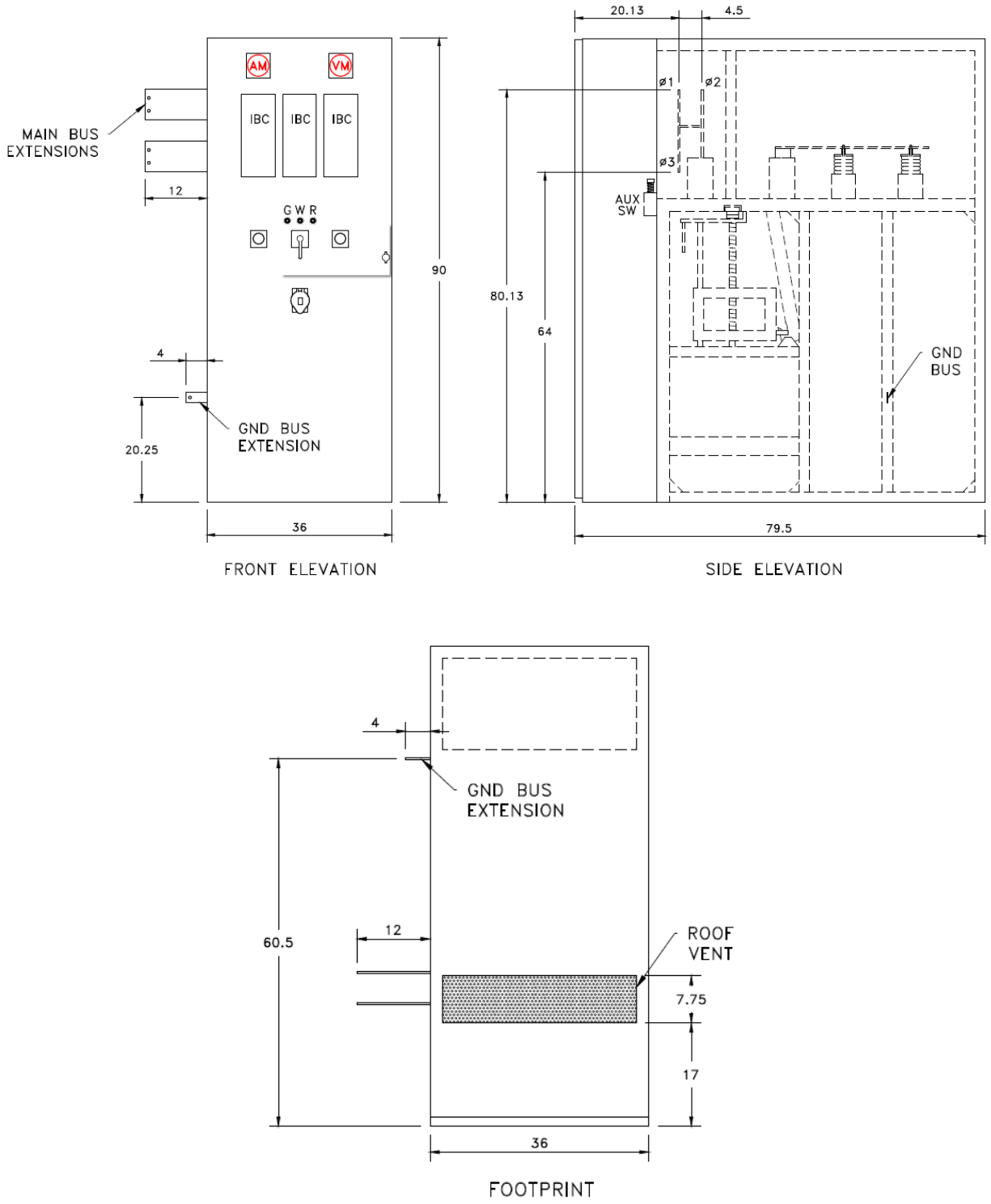


**Figure 6. Drawing of Switchgear Enclosure (dimensions in inches)**

### 1.4.2 Medium-voltage non-segregated phase bus duct

Six medium-voltage non-segregated bus ducts (NSBD) were procured new. Figure 7 provides an illustration of the bus duct assembly. The NSBD consist of straight sections measuring 1.9 m (6 ft) in length and a connecting 90-degree elbow section. The arc will be located in the middle of the straight section. The duct will be supported by a Unistrut structure described in Section 2.1. One end of the bus bars will be connected to the KEMA Labs power supply, while the other end, closes to elbow, will be left unterminated, but insulted. The end of the straight section opposite of the power supply connection will be connected to the 90-degree elbow. The elbow will be supported by a structure to provide added rigidity and support during the experiment.

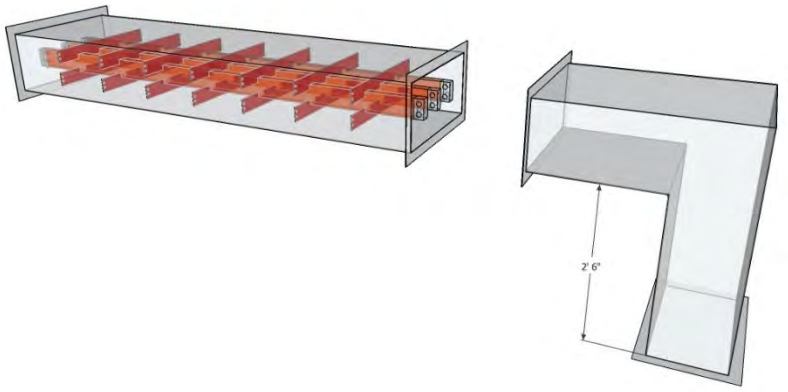


**Figure 7. Illustration of medium-voltage non-segregated bus duct (dimensions in inches) non-fully representative of procured equipment.**

The bus bars are either aluminum or copper depending on the specific experiment configuration. The dimensions of the bus bars differ, as does the duct housing for the respective bus bars, as shown in Figure 8. The copper bars are (4 in) wide by (0.5 in) thick. The aluminum bars are (6 in) wide by (0.63 in) thick. The NSBD ratings are presented in Table 2.

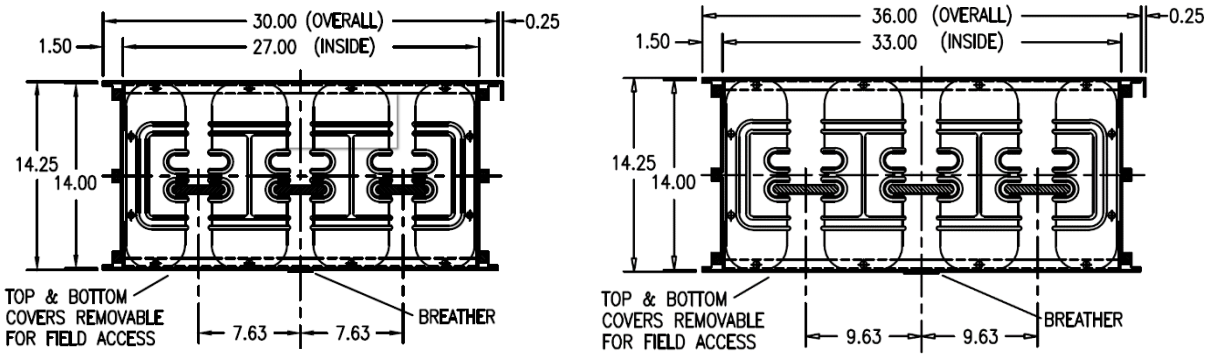


**Figure 8. Drawing of NSBD cross-section. Copper bus bars – Left; Aluminum bus bars – Right (Dimensions in inches)**

**Table 2. NSBD Ratings for bus conductors.**

| RATING | COPPER | ALLUMINIUM |
|---|---|---|
| **Nominal operating voltage** | 4,160 V | 4,160 V |
| **Rated voltage** | 5,000 V | 5,000 V |
| **Continuous rating** | 2,000 A | 2,000 A |
| **Momentary** | 80,000 A (asym.)<br>51,613 (sym.) | 80,000 A (asym.)<br>51,613 (sym.) |
| **BIL rating** | 19 kV | 19 kV |
| **System Frequency** | 60 Hz | 60 Hz |
| **Enclosure Thickness** | N/A | 1.5 MIL |
| **Enclosure weight** | N/A | 41 lbs/foot |
| **Insulation** | Epoxy | Epoxy |
| **Supports** | Polyester | Polyester |

## 1.5 Determination of Experimental Parameters

A number of experimental parameters require determination to support a realistic evaluation of the hazard. The following provides details for determining the experimental parameters.

### 1.5.1 Arc Initiation / Location

Arcs will be initiated using a stranded copper wire 0.51 mm diameter (#24 American Wire Gauge [AWG]), strung across the three phase conductors within the electrical enclosure, at the desired initial arc location. This is consistent with IEEE guide on testing switchgear for internal arcing faults [6]. Each initial arc will be created when the three-phase electrical supply to the switchgear enclosure or bus duct is energized, causing a direct short circuit at the desired location for the arc to occur. Operating experience from HEAF events has identified representative arc locations within equipment.

For the non-segregated bus ducts, the arc location will be in the mid-section of the straight duct enclosure. Several operational events have occurred in straight sections and at locations where the non-segregated phase bus duct changes direction (e.g., elbows and tee-intersections). While both locations have operational experience (OE), performing experiments on a straight section provide advantages from a measurement and repeatability standpoint. A straight section reduces the orientation variable, allowing for the instrumentation to be placed where the arc is to be established and maintained.

For the electrical switchgear enclosures, the arc location will be in the primary cable connection compartment. This location is consistent with past testing [1] and provides a direct comparison to aluminum bus configurations. While other locations have had OE, such as breaker stabs, testing in those locations provide additional complexity to the experiments that are difficult, if not, impossible to measure their impact to support the objective of these experiments (modeling validation).

The use of a shorting wire across all three phases is necessary during testing to provide predictable arc initiation process and to provide for sustained arc duration at the desired position within the electrical enclosure or bus duct. Within milliseconds of energy delivery, the shorting wire vaporizes, becoming a column of ionized gas and plasma, as would be found in a typical arc column. Electrical arcs that occur in the field commonly initiate phase-to-phase or phase-to-ground, then transition to a three-phase fault typically within a fraction of a cycle (i.e., less than one-sixtieth of a second) [7], even for equipment with insulated conductors based on operating experience from 2021. The transition period between a phase-to-ground or a two-phase fault to a three phase fault is small (less than 0.8% of the total energy for a 2 second event and less than 0.2% of the total energy for an 8 second event) relative to the duration of the three phase arc. Given the breaker control system at the testing laboratory can breaker a circuit +0.05 s to +0.15 s beyond the desired arc time, controlling the arc duration to account for the transition time is not achievable and not necessary for the validation purposes.

### 1.5.2 Arc Current /Voltage

KEMA Labs, located in Chalfont, PA, is an electrical test facility providing the electrical energy (voltage, current, duration) for sustained arcing within the subject enclosures independent of the local electric grid. KEMA will also provide the electrical measurement results required to quantify the characteristics of the power supplied to the enclosures during the arcing experiments.

During a public workshop held in 2018, the NRC communicated the results of an informal analysis to estimate the arcing fault current for a number of U.S. nuclear power plants [8]. These results indicated that arcing fault currents ranged from 13.5kA to 59.6kA. For equipment at a nominal operating voltage of 4.16kV a mean of 29.5kA and median of 29.3kA was reported, while equipment operating at a nominal voltage of 6.9kV calculations demonstrated a mean of 31.2kA and a median of 31.9kA. Note that these estimates are based on the entire population, but a limited sample of units (23 for 4.16kV and 9 for 6.9kV) with electrical distribution system information available to the NRC for performing the calculation.

The Electric Power Research Institute (EPRI) performed a comprehensive review of HEAF OE [9]. From that review, the arcing fault current for most events could not be determined. However, there are approximately 4 events that occurred in medium-voltage where the fault current is known, as presented below. The range of fault currents collected through review of the HEAF OE varied from 28 kA to 32 kA. Note that the 13 kA event was not used as it was significantly lower than that typically associated with medium-voltage available fault current.

**Table 3. Operational experience with reported fault current from medium-voltage equipment**

| Event ID | Date | HEAF Location | Generator-fed Fault | Reported Fault Current |
|---|---|---|---|---|
| 51764 | 1/17/2017 | NSBD | No | 13 kA |
| 50910 | 3/28/2010 | SWGR | No | 28 kA |
| 732 | 7/6/1988 | SWGR | No | 32 kA |

| Event ID | Date | HEAF Location | Generator-fed Fault | Reported Fault Current |
|---|---|---|---|---|
| 74 | 6/10/1995 | SWGR | Yes | 28 kA |

To evaluate the influence arcing fault current has on the HEAF hazard, testing at more than one current level was desired. As such, in the 2018 series of experiments involving switchgear with aluminum bus bars [1], two arcing fault current levels were selected, 25kA and 32kA. Given the information gained from that series of experiments along with insights gained from developing models to predict the HEAF hazard, comparative tests at 32kA for medium voltage switchgear are planned for this series of experiments. For the medium voltage non-segregated bus ducts, a comparative test to the switchgear experiments (32kA) was not needed. As such, testing at 30kA is between the 28kA and 32kA OE and a current level used in HEAF hazard modeling efforts. Therefore, medium-voltage non-segregated bus ducts will be tested at 30kA while medium-voltage switchgear will be tested at 32kA.

The arc voltage will be selected to replicate typical power distribution systems commonly found within NPP's. For medium-voltage, 4.16kV and 6.9kV is common, with some units use 2.7kV and 13.8kV. Given that the 2018 series of medium voltage switchgear were tested at 6.9kV [1], that voltage will be used for the medium voltage switchgear tested in this series. For the medium-voltage non-segregated phase bus ducts, 4.16kV will be used. This change from the switchgear tests allows for addition evaluation of the impact voltage has on the HEAF phenomena. The current state of knowledge suggest that it will have minimal impact, as arc impedance and equipment configuration play a large role in the arc voltage and subsequently the arc power during the arc fault.

The nominal current and voltage directly contributed to the total arc energy released during the event and were identified as key parameters for future model input in a recent international HEAF PIRT expert elicitation exercise [Ref. 5].

### 1.5.3 Duration

Review of operating experience for NPP HEAF events has shown that protective devices have not always worked as designed. Problems such as incorrect breaker settings and fuse sizing due to design errors can increase the likelihood of a HEAF and allow for extended duration HEAF events. Operating experience has also indicated that faults can be initiated in locations not protected by fault clearance devices, allowing for extended fault exposure times. In 2021, EPRI issued a reported summarizing industry survey results relative to HEAF [10]. The EPRI report identified that based on the fault clearing time of the station auxiliary transformer (SAT), 45% of HEAFs last longer than 2 seconds, with the longest maximum fault clearing time (FCT) being approximately 5 seconds (approximately 8% have FCT greater than 5 seconds). The report goes on to state,

> The FCT for a unit auxiliary transformer (UAT) powered from the main generator could not be directly correlated to HEAF duration since the HEAF may continue for an addition 4 to 10 seconds

due to the un-isolated main generator's ability to continue feeding the fault until the residual generator energy (field flux) decays.

From this information, arc duration has a very broad range and direct influence on arc energy. For some arcing events the arc duration could be a fraction of a second while other scenarios could persist for up to 15 seconds (assuming 5 second constant current (stiff) followed by a 10 second generator fed decay).

Lessons learned from the testing performed to date, indicate there are a few key aspects of arc duration that need to be addressed in selection of durations for experimentation. First the arc needs to be long enough to ensure breach in the enclosure. This is a key phenomenon that needs to be accurately predicted in HEAF hazard modeling. Secondly, a duration sufficiently different from other identical experimental configurations is desirable to evaluate the duration parameter influence. Third, for experiments that are used for direct comparison, durations should be identical to the experiment to be compared. Lastly, the testing facility must have the capability to provide the arc power for the intended duration. Based on these three attributes, the selected durations for the medium-voltage non-segregated bus ducts and medium-voltage switchgear enclosure experiments will be either 2 or 4 seconds.

## **1.6** Instrumentation

A list of measurements and the corresponding measurement devices is provided in Table 4. The thermal environment around the cabinet during the HEAF experiments will be characterized by measurements of time varying and average heat flux and incident energy. The time varying and maximum pressure inside of the electrical switchgear enclosure will also be measured during the experiments. HEAF generated deposits will be collected on vertical coupons of double sided carbon tape and analyzed to quantify evolved particle sizes and chemical composition after the experiments. The analysis will use scanning electron microscopy (SEM) and energy dispersive spectroscopy (EDS). Standards of 99% aluminum oxide ($Al_2O_3$) and copper oxide (CuO) will be used as reference samples.

The geometrical extent of the arc plasma and fire will be characterized using optical (visible and IR spectrum video) means. IR imaging will provide information as to the extent of the arc plasma and fire, as well as cabinet surface temperature information.

Atmospheric conditions will be recorded on the test days including ambient temperature and humidity. The equipment components such as bus bars and enclosure panels will be weighed before and after experiments to obtain mass loss information associated with the loss of the bus bars through arcing.

**Table 4. Metrology**

| Measurement | Device |
|---|---|
| Temperature | Infrared (IR) imaging, Plate Thermometer (PT) |
| Heat flux (time-varying) | Plate Thermometer (PT) |
| Heat flux (average) | Plate Thermometer (PT), Thermal Capacitance Slug ($T_{cap}$ Slug) |
| Incident energy | ASTM F1959 Slug calorimeter (slug), Thermal Capacitance Slug ($T_{cap}$ Slug) |
| Enclosure internal pressure | Piezoelectric pressure transducer |
| Arc plasma / fire geometry | Videography (with and without neutral density filter), IR imaging |
| Surface deposit analysis | Sample collection (black carbon tape), post-test experiment laboratory analysis (Scanning Electron Microscope, Energy dispersive spectroscopy) |
| Qualitative damage | Cable samples |

### 1.6.1 Digital Imaging

NIST and SNL will field numerous imaging technologies to provide high-speed quantitative and qualitative imaging during this HEAF experimental series evolution. The measurement methods include visible high-speed and high-definition imaging, high-speed high dynamic range visible imaging, and high-speed thermal imaging. The equipment fielded by NIST includes high-definition video cameras and a high-definition thermal imager like that used in the Phase 1 experiments and 2018 medium-voltage HEAF experiments to capture high-definition visible and high-speed thermal images. NIST will also field a high speed, high dynamic range, thermal imager. Equipment fielded by SNL will be a subset of equipment fielded in the 2018 experiment. The equipment selection was scaled down based on results and lessons learned. SNL reports document the approach, and uncertainties.

The processed images will be accessible through an NRC or OECD website as determined by the management board. The digital imaging will include High-Speed Videography, High-Definition Videography, and Thermography.

### 1.6.2 Calorimetry

Several different calorimeter devices will be used to span a range of thermal exposure conditions that may occur during and subsequent to the HEAF experiment. These devices include modified plate thermometers, ASTM slug calorimeters, and tungsten slug calorimeters. These devices have been used in past experiments and are described next.

#### *1.6.2.1 Plate Thermometer*

Modified plate thermometers (PTs) are robust thermal sensors that can survive in hostile HEAF environments [1][4][11]. They were chosen for heat flux measurements in the HEAF experiments

due to their rugged construction, low cost, lack of cooling water, and known emissivity and convective heat flux coefficients.

The modified plate thermometer used in the HEAF experiments is shown in Figure 9. It consists of two 0.51 mm (0.02 in) nominal diameter (24 AWG) Type K thermocouple wires welded directly to the rear of a 0.787 mm ± 0.051 mm (0.031 in ± 0.002 in, 99 percent confidence interval per manufacture specifications) thick Inconel 600 plate, approximately 100 mm (3.94 in) by 100 mm (3.94 in) in size. The plate is backed by a mineral fiber blanket approximately 25.4 mm (1.0 in) thick to minimize heat loss. Machine screws with ceramic washers allow for legs to be attached at the rear of the plate thermometer to simplify installation onto instrumentation racks.

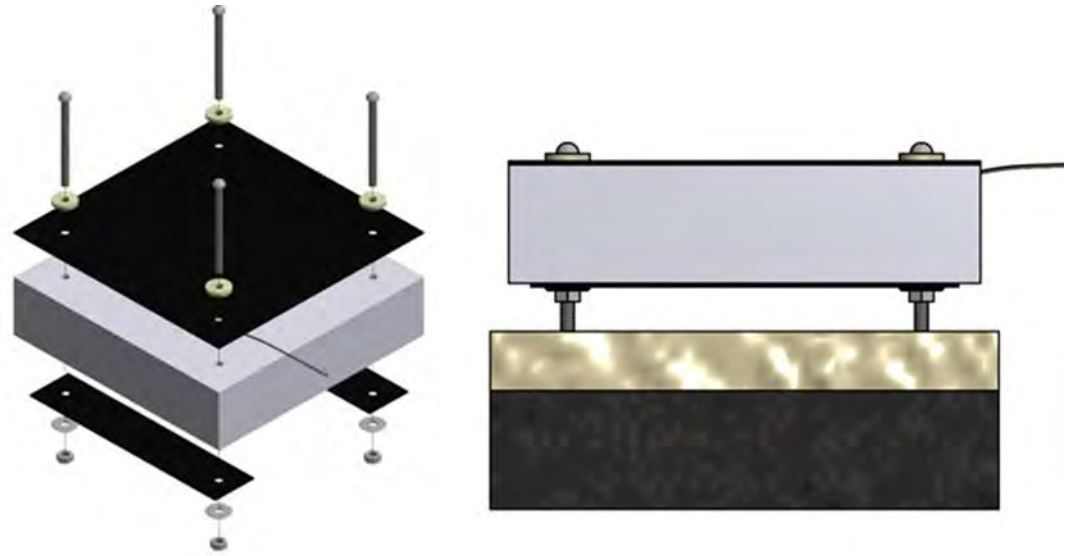

Figure 9. Exploded view of modified plate thermometer (left); cross-sectional view of modified plate thermometer placed on cone calorimeter sample holder (right).

The incident heat flux on a plate thermometer can be calculated from a heat balance using the following equation, a rearrangement of Equation 18 from Ingason and Wickstrom [12]:

$$\dot{q}''_{inc} = \sigma \cdot T_{PT}^4 + \frac{(h_{PT} + K_{cond})(T_{PT} - T_\infty)}{\varepsilon_{PT}} + \frac{\rho_{PT} \cdot C_{PT} \cdot \delta \cdot \left(\frac{\Delta T_{PT}}{\Delta t}\right)}{\varepsilon_{PT}}$$

Here $\dot{q}''_{inc}$ is the incident heat flux, $\sigma$ is the Stefan-Boltzmann Constant, $5.670\times10^{-8}$ W/(m$^2$·K$^4$), $T_{PT}$ is the temperature of the plate (K), $h_{PT}$ is the convection heat transfer coefficient, 10 W/(m$^2$·K), $K_{cond}$ is the conduction correction factor determined from NIST cone calorimeter data, 4 W/(m$^2$·K), $T_\infty$ is the ambient temperature (K), $\varepsilon_{PT}$ is the plate emissivity, 0.85 at 480 °C as rolled and oxidized and specified by the alloy manufacturer, $\rho_{PT}$ is the alloy plate density, 8470 kg/m$^3$ from the alloy manufacturer, $C_{PT}$ is the alloy plate heat capacity, 502 J/(kg·K) at 300 °C from the alloy manufacturer, $\delta$ is the alloy plate thickness, 0.79 mm (0.03 in), and $\Delta t$ is the data acquisition time step of 0.1 s.

The gauge heat flux can also be calculated and is the heat flux listed in the tables of this report. The gauge heat flux is the heat flux that would be reported by an ideal water-cooled transducer

such as a Schmidt-Boelter or Gardon gauge operating at a constant temperature of $T_{gauge}$. The gauge heat flux, $\dot{q}''_{gauge}$, is calculated from [13]:

$$\dot{q}''_{gauge} = \sigma \cdot T_{PT}^4 + \frac{(h_{PT} + K_{cond})(T_{PT} - T_\infty)}{\varepsilon_{PT}} + \frac{\rho_{PT} \cdot C_{PT} \cdot \delta \cdot \left(\frac{\Delta T_{PT}}{\Delta t}\right)}{\varepsilon_{PT}} - \sigma \cdot T_{gauge}^4$$

Type A evaluation of uncertainty is performed by the statistical analysis of a series of measurements. Type B evaluation of uncertainty is based on scientific judgement using relevant available information such as manufacturer specifications, calibration data, handbook data, previous experiments, and knowledge of the behaviors of materials and measurement equipment [12][14][15].

The plate thermometer temperature increase, $\Delta T_{PT}$, is reported along with the gauge heat flux. The uncertainty in the temperature of the Type K thermocouple wire is given by the manufacturer as ± 1.1 °C or 0.4 percent with a 99 percent confidence interval [16]. The expanded uncertainty in a PT temperature change of 0 °C to 1250 °C is 0.3 percent, with a coverage factor of 2, which corresponds to a confidence interval of 95 percent [14]. The expanded uncertainty in the heat flux measurement is ± 1 kW/m2 or ± 5 percent, with a coverage factor of 2, which corresponds to a confidence interval of 95 percent. Additional detail on the uncertainty determination can be found in the previous report [1].

#### *1.6.2.2 ASTM Slug Calorimeters (Slug)*

Incident energy will be measured using slug calorimeters described in ASTM F1959 [17] and shown in Fig. 12. These instruments are customarily used to measure radiant energy and determine the arc flash hazard to personnel in the area of electrical enclosures. Due to the characteristics of the HEAF phenomena, which can result in convective arc jets, the calorimeters are reacting to convective heat transfer in addition to radiant heat transfer. ASTM slug calorimeters consist of a copper disc with a nominal thickness of 1.6 mm (0.063 in) and nominal diameter of 40 mm (1.6 in). An iron-constantan thermocouple (Type J), composed of two 0.255 mm (0.01 in) nominal diameter (30 AWG) wires, is soldered to the back of the copper disc using silver solder. The ASTM standard specifies that the copper disc be installed in an insulation board. The KEMA slug calorimeters are installed in a G-11 fiberglass epoxy phenolic cup, which is then placed in a calcium silicate board holder nominally 100 mm by 100 mm by 32 mm thick (4 in by 4 in by 1.25 in nominal thickness) for mounting on the instrument rack. The instruments are provided by KEMA. The slug temperatures are reported by the KEMA data acquisition system at a rate of 20 Hz.

The incident energy absorbed by the slug calorimeter during the HEAF experiments is calculated according to the methodology in ASTM F1959 [17]. The method reports the net heat absorbed over the arc duration and assumes that there are no losses from the disc due to re-radiation, convection, or conduction to the disc holder. The absorptivity of the disc is assumed to be one.

The total energy per unit area, $Q''$, is calculated by:

$$Q'' = \frac{m \cdot \overline{C_p} \cdot (T_f - T_i)}{A}$$

where m is the mass of the copper disc, $\overline{C_P}$ is the average heat capacity of the copper disc, $T_f$ is the temperature of the disc at the end of the arc, $T_i$ is the temperature of the disc before the arc, and A is the front surface area of the disc. The total energy per unit area resulting from the arc is reported in a summary table for each sensor location in each experiment. The ASTM F1959 standard also refers to the total energy per unit area as incident energy ($cal/cm^2$ or $kJ/m^2$).

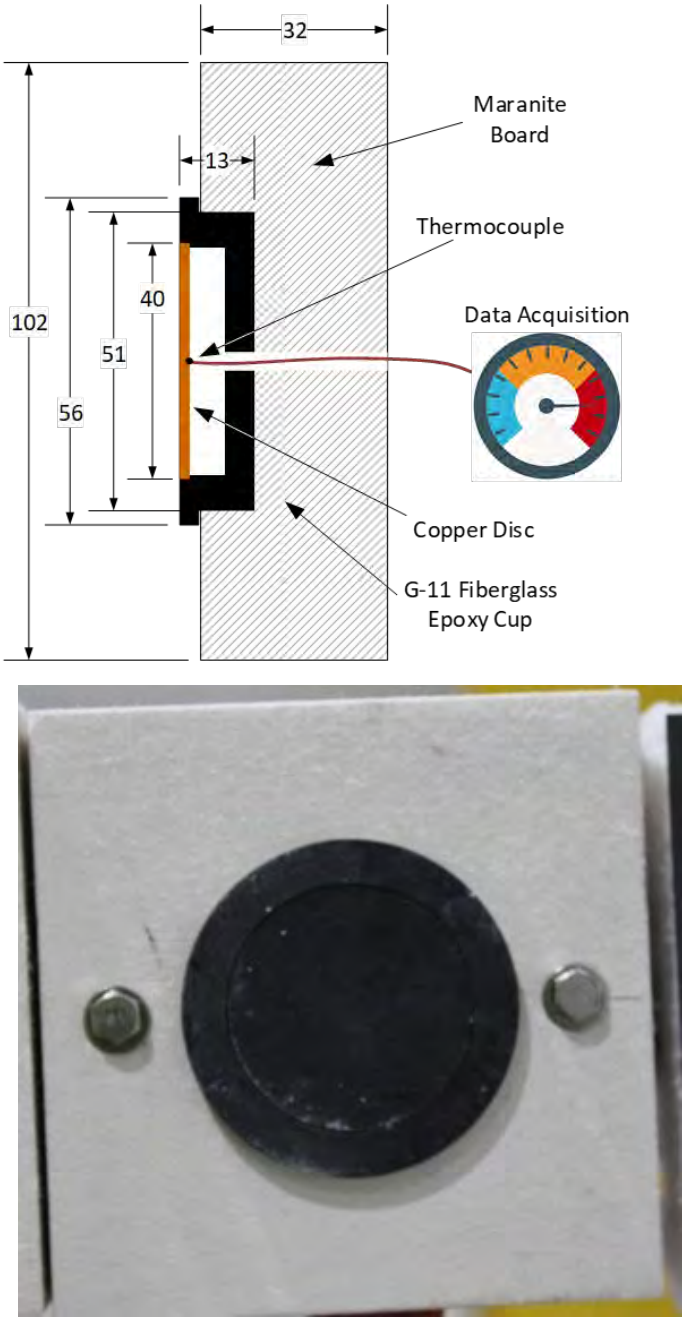


**Figure 10** **Cross-section of ASTM Slug (top) nominal dimensions in millimeters, photo of device being prepared in the field (bottom). Note that the two bolts on each side of the device are used for mounting to the DIN rail of the instrumentation rack.**

The Type B standard uncertainty in the thermocouple measurement, derived from typical thermocouple manufacturer data, with a coverage factor of 2, is 2.2 °C or 0.75 percent. The ASTM calculation method assumes that the absorptivity of the disc is 1.0; however, inspection of the discs over the course of the experiments suggests that the emissivity may vary from approximately 0.9 to 1.0, in a rectangular probability distribution. The expanded uncertainty in the incident energy measurement is ± 18 kJ/m$^2$ or ± 4 percent, with a coverage factor of 2, which

corresponds to a confidence interval of 95 percent. Additional detail on the uncertainty determination can be found in the previous report [1].

### *1.6.2.3 Thermal Capacitance Slugs (Tcap slug)*

Tungsten thermal capacitance slugs ($T_{cap}$ slug) were used to measure the heat flux and incident energy during the HEAF experiment. These sensors were developed as a result of experience gained in Phase 1, where the thermal conditions during some experiments exceeded the measurement capabilities and caused destruction of the ASTM slug calorimeters and modified plate thermometers. A cross section of a $T_{cap}$ slug is shown in Figure 11, which is a modified example of the thermal capacitance slug described in ASTM E457-08 [18]. The slug is composed of a tungsten cylinder approximately 15 mm (0.59 in) long mounted in calcium silicate board. A type K thermocouple is attached to the rear of the tungsten to measure the temperature during heating. The development of the $T_{cap}$ is described in the previous report [1].

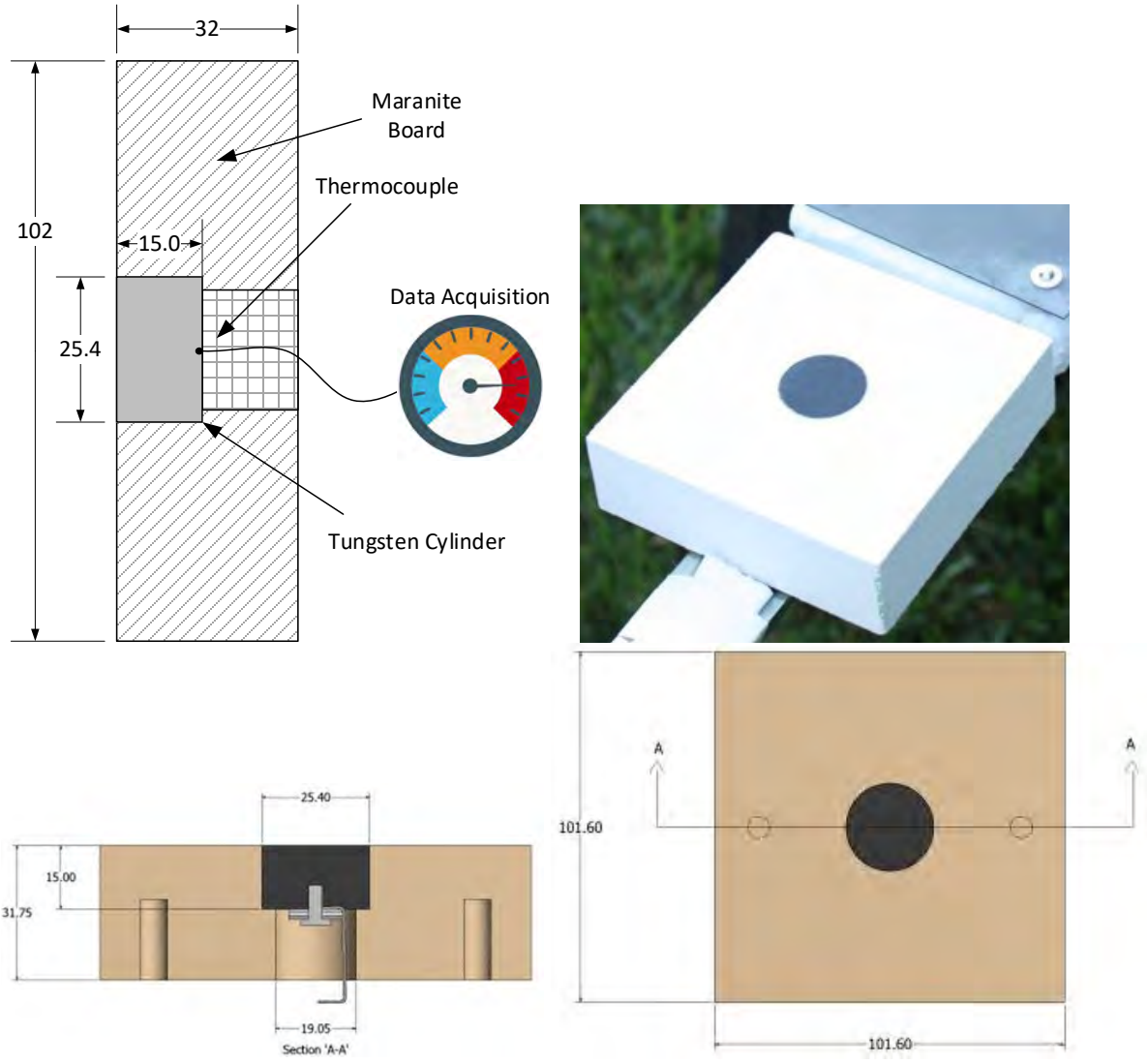


**Figure 11.** Thermal capacitance style slug, illustration (top left), photo of device being prepared in the field (top right), dimensional drawings showing internal construction (bottom left and right). All nominal dimensions in mm.

The maximum heat flux was determined from Equation (5), where $(q")^{\cdot\cdot}$ is the heat flux into the surface of the tungsten slug (kW/m$^2$), ρ is the density of the tungsten slug (kg/m$^3$), $\overline{C_P}$ is the average heat capacity of the tungsten slug (kJ/[kg K]), l is the thickness (m), ΔT is the change in temperature of the tungsten slug (°C), and Δt is the corresponding change in time (s).

$$\dot{q}" = \rho \cdot \overline{C_P} \cdot l \cdot \left(\frac{\Delta T}{\Delta t}\right)$$

An uncertainty analysis using Type A and Type B components was performed on the $T_{cap}$ slug at 50 kW/m$^2$ and 5 MW/m$^2$ using the NIST Uncertainty Machine [19] with cone calorimeter data and fire dynamics simulator (FDS) [20] simulations. The expanded uncertainty in the heat flux measurement is ± 1.5 kW/m$^2$ or ± 2.9 percent, with a coverage factor of 2, which corresponds to a confidence interval of 95 percent.

The expanded uncertainty of the incident energy over the measurement range is estimated at ± 2.4 KJ/m$^2$ or ± 5 percent, with a 95 percent confidence interval, which includes the estimated error due to conduction effects. Additional details on the development of the $T_{cap}$, heat transfer analysis, and uncertainty determinations can be found in the previous report [1].

# 2 TEST APPARATUS AND EXPERIMENTAL SETUPS

## 2.1 Bus Duct Experimental Setup and Configuration

The setup of a typical bus duct experiment is shown in Figure 12-14. The bus bars in the bus duct are attached to the power supply bus mounted on the wall or connected to the Cell 9 breaker unit and terminate at the electrical cabinet. The bus bar will be fully insulated with insulation. The experimental setup calls for a notch to be made in the insulation on the lower portion of the bus bar where the arcing wire will be connected. The notch should provide an anchor point for the arc to limit the possibility for arc migration down the bus bars and into the electrical enclosure. The experimental configuration will be evaluated as testing begins with the potential to implement a full break in the bus bars if needed. Based on experience from previous bus duct testing the physical break is not necessary when bus bar insulation material is employed. This will be evaluated further on a limited number of tests. Thermal transducers and samples are mounted on steel horizontal test stands located above and below the bus duct (see Figure 13).

The primary arc plasma and fire are expected to eject from either the top or bottom of the bus duct near the location of the arc wire. The instrument stands are located at approximately 0.9 m from the top, bottom and side surfaces of the bus duct. The number of instrument stands will be evaluated on an as needed basis depending on expected damage states and laboratory configuration. The preferential arrangement is shown in Figure 12 which depicts two instrumentation racks centered under the desired arc location. The lower instrumentation rack will be slightly offset in the direction of the incoming power supply to limit potential shadowing effects from the higher rack. Sensors, target samples, and imaging techniques will be used in the

same manner as in the electrical cabinet experiments. The general arrangement of each instrumentation stand is depicted in Figure 15.

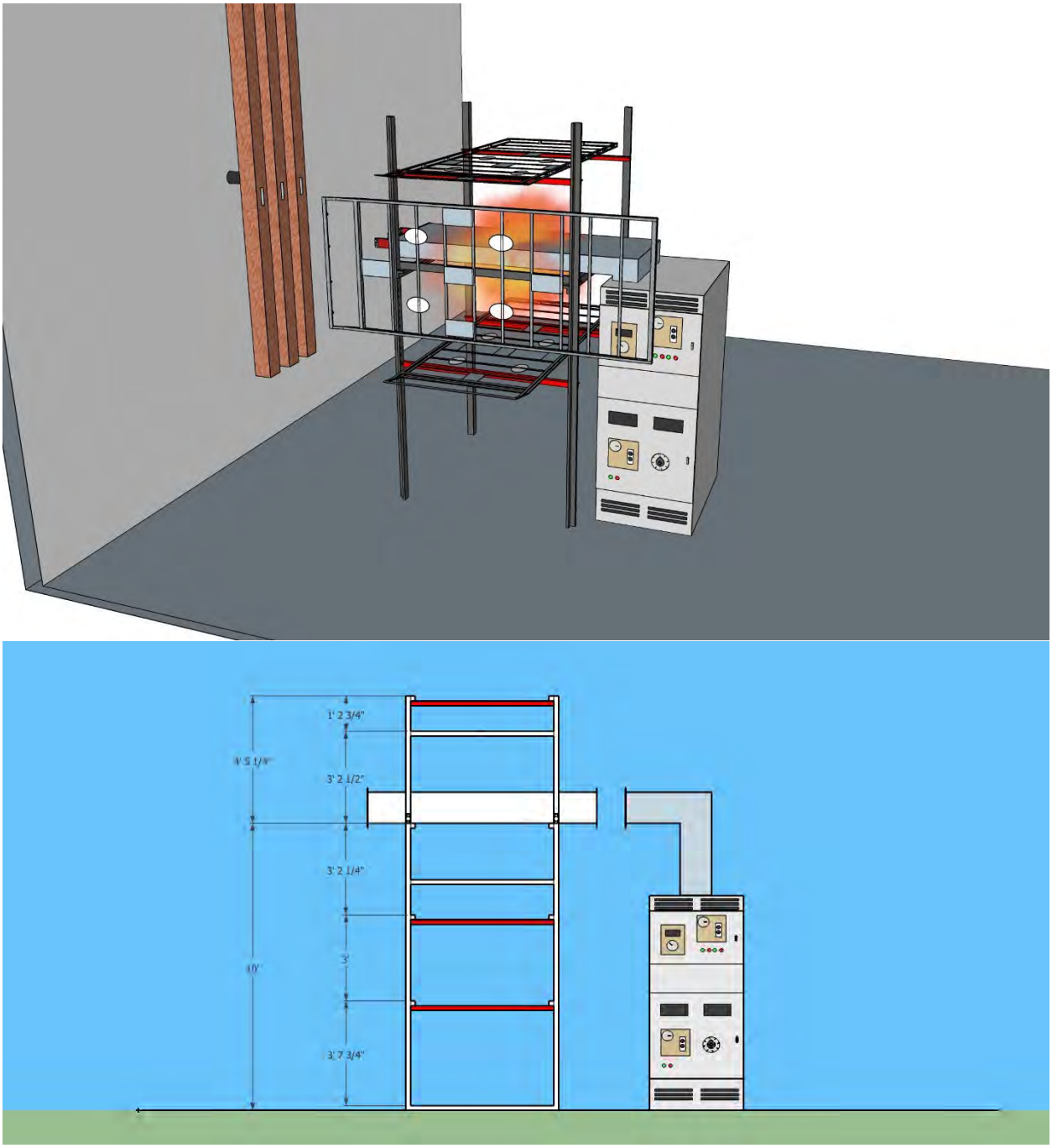


**Figure 12. Bus duct experiment. Elevation view of bus duct and instrument stands.**

**Figure 13. Isometric View of Bus Duct Orientation**

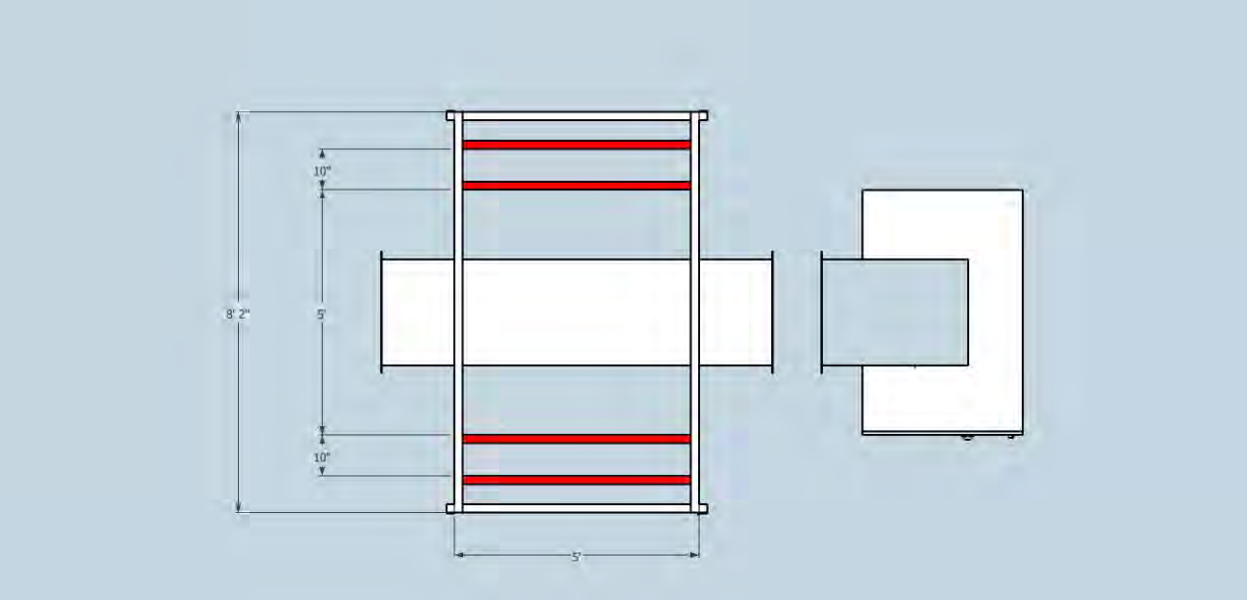


**Figure 14. Plan View of Bus Duct Orientation**

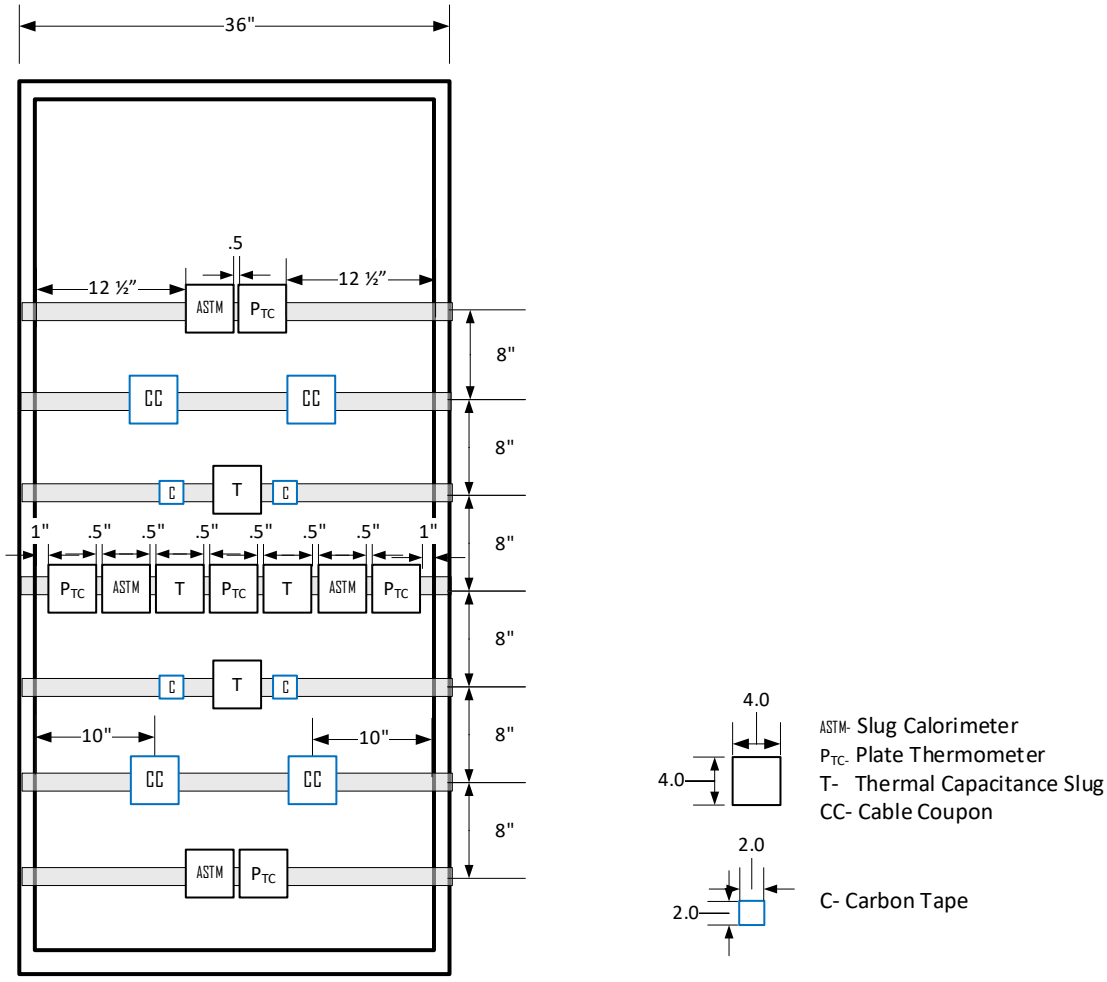


**Figure 15. Instrumentation Rack general assembly**

## 2.2 Test Parameters

**Table 5.** HEAF Test Matrix and Experimental Parameters

| Test ID | Equipment | | Current [kA] | | Target Arc-Duration [s] | | Bus Bar Material | | Enclosure Material | | Comment |
|---|---|---|---|---|---|---|---|---|---|---|---|
| | Duct/Enclosure | 4160 | 30 | 32 | 2 | 4 | Al | Cu | Steel | Aluminum | |
| 2-25 | Duct | X | X | | X | | | X | X | | |
| 2-26 | Duct | X | X | | | X | | X | X | | |
| 2-28 | Duct | X | X | | X | | | X | | X | |
| 2-29 | Duct | X | X | | X | | X | | X | | |
| 2-30 | Duct | X | X | | | X | X | | X | | |
| 2-32 | Duct | X | X | | | X | X | | | X | |
| 2-10 | Enclosure | X | | X | X | | | X | X | | |
| 2-12 | Enclosure | X | | X | | X | | X | X | | |

## 2.3 Timeline and Milestones

Several deliverables shall be supplied to OECD HEAF 2 members for their review, comment and resolution, including:

(1) Test plan
   a. Draft: May 2, 2022
   b. Comments on Draft: June 1, 2022 (30-day OECD review)
   c. Revised draft: June 17, 2022 (15-day NRC-RES response)
   d. Final test plan: July 1, 2022

Note: Final test plan must be submitted to testing laboratory 30-days prior to test

(2) Test report
   a. Draft 90-days after completion of test series
   b. 30-day OECD review
   c. 15-day NRC-RES response
   d. 45-day publication as a RIL

## 2.4 Reporting

A report of test will document the results from this testing program. The report will describe the experimental setup including characteristics of the power supply, description of the tests performed, quantitative results, observations, and any general conclusions or findings. The report will not specify new methods for assessing risk to plants from HEAF events.

# 3 REFERENCES


[1] Taylor, G.,Putorti, A.D., LaFleur, C., et.al., Report on High Energy Arcing Fault Experiments, Experimental Results from Medium Voltage Electrical Enclosures, https://doi.org/10.6028/NIST.TN.2188, RIL2021-10, (ADAMS Accession No. ML21334A196), U.S. Nuclear Regulatory Commission, Washington, DC 20555-0001, NIST TN 2188, National Standards of Science and Technology (NIST), Gaithersburg, MD, SAND2021-12049 R, Sandia National Laboratories (SNL), Albuquerque, NM, 2021.

[2] McGrattan, K., Hostikka, S., et.al., Fire Dynamics Simulator User's Guide, NIST Special Publication 1019, http://dx.doi.org/10.6028/NIST.SP.1019, National Institute of Standards and Technology (NIST), Gaithersburg, MD, VTT Technical Research Centre of Finland, Espoo, Finland, 2021.

[3] Taylor, G., LaFleur, C., Predicting High Energy Arcing Fault Zones of Influence for Aluminum using a Modified Arc Flash Model, Evaluation of a Modified model bias, uncertainty, parameters sensitivity and zone of influence estimation, Draft for Comment, (ADAMS Accession No. ML22095A236), U.S. Nuclear Regulatory Commission, Washington, DC 20555-0001, 2022.

[4] NEA HEAF Project – TOPICAL REPORT No. 1, Experimental Results from the International High Energy Arcing Fault (HEAF) Research Program – Phase 1 Testing 2014 to 2016, Nuclear Energy Agency, Committee on The Safety of Nuclear Installations, Organization for Economic Cooperation and Development, May 2017.

[5] Hamburger, K., An International Phenomena Identification and Ranking Table (PIRT) Expert Elicitation Exercise for High Energy Arcing Faults (HEAF), NUREG-2218, U.S. Nuclear Regulatory Commission, Washington, DC 20555-0001, 2018.

[6] IEEE Guide for Testing Switchgear Rated up to 52kV for Internal Arcing Faults, IEEE C37.20.7-2017, Institute of Electrical and Electronic Engineers, New York, NY, 2017.

[7] Taylor, G.,Putorti, A.D., LaFleur, C., et.al., Report on High Energy Arcing Fault Experiments, Experimental Results from Open Box Enclosures, https://doi.org/10.6028/NIST.TN.2198, RIL2021-18, (ADAMS Accession No. ML21361A176), U.S. Nuclear Regulatory Commission, Washington, DC 20555-0001, NIST TN 2198, National Standards of Science and Technology (NIST), Gaithersburg, MD, SAND2021-16075 R, Sandia National Laboratories (SNL), Albuquerque, NM, 2021.

[8] Taylor, G., Hamburger, K., et.al., Proceedings of the Information-Sharing Workshop on High Energy Arcing Faults (HEAF), NUREG/CP-0311, (ADAMS Accession Nos. ML19212A150 (page 10-22) and ML18108A210 (pages 260-261)) U.S. Nuclear Regulatory Commission, Washington, DC, 20555-0001, 2018.

[9] Fire Events Database Update for the Period 2010–2014: Revision 1. Electric Power Research Institute (EPRI), Palo Alto, CA: 2016. 3002005302.

[10] Survey and Analysis of U.S. Nuclear Industry Relative to High Energy Arcing Faults in the Presence of Aluminum, EPRI 3002020692, Electric Power Research Institute, Palo Alto, CA, 2021.

[11] Putorti, A., Melly, M., Bareham, S., and Praydis Jr., J., "Characterizing the Thermal Effects of High Energy Arc Faults." 23rd International Conference on Structural Mechanics in Reactor Technology (SMiRT 23) – 14th International Post-Conference Seminar on "FIRE SAFETY IN NUCLEAR POWER PLANTS AND INSTALLATIONS," Salford, UK, August 17-18, 2015, http://www.grs.de/en/publications/grs-a-3845.

[12] Joint Committee for Guides in Metrology. International vocabulary of metrology – Basic and general concepts and associated terms (VIM), Sèvres, France: International Bureau of Weights and Measures (BIPM), 3rd ed., URL www.bipm.org/en/publications/guides/vim.html, BIPM, IEC, IFCC, ILAC, ISO, IUPAC, IUPAP and OIML, JCGM 200:2012 (2008 version with minor corrections) (2012).

[13] Ingason, H. and Wickstrom, U., "Measuring incident radiant heat flux using the plate thermometer," Fire Safety Journal, Vol. 42, No. 2, 2007, pp. 161-166.

[14] Taylor, B.N. and Kuyatt, C.E., "Guidelines for evaluating and expressing the uncertainty of NIST measurement results," NIST Technical Note 1297, National Institute of Standards and Technology, Gaithersburg, MD, USA, 1994.

[15] Joint Committee for Guides in Metrology. Evaluation of measurement data – Guide to the expression of uncertainty in measurement, Sèvres, France: International Bureau of Weights and Measures (BIPM), URL www.bipm.org/en/publications/guides/gum.html, BIPM,

IEC, IFCC, ILAC, ISO, IUPAC, IUPAP and OIML, JCGM 100:2008, GUM 1995 with minor corrections (2008).

[16] ASTM (1993), Manual on the Use of Thermocouples in Temperature Measurement, ASTM Manual Series: MNL12, Revision of Special Publication (STP) 470B, 4th ed., ASTM International, West Conshohocken, PA, 1993, United States.

[17] ASTM Standard F1959 / F1959M-14, 2014, "Standard Experiment Method for Determining the Arc Rating of Materials for Clothing," ASTM International, West Conshohocken, PA, 2014.

[18] ASTM Standard E457-08, "Standard Test Method for Measuring Heat-Transfer Rate Using a Thermal Capacitance (Slug) Calorimeter," ASTM International, West Conshohocken, PA, 2008.

[19] Lafarge, T. and Possolo, A, "The NIST Uncertainty Machine," NCLSI Measure J. Meas. Sci., Vol. 10, No. 3, pp.20-27, September 2015.

[20] McGrattan, K., Hostikka, S., McDermott, R., Floyd, J., Weinschenk, C., Overholt, K., Fire Dynamics Simulator, Technical Reference Guide. National Institute of Standards and Technology, Gaithersburg, MD, USA, and VTT Technical Research Centre of Finland, Espoo, Finland, sixth edition, September 2013. Vol. 1: Mathematical Model; Vol. 2: Verification Guide; Vol. 3: Validation Guide; Vol. 4: Configuration Management Plan.

KEMA Labs

# END OF DOCUMENT